Nutrients and Metabolism: Using mass spectrometric techniques to investigate the metabolic effects of nutrition in health and environmental applications

A Dissertation Presented for the
Doctor of Philosophy
Degree
The University of Tennessee, Knoxville

Katarina Alexis Jones
December 2021

Copyright © 2021 by Katarina A. Jones
All rights reserved.

DEDICATION

Soli Deo Gloria. To God alone be the glory.

ACKNOWLEDGEMENTS

I would like to first thank my advisor, Dr. Shawn Campagna for providing me many opportunities to learn and grow as a scientist. While working in his research group I have learned many valuable skills extending beyond the lab. I would also like to thank Drs. Bhavya Sharma, Michael Best, and Brynn Voy for taking the time to serve on my committee and provide valuable feedback and advice throughout my graduate career.

I have also had the pleasure of working with many collaborators during my time in graduate school. Through these interactions I have been given the opportunity to learn about a vast array of biological systems and how to better use mass spectrometry to answer biological questions. I would like to specifically thank Dr. Alison Buchan for introducing me to the world of bacteriophages and giving me advice and guidance through this journey. Dr. Jonelle Basso has always been exceptionally patient with all of my basic biology questions and encouraging me through graduate school and has become a good friend. I would also like to thank Drs. Allison Richards and Jackie Stephens as they have been gracious and supportive while I've been writing.

Over the years I have be grateful to be surrounded with wonderful friends and colleagues in the Campagna lab: Dr. Hector Castro, Dr. Amanda May, Sara Howard, Dr. Allen Bourdon, Dr. Abigail Tester, Dr. Eric Tague, Dr. Brandon Kennedy, Dr. Caleb Gibson, Dr. Alex Fisch, Dr. Josh Powers, Jordan Rogerson, Haley Fielland, Katha Höland, Ashley Starck, Courtney Christopher, Zarin Tasnim, Brittni Woodall, Lindsay Brown, Zane Vickery, Wesley Seaton, Alex Walls, and Maliha Tabassum. I would like to especially thank a few people. Dr. Hector Castro has always supported and encouraged me to pursue my goals, while providing me opportunities to work on different projects and diversify my learning. Dr. Amanda May has always been there to talk through problems with and provide advice. Katha Höland for our many discussions about data analysis and trying to find a better way to display data, and it has been such a relief and help to work on our

dissertations at the same time. Courtney Christopher for always listening to my crazy ideas and letting me talk through research questions and willingness to always proofread anything. Lindsay Brown, thank you for always being eager to help with data processing and analysis so that I could have time to write. And everyone else, thank you for all you do and for supporting and encouraging each other.

And finally, I would like to thank my family, I would not be here today without them. Specifically, my parents Kenny and Maria Jones for teaching me the value of hard work and time management even at a young age. They have always pushed me to do my best in all that I do, but also that my best is all that I can do. Thank you for reminding me to remember “who you are and whom you are” and always being there for me. To my brothers, Joshua, Jacob, Matthew, and Micah, thank you for making trips home always fun and exciting and inspiring me to keep going. I always cherish the time we are able to be together, whether playing at the lake, celebrating birthdays and holidays, or just being together. To my grandparents, Jerry and Susan Burgess, thank you for always being willing to lend a helping hand and supporting me in all that I do. I could keep going on, but for now I will suffice it to say, to my entire family, thank you for everything and for supporting me in this endeavor.

ABSTRACT

For all biological systems nutrients, including small molecules, are necessary for life. Small molecules in particular are used for biological processes such as energy metabolism and as building blocks for larger biomolecules like DNA, proteins, and lipids. Because of this, nutrition and metabolism are intrinsically linked, making metabolomics advantageous to nutritional studies. This work describes three separate studies using metabolomics to probe the effects of specific nutrients and diets in different conditions.

While exercise is documented to provide health benefits, the underlying metabolic mechanisms are not well known. Additionally, exercise is often used to reverse or prevent the negative effects of an unhealthy diet, such as gut dysbiosis. As gut dysbiosis has been seen to be sufficient cause metabolic and neurologic disorders, the interaction between an unhealthy diet, exercise, and the gut microbiome was investigated. From these studies using C57Bl/6J mice, it was determined that while diet had the most significant influence, exercise impacted cecal metabolism most.

Another approach that is commonly used to combat the negative affect of unhealthy diets is through dietary supplements. One of these supplements is fenugreek seeds (*Trigonella foenum-graecum*), which has been used in traditional herbal remedies to treat Type 2 diabetes and obesity. A proposed method by which fenugreek provides benefit is through gut microbiome alterations, which then alters the metabolome. Investigations of the metabolome of C57Bl/6J mice given ground fenugreek seeds (2% [percent] w/w) revealed that the large intestinal and liver metabolite profiles were significantly impacted by fenugreek.

The significant impact of nutrients on the metabolism is not limited to multicellular organisms. Using a unique one-host-two-temperate phage model system from the environmentally relevant Roseobacter clade, the influence of nutrients and phages were evaluated. The effects of a complex growth substrate were compared to glutamate and acetate on the metabolism and lipid regulation

of two *Sulfitobacter* lysogens. From these analyses it was discovered that while there were small differences in the metabolome between strains, the lipids display dramatic differences based on growth substrate. Additionally, it was determined that phages impact the metabolite and lipid profiles in a nutrient dependent way.

TABLE OF CONTENTS

Introduction 1
Nutrition and metabolism 2
Overview of metabolomics 3
Outline of dissertation 5
Chapter 1 Western Diet and Short-Term Voluntary Exercise Induce Intestinal Metabolome Changes 6
1.1 Abstract 7
1.2 Introduction 8
1.3 Results 10
1.3.1 Metabolic profiles display differences between intestinal regions and serum 10
1.3.2 Western diet has greater influence on metabolomes than exercise 13
1.3.3 Immediate effects of exercise 14
1.3.4 Enduring effects of exercise 17
1.4 Discussion 21
1.4.1 Western diet alters metabolism of specific amino acids 22
1.4.2 Exercise impacts metabolites most greatly altered by Western Diet 24
1.4.3 Cecum contents are most greatly impacted by exercise 26
1.5 Methods 27
1.5.1 Animals 27
1.5.2 Metabolomics sample preparations 28
1.5.3 Liquid chromatography 28
1.5.4 Mass Spectrometry 29
1.5.5 Data processing 29
1.5.6 Statistical analysis 30
1.6 Conclusions 30
Appendix 31
Chapter 2 Fenugreek Supplementation to High Fat and Western Diets Significantly Alters Liver and Intestinal Metabolome 44
2.1 Abstract 45
2.2 Introduction 46
2.3 Results 48
2.3.1 Significant differences between small intestine, large intestine, liver, and serum 48
2.3.2 Metabolomics data indicate significant differences as a result of fenugreek supplementation 50
2.3.3 Fenugreek supplementation modulates HDL balance and total cholesterol in both HF diet- and WD-fed mice 65
2.4 Discussion 68
2.4.1 High fat diet influences purine metabolite abundances 72
2.4.2 Fenugreek induces considerable changes in the large intestines 72
2.4.3 Liver and serum metabolomes are affected by fenugreek 74

2.4.4 Fenugreek impacts specific pathways by location and diet.....76
2.5 Methods.....78
2.5.1 Animals and diets 78
2.5.2 Metabolic phenotyping.....80
2.5.3 Metabolite extractions.....80
2.5.4 UHPLC-HRMS.....81
2.5.5 Metabolomics Data Processing 81
2.5.6 Statistical Analysis 82
2.6 Conclusions.....82
Appendix 84
Chapter 3 Metabolomics And Lipidomics Demonstrate Two Genetically Similar Lysogens Influence Host Metabolism Based on Growth Substrate 101
Preface.....102
3.1 Abstract 104
3.2 Introduction.....105
3.3 Results 107
3.3.1 Growth physiologies of strains are different across substrates. 108
3.3.2 Diversity of metabolites detected varies strongly with growth substrate. 110
3.3.3 Lipid profiles vary with growth substrate and strain. 110
3.3.4 Presence of amino lipids correlates with nutrients. 113
3.3.5 Detection of an abundant, but unidentified lipid class. 117
3.4 Discussion.....119
3.5 Materials and Methods 125
3.5.1 Bacterial propagation in different growth conditions. 125
3.5.2 Sampling methodology. 125
3.5.3 Metabolomics.....126
3.5.4 Lipidomics.....127
3.5.5 Spot plating assays for SPI detection. 127
3.5.6 Statistical analysis. 128
3.6 Conclusions.....128
Appendix 130
Conclusion 140
References 144
Vita.....163

LIST OF TABLES

Table 1.1 Summary of diets, activity group, and experimental duration 11
Table 1.2 Summary of identified metabolites and unique spectral features 13
Table 2.1 Summary of identified metabolites and mass spectral features from HF metabolomics data. 52
Table 2.2 Summary of identified metabolites and mass spectral features from WD metabolomics data. 54
Table 2.3 Summary of diets and animals per diet for fenugreek studies 79
Table 2.4 Fenugreek supplementation does not alter body weight, body composition or liver weight in mice fed a LF_{HF} or HF diet. 97
Table 2.5 Fenugreek supplementation does not alter body weight or body composition in mice fed a LF_{WD} or WD diet, but does alter liver weight in mice fed a WD diet. 97
Table 3.1 Media comparisons for complex, glutamate, and acetate carbon sources 130
Table 3.2 Incidence of SPI from *Sulfitobacter* sp. strains CB-D and CB-A cells grown in SMM 131
Table 3.3 Incidence of SPI from *Sulfitobacter* sp. strains CB-D and CB-A cells grown in glutamate 132
Table 3.4 Incidence of SPI from *Sulfitobacter* sp. strains CB-D and CB-A cells grown in acetate 133
Table 3.5 Optical density and viable counts data for *Sulfitobacter* sp. strains CB-A and CB-D grown in SMM. 134
Table 3.6 Optical density and viable counts data for *Sulfitobacter* sp. strains CB-A and CB-D grown on glutamate 135
Table 3.7 Optical density and viable counts data for *Sulfitobacter* sp. strains CB-A and CB-D grown on acetate 136

LIST OF FIGURES

Figure 1.1 Partial least squares discriminant analysis (PLS-DA) of all identified metabolites according to sample matrix. 11
Figure 1.2 Pairwise PLS-DA analysis of cecum content metabolomics data 13
Figure 1.3 Average normalized peak area for taurodeoxycholate from the 10-week study. 15
Figure 1.4 PLS-DA of total unique features detected from metabolomics analysis of (A) jejunum contents, (B) ileum contents, (C) cecum contents, and (D) colon contents of low fat (LF) and Western diet (WD) fed sedentary (Sed) and exercise (Ex) mice from the 10 week study. 16
Figure 1.5 Heatmap analysis of select metabolites from (A) 10-week experiment and (B) 18-week experiment. 18
Figure 1.6 PLS-DA of total unique features detected from metabolomics analysis of (A) cecum contents, (B) colon contents, (C) serum of low fat (LF) and Western diet (WD) fed sedentary (Sed) and exercise (Ex) mice from the 18-week study. 19
Figure 1.7 PLS-DA of total unique features detected from metabolomics analysis of (A) cecum contents, (B) colon contents, (C) serum of low fat (LF) and Western diet (WD) fed sedentary (Sed) and exercise (Ex) mice from the 18-week study. 20
Figure 1.8 Cysteine and methionine metabolism and taurine metabolism pathways 23
Figure 1.9 Pairwise PLS-DA of jejunum contents. 31
Figure 1.10 Pairwise PLS-DA of ileum contents.. 31
Figure 1.11 Pairwise PLS-DA of colon contents. 32
Figure 1.12 Pairwise PLS-DA of serum metabolomics. 32
Figure 1.13 Average normalized peak area for cholate from the (A) 10-week study and (B) 18-week study.. 33
Figure 1.14 Average normalized peak area for cystathionine from the (A) 10-week study and (B) 18-week study. 34
Figure 1.15 Average normalized peak area for cysteate from the (A) 10-week study and (B) 18-week study.. 35
Figure 1.16 Average normalized peak area for cysteine from the (A) 10-week study and (B) 18-week study. 36
Figure 1.17 Average normalized peak area for homocysteic acid from the (A) 10-week study and (B) 18-week study. 37
Figure 1.18 Average normalized peak area for methionine from the (A) 10-week study and (B) 18-week study.. 38
Figure 1.19 Average normalized peak area for taurine from the (A) 10-week study and (B) 18-week study. 39
Figure 1.20 Average normalized peak area for taurodeoxycholate from the 18-week study. 40
Figure 1.21 Heatmap visualization comparing WD-fed to LF-fed mice.. 41

Figure 1.22 PLS-DA of identified metabolites detected from metabolomics analysis of (A) jejunum contents, (B) ileum contents, (C) cecum contents, and (D) colon contents of low fat (LF) and Western diet (WD) fed sedentary (Sed) and exercise (Ex) mice from the 10 week study. 42
Figure 1.23 PLS-DA of (A) identified metabolites and (B) total unique features detected from metabolomics analysis of serum of low fat (LF) and Western diet (WD) fed sedentary (Sed) and exercise (Ex) mice from the 10-week study. 42
Figure 1.24 PLS-DA of identified metabolites detected from metabolomics analysis of (A) jejunum contents, (B) ileum contents, (C) colon contents, and (D) serum of low fat (LF) and Western diet (WD) fed sedentary (Sed) and exercise (Ex) mice from the 18 week study. 43
Figure 1.25 PLS-DA of total unique features detected from metabolomics analysis of (A) jejunum contents and (B) ileum contents of low fat (LF) and Western diet (WD) fed sedentary (Sed) and exercise (Ex) mice from the 18-week study. 43
Figure 2.1 Venn diagrams depicting the overlap of identified metabolites between the small intestines, large intestines, liver, and serum from (A) HF-fed and LF_{HF}-fed mice both with and without fenugreek supplementation and (B) WD-fed and LF_{WD}-fed mice both with and without fenugreek supplementation. 49
Figure 2.2 Partial least squares discriminant analysis (PLS-DA) comparing metabolomes for each intestinal region (jejunum, ileum, cecum, and colon), liver, and serum and associated with (A) HF and HFFG diets or (B) WD and WDFG diets. 51
Figure 2.3 PLS-DA display minimal differences in metabolic profiles between diets and the respective FG supplemented diet in small intestines. Untargeted metabolomics was performed on the jejunum and ileum contents mice fed HF, HFFG, LF_{HF}, or LF_{HF}FG diets for 14 weeks. PLS-DA were performed for (A) identified jejunum metabolites, (B) all jejunum spectral features, (C) identified ileum metabolites and (D) all ileum spectral features. 54
Figure 2.4 PLS-DA display some differences in metabolic profiles between diets and the respective FG supplemented diet in small intestines. Untargeted metabolomics was performed on the jejunum and ileum contents mice fed WD, WDFG, LF_{WD}, or LF_{WD}FG diets for 14 weeks. PLS-DA were performed for (A) identified jejunum metabolites, (B) all jejunum spectral features, (C) identified ileum metabolites and (D) all ileum spectral features. 55
Figure 2.5 Diet and FG supplementation induce distinct differences in the large intestine metabolome as shown by PLS-DA. Untargeted metabolomics was performed on the cecum and colon contents of mice fed either HF, HFFG, LF_{HF}, or LF_{HF}FG diets after 14 weeks of diet exposure. PLS-DA were performed for (A) identified jejunum metabolites, (B) all jejunum spectral

features, (C) identified ileum metabolites and (D) all ileum spectral features. 57
Figure 2.6 Normalized intensities of xanthosine from both cecum and colon data from HF-, HFFG-, LF_{HF}-, and LF_{HF}FG-fed mice. 58
Figure 2.7 Normalized intensities of carnitine from both cecum and colon data from HF-, HFFG-, LF_{HF}-, and LF_{HF}FG-fed mice. 58
Figure 2.8 Diet and FG supplementation induce distinct differences in the large intestine metabolome as shown by PLS-DA. Untargeted metabolomics was performed on the cecum and colon contents of mice fed either WD, WDFG, LF_{WD}, or LF_{WD}FG diets after 14 weeks of diet exposure. PLS-DA were performed for (A) identified jejunum metabolites, (B) all jejunum spectral features, (C) identified ileum metabolites and (D) all ileum spectral features. 60
Figure 2.9 Over a quarter of unique spectral features detected in metabolomics investigations of cecum contents of mice were significantly different in WD-fed mice compared to LF_{WD} fed mice. Of these features, over 90% were detected with higher abundance in WD-fed mice relative to LF-fed mice, but lower abundance in WDFG-fed mice relative to WD-fed mice. 61
Figure 2.10 PLS-DA of liver and serum samples reveal subtle distinctions between the metabolic profiles associated with each diet, more notably in the unidentified features. Untargeted metabolomics was performed on the liver samples from mice fed either HF, HFFG, LF_{HF}, or LF_{HF}FG diets. PLS-DA were performed for (A) identified liver metabolites, (B) all liver spectral features, (C) identified serum metabolites, and (D) all serum spectral features. 63
Figure 2.11 16% of unique spectral features detected in metabolomics investigations of livers of mice were significantly different in WD-fed mice compared to LF_{WD} fed mice. Of these features, nearly 90% were detected with higher abundance in WD-fed mice relative to LF-fed mice, but lower abundance in WDFG-fed mice relative to WD-fed mice. 64
Figure 2.12 PLS-DA of serum samples reveal distinctions, although minimal, between the metabolic profiles associated with each diet, more noticeably in the unidentified features. Untargeted metabolomics was performed on the liver samples from mice fed either WD, WDFG, LF_{WD}, or LF_{WD}FG diets. PLS-DA were performed for (A) identified serum metabolites and (B) all serum spectral features. 66
Figure 2.13 Nearly 40% of unique spectral features detected in metabolomics investigations of livers of mice were significantly different in WD-fed mice compared to LF_{WD} fed mice. Of these features, over 50% were detected with lower abundance in WD-fed mice relative to LF-fed mice, but higher abundance in WDFG-fed mice relative to WD-fed mice. 67
Figure 2.14 Fenugreek supplementation improves cholesterol levels and high-density lipoprotein (HDL) balance in HF diet-fed mice. Whole blood was collected from fasted mice following 14 weeks on LF_{HF}, LF_{HF}FG, HF, or

HFFG diet, and serum was separated and analyzed for total cholesterol, HDL, and low-density lipoprotein (LDL). (A) and (B) HDL and LDL are represented as percent cholesterol. (C – E) show the absolute levels of total cholesterol, HDL, and LDL.....69
Figure 2.15 Fenugreek supplementation improves cholesterol levels and high-density lipoprotein (HDL) balance in WD-fed mice. Whole blood was collected from fasted mice following 14 weeks on LF_{WD}, LF_{WD}FG, WD, or WDFG diet, and serum was separated and analyzed for total cholesterol, HDL, and low-density lipoprotein (LDL). (A) and (B) HDL and LDL are represented as percent cholesterol. (C – E) show the absolute levels of total cholesterol, HDL, and LDL.....70
Figure 2.16 Only 5% of unique spectral features detected in metabolomics investigations of jejunum contents of mice were significantly different in WD-fed mice compared to LF_{WD} fed mice. Of these features, over 50% were detected with higher abundance in WD-fed mice relative to LF-fed mice, but lower abundance in WDFG-fed mice relative to WD-fed mice.....84
Figure 2.17 A third of unique spectral features detected in metabolomics investigations of ileum contents of mice were significantly different in WD-fed mice compared to LF_{WD} fed mice. Of these features, over 80% were detected with higher abundance in WD-fed mice relative to LF-fed mice, but lower abundance in WDFG-fed mice relative to WD-fed mice.....84
Figure 2.18 Top 10 metabolites with the highest VIP scores from PLS-DA of (A) cecum contents and (B) colon contents comparing LF_{HF}, LF_{HF}FG, HF and HFFG diets. 85
Figure 2.19 Normalized intensities of (A) adenine and (B) guanosine from both cecum and colon data from HF-, HFFG-, LF_{HF}-, and LF_{HF}FG-fed mice. 86
Figure 2.20 Normalized intensities of (A) inosine and (B) myo-inositol from both cecum and colon data from HF-, HFFG-, LF_{HF}-, and LF_{HF}FG-fed mice. 87
Figure 2.21 Pairwise PLS-DA of identified metabolites from (A) cecum contents and (B) colon contents of HF- and HFFG-fed mice. Experimental replicates and 95% confidence intervals are shown. Top 10 metabolites with highest VIP scores are shown for (C) cecum contents and (D) colon contents.....88
Figure 2.23 Normalized intensities of 6-phospho-D-gluconolactone from both cecum and colon data from WD-, WDFG-, LF_{WD}-, and LF_{WD}FG-fed mice.. .89
Figure 2.22 Normalized intensities of 2,3-dihydroxybenzoate from both cecum and colon data from HF-, HFFG-, LF_{HF}-, and LF_{HF}FG-fed mice.....89
Figure 2.24 Normalized intensities of (A) glucose phosphate and (B) gluconolactone from both cecum and colon data from WD-, WDFG-, LF_{WD}-, and LF_{WD}FG-fed mice.....90
Figure 2.25 Normalized intensities of (A) myo-inositol and (B) homocarnosine from both cecum and colon data from WD-, WDFG-, LF_{WD}-, and LF_{WD}FG-fed mice. 91

Figure 2.26 Top 10 metabolites with the highest VIP scores from PLS-DA of (A) cecum contents and (B) colon contents comparing LF_{WD}, $LF_{WD}FG$, WD and WDFG diets. 92
Figure 2.27 Nearly one third of unique spectral features detected in metabolomics investigations of colon contents of mice were significantly different in WD-fed mice compared to LF_{WD} fed mice. Of these features, around 40% were detected with higher abundance in WD-fed mice relative to LF-fed mice, but lower abundance in WDFG-fed mice relative to WD-fed mice. 93
Figure 2.28 Normalized intensities of glycodeoxycholate detected in liver samples of LF_{HF}, $LF_{HF}FG$, HF and HFFG fed mice. 93
Figure 2.29 Pairwise (A) PLS-DA of identified metabolites from liver samples of HF- and HFFG-fed mice, and (B) Top 10 metabolites with highest VIP scores. 94
Figure 2.30 PLS-DA of (A) identified metabolites and (B) total unique features from the liver of mice fed WD, WDFG, LF_{WD}, or $LF_{WD}FG$ diets for 14 weeks. Experimental replicates are shown. Top 10 metabolites with highest VIP scores for components 1-3 from PLS-DA of identified metabolites are shown in (C). 95
Figure 2.31 Sum of the average intensity for each metabolite identified from the contents of the jejunum, ileum, cecum, and colon, and liver and serum samples of mice fed (A) HF or LF_{HF} with and without fenugreek (FG; 2% w/w) or (B) WD or LF_{WD} with and without FG (2% w/w). 96
Figure 2.32 Heatmap analysis of metabolomics data from HF study.. 98
Figure 2.33 Heatmap analysis of metabolomics data from WD study. 99
Figure 2.34 Normalized intensities of (A) xanthine detected in serum and (B) cholate detected in liver samples of LF_{WD}, $LF_{WD}FG$, WD and WDFG fed mice. 100
Figure 3.1 Growth dynamics and cell size data for *Sulfitobacter* sp. strains CB-D (light gray) and CB-A (dark gray) in (A) Standard Marine Media (SMM), (C) glutamate and (E) acetate. Cell size was measured by forward scatter through flow cytometry for cells grown in (B) SMM, (D) glutamate and (F) acetate. 109
Figure 3.2 Metabolomics heatmap analysis of SMM, glutamate and acetate grown cells. 111
Figure 3.3 Partial least squares discriminant analysis (PLSDA) plots illustrate significant clustering by substrate, and to a lesser extent, by strain. (A) *Sulfitobacter* sp. strains CB-D and CB-A metabolites comparison and (B) lipids comparison were analyzed using MetaboAnalyst 112
Figure 3.4 Lipidomics heatmap analysis of SMM, glutamate and acetate grown cells 114
Figure 3.5 Pie charts display relative proportions of the sum of phospholipid concentrations in *Sulfitobacter* sp. strains CB-D and CB-A for each timepoint and substrate 115

Figure 3.6 Ornithine Lipid (OL) and glutamate lipid (QL) in *Sulfitobacter* sp. strains CB-A (orange) and CB-D (blue). Box & whisker plots highlight differences between strains and time, and between substrates. These plots are shown for all substrates for (A), (B), (C) ornithine lipid (OL) and (D), (E), (F) glutamine (QL) lipid. Significant differences are denoted by asterisks (* = p<0.1; ** = p<0.05; *** = p<0.01). Averages of biological replicates are reported for all treatments (n= 3 in SMM grown cells; n= 5 in glutamate and acetate grown cells). All data are normalized according to optical density. Structures of (G) ornithine lipid (OL) and (H) glutamine lipid (QL), with respective retention times. (I) OL and QL biosynthesis gene organization in *Sulfitobacter* sp. strains CB-D and CB-A. 116
Figure 3.7 Percentages of significantly different (A) metabolites and (B) lipids of SMM (dark gray), glutamate (light gray) and acetate grown cells (medium gray). 137
Figure 3.8 Lysine lipid (KL) in *Sulfitobacter* sp. strains CB-A (orange) and CB-D (blue). Box & whisker plots highlight differences between strains and time, and between substrates. These plots are shown for all substrates, (A) standard marine media (SMM), (B) glutamate, and (C) acetate.. 138
Figure 3.9 Pie charts display relative proportions of the sum of lipid intensities to total detected lipid intensities in *Sulfitobacter* sp. strains CB-D and CB-A for each timepoint and substrate.....139

Introduction

Nutrition and metabolism

“Eat your vegetables.” This is commonly told to children as a reminder that what you eat, or your nutrition, matters. An unhealthy diet leads to malnutrition, specifically either overnutrition or micronutrient deficiencies. Malnutrition increases the chances for cardiovascular disease as well as metabolic diseases such as Type 2 Diabetes and obesity.[1-2] In children and adolescents, dietary patterns have been correlated with mental health, specifically less healthy diets have been associated with less healthy mental states.[3] This has also been observed in adults, for example, Western diets including processed and fried foods and high sugar has been linked to depression in women, and certain dietary fats have been correlated with increased risk for depression for both men and women.[4-5] In addition to these metabolic and mental health effects, nutrition also has been correlated with both the gut microbiome and the immune system.[6-7] With these widespread impacts, the importance of proper nutrition is evident. Despite this, healthy diets are often unattainable making alternative means of reversing or preventing the negative effects of unhealthy diets necessary.

Two of the most common ways that are used to reverse the effects of an unhealthy diet are exercise and dietary supplements. Exercise can be effective and more economical. Additionally, exercise programs can be customized for individual lifestyles. Because of this, exercise is a popular method for preventing the effects of unhealthy diets. The underlying mechanism behind the benefits of exercise are not fully known, but a proposed mechanism is that exercise alters the gut microbiome, and thus influencing absorbed nutrients. However, exercise does not address the micronutrient deficiencies caused by western style diets. In contrast, dietary supplements play a more direct role in preventing and reversing micronutrient deficiencies. A variety of different supplements are available ranging from probiotics, herbal medicines, and vitamins. For example, researchers have investigated lycopene, which is naturally found in tomatoes, and vitamin D as potential diet-induced obesity treatments.[8-9] Vitamin D has also been found to have

hepato- and cardio-protective properties, while probiotics and polyphenols alter the gut microbiome.[10-12] Despite the wide range of dietary supplements available, research is still needed to determine if specific supplements are sufficient to reverse the effects of unhealthy diets, and the underlying mechanisms by which they provide benefits.

While it is well known that nutrition is important for human health, the significance of nutrition extends to all living organisms. At the most simplistic level, essential nutrients are molecules not produced by an organism, which can be used for energy metabolism via pathways such as the tricarboxylic acid (TCA) cycle or as molecular building blocks for proteins or lipids. Because of this, all living organisms have specific nutritional requirements which influences intracellular metabolism. Although, all living organisms have nutritional requirements, the essential nutrients vary by organisms. For example, plants can produce glucose via photosynthesis, but most bacteria and all animals cannot undergo photosynthesis, so exogenous glucose or another energy source is required. However, bacteria can adapt to its environment and the available nutrients. This can be significant as it can alter the structure and function of the cell, and potentially even how the cells interact with the surrounding environment. Due to this significance and the inherent connection between nutrition and metabolism, the effect of nutrients, or growth substrates, on metabolism warrants further study.

Overview of metabolomics

Metabolomics is the latest addition to the omics cascade, focusing on the detection of all small molecules, or metabolites, with a system. Whereas genomics, transcriptomics, and proteomics are indirect measurements of the phenotype, metabolomics is a direct measurement of the biochemical phenotype of a system. However, because of the indirect nature of genomics, transcriptomics, and proteomics, detected alterations do not always correlate to the phenotype.[13] In contrast, metabolites can be influenced by both intrinsic and extrinsic factors, making metabolomics a more functional analysis.[13-15] Because of this, the

metabolome has been described as a looking glass revealing insights to the physiological, developmental, and pathological state of a biological system.[14] This makes metabolomics useful for a wide variety of applications including pharmaceutical science, food science, microbiology, and human health.[15-17]

Metabolomics is not without its challenges, however. Two of the greatest challenges facing metabolomics is the high quantity and diversity of metabolites, both in structure and concentration.[14] Advances in analytical technology have helped to address these challenges. Ultra-high performance liquid chromatography high resolution mass spectrometry (UHPLC-HRMS) in particular has driven these technological advances in metabolomics. Benchtop orbitrap mass analyzers allow for quantitative high resolution analyses, while rapid scan times and efficient separations increase the sensitivity and throughput. The use of an ion pairing reagent with reversed phase separations further increases the sensitivity by reducing ion suppression from coeluting metabolites.[18] An additional advantage provided by orbitrap mass spectrometry is the full scan capabilities. Full scan analyses allow all ions within a select mass range to be detected. Resulting from this, metabolomics analyses can be untargeted meaning that all water-soluble metabolites can be detected in a single analysis.

Any overview of metabolomics would be remiss if lipidomics was not included in the discussion. Lipids are an often overlooked in metabolomics studies, however in recent years have been gaining attention for their significant biological changes and functions.[19-20] The accepted roles of lipids include energy storage, membranes, and signaling. As metabolites are the molecular building blocks of lipids, these amphiphilic compounds can be informative of metabolome changes. This is because the reaction rates for lipid pathways is slower than metabolic pathways. The rates of metabolic pathways can often provide difficulties to metabolomics studies, as metabolism must be stopped, but not altered for effective analyses. Combined with the biological roles of lipids, this makes lipidomics a valuable addition to metabolomics studies.

Outline of dissertation

With these advantages of metabolomics and the natural connection between metabolism and nutrition, metabolomics provides a significant advantage to increasing the understanding of nutrients and specific diets. In the following chapters, investigations of the effects of nutrients and diet in various conditions using metabolomics will be described. In the first chapter, a metabolomics approach was used to study the interaction between an unhealthy western style diet, short term voluntary exercise, and the gut microbiome. To do this, C57Bl/6J mice were used in an animal model system and serum and intestinal contents were analyzed for global metabolome changes. In the second chapter, the effect of an herbal supplement, specifically ground fenugreek seeds, was evaluated via metabolomics. For this research, the serum, liver, and intestinal contents were analyzed for metabolic alterations caused by high fat or western style diets and reversed by fenugreek supplementation. The third chapter describes research in which metabolomics and lipidomics were used to probe the host-phage interactions of an environmentally relevant bacteria when provided different nutrients. *Sulfitobacter* spp. CB-D and CB-A were grown with either a complex media or minimal media in which the only carbon substrate was either glutamate or acetate. From these cultures, the impact of nutrients on host-phage interactions were investigated throughout the growth curve.

Chapter 1 Western Diet and Short-Term Voluntary Exercise Induce Intestinal Metabolome Changes

A version of this chapter is expected to be a part of a future publication.

Proposed authors:

Katarina A. Jones, Allison J. Richard, Annadora J. Bruce-Keller, Jacqueline M. Stephens, Shawn R. Campagna

1.1 Abstract

High caloric diets, such as typical Western diets, disrupt the gut microbiome which leads to health problems, including obesity and the related comorbidities. Exercise is commonly assumed to be an effective method to prevent the negative effects of unhealthy diets. Although exercise is known to provide health benefits, the combined impact of unhealthy diets, exercise, and the gut microbiome is remains unclear. This study was designed to elucidate this interaction between diet, exercise, and the gut microbiome at the metabolite level. For this reason, untargeted metabolomics was performed on the serum and intestinal contents of male C57Bl/6J mice fed either Western diet (WD) or a low-fat control diet for the entire experiment and each with and without short term voluntary exercise. The experiment was performed in two time intervals, specifically 10 weeks and 18 weeks to evaluate the immediate and enduring effects of exercise, respectively. Partial least squares discriminant analysis revealed that diet leads to more clear separation between the metabolic profiles of either the serum or intestinal contents. Metabolites relating to methionine metabolism and bile acid biosynthesis were found to be significantly different between WD- and LFD-fed mice. While exercise had a minimal impact on the metabolic profiles of serum and jejunum, ileum, and colon contents of WD-fed mice, exercise did have a noticeable effect on the metabolic profiles of the cecum contents of WD-fed mice. However, no clear trend was observed in the metabolites driving these differences suggesting that exercise influences multiple metabolic pathways.

1.2 Introduction

The gut microbiome is important for human health and has been correlated with several adverse health outcomes.[21-26] With up to 100 trillion microorganisms residing in the average adult human intestines, the microbiome is complex and far more genetically diverse than the mammalian host.[23, 27-28] However, the microbiome can be altered by a variety of influences including exposure to environmental stressors such as heavy metals and pesticides, lifestyle and behavioral changes such as exercise and physical activity, and dietary changes.[22, 24, 26, 29-31] Some of these microbiome alterations result in gut dysbiosis, or a disrupted microbiome, which has been associated with human diseases.[23] Specifically, gut dysbiosis has been correlated with metabolic diseases including obesity, type 2 diabetes, and non-alcoholic fatty liver disease, and autoimmune diseases including type 1 diabetes, inflammatory bowel disease, and multiple sclerosis.[26, 29, 32] With the growing prevalence of obesity and its comorbidities, modulation of gut microbiota has been of interest for potential therapeutic options. Additionally, these same disorders are often linked to unhealthy diets, specifically diets such as a typical Western style diet, which is characterized by high fat and sucrose content.[33] With this association and because significant dietary changes are often unattainable, alternative means of providing resiliency to diet-induced gut dysbiosis is needed.

Exercise is commonly perceived as an option to counteract the negative effects of unhealthy diets. Exercise is documented to assist in preventing many of the same health conditions which are related to unhealthy diets, but the mechanisms of these beneficial effects are not well known.[34] A previous study has shown that voluntary exercise is able to induce beneficial changes in the gut microbiome of mice as well as reducing inflammation.[35] Other studies have demonstrated similar outcomes, specifically that exercise was able to alter the gut microbiome in both mice and humans.[29-30, 36-38] In addition to microbiome alterations, these studies have displayed beneficial effects of exercise on host health. However, the underlying mechanisms leading to these advantages, and

the interaction between diet, exercise, and the gut microbiome is still largely unknown.[35-36] This work sought to investigate the relationship between diet, exercise, and the gut microbiome, and specifically to determine if short term voluntary exercise is sufficient to provide metabolic resiliency to a Western style diet in C57Bl/6J mice.

The gut microbiome and the metabolome are closely related, each influencing the mammalian host health.[39] The microbiome interacts with the metabolome through multiple pathways. One common example is dietary fiber and complex carbohydrates, which human enzymes are incapable of digesting.[28] However, gut microbiota ferment these compounds to produce short chain fatty acids (SCFAs) such as acetate, propionate, and butyrate.[23-24, 28, 32] SCFAs have diverse functions, but are primarily associated with energy metabolism.[23-24, 28] Additionally, gut microbiota have been associated with other metabolites including the production of bile acids and choline, and digestion of polyphenols.[23, 39-40] From this it can be concluded that the gut microbiome aids in the absorption, digestion, metabolism, and excretion of a variety of bioactive compounds, often coming from dietary sources.[23] The significance of the microbiome is particularly evident in that when germ free mice were colonized with only a single bacterial species it was found to be sufficient for microbial metabolites to be detected in the bloodstream.[40] Because of the intertwined nature of the metabolome and microbiome, it is of great benefit to include metabolic profile analyses in gut microbiome research.

Untargeted metabolomics provides high throughput analysis of all metabolites within a biological system. This research utilized the advantages of high resolution mass spectrometry based metabolomics to investigate the interactions between diet, exercise, and the gut microbiome on a molecular level. Specifically, this work sought to determine alterations in intestinal and circulating metabolite profiles of C57Bl/6J mice provided either a low fat, or Western-style diet, and within each dietary group were both sedentary and physically active (exercise) mice. This research additionally evaluated the immediate versus lasting effects of exercise, via a 10 week long experiment and an 18 week long

experiment. From each of these experiments, both intestinal contents and serum samples were collected and analyzed via metabolomics. Insights gained from this study will contribute to the understanding of the underlying mechanisms from the interaction of diet, exercise, and the gut microbiome.

1.3 Results

1.3.1 Metabolic profiles display differences between intestinal regions and serum

This study utilized untargeted metabolomics to investigate the immediate and lasting impact of both a Western style diet (WD) and short-term voluntary exercise on the serum and intestinal metabolism of C57BL/6J mice. A total of 76 mice were initially divided into two groups and assigned either WD or a nutritionally matched low fat (LF) diet, then each of these dietary groups were divided and assigned to either an exercise (Ex) or sedentary (Sed) group. This process was completed for both a 10-week study and an 18-week study to evaluate the immediate and lasting effects, respectively, of short-term voluntary exercise with WD. The mice were separated into a total of eight experimental groups based on diet, activity level, and length of study (Table 1.1). Water soluble metabolites were extracted and analyzed from serum and intestinal content samples, which were collected at euthanasia, via ultra-high performance liquid chromatography coupled to high resolution mass spectrometry (UHPLC-HRMS). After the mass spectral analysis, known metabolites were identified by exact mass and retention time compared to an in-house standard library containing 279 small molecules. A total of 151 unique metabolites were identified from serum and contents from the jejunum, ileum, cecum, and colon of the mice used in this study. As anticipated, analysis of these identified metabolites across all samples reveals that the sample matrix (serum or intestinal contents from jejunum, ileum, or large intestine regions) has the greatest influence on the metabolic profiles regardless of diet, exercise level, or length of experiment (Fig 1.1).

Table 1.1 Summary of diets, activity group, and experimental duration assigned to mice used in this study.

Western diet and exercise metabolomics

No. of replicates	Diet	Activity group	Experimental duration
10	LF	Sed	10 weeks
10	LF	Sed	18 weeks
10	LF	Ex	10 weeks
9	LF	Ex	18 weeks
10	WD	Sed	10 weeks
9	WD	Sed	18 weeks
10	WD	Ex	10 weeks
8	WD	Ex	18 weeks

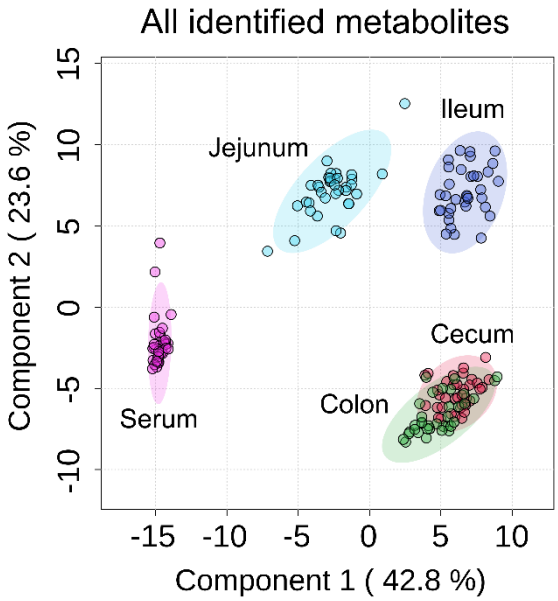


Figure 1.1 Partial least squares discriminant analysis (PLS-DA) of all identified metabolites according to sample matrix. This analysis displays distinct metabolic profiles for serum, jejunum, ileum, and large intestinal regions.

In addition to the identified metabolites, this study also investigated the effects of diet and exercise on the global metabolome, including unidentified spectral features. Interestingly, while there was almost no difference in the number of identified metabolites between the intestinal regions, there are vast differences in the number of unidentified features (Table 1.2). In the jejunum contents only 443 features were detected, while in the ileum, cecum, and colon contents there were 2959, 4503, and 2434 features detected, respectively. Only 245 features were detected in serum. These dramatic differences in the complexity of the metabolomes by matrix confirm the observation in the identified metabolites that the sample matrix has the most influence on the metabolic profiles. However, the alterations resulting from diet and exercise within each region are of greater interest to this study and will be reported in the following sections.

1.3.2 Western diet has greater influence on metabolomes than exercise

Metabolomics analysis detected a wide range of spectral features between intestinal regions and serum samples (Table 1.2). However, only a fraction of these features were identified as known metabolites with 65 metabolites identified from the 245 spectral features in serum. In the intestinal contents just over 140 metabolites were identified, but 443, 2959, 4503, and 2434 total features were detected the jejunum, ileum, cecum, and colon contents, respectively (Table 1.2). The analysis of both the total spectral features and the identified metabolites for each matrix (serum or intestinal contents) and region (jejunum, ileum, cecum, or colon) individually reveals that the most significant influence on the metabolomes is the diet. This can be seen in partial least squares discriminant analysis (PLS-DA) for the pairwise comparisons between WD versus LFD and exercise versus sedentary groups using the identified metabolites (Representative example is shown in Fig 1.2, see appendix Figs. 1.9-1.12 for other matrices). From the PLS-DA, metabolite variable importance in projection (VIP) scores are calculated and inform which metabolites are contributing most to the observed metabolic profiles.

Table 1.2 Summary of identified metabolites and unique spectral features from this study.

Short term voluntary exercise metabolomics					
	Serum	Jejunum	Ileum	Cecum	Colon
Total identified	**65**	**141**	**144**	**143**	**144**
Significantly altered by exercise (LF)	6	37	14	8	11
Significantly altered by exercise (WD)	1	3	6	9	11
Total unidentified	**245**	**443**	**2959**	**4503**	**2434**
Significantly altered by exercise (LF)	55	190	261	702	192
Significantly altered by exercise (WD)	6	7	232	205	212

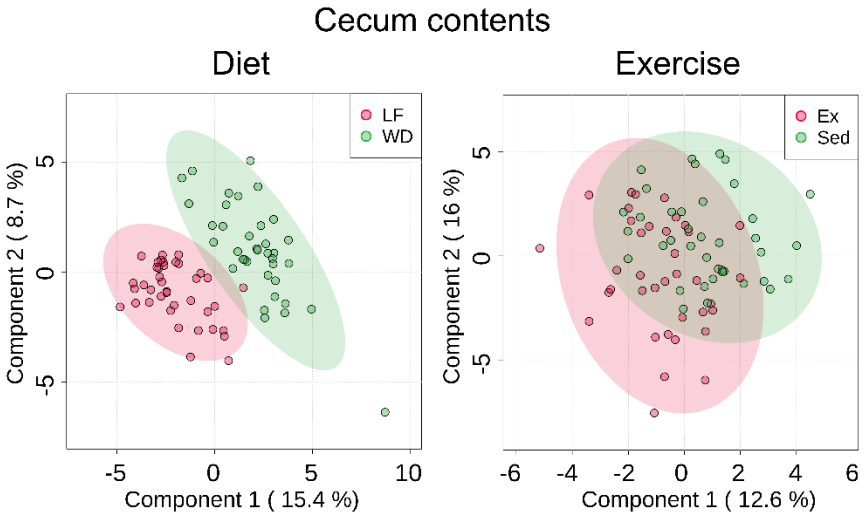


Figure 1.2 Pairwise PLS-DA analysis of cecum content metabolomics data. The left plot displays the pairwise comparison between low fat diet (LF) and Western diet (WD) groups, with only minimal overlap. The right plot shows much greater overlap between metabolic profiles of exercise (Ex) and sedentary (Sed) groups.

Using these VIP scores, it was determined that metabolites involved in cysteine and methionine metabolism as well as taurine metabolism are more significantly contributing to the differences (VIP>1) in the intestinal metabolic profiles of WD- and LF-fed mice. These pathways are related in that cysteate is a downstream product of methionine, but also is a precursor to taurine. Specifically, the detected metabolites involved in these pathways include, homocysteine, cystathionine, cysteine, cysteate, taurine, cholate, and taurodeoxycholate (Representative example shown in Fig 1.3. For other selected metabolites see appendix Figs. 1.13-1.20).

1.3.3 Immediate effects of exercise

In addition to the effects of WD, this study investigated both the immediate and enduring effects of exercise. For this experiment mice were kept in standard cages for 8 weeks, transferred to cages in which a subset of mice were allowed short term voluntary exercise. This study was designed to evaluate the immediate effects of short-term voluntary exercise on the metabolic profiles of mice fed an unhealthy WD. Metabolomics analysis determined that the majority of identified metabolites in the intestinal contents were detected in higher abundance in LF-fed mice than in WD-fed mice (Appendix Fig 1.20. PLS-DA analysis revealed no noticeable differences between the WD exercise and sedentary groups in any of the identified metabolites in the analyzed intestinal regions or serum (Appendix Figs 1.22 & 1.23). Analysis of the total detected, including unidentified, features reveal small differences between the WD exercise and sedentary groups, in the jejunum and cecum contents, but none in the ileum or colon contents (Fig 1.4). Alternatively, the same PLS-DA of identified metabolites display much greater separation between LFD exercise and sedentary groups in each of the intestinal content analyses (Appendix Figs 1.22 & 1.23). Although there are minimal global metabolome alterations due to exercise, there are immediate changes in certain metabolites. In particular, evaluation of metabolites which were determined to be

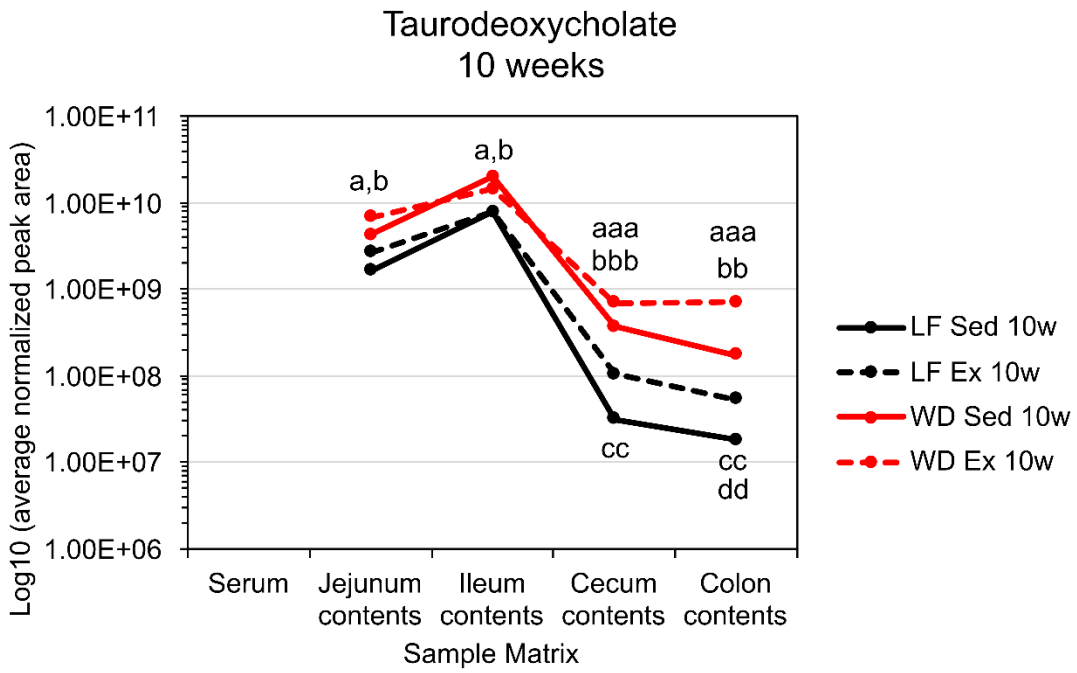


Figure 1.3 Average normalized peak area for taurodeoxycholate from the 10-week study. Data is shown for low fat (LF) fed sedentary (Sed) and exercise (Ex) mice, and Western diet (WD) fed Sed and Ex mice after 8 weeks of exposure to the assigned diet and 2 weeks of short-term voluntary exercise for a total of 10 weeks (10w). The data is shown on a $\log_{10}$ scale and p-values are indicated as follows: "a" is used for LF/WD comparison of Sed mice, "b" is used for LF/WD comparison of Ex mice, "c" is used for Ex/Sed comparison of LF mice, "d" is used for Ex/Sed comparison of WD mice. Significance levels are as follows: a, b, c, d = $p<0.1$; aa, bb, cc, dd = $p<0.05$; aaa, bbb, ccc, ddd = $p<0.01$.

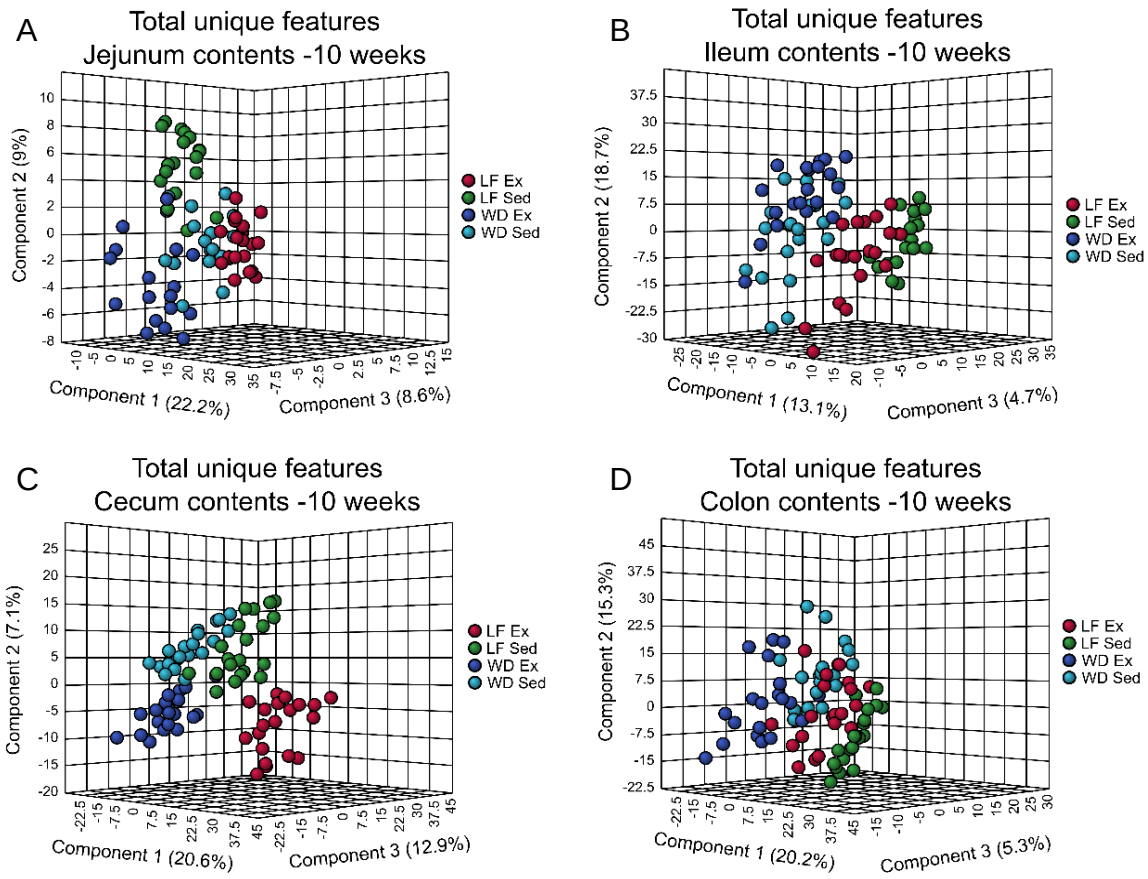


Figure 1.4 PLS-DA of total unique features detected from metabolomics analysis of (A) jejunum contents, (B) ileum contents, (C) cecum contents, and (D) colon contents of low fat (LF) and Western diet (WD) fed sedentary (Sed) and exercise (Ex) mice from the 10 week study.

When comparing the exercise to sedentary mice, in the jejunum contents, nearly all of these selected metabolites were detected in higher abundance in sedentary mice, regardless of diet (Fig 1.5A). However, in the colon contents, these same metabolites were detected in higher abundance in either LF- or WD-fed exercise mice, and in the ileum contents there were minimal differences in abundance (Fig 1.5A). Interestingly, the selected metabolites are also significantly higher in abundance in the cecum contents of exercise LF-fed mice compared to sedentary LF-fed mice, but this trend was not apparent in WD-fed mice (Fig 1.5A).

1.3.4 Enduring effects of exercise

To investigate the enduring effects of exercise, an 18-week study was performed. In this study, after 8 weeks in standard cages, a subset of mice were allowed short term voluntary exercise for 2 weeks and returned to the original cages for 8 weeks. Contrasting with the 10-week study, a greater percentage of identified metabolites in the intestinal contents were detected in higher abundance in the WD-fed mice relative to the LF-fed mice, in the 18-week study (Appendix Fig. 1.21). However, analysis of the identified metabolites from the intestinal contents displays minimal differences between exercise and sedentary groups, with the exception of the cecum contents (Fig. 1.6 & Appendix Fig. 1.24). Specifically, analysis of the identified metabolites within the cecum contents displays a greater difference between exercise and sedentary groups of WD-fed mice (Fig. 1.6). Evaluation of the enduring effects of exercise on the metabolites altered by WD illustrate minimal fold differences between exercise and sedentary mice for either diet (Fig. 1.5B). Despite the lack of obvious changes in the identified metabolites from the intestinal contents or serum, PLS-DA of the total detected features show greater separation (Fig. 1.7 & Appendix Fig. 1.25). In particular differences between exercise and sedentary groups of LF-fed mice in the serum metabolomes, and between exercise and sedentary groups of WD-fed mice in the large intestine (cecum and colon) metabolomes were more apparent (Fig 1.7).

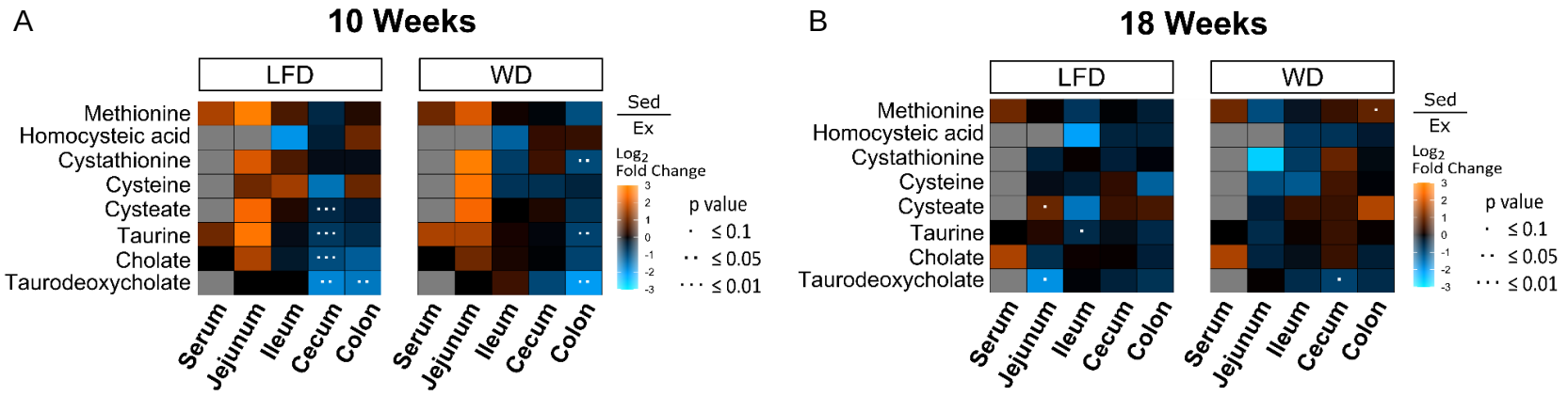


Figure 1.5 Heatmap analysis of select metabolites from (A) 10-week experiment and (B) 18-week experiment. Log base 2 fold changes of sedentary relative to exercise groups and significance determined by a Student's T test are shown. Results from low fat diet-fed mice are shown on the left, and Western diet-fed mice on the right. Orange indicates higher abundance in sedentary mice, and blue indicates higher abundance in exercise mice. Brightness indicates the magnitude of fold change.

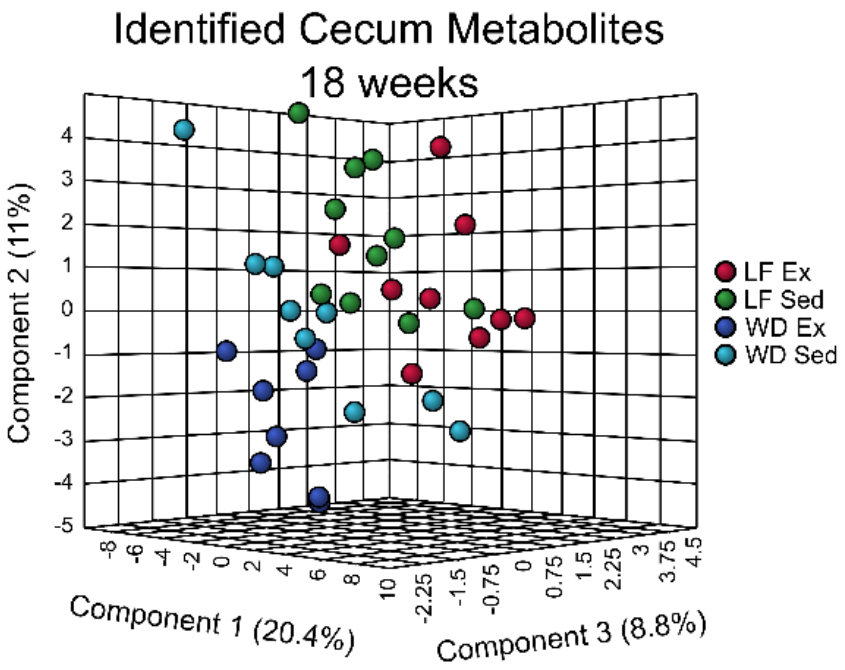


Figure 1.6 PLS-DA of total unique features detected from metabolomics analysis of (A) cecum contents, (B) colon contents, (C) serum of low fat (LF) and Western diet (WD) fed sedentary (Sed) and exercise (Ex) mice from the 18-week study.

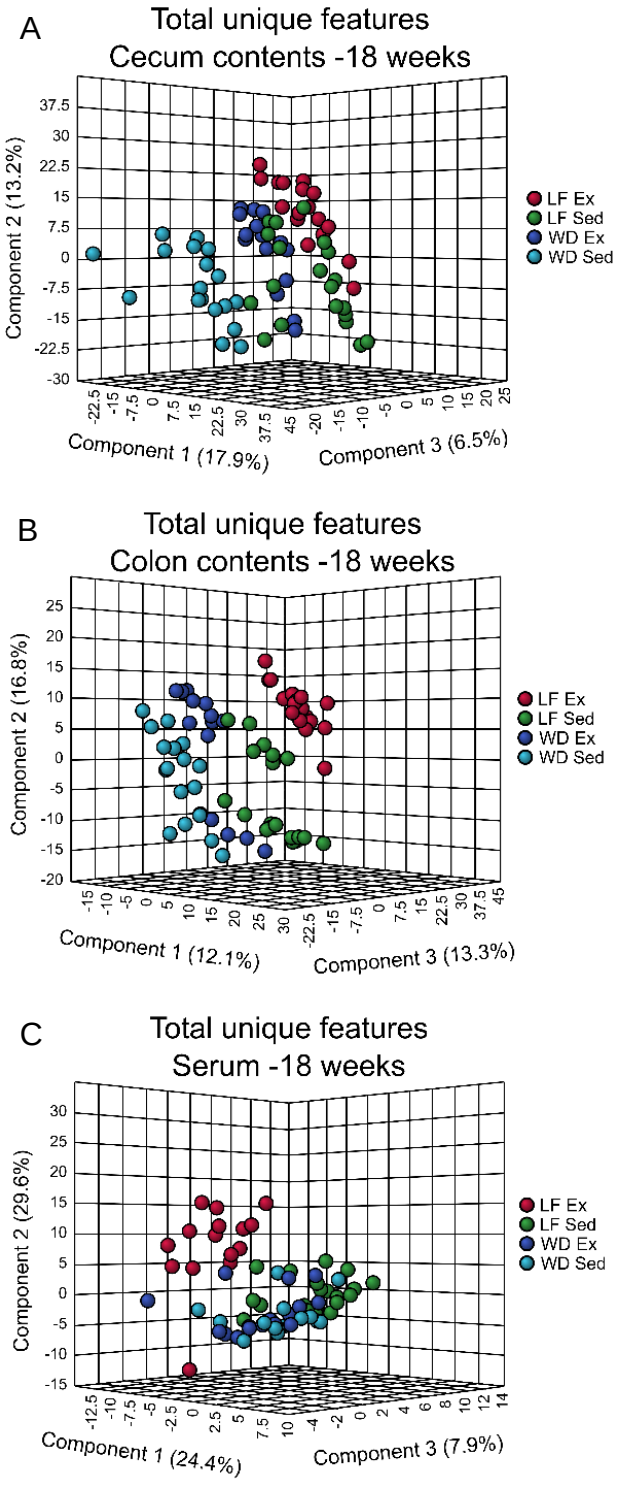


Figure 1.7 PLS-DA of total unique features detected from metabolomics analysis of (A) cecum contents, (B) colon contents, (C) serum of low fat (LF) and Western diet (WD) fed sedentary (Sed) and exercise (Ex) mice from the 18-week study.

1.4 Discussion

Standard Western style diets have been linked to several adverse health effects, resulting from the malnutrition of these diets.[33, 41] These health effects include, but are not limited to, gut dysbiosis and obesity. This is significant not only because of the prevalence of Western style diets and obesity, but also as the impact of gut dysbiosis on the mammalian host. The gut microbiome has been linked to the host's immune system, neurologic function, cardiovascular system, and metabolic health.[42-46] Often times, exercise is used to counteract the negative impact of an unhealthy diet, including gut dysbiosis, and obtain a healthier lifestyle. While exercise is documented to provide significant health benefits (i.e., gut microbiome alterations, body weight), the combined effect of unhealthy diets and exercise on the gut microbiome and the resulting effect on metabolism is understudied.[34, 36, 38, 47]

Metabolomics is a valuable addition to nutritional and exercise studies as it allows for both high throughput and high-resolution analyses at the small molecule level. Additionally, metabolites can be influenced by a variety of both internal and external factors. Using mass spectrometry based untargeted metabolomics analysis, all water-soluble small molecules, rather than limiting the analysis to known metabolites, can be directly measured, and analyzed. These factors make metabolomics a practical way to gain insights into the phenotype of a biological system. This research, utilizing the advantages offered by UHPLC-HRMS based metabolomics, was designed to evaluate the immediate and enduring effects of short-term voluntary exercise on the serum and intestinal metabolism of mice fed a Western style diet. By including serum in this study, insights were gained about the absorbed nutrients and circulating metabolite abundances.

Initial analysis of metabolomics results revealed that the sample matrix is most influential factor in shaping the metabolome. This is an anticipated result, as the intestinal regions and serum have diverse biological roles and functions. Additionally, the microbiota found within the intestines can vary by regions, which

alters the metabolome found in these matrices.[48] While this result can be clearly observed in the identified metabolites, it is also evident by the vast differences in the number of unique spectral features in each sample type. In particular, the greater number of features detected in the ileum, cecum, and colon contents suggests greater microbial diversity in these intestinal regions. However, the effects of diet and exercise profiles are the main focus of the remainder of this chapter.

1.4.1 Western diet alters metabolism of specific amino acids

In this research, diet was found to have a greater influence on the metabolome than exercise. This is particularly clear in the intestinal content metabolite profiles. Metabolites which were determined to significantly contribute to the distinctions between the profiles of mice fed WD and LF diet are involved in the metabolism of methionine. Typical Western diets include high intake of red meats and dairy products.[41] Methionine, which is an added component in the WD used in this study, is most abundantly found in red meats and dairy products.[49-50] Methionine is related to multiple biological processes, including glutathione metabolism and antioxidant activity, and the activated methyl cycle and DNA methylation.[51-52] These pathways are of interest as western diets lead to inflammation which can be a result of an imbalance of antioxidants.[53-54] Additionally, DNA methylation is linked to several health conditions including cancer, autoimmune disease, and metabolic disorders.[55] However, methionine metabolism is also linked to taurine biosynthesis, which can then be used to produce taurine conjugated bile acids.

In this study the metabolites which connect methionine and taurine metabolic pathways are significantly different between WD- and LF-fed mice. The intermediate metabolites include homocysteine, cystathionine, cysteine, and cysteate (Fig. 1.8), all of which have significant VIP scores in at least one intestinal region. Cysteate, which is significantly different in all four analyzed intestinal regions, is converted into taurine, which can then be conjugated to form the bile

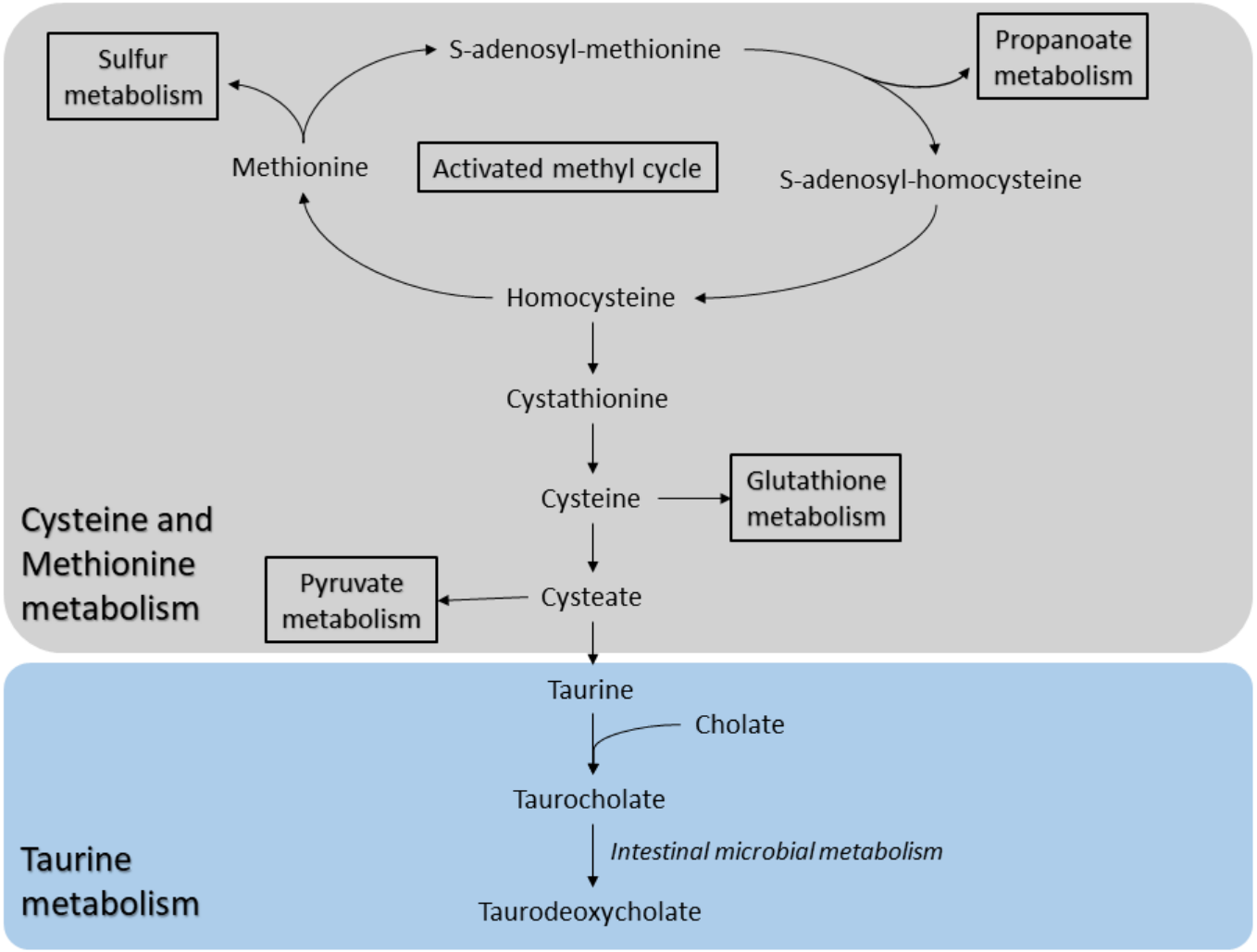


Figure 1.8 Cysteine and methionine metabolism and taurine metabolism pathways.

acid, taurodeoxycholate. Taurodeoxycholate is also significantly altered in all analyzed intestinal regions and is involved in regulating cholesterol levels. Cholesterol is found in the same dietary sources as methionine and is elevated in WD, thus making it unsurprising that taurodeoxycholate is significantly altered in WD-fed mice. This suggests that with high levels of both methionine and cholesterol in the WD used in this study, the production of bile acids is increased. As the primary biological function of bile acids is to assist in forming micelles and lipid absorption in the small intestines, an increase in bile acids may be an attempt to regulate cholesterol levels. As these metabolites are altered by WD, they were selected for further investigation of the impact of exercise on their relative abundances.

1.4.2 Exercise impacts metabolites most greatly altered by Western Diet

Metabolites involved in methionine and taurine pathways were investigated for both the immediate and lasting effects of exercise. Exercise can increase high density lipoprotein (HDL) levels, and thus was anticipated to alter cholesterol metabolism.[56] As methionine and taurine metabolic pathways are precursors to bile acids, and therefore cholesterol metabolism, it would be reasonable to expect that the metabolic pathways most significantly affected by WD may also be affected by exercise. These metabolites showed the greatest changes between WD-fed exercise and sedentary mice during the 10-week study as compared to the 18-week study (Figs 1.5 & 1.6). This implies that short term voluntary exercise has a greater immediate impact than enduring impact on these metabolites. Interestingly, these changes display opposite trends in the contents of the jejunum versus the colon, in which most of these metabolites were decreased with exercise in the jejunum contents but increased with exercise in the colon contents (Fig 1.5A).

Of these metabolites, taurodeoxycholate is of particular interest, as it is a bile salt, used to aid in the digestion and absorption of dietary lipids such as

triglycerides, cholesterol esters, and phospholipids. The increased levels of taurodeoxycholate in the large intestinal regions is intriguing as bile salts are secreted into the duodenum and jejunum and are reabsorbed into enterohepatic circulation from the ileum. Because of this, bile salts are typically high in concentration throughout the small intestines, but much lower in the large intestines as only a small fraction is excreted. However, in this study the abundance of taurodeoxycholate in the large intestines was increased with exercise relative to sedentary mice for both diets. A possible explanation for this is that with exercise, fewer dietary lipids can be digested into forms that can be absorbed in the small intestines. This would lead to reduced uptake and recycling of bile salts from the ileum, and thus higher concentrations in the large intestines. Additionally, with fewer bile salts being recycled, the liver would increase biosynthesis of bile acids which would reduce circulating cholesterol abundance as well.

However, beyond these specific metabolites, the global metabolic profiles resulting from short term voluntary exercise were evaluated. While there were minimal effects on the metabolomes of WD-fed mice resulting from short term voluntary exercise, greater effects were present in LF-fed mice. This suggest that short term voluntary exercise alone may not be sufficient to reverse the metabolic effects of WD, which could be linked to gut dysbiosis. In contrast to the intestinal content metabolic profiles, there were small, but noticeable differences in the serum profiles of exercise versus sedentary mice, in the 18-week study. This implies that while exercise has a more immediate effect on the intestinal metabolome, there is a more modest, but significant enduring effect on the circulating metabolite profiles. A possible explanation for these differences could be related to the gut microbiome, specifically that the microbial metabolism will reflect alterations as the composition of the microbiome is being changed. However, nutrients and other small molecules, which have been affected by microbial activity, are absorbed from the intestines into the bloodstream. Therefore, even small changes can be enhanced over time, which could explain

the observed differences in the serum metabolome of mice from the 18-week study.

1.4.3 Cecum contents are most greatly impacted by exercise

Although exercise induces only minimal global metabolome alterations in WD-fed mice in most analyzed sample matrices, significant alterations were found in the cecum contents. Within the analysis of identified metabolites, there was more clear separation between the WD-fed exercise and sedentary groups after 18 weeks than after 10 weeks. From the 18-week study, the metabolites with an average VIP score greater than two include a bile salt (taurodeoxycholate), a vitamin (ascorbate or vitamin C), a lipid biosynthesis precursor (phosphorylethanolamine) and two phosphorylated nucleosides (UMP and dTMP). The diversity of these metabolites which drive the separation between not only WD-fed exercise and sedentary groups, but also the groups from LF-fed mice, suggests that neither diet nor exercise effect only one pathway, but rather several metabolic pathways. As metabolic pathways are complex and intertwined, it is likely that these small changes across multiple metabolic pathways will have a significant impact on the mammalian host function.

The metabolic profile changes may have been minimal in the identified metabolite analysis of the cecal contents, but the global metabolome analysis of all detected features show clear distinctions between diet and exercise versus sedentary groups. This is particularly apparent in the PLS-DA of the total detected spectral features which includes thousands of unidentified features, at either 10 weeks or 18 weeks. Generally speaking, the large intestines contain a greater number or microorganisms, which could explain the large number of unique spectral features which are evident in the cecal contents in this study.[48] Although the identified metabolites show less separation between the groups, this can be easily explained in that many of the known primary metabolites are often conserved across different organisms, and thus less likely to reflect microbiome alterations. However, as metabolic profile differences are observed in both the

identified and global metabolome analyses of cecal contents in both 10- and 18-week studies, it was determined that short term voluntary exercise has a significant impact on cecal metabolism. While this impact was immediately apparent after exercise, the differences in metabolic profiles do not diminish in the 18 weeks study, indicating that exercise has both immediate and enduring effects on cecal metabolism.

1.5 Methods

1.5.1 Animals

Seventy-six male C57BL/6J mice were randomly divided between either Western style diet (WD) or a nutritionally matched low fat control diet (LF). The mice were purchased at 8 weeks of age (WOA) from Jackson Laboratories. Prior to starting the studies, the mice were randomized and divided into experimental groups. In addition to differing diets, the mice from each diet were divided into sedentary and exercise groups, and by length of study either 10 weeks or 18 weeks. This gave a total of eight experimental groups, for the 18-week study the groups were: 1) WD with exercise (WD-Ex, n=8), 2) WD with no exercise (WD-Sed, n=9), 3) LF diet with exercise (LF-Ex, n=9), 4) LF diet with no exercise (LF-Sed, n=10) (Table 1.1). The four experimental groups from the 10-week study were the same as in the 18-week study, and for each 10-week group n=10. The 10-week study began when the mice were 11 WOA and the 18-week study began when the mice were 9 WOA. For both studies the mice were exposed to the assigned diets for 8 weeks followed by 2 weeks with wheels, either upright for the exercise groups or on its side for the sedentary groups as an enrichment control for 2 weeks. After these 2 weeks of short-term voluntary exercise, the 10 weeks study mice were euthanized, but the 18-week study mice were transferred back to standard cages for 8 additional weeks of extended recovery prior to euthanasia. The mice were fed the respective diets throughout the entire study and cage changes. Serum and intestinal contents were collected at euthanasia for metabolomics. These studies

were conducted in strict accordance with the National Institutes of Health guidelines on the care and use of laboratory animals, and all experimental protocols were approved by the Institutional Animal Care and Use Committee at Pennington Biomedical Research Center.

1.5.2 Metabolomics sample preparations

Serum and intestinal content samples from the jejunum, ileum, cecum, and colon were weighed prior to sample preparation procedures. The pre-weighed samples were subjected to an acidic acetonitrile extraction, adapted from the protocol described by Rabinowitz and Kimball.[57] Using HPLC grade solvents, 1.3 mL of metabolomics extraction solvent (4:4:2 acetonitrile: methanol: water with 0.1 M formic acid) was added to the pre-weighed samples. The sample suspension was stored at -20 °C for 20 minutes prior to centrifugation. The supernatant was collected, and the pellet was re-extracted with 0.2 mL extraction solvent. The collected supernatants were dried under nitrogen and stored at -80 °C. Immediately before analysis, samples were thawed and resuspended in 300 µL water.

1.5.3 Liquid chromatography

Water soluble metabolites were analyzed utilizing ultra-high performance liquid chromatography coupled to high resolution mass spectrometry (UHPLC-HRMS). Resuspended samples were stored at 4°C in an UltiMate 3000 RS autosampler (Dionex, Sunnyvale, CA) until analysis. An injection volume of 10 µL was used and samples were analyzed in duplicate. Metabolites were chromatographically separated using a Synergi 2.6 µm Hydro RP column (100 mm x 2.1 mm, 100 Å; Phenomenex, Torrance, CA). The gradient was performed as follows: 0 to 5 min 0%B, 5 to 13 min 20% B, 13 to 15.5 min 55% B, 15.5 to 19 min 95% B, 19 to 25 min 0% B.[58] All solvents were HPLC grade and solvent A was 97:3 water: methanol with 15 mM acetic acid and 10 mM tributylamine as an ion pairing reagent. Solvent B was 100% methanol. Both the solvent flow rate (200 µL/min) and the

temperature of the column compartment (25 °C) were held constant throughout the analysis.

1.5.4 Mass Spectrometry

Following the reversed phase separations, the metabolites were introduced into the mass spectrometer (MS) via negative mode electrospray ionization (ESI). The ionization parameters were as following: spray voltage was set at 3 kV, nitrogen sheath gas was set at 10 arbitrary units, and capillary temperature was set at 320°C. The mass analysis was performed in full scan mode on an Exactive Plus Orbitrap MS (Thermo Scientific, San Jose, CA). The automatic gain control (AGC) target was set to 3e6 and resolution set at 140,000. The scan range was set at 85 to 800 *m/z* for 0 to 9 min and at 100 to 1000 *m/z* from 9 to 25 minutes.[58]

1.5.5 Data processing

Mass spectral data files were converted from .raw file generated by Thermo's Xcalibur software to .mzML files. This conversion was performed using msConvert, an open source software package from ProteoWizard.[59] These converted files were uploaded to Metabolomic Analysis and Visualization Engine (MAVEN), and metabolites were identified by comparison of exact mass (±5 ppm) and retention time to an in-house spectral database.[60-61] The chromatographic peaks were integrated and the area under the curve for each metabolite was exported for further analysis. For global metabolome analysis, the R packages XCMS and CAMERA were used to automatically detect and integrate all unique spectral features and annotate isotope and adduct peaks.[62-64] All isotope and adduct annotated features were removed before further analysis. Additionally, only features with a signal to blank ratio of equal to or greater than 3 in at least half of the biological replicates in at least one condition were used for the remainder of the study and are reported here.

1.5.6 Statistical analysis

Peak areas were background subtracted and normalized according to mass. Fold changes and p-values calculated by a Student's T-test were calculated in excel, and visualized on a $\log_2$ scale in heatmaps prepared using R (version 4.0.3).[64] Partial least squares discriminant analyses (PLS-DA) were performed using MetaboAnalyst 5.0 online.[65-66] Prior to PLS-DA, normalized data was preprocessed using interquartile range (IQR) filtering, log transformed, and Pareto scaled using the MetaboAnalyst 5.0 software. Cross validation of PLS-DA was performed using the leave one out (LOOCV) method in the same software.[66]

1.6 Conclusions

In conclusion, this study used an untargeted metabolomics approach to analyze the intestinal and circulating metabolite profiles of mice to evaluate the combined effects of diet, exercise, and the gut microbiome. Specifically, the metabolome was analyzed from the serum, and the contents from each of the jejunum, ileum, cecum, and colon of exercise and sedentary mice fed either a WD or LFD both immediately after exercise and after an extended recovery period following exercise. There are a few limitations to this study, particularly that only male mice were used and that only water-soluble metabolites were analyzed, which excludes lipids. Additionally, serum samples were small volumes, which may contribute to more metabolites at a concentration less that the limit of detection for these analyses. From these studies it was determined that diet has a more significant influence on the metabolic profiles of the mice, however exercise has small but significant impact on the metabolites in a diet-dependent manner. Additionally, this research revealed that exercise has the greatest impact on cecal metabolism. This work contributes to the existing literature investigating the interaction between diet, exercise, and the gut microbiome by monitoring the metabolic changes resulting from these interactions.

Appendix

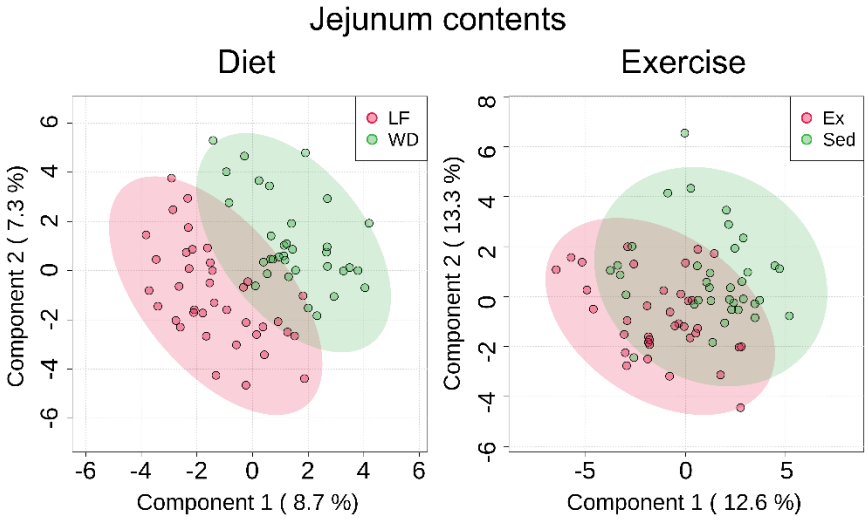


Figure 1.9 Pairwise PLS-DA of jejunum contents. The left plot is a comparison of low-fat diet (LF) versus Western diet (WD) groups. The right plot is a comparison of exercise (Ex) versus sedentary (Sed) groups.

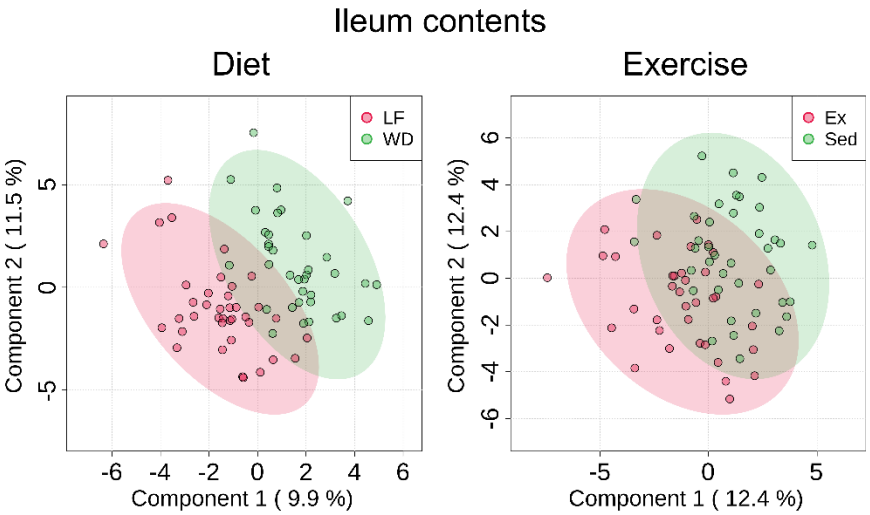


Figure 1.10 Pairwise PLS-DA of ileum contents. The left plot is a comparison of low-fat diet (LF) versus Western diet (WD) groups. The right plot is a comparison of exercise (Ex) versus sedentary (Sed) groups.

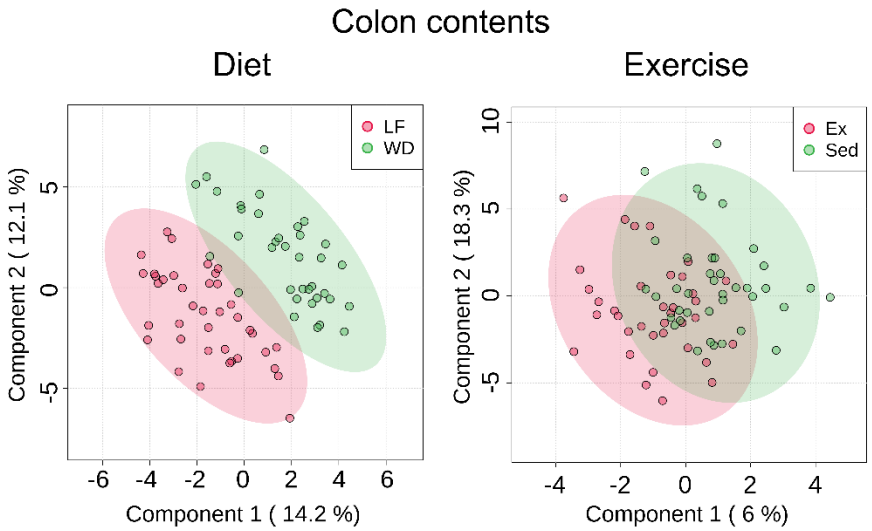


Figure 1.11 Pairwise PLS-DA of colon contents. The left plot is a comparison of low-fat diet (LF) versus Western diet (WD) groups. The right plot is a comparison of exercise (Ex) versus sedentary (Sed) groups.

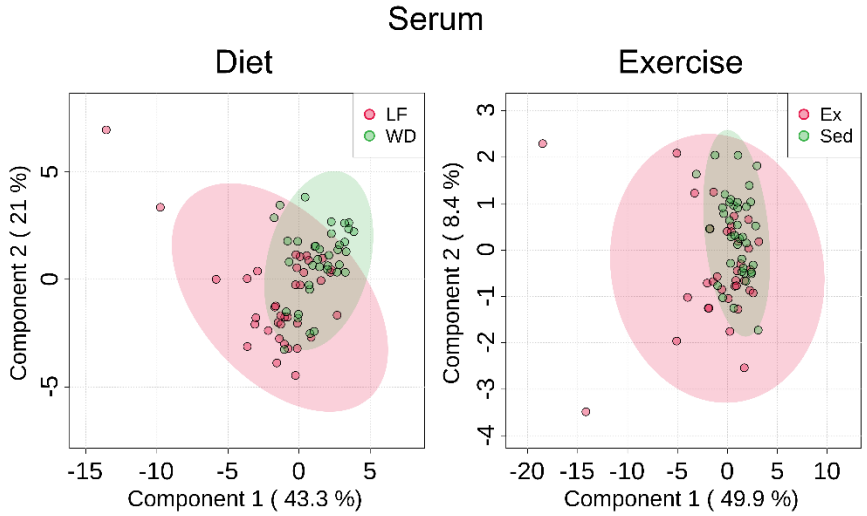


Figure 1.12 Pairwise PLS-DA of serum metabolomics. The left plot is a comparison of low-fat diet (LF) versus Western diet (WD) groups. The right plot is a comparison of exercise (Ex) versus sedentary (Sed) groups.

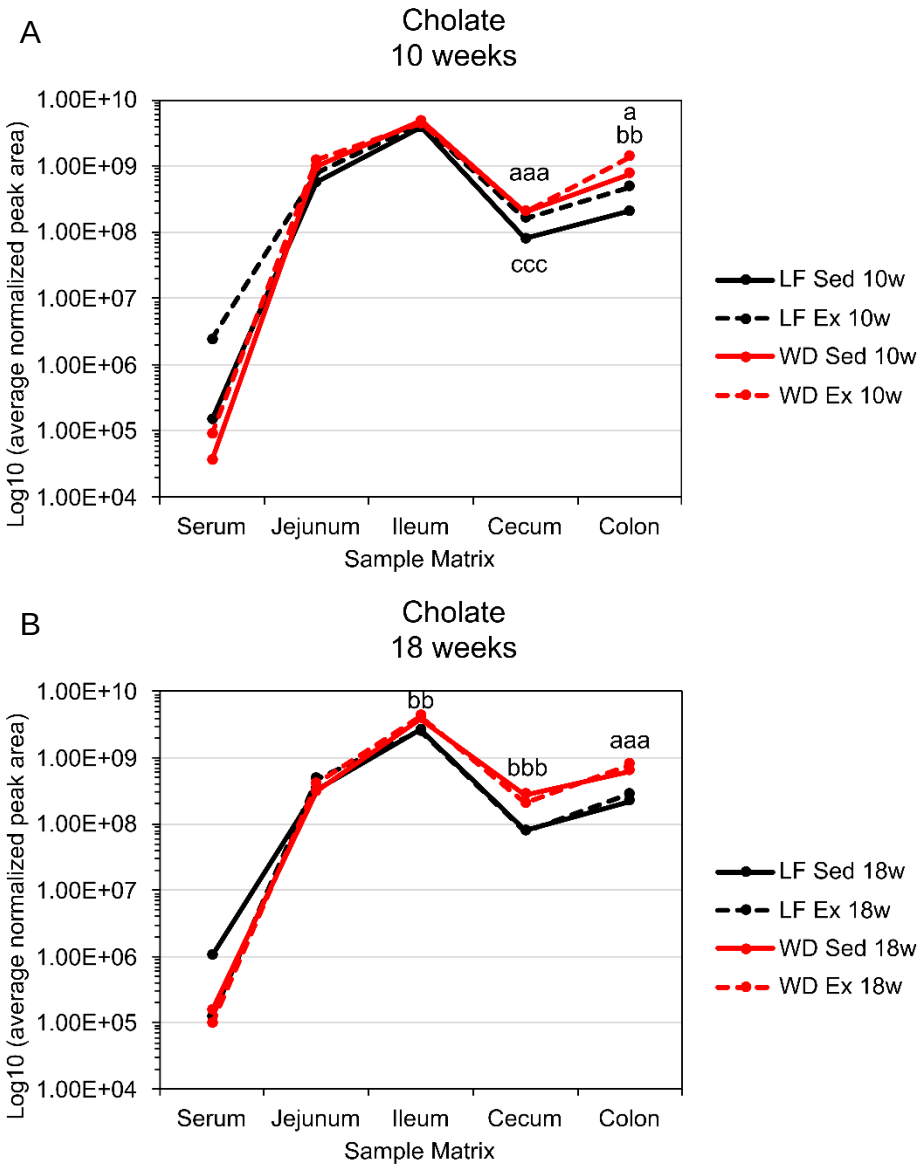


Figure 1.13 Average normalized peak area for cholate from the (A) 10-week study and (B) 18-week study. Data is shown for low fat (LF) fed sedentary (Sed) and exercise (Ex) mice, and Western diet (WD) fed Sed and Ex mice. The data is shown on a $\log_{10}$ scale and p-values are indicated as follows: "a" is used for LF/WD comparison of Sed mice, "b" is used for LF/WD comparison of Ex mice, "c" is used for Ex/Sed comparison of LF mice, "d" is used for Ex/Sed comparison of WD mice. Significance levels are as follows: a, b, c, d = $p<0.1$; aa, bb, cc, dd = $p<0.05$; aaa, bbb, ccc, ddd = $p<0.01$.

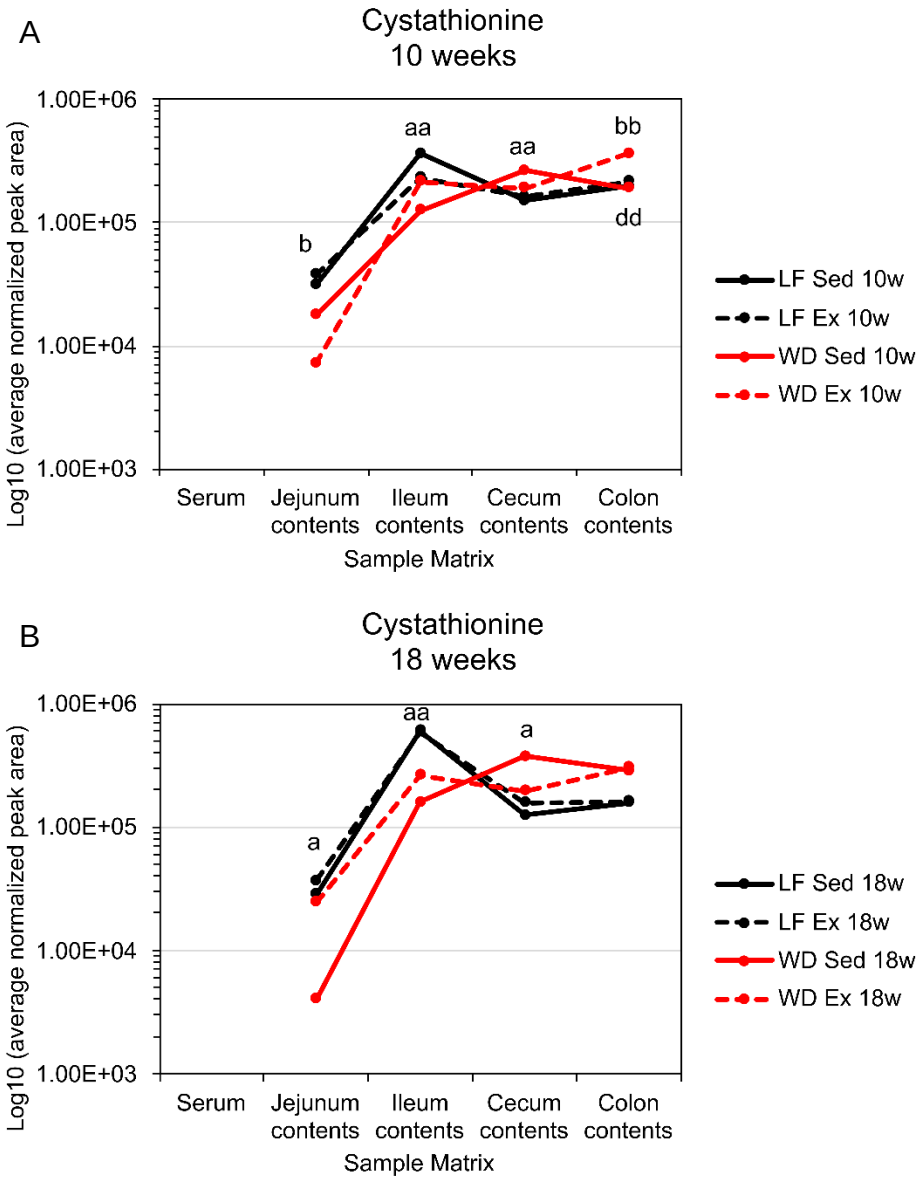


Figure 1.14 Average normalized peak area for cystathionine from the (A) 10-week study and (B) 18-week study. Data is shown for low fat (LF) fed sedentary (Sed) and exercise (Ex) mice, and Western diet (WD) fed Sed and Ex mice. The data is shown on a $\log_{10}$ scale and p-values are indicated as follows: "a" is used for LF/WD comparison of Sed mice, "b" is used for LF/WD comparison of Ex mice, "c" is used for Ex/Sed comparison of LF mice, "d" is used for Ex/Sed comparison of WD mice. Significance levels are as follows: a, b, c, d = $p<0.1$; aa, bb, cc, dd = $p<0.05$; aaa, bbb, ccc, ddd = $p<0.01$.

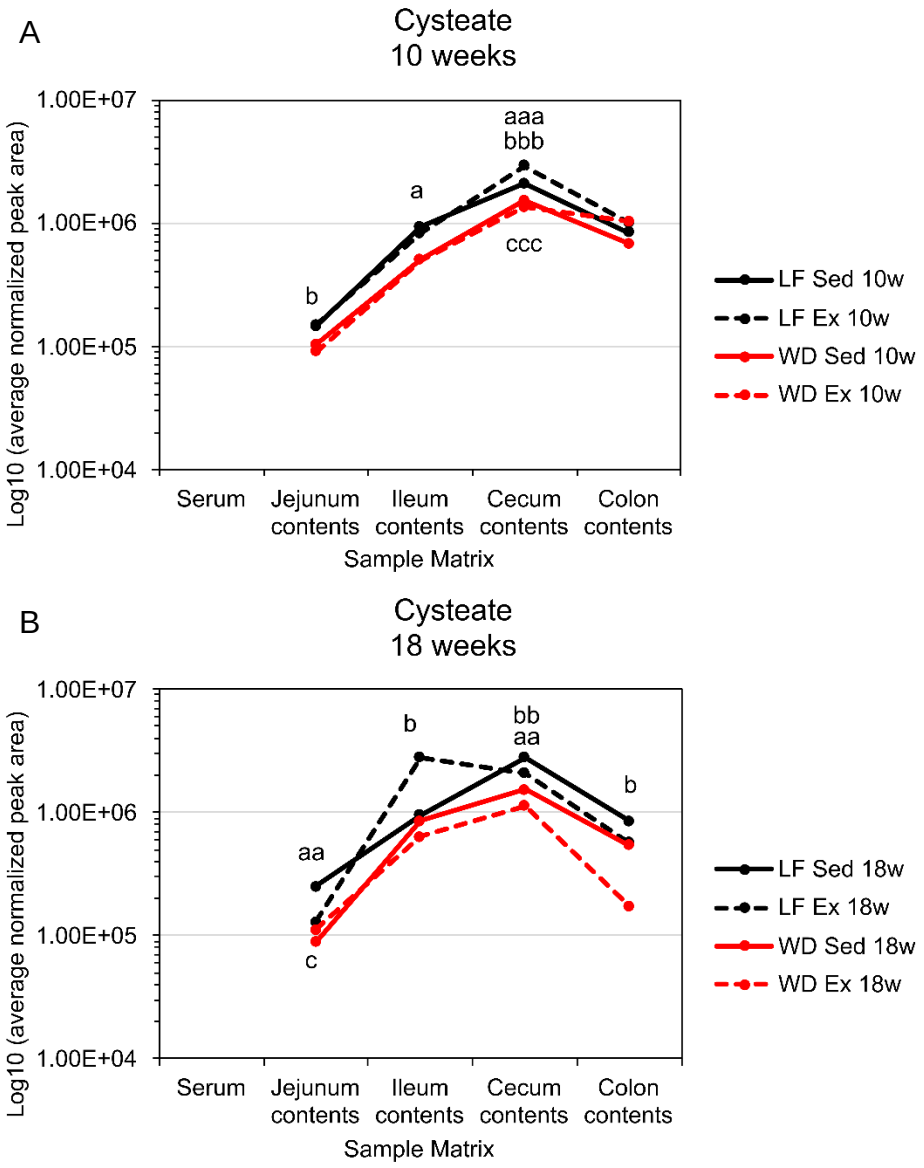


Figure 1.15 Average normalized peak area for cysteate from the (A) 10-week study and (B) 18-week study. Data is shown for low fat (LF) fed sedentary (Sed) and exercise (Ex) mice, and Western diet (WD) fed Sed and Ex mice. The data is shown on a $\log_{10}$ scale and p-values are indicated as follows: "a" is used for LF/WD comparison of Sed mice, "b" is used for LF/WD comparison of Ex mice, "c" is used for Ex/Sed comparison of LF mice, "d" is used for Ex/Sed comparison of WD mice. Significance levels are as follows: a, b, c, d = $p<0.1$; aa, bb, cc, dd = $p<0.05$; aaa, bbb, ccc, ddd = $p<0.01$.

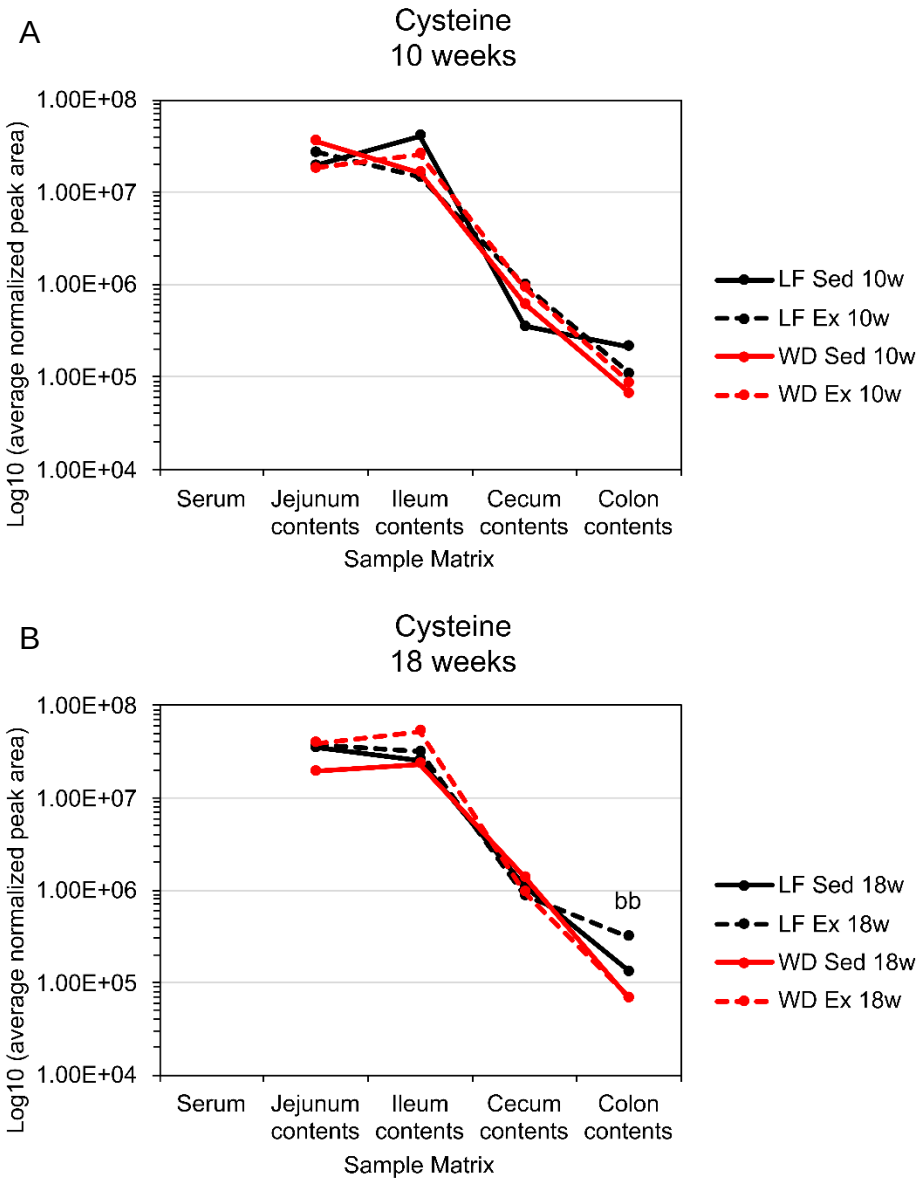


Figure 1.16 Average normalized peak area for cysteine from the (A) 10-week study and (B) 18-week study. Data is shown for low fat (LF) fed sedentary (Sed) and exercise (Ex) mice, and Western diet (WD) fed Sed and Ex mice. The data is shown on a $\log_{10}$ scale and p-values are indicated as follows: "a" is used for LF/WD comparison of Sed mice, "b" is used for LF/WD comparison of Ex mice, "c" is used for Ex/Sed comparison of LF mice, "d" is used for Ex/Sed comparison of WD mice. Significance levels are as follows: a, b, c, d = $p<0.1$; aa, bb, cc, dd = $p<0.05$; aaa, bbb, ccc, ddd = $p<0.01$.

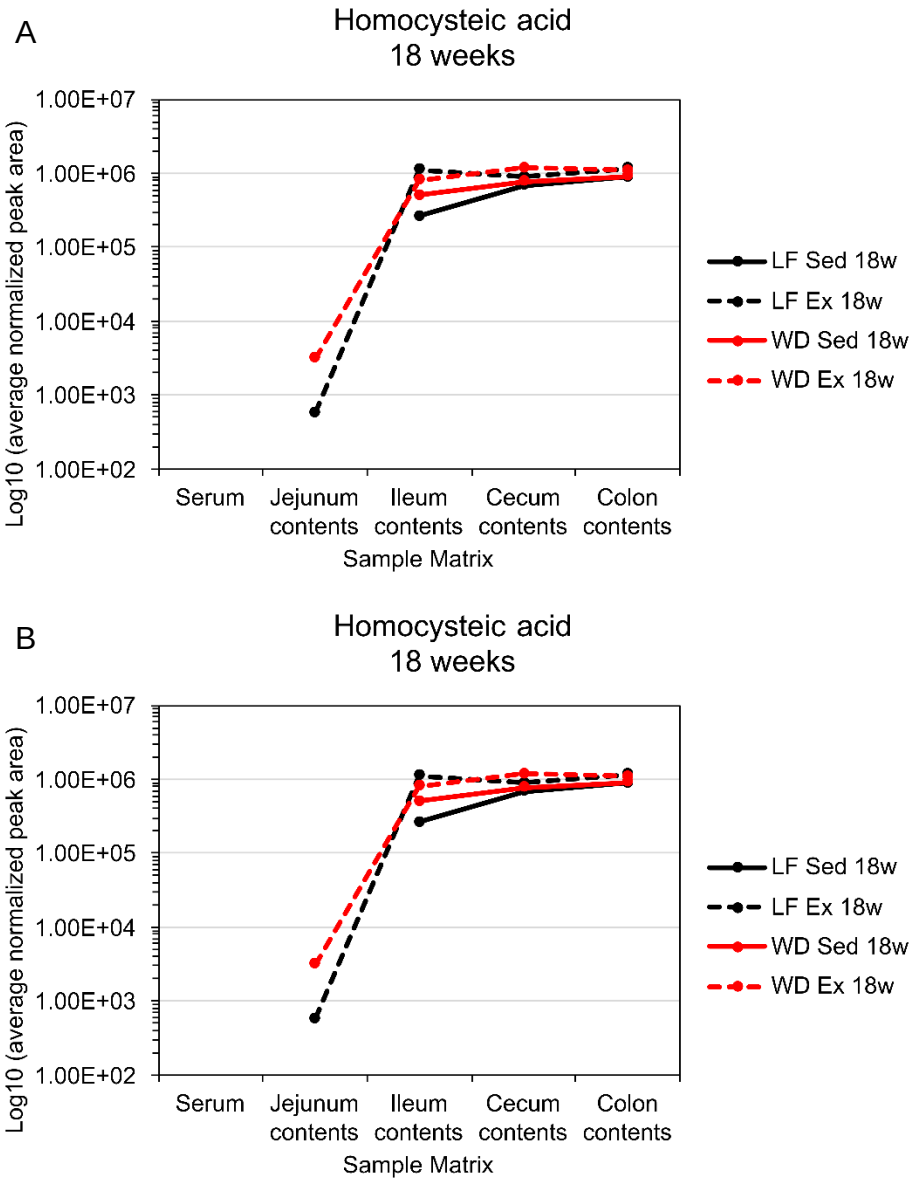


Figure 1.17 Average normalized peak area for homocysteic acid from the (A) 10-week study and (B) 18-week study. Data is shown for low fat (LF) fed sedentary (Sed) and exercise (Ex) mice, and Western diet (WD) fed Sed and Ex mice. The data is shown on a $\log_{10}$ scale and p-values are indicated as follows: "a" is used for LF/WD comparison of Sed mice, "b" is used for LF/WD comparison of Ex mice, "c" is used for Ex/Sed comparison of LF mice, "d" is used for Ex/Sed comparison of WD mice. Significance levels are as follows: a, b, c, d = $p<0.1$; aa, bb, cc, dd = $p<0.05$; aaa, bbb, ccc, ddd = $p<0.01$.

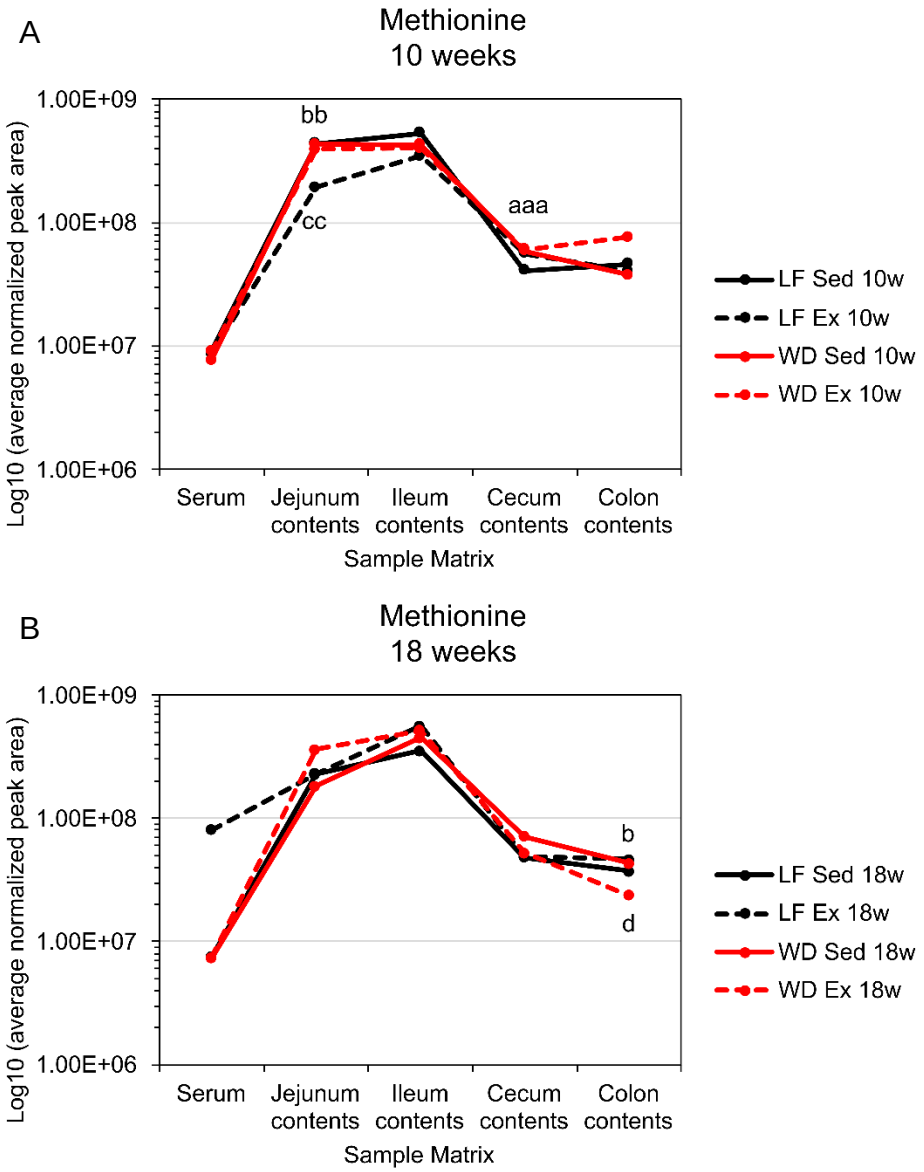


Figure 1.18 Average normalized peak area for methionine from the (A) 10-week study and (B) 18-week study. Data is shown for low fat (LF) fed sedentary (Sed) and exercise (Ex) mice, and Western diet (WD) fed Sed and Ex mice. The data is shown on a $\log_{10}$ scale and p-values are indicated as follows: "a" is used for LF/WD comparison of Sed mice, "b" is used for LF/WD comparison of Ex mice, "c" is used for Ex/Sed comparison of LF mice, "d" is used for Ex/Sed comparison of WD mice. Significance levels are as follows: a, b, c, d = $p<0.1$; aa, bb, cc, dd = $p<0.05$; aaa, bbb, ccc, ddd = $p<0.01$.

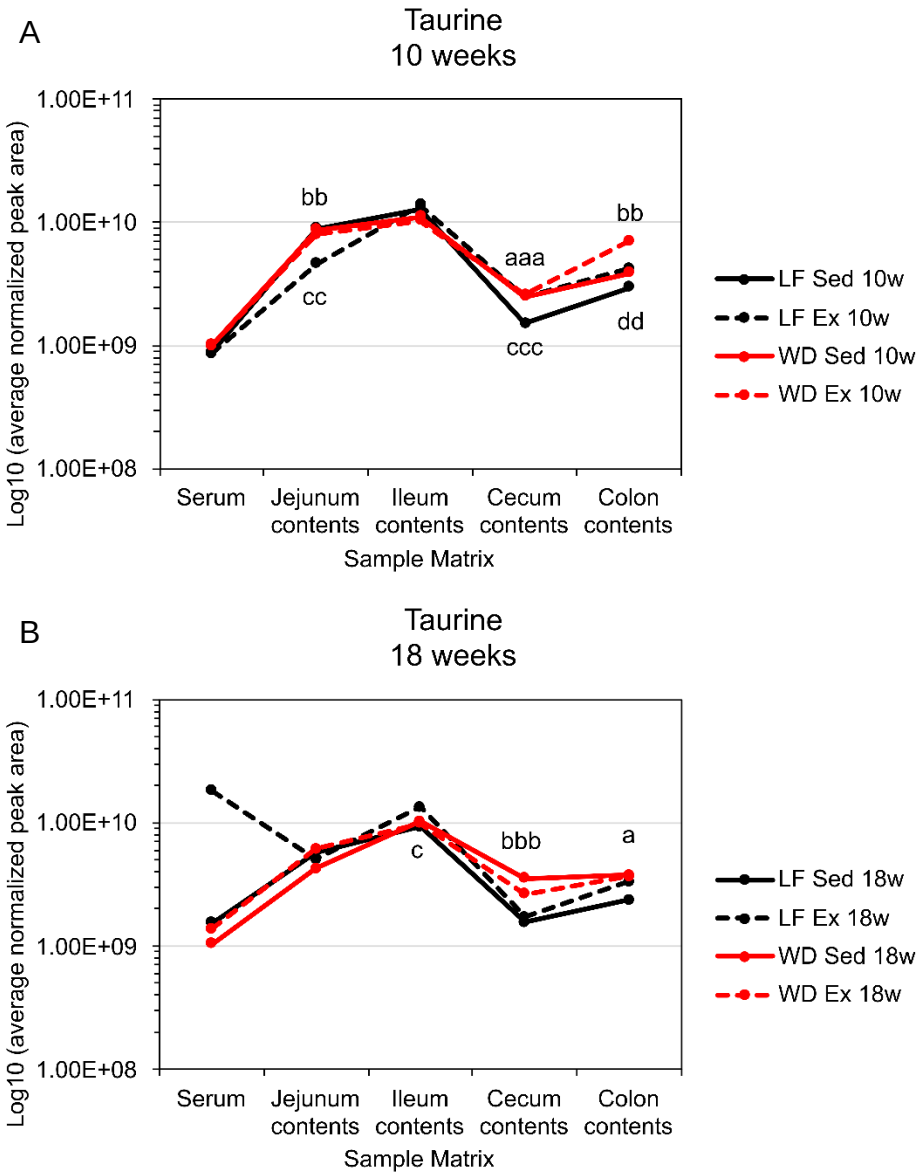


Figure 1.19 Average normalized peak area for taurine from the (A) 10-week study and (B) 18-week study. Data is shown for low fat (LF) fed sedentary (Sed) and exercise (Ex) mice, and Western diet (WD) fed Sed and Ex mice. The data is shown on a $\log_{10}$ scale and p-values are indicated as follows: "a" is used for LF/WD comparison of Sed mice, "b" is used for LF/WD comparison of Ex mice, "c" is used for Ex/Sed comparison of LF mice, "d" is used for Ex/Sed comparison of WD mice. Significance levels are as follows: a, b, c, d = $p<0.1$; aa, bb, cc, dd = $p<0.05$; aaa, bbb, ccc, ddd = $p<0.01$.

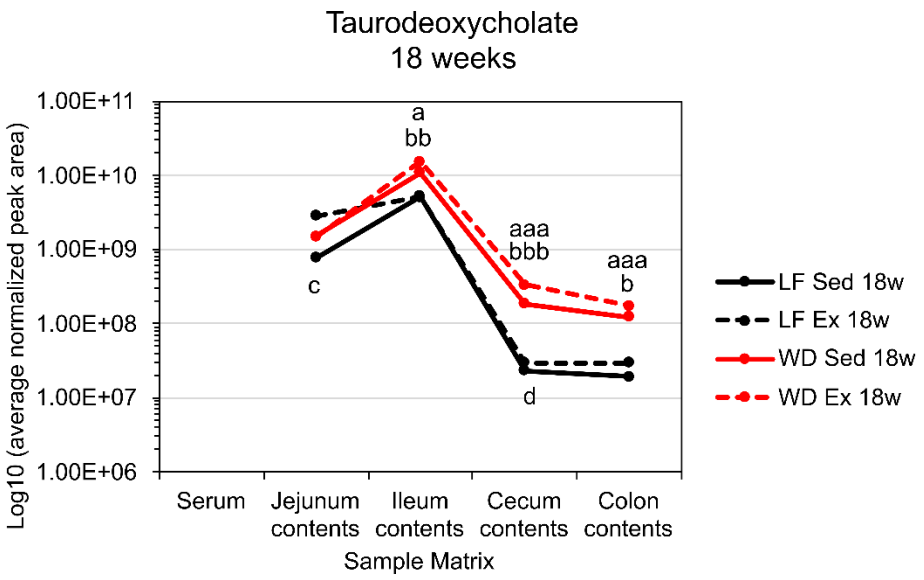


Figure 1.20 Average normalized peak area for taurodeoxycholate from the 18-week study. Data is shown for low fat (LF) fed sedentary (Sed) and exercise (Ex) mice, and Western diet (WD) fed Sed and Ex mice. The data is shown on a $\log_{10}$ scale and p-values are indicated as follows: "a" is used for LF/WD comparison of Sed mice, "b" is used for LF/WD comparison of Ex mice, "c" is used for Ex/Sed comparison of LF mice, "d" is used for Ex/Sed comparison of WD mice. Significance levels are as follows: a, b, c, d = $p<0.1$; aa, bb, cc, dd = $p<0.05$; aaa, bbb, ccc, ddd = $p<0.01$.

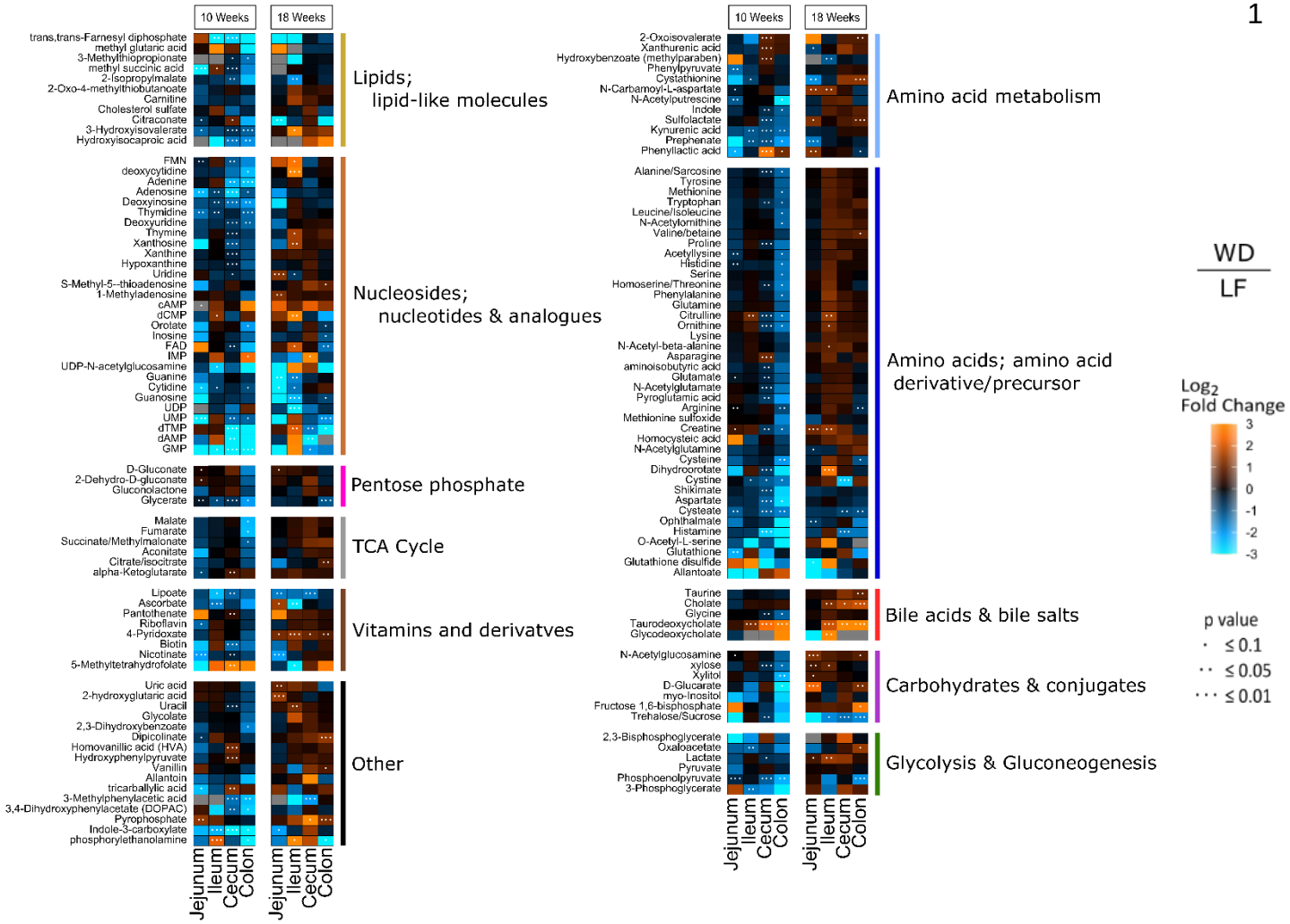


Figure 1.21 Heatmap visualization comparing WD-fed to LF-fed mice. Metabolomics data from the 10-week study is shown on the left, and 18-week study on the right. Log base 2 fold changes are shown, and significance indicated.

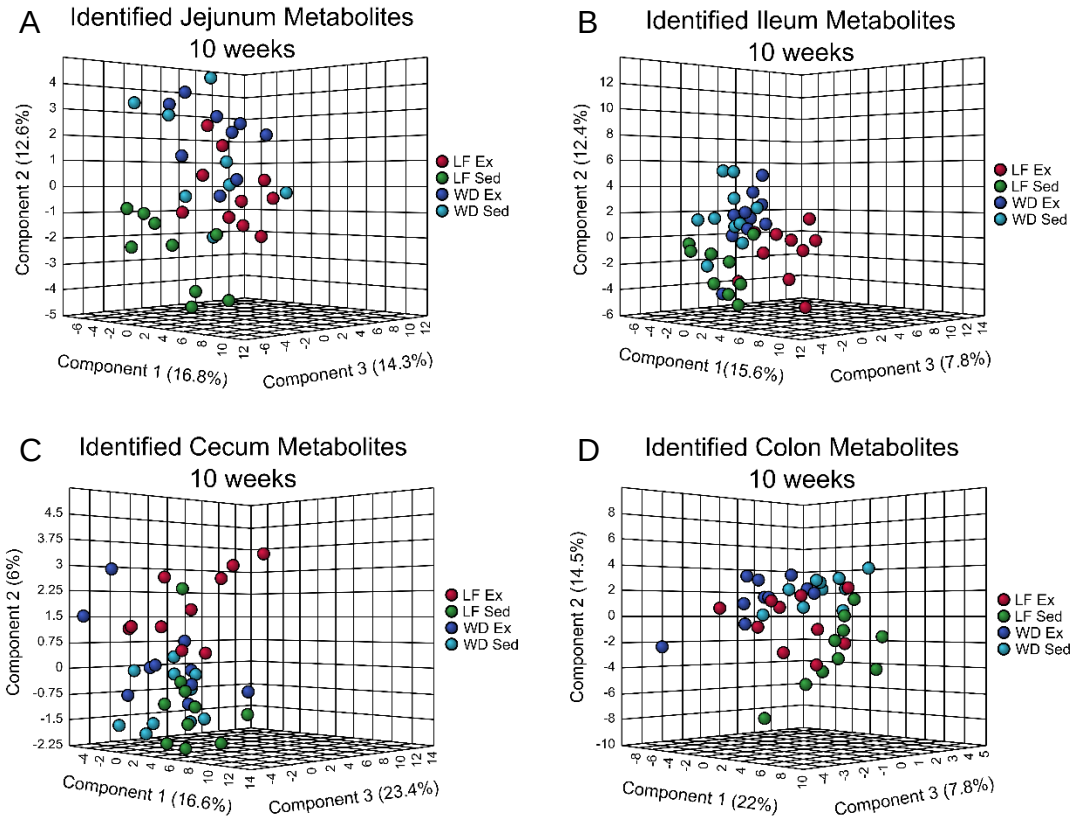


Figure 1.22 PLS-DA of identified metabolites detected from metabolomics analysis of (A) jejunum contents, (B) ileum contents, (C) cecum contents, and (D) colon contents of low fat (LF) and Western diet (WD) fed sedentary (Sed) and exercise (Ex) mice from the 10 week study.

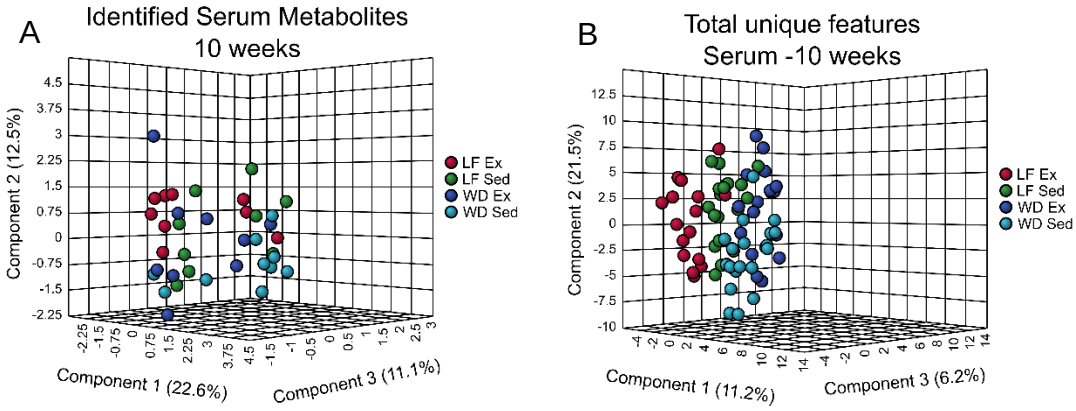


Figure 1.23 PLS-DA of (A) identified metabolites and (B) total unique features detected from metabolomics analysis of serum of low fat (LF) and Western diet (WD) fed sedentary (Sed) and exercise (Ex) mice from the 10-week study.

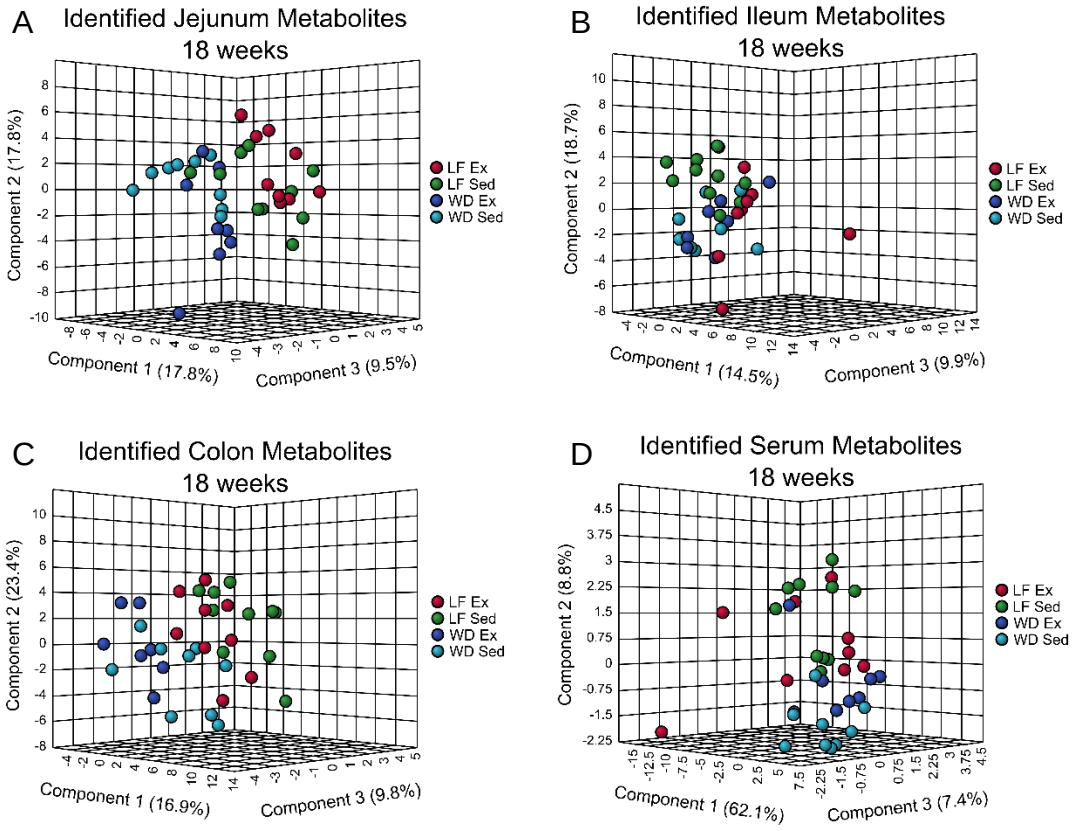


Figure 1.24 PLS-DA of identified metabolites detected from metabolomics analysis of (A) jejunum contents, (B) ileum contents, (C) colon contents, and (D) serum of low fat (LF) and Western diet (WD) fed sedentary (Sed) and exercise (Ex) mice from the 18 week study.

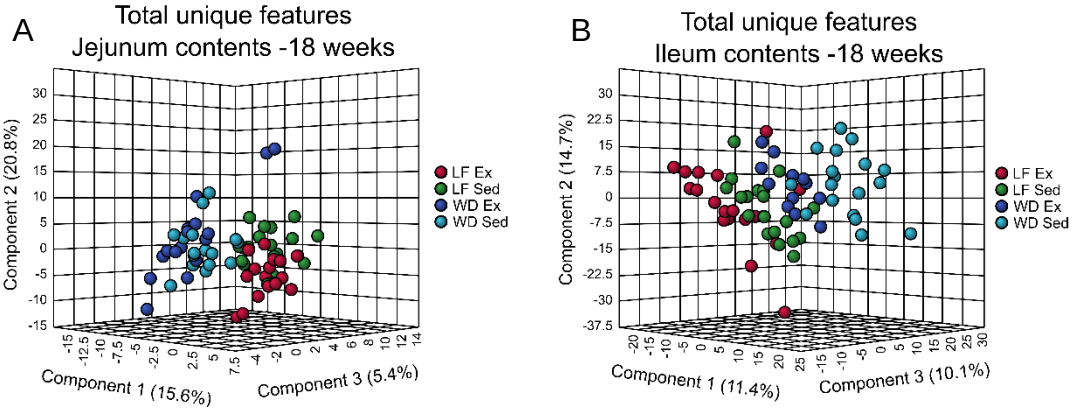


Figure 1.25 PLS-DA of total unique features detected from metabolomics analysis of (A) jejunum contents and (B) ileum contents of low fat (LF) and Western diet (WD) fed sedentary (Sed) and exercise (Ex) mice from the 18-week study.

Chapter 2 Fenugreek Supplementation to High Fat and Western Diets Significantly Alters Liver and Intestinal Metabolome

A version of this chapter will be a part of a future publication titled:

Cross-omics Analysis of Fenugreek Supplementation Reveals Beneficial Effects are Caused by Gut Microbiome Changes Not Mammalian Host Physiology

Proposed authors:

Katarina A. Jones, Allison J. Richard, Annadora J. Bruce-Keller, Jacqueline M. Stephens, Shawn R. Campagna

Author contributions

KAJ performed metabolomics experiments, processed, and analyzed the data, and wrote the manuscript. AJR and JMS helped write and edit the manuscript. ABK and SRC designed the experiment. SRC assisted in editing the manuscript.

2.1 Abstract

Herbal remedies and plant materials are increasing in popularity as potential treatments for metabolic conditions such as obesity and Type 2 Diabetes. One potential therapeutic option is fenugreek seeds (*Trigonella foenum-graecum*), which have been used for treating high cholesterol and Type 2 diabetes. A possible mechanism for these benefits is through alterations in the microbiome that can impact mammalian host metabolic function. This study used untargeted metabolomics to investigate the fenugreek-induced alterations in the intestinal, liver, and serum small molecules of male C57BL/6J mice fed either a 60% high fat, western style diet, or nutritionally matched low fat control diets each with or without fenugreek supplementation (2% w/w) for 14 weeks. Metabolomics analyses were performed on the contents of the jejunum, ileum, cecum, and colon, as well as liver and serum samples. Partial least squares discriminant analysis (PLS-DA) reveals that the supplementation of very high fat diet or western diet with ground fenugreek seeds induces substantial changes in the metabolome of the large intestines, as compared to the small intestines and liver. However, it was also observed that while the magnitude of changes was less, significant modifications were present

in the liver tissues resulting from fenugreek supplementation. Further analyses reveal the pathways affected by fenugreek and indicate that rather than only impacting one single pathway, fenugreek supplementation affects multiple pathways, including carnitine biosynthesis, cholesterol and bile acid metabolism, and the arginine biosynthesis pathways that may play important roles in the beneficial effects of fenugreek.

2.2 Introduction

Obesity is a global epidemic which has been steadily increasing over the last few decades, and now affects more than two billion people worldwide.[67] Accompanying obesity are several comorbidities including, but not limited to, metabolic and endocrine disorders such as Type 2 diabetes, dyslipidemia, and cardiovascular disease, and it is frequently linked to mental health, specifically anxiety and depression.[68-72] These diseases are often related to an unhealthy diet, particularly, high fat or high caloric diets. Despite this being well known, it is often unattainable for subjects with obesity to have consistently healthy diets due to societal and physiological barriers. To combat this growing problem, ongoing research is aiming to develop more effective treatments. However, many pharmacological therapies are limited by high costs and detrimental side effects.[73-75] Herbal remedies and specific plant materials, which have traditionally been used for obesity and metabolic diseases, are an alternative approach to therapy development.[76-77] Many of these traditional remedies include fenugreek (*Trigonella foenum-graecum*), an annual herbaceous plant belonging to the *Fabaceae* (also known as the *Leguminoseae*) family.[77-79]

Fenugreek is grown in several regions globally, including parts of Africa, Asia, and Europe and is used for both medicinal properties and for food purposes, as a seasoning.[78-80] It has been used for its anti-diabetic, anti-inflammatory, anti-cancer, anti-hyperlipidemic, and hepatoprotective properties.[79-81] The anti-diabetic effects of fenugreek have been suggested to result from the inhibition of glucose absorption in the intestines and/or insulinotropic activity.[81] Fenugreek seeds

contain several bioactive compounds including diosgenin, trigonelline, galactomannan, and 4-hydroxyisoleucine, among others, however the source of the beneficial effects of fenugreek is not well known.[77-79] Studies have shown that fenugreek supplementation is sufficient to alter intestinal microbiota, and thus influence the host physiology.[81-83] Microbiome changes as a result of fenugreek diet supplementation are a possible explanation for the therapeutic effects of fenugreek. A previous study using metabolomic and microbiome analyses has shown that microbiota from the *Lachnospiraceae* and *Ruminococcacea* families (in the Firmicutes phylum) increase coprostanol production in healthy humans, and thus reduced blood cholesterol levels through increased fecal cholesterol excretion.[84] More recent microbiome data demonstrates that a fenugreek-supplemented high fat diet was able to alter the expression of several taxa belonging to these two families, suggesting that fenugreek may encourage fecal fat excretion.[81] This may be a possible explanation for the anti-hyperlipidemic properties of fenugreek.

Metabolic health is influenced by gut microbiota, and is often mutually beneficial to both microbiota and the host.[40, 81, 85] The gut microbiome is a complex heterogeneous mixture of primarily bacteria, but also other types of microbes, with the greatest concentration found in the large intestines.[85] Intestinal microbiota has several important roles including aiding in digestion, synthesis of vitamins, as well as neutralizing carcinogens, toxins, and pathogenic bacteria.[81, 86] In healthy gut microbiomes, there is high diversity between bacterial species (alpha diversity), but the majority of bacteria belong to three phyla, specifically gram-positive Firmicutes (60%), gram-negative Bacteroidetes and gram-positive Actinobacteria (combined ~10%).[85] However, high fat and caloric diets, such as Western style diets which are high in fat, sucrose, and animal protein, significantly alter the composition of the microbiome.[85, 87-88] These diets, including Western style diets, result in decreased microbial diversity, and an increase in pathogenic and pro-inflammatory producing bacteria.[81, 85, 89] These changes not only alter the microbiome, but are also sufficient to cause detrimental metabolic effects.[81]

Fenugreek seeds are known to alter the microbiome and a previous study found that fenugreek was able to partially restore a healthy microbiome to mice fed a high fat diet, thus providing metabolic resiliency and improving metabolic health in mice.[81]

This study was designed to determine how the structure and function of the mammalian host is altered by high fat or western style diets and fenugreek seeds and the expected microbiome changes associated with these diets. High resolution mass spectrometry-based untargeted metabolomics was used to study male C57BL/6J mice that were fed either a 60% high fat diet, western style diet or low-fat control diets nutritionally matched to either high fat or western style diets. A subset of each experimental group received diets supplemented with ground fenugreek seeds (2% w/w) for 14 weeks and the effects of the diets on the metabolome were determined. Metabolomics permits high throughput analysis of all water-soluble small molecules, which allows for a systems-level phenotype analysis of the gut metabolome. To contribute to this analysis, liver and serum analyses were included to provide insight into circulating nutrients resulting from fenugreek supplementation. These data reveal significant alterations to the metabolic profiles as a result of fenugreek supplementation.

2.3 Results

2.3.1 Significant differences between small intestine, large intestine, liver, and serum

Untargeted metabolomics was used to analyze the metabolic effects of fenugreek on the gut, liver, and serum of mice fed either HF or WD diets for 14 weeks. From these analyses, a total of 209 and 208 metabolites (HF and WD respectively) were identified by exact mass and retention time across the contents of four intestinal regions (jejunum, ileum, cecum, and colon), livers, and serum of mice fed experimental diets. The diets, which were determined to evaluate the

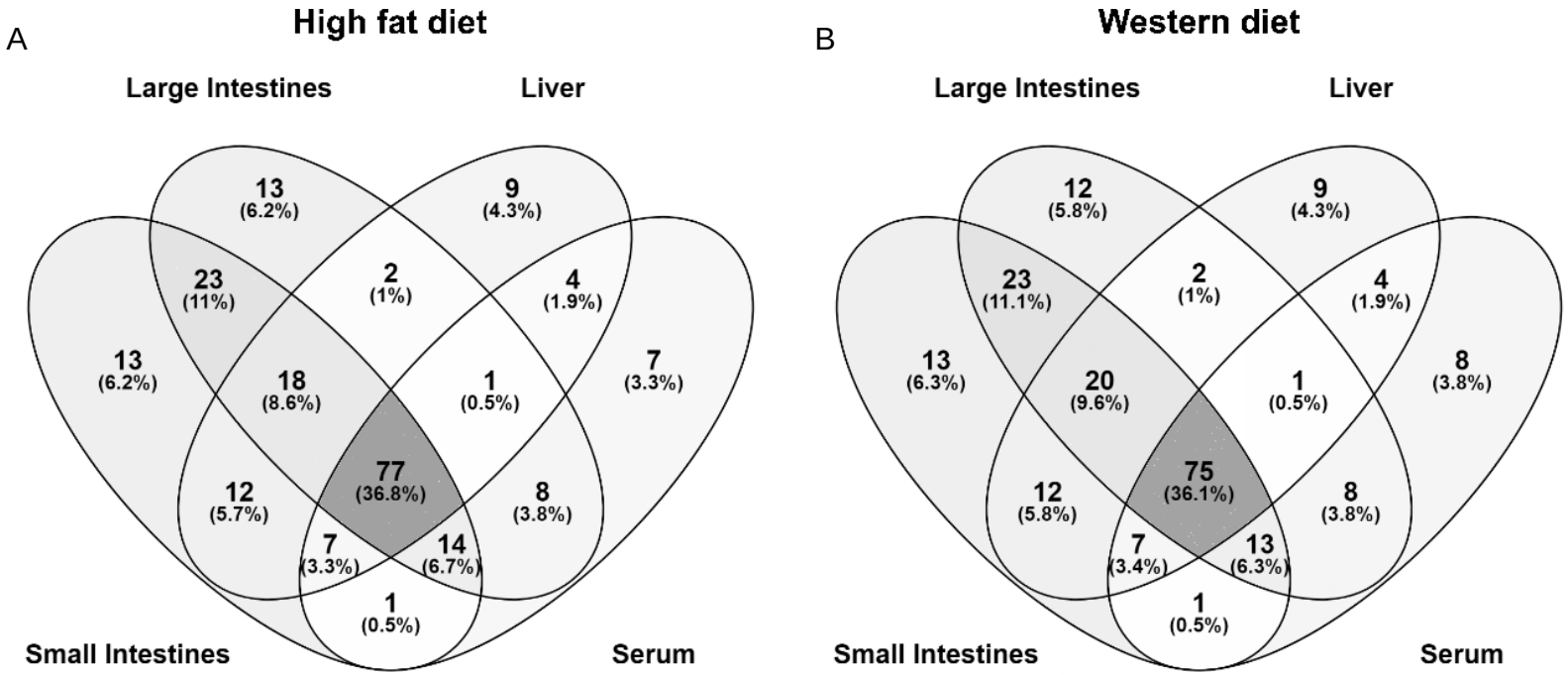


Figure 2.1 Venn diagrams depicting the overlap of identified metabolites between the small intestines, large intestines, liver, and serum from (A) HF-fed and LF_{HF}-fed mice both with and without fenugreek supplementation and (B) WD-fed and LF_{WD}-fed mice both with and without fenugreek supplementation.

effects of fenugreek in a diet specific manner, consisted of either HF or WD diets and two separate LF diets nutritionally matched to HF (LF_{HF}) and WD (LF_{WD}), and each with and without fenugreek for a total of 8 different diets: HF, HFFG, LF_{HF}, and LF_{HF}FG (HF control) or WD, WDFG, LF_{WD}, and LF_{WD}FG (WD control). Of these 209 metabolites detected in the HF study, 77 (37%) were detected in the small intestine, large intestine, liver, and serum (Fig. 2.1A). Similarly, of the 208 metabolites detected in the WD study, 75 (36%) were detected in the small intestine, large intestine, liver, and serum (Fig. 2.1B). As anticipated, the greatest influence on the metabolic profiles was due to the origin of the sample (jejunum, ileum, cecum, colon, liver, or serum), rather than the specific diet. PLS-DA analysis (Fig. 2.2), when including groups for different sample location and diet, show four clear and distinct groupings – small intestine (jejunum and ileum), large intestine (cecum and colon), liver, or serum – but the difference resulting from fenugreek supplementation is indistinguishable. However, when focusing on only one sample location at a time, the influence of diet and fenugreek supplementation is apparent.

2.3.2 Metabolomics data indicate significant differences as a result of fenugreek supplementation

Small intestine

From the metabolomics data of the HF analysis, nearly 7,000 unique spectral features were detected in the jejunum and ileum samples (6,837 and 6,823 for jejunum and ileum, respectively; Table 2.1). Of these features, 145 and 140 were identified as metabolites in the jejunum and ileum samples, respectively. While there were similar numbers of features and identified metabolites, there were vast differences in the number of features which were determined to be significantly different ($p<0.05$ and fold change>|1.5|) with fenugreek supplementation between the two small intestine regions. Specifically, in the jejunum contents, no identified metabolites and only 331 unidentified features were significantly different with fenugreek (Table 2.1).

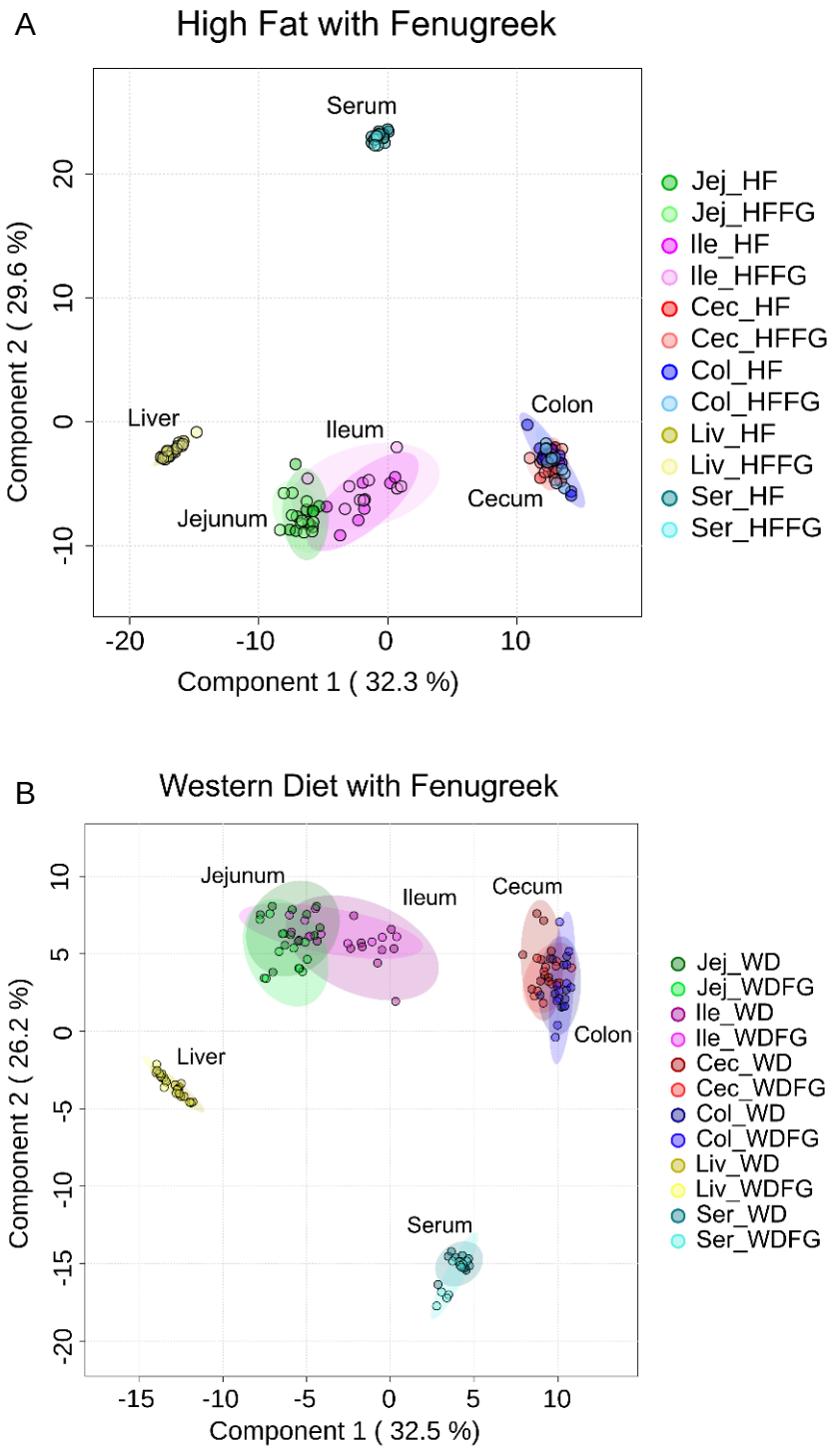


Figure 2.2 Partial least squares discriminant analysis (PLS-DA) comparing metabolomes for each intestinal region (jejunum, ileum, cecum, and colon), liver, and serum and associated with (A) HF and HFFG diets or (B) WD and WDFG diets. Experimental replicates are shown with respective 95% confidence intervals.

Table 2.1 Summary of identified metabolites and mass spectral features from HF metabolomics data. Features with p-values less than 0.05 and fold change (HFFG/HF) greater than 1.5 were counted as significantly increased with fenugreek. Features with p-value less than 0.05 and fold change (HFFG/HF) less than 0.667 were counted as significantly decreased with fenugreek.

High fat diet metabolomics

	Jejunum	Ileum	Cecum	Colon	Liver	Serum
Total identified metabolites	**145**	**140**	**141**	**137**	**130**	**120**
Significantly increased w/FG	0	0	5	11	0	2
Significantly decreased w/FG	0	9	7	4	2	0
Total unique spectral features	**6837**	**6823**	**11157**	**8974**	**3323**	**1772**
Significantly increased w/FG	41	37	579	580	92	58
Significantly decreased w/FG	290	1580	1679	543	204	30

Additionally, using visualization tools such as PLS-DA, minimal to no separation was observed between the groups with and without fenugreek, although there is slight separation between HF and LF_{HF} diets in the identified metabolome (Fig. 2.3A). However, there was more separation between the profiles associated with the diets and resulting from fenugreek supplementation of LF_{HF} diet when comparing the unidentified and identified features (Fig. 2.3B). In the ileum content samples, 1,617 spectral features, including nine identified metabolites were determined to be significantly different with 1,580 of these features having been decreased with fenugreek supplementation (Table 2.1). While the PLS-DA for the identified metabolites again only shows a little separation between the groups (Fig. 2.3C), similar to the jejunum samples, including the unidentified features increases the distinction (Fig. 2.3D) between all four diets.

Similar to the HF study, nearly 7,000 unique features were detected in the small intestines of mice using untargeted metabolomics for the WD experiments. Specifically, 6,786 features were detected in the jejunum contents, and 6,871 features were detected in the ileum contents (Table 2.2). Of these features, 1,236 and 965 were significantly different with FG supplementation in the jejunum and ileum, respectively (Table 2.2). However, 310 and 1,951 (jejunum and ileum) features were significantly different between WD and control diet, of which 73% or 89% (226 or 1,736 features, jejunum, and ileum) were reversed in WDFG (Appendix Figs. 2.16 & 2.17). From the total spectral features, 144 and 139 metabolites were identified using exact mass and retention time. In the jejunum, 15 of the identified metabolites were significantly different with FG supplementation, while in the ileum, 39 of the identified metabolites were significantly different (Table 2.2). Using PLS-DA to analyze both the identified and total detected features reveals that the metabolomes of each region are distinguished between WD and LF_{WD} diet groups (Fig 2.4). However, the PLS-DA analysis of the total features in jejunum as well as both identified and total features in the ileum, also exhibit separation between WD and WDFG groups (Fig 2.4B, C, D).

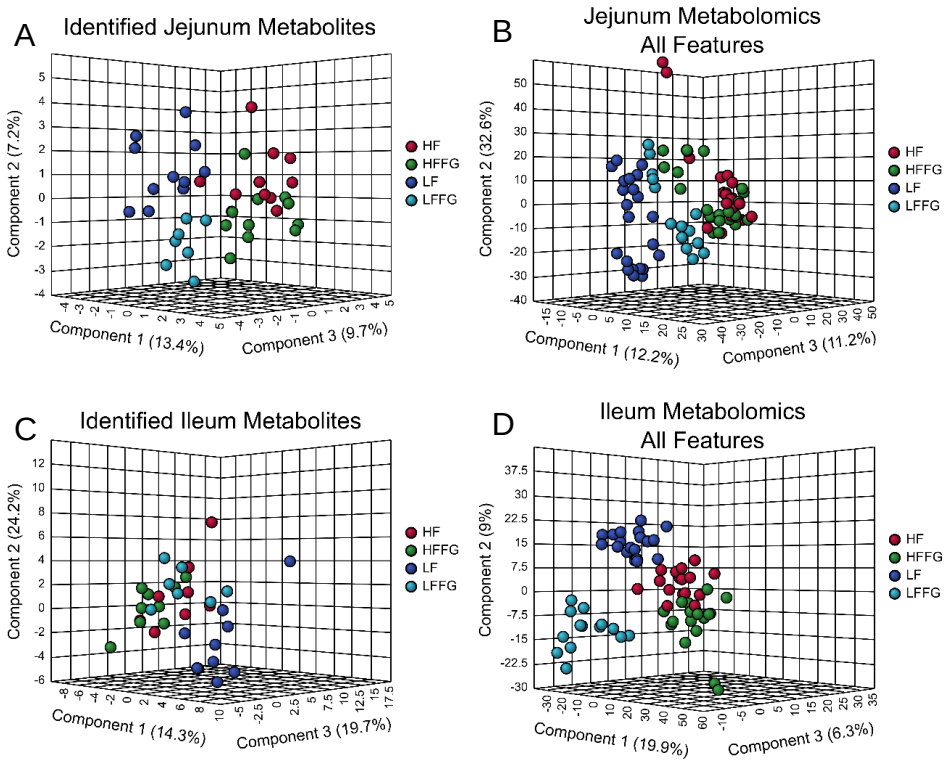


Figure 2.3 PLS-DA display minimal differences in metabolic profiles between diets and the respective FG supplemented diet in small intestines. Untargeted metabolomics was performed on the jejunum and ileum contents mice fed HF, HFFG, LF_{HF}, or $LF_{HF}FG$ diets for 14 weeks. PLS-DA were performed for (A) identified jejunum metabolites, (B) all jejunum spectral features, (C) identified ileum metabolites and (D) all ileum spectral features. Experimental replicates are shown; HF samples are shown in red, HFFG samples are shown in green, LF_{HF} samples are shown in dark blue, and $LF_{HF}FG$ samples are shown in light blue.

Table 2.2 Summary of identified metabolites and mass spectral features from WD metabolomics data. Features with p-values less than 0.05 and fold change (WDFG/WD) greater than 1.5 were counted as significantly increased with fenugreek. Features with p-value less than 0.05 and fold change (WDFG/WD) less than 0.667 were counted as significantly decreased with fenugreek.

Western style diet metabolomics

	Jejunum	Ileum	Cecum	Colon	Liver	Serum
Total identified metabolites	**144**	**139**	**140**	**136**	**130**	**117**
Significantly increased w/FG	1	36	15	20	8	0
Significantly decreased w/FG	14	3	47	11	0	1
Total unique spectral features	**6786**	**6871**	**10973**	**8721**	**3247**	**1750**
Significantly increased w/FG	440	517	413	351	130	512
Significantly decreased w/FG	796	448	901	1056	60	4

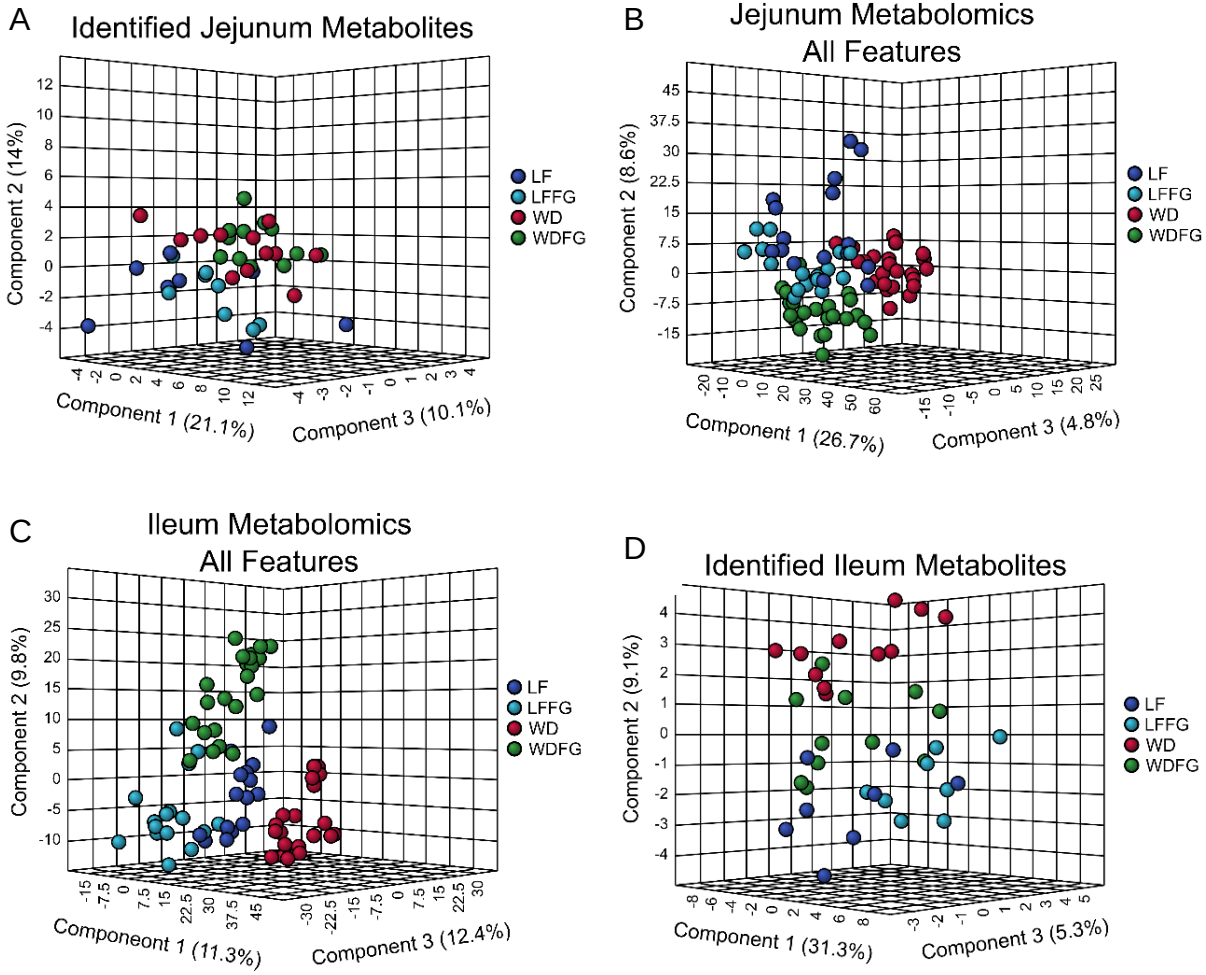


Figure 2.4 PLS-DA display some differences in metabolic profiles between diets and the respective FG supplemented diet in small intestines. Untargeted metabolomics was performed on the jejunum and ileum contents mice fed WD, WDFG, LF_{WD}, or $LF_{WD}FG$ diets for 14 weeks. PLS-DA were performed for (A) identified jejunum metabolites, (B) all jejunum spectral features, (C) identified ileum metabolites and (D) all ileum spectral features. Experimental replicates are shown; WD samples are shown in red, WDFG samples are shown in green, LF_{WD} samples are shown in dark blue, and $LF_{WD}FG$ samples are shown in light blue.

Large intestine

Large intestine contents show dramatic differences with fenugreek supplementation in these metabolomics data. Specifically, of the 209 total metabolites identified in these studies, 141 and 137 were detected in the cecum and colon contents, respectively (67% and 66%). Moreover, a total of 11,157 (cecum) and 8,974 (colon) spectral features were detected in the large intestines contents of mice used in this study (Table 2.1). Among these features, 2,258 (cecum) and 1,123 (colon) were determined to be significantly increased or decreased with the addition of fenugreek to HF diet (Table 2.1). Using PLS-DA to visualize the small molecule profiles in the cecum and colon contents, it is apparent that the profiles of mice fed fenugreek are distinctly different from the profiles of mice not given fenugreek. This is in addition to alterations caused by either HF or LF_{HF} diets for both identified and unidentified small molecules (Fig. 2.5).

Among the identified small molecules, many of these have been determined to be involved in central carbon pathways. PLS-DA plots for these identified metabolites display no overlap between the HF and HFFG groups (Fig. 2.5 A & B). Using the variable importance in projection (VIP) score, it was determined that of the top 10 highest VIP scoring metabolites, five metabolites were conserved between cecum and colon and have a compelling impact on the separation of these groups for both regions. These metabolites are inosine, adenine, myo-inositol, xanthosine, and guanine (Appendix Fig. 2.18). These metabolites are significantly altered by HF diet, particularly, inosine, myo-inositol, xanthosine, and guanine decrease in HF- relative to LF_{HF}-fed mice, but adenine increases in HF- relative to LF_{HF}-fed mice (Fig. 2.6; Appendix Figs 2.19 & 2.20). No consistent trend of increasing or decreasing with fenugreek supplementation is evident for these metabolites. However, for each region, a pairwise PLS-DA comparison of HF and HFFG groups, which are clearly separated, (Appendix Fig. 2.21) found that while several metabolites contribute to the separation of these profiles, two specific metabolites, carnitine and 2,3-dihydroxybenzoate, heavily influenced the separation (Fig 2.7; for 2,3-dihydroxybenzoate see Appendix Fig. 2.22).

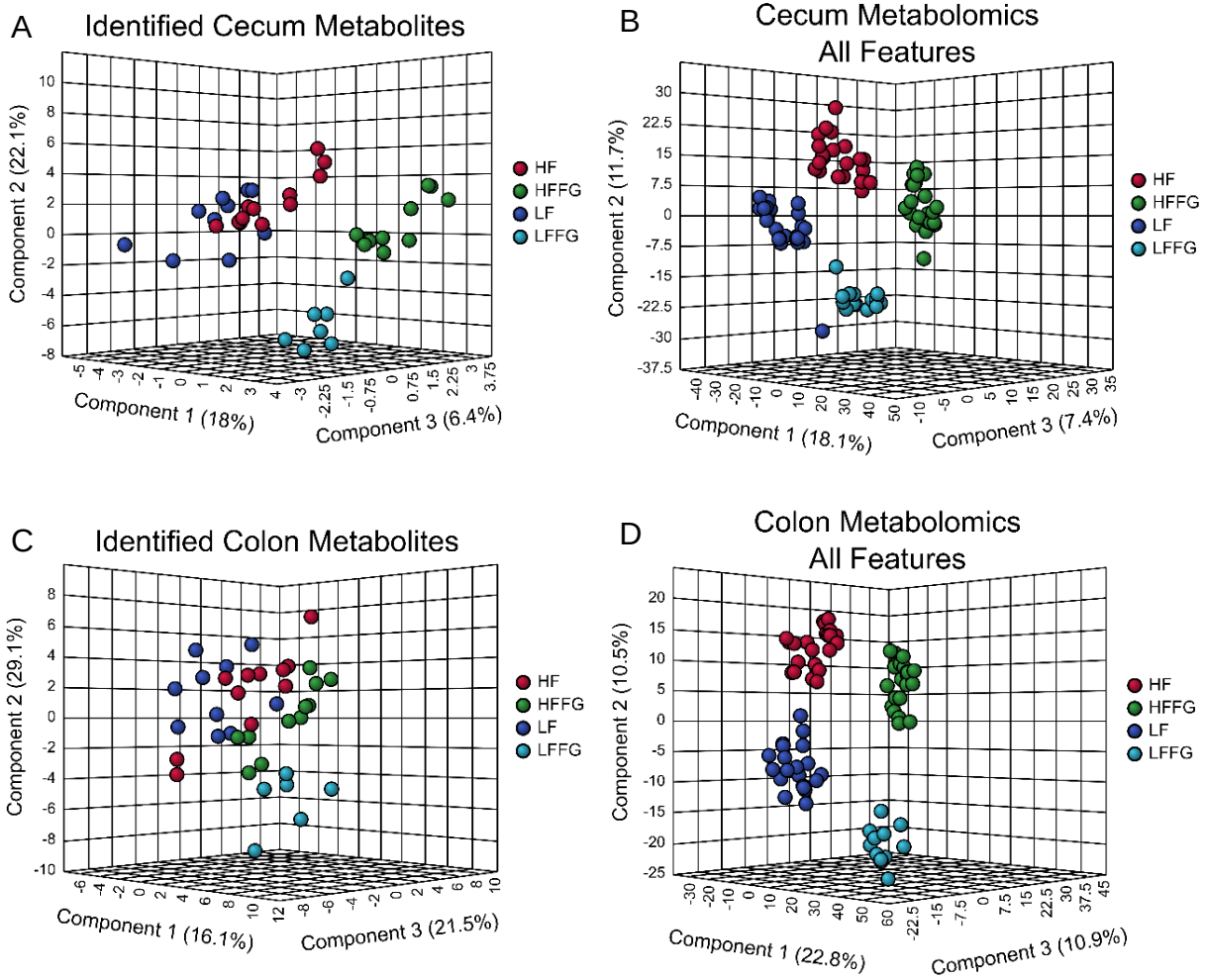


Figure 2.5 Diet and FG supplementation induce distinct differences in the large intestine metabolome as shown by PLS-DA. Untargeted metabolomics was performed on the cecum and colon contents of mice fed either HF, HFFG, LF_{HF}, or $LF_{HF}FG$ diets after 14 weeks of diet exposure. PLS-DA were performed for (A) identified jejunum metabolites, (B) all jejunum spectral features, (C) identified ileum metabolites and (D) all ileum spectral features. Experimental replicates are shown; HF samples are shown in red, HFFG samples are shown in green, LF_{HF} samples are shown in dark blue, and $LF_{HF}FG$ samples are shown in light blue.

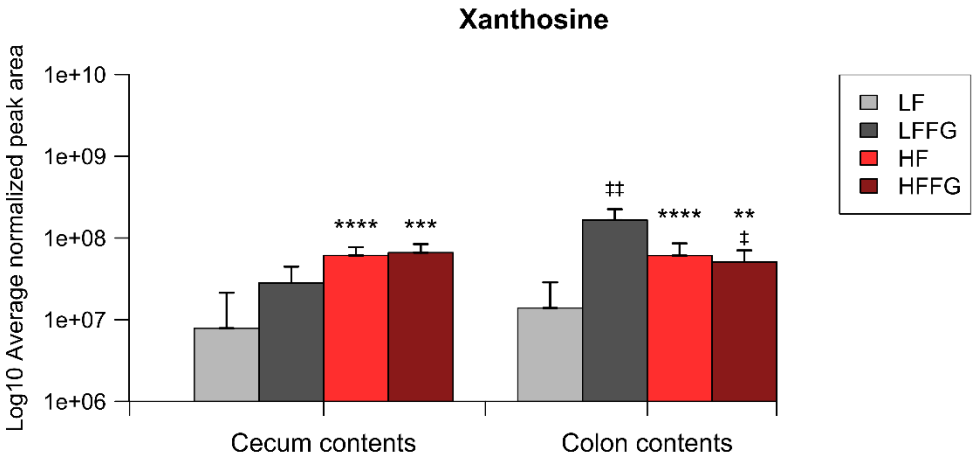


Figure 2.6 Normalized intensities of xanthosine from both cecum and colon data from HF-, HFFG-, LF_{HF}-, and $LF_{HF}FG$-fed mice. Data was normalized according to mass and the normalized peak area is represented on a log_{10} scale as mean ± standard deviation. Significance was determined using a Student's t-test. Significance is represented as *p<0.05, **p<0.01, ***p<0.001, and ****p<0.0001 for comparisons against respective LF groups or ‡ p<0.05, ‡‡ p<0.01, ‡‡‡ p<0.001, and ‡‡‡‡ p<0.0001 for comparisons against either HF or LF, respectively.

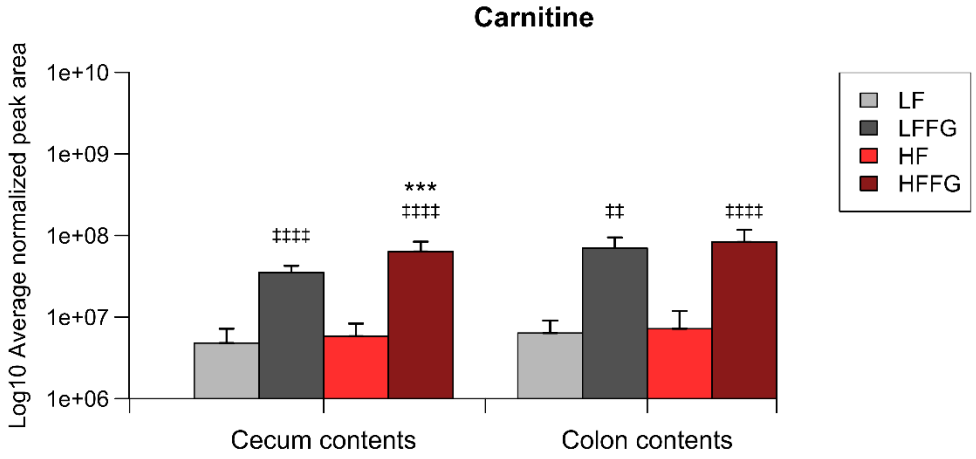


Figure 2.7 Normalized intensities of carnitine from both cecum and colon data from HF-, HFFG-, LF_{HF}-, and $LF_{HF}FG$-fed mice. Data was normalized according to mass and the normalized peak area is represented on a log_{10} scale as mean ± standard deviation. Significance was determined using a Student's t-test. Significance is represented as *p<0.05, **p<0.01, ***p<0.001, and ****p<0.0001 for comparisons against respective LF groups or ‡ p<0.05, ‡‡ p<0.01, ‡‡‡ p<0.001, and ‡‡‡‡ p<0.0001 for comparisons against either HF or LF, respectively.

Representatively shown in Figure 2.7, these metabolites consistently display high fold changes in $LF_{HF}FG$ and HFFG relative to LF_{HF} and HF groups, respectively.

Metabolomics analysis of large intestinal contents of mice in the WD study, reveal significant alterations related to diet. There were 10,973 and 8,721 features detected, of which 140 and 136 were identified in the cecum and colon contents, respectively (Table 2.2). Using only the identified features, three separate groups in the PLS-DA plots for cecum contents corresponding to WD, WDFG, and overlapping LF_{WD} and $LF_{WD}FG$ groups, denoting a similarity in the metabolic profile between these two groups (Fig. 2.8). This separation is driven by several metabolites, however five metabolites which are significantly influencing this separation (VIP >1) in both regions (appendix Figs. 2.26). These metabolites are 6-phospho-D-gluconolactone, glucose phosphate, gluconolactone, myo-inositol, and homocarnosine (appendix Figs. 2.23-2.25). These metabolites also have fold changes ranging from 7-35 (cecum) or 5-38 (colon) and p-values, determined by a Student's T-test, less than 0.05 (except for 6-phospho-D-gluconolactone) for comparison between WD and WDFG groups. The analysis of the total spectral features reveals similar grouping in the PLS-DA of the cecum as in the identified metabolites in which the only overlapping groups are the LF_{WD} and $LF_{WD}FG$ control groups (Fig. 2.8A). Alternatively, in the PLS-DA of the colon contents, all four dietary groups were separated indicating distinct metabolic profiles (Fig. 2.8 C & D). Additionally, of the 10,973 and 8,721 features, 2,301 and 2,232 features (26% and 32% of features detected in all diets, respectively) were significantly different between WD and LF_{WD} diets (Fig. 2.9 & appendix Fig. 2.27). Greater than 75% of the features altered by WD were significantly reversed by FG, specifically 94% and 78% (2,164 and 1,730 features) from cecum and colon contents. Interestingly, in the cecum, the majority of significantly altered features are elevated in WD and diminished in WDFG (2100 features) (Fig. 2.9). However, in the colon contents the features reversed by FG are split more evenly, with 927 features elevated in WD, and 803 diminished in WD (Appendix Fig. 2.27).

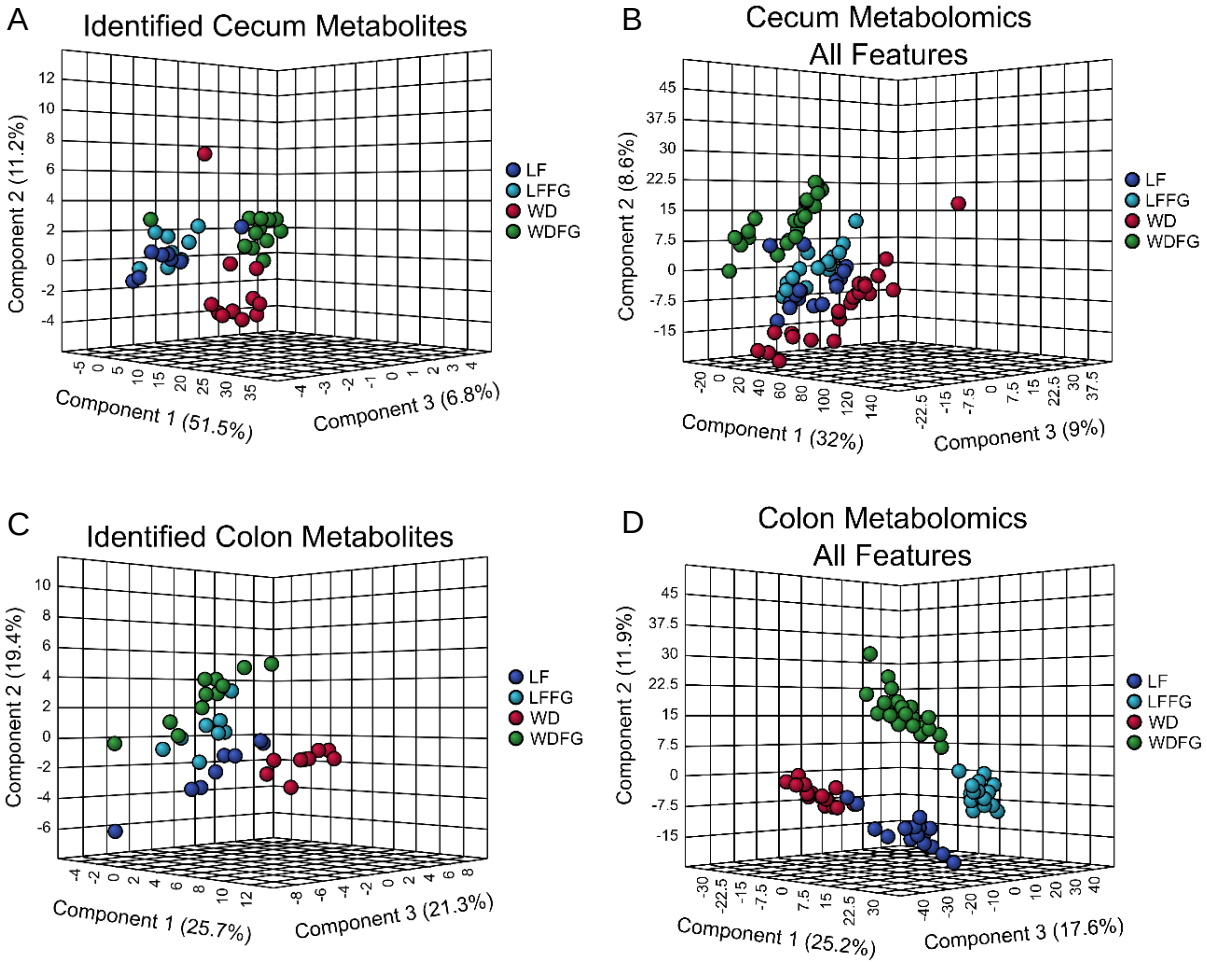


Figure 2.8 Diet and FG supplementation induce distinct differences in the large intestine metabolome as shown by PLS-DA. Untargeted metabolomics was performed on the cecum and colon contents of mice fed either WD, WDFG, LF_{WD}, or $LF_{WD}FG$ diets after 14 weeks of diet exposure. PLS-DA were performed for (A) identified jejunum metabolites, (B) all jejunum spectral features, (C) identified ileum metabolites and (D) all ileum spectral features. Experimental replicates are shown; WD samples are shown in red, WDFG samples are shown in green, LF_{WD} samples are shown in dark blue, and $LF_{WD}FG$ samples are shown in light blue.

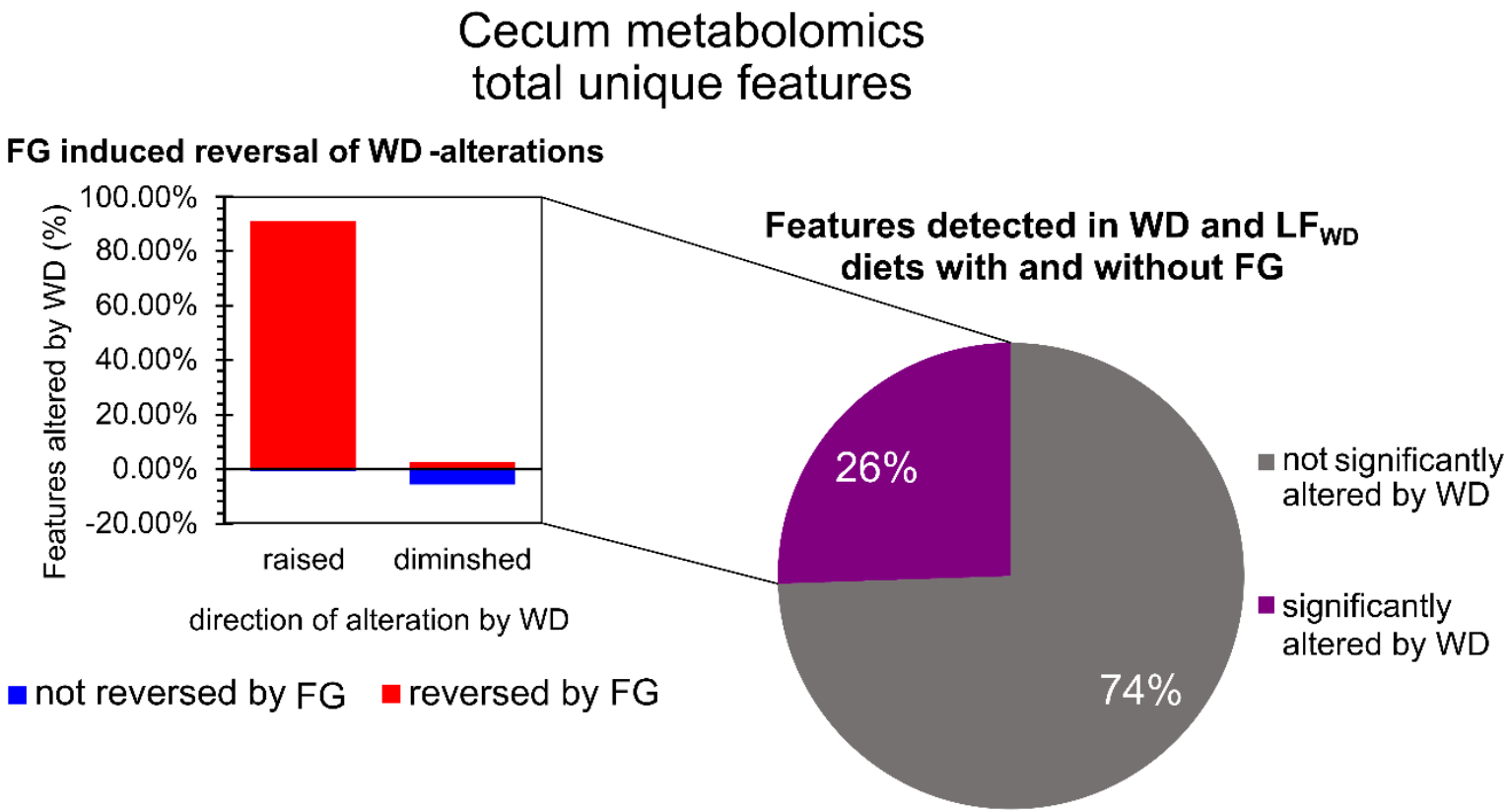


Figure 2.9 Over a quarter of unique spectral features detected in metabolomics investigations of cecum contents of mice were significantly different in WD-fed mice compared to LF_{WD} fed mice. Of these features, over 90% were detected with higher abundance in WD-fed mice relative to LF-fed mice, but lower abundance in WDFG-fed mice relative to WD-fed mice.

Liver

While not as dramatic as in the large intestines, metabolomics data reveal the liver metabolome is also altered by fenugreek. From the livers in the HF study, a total of 3,323 spectral features were detected, from which 131 features were identified as water-soluble metabolites when compared to an in-house standard library (Table 2.1). Of the unidentified spectral features, 296 were determined to be significantly altered with the addition of fenugreek to HF diet. From the PLS-DA, which only includes the identified metabolites (Fig. 2.10A), and another that includes all features (Fig. 2.10B), it is clear that the metabolite profiles in the livers of mice are moderately different when the diet is supplemented with fenugreek. From the multivariate analysis of the identified metabolites within HF and HFFG groups, it was determined that the metabolite with the highest VIP score and thus most substantially driving this separation is the bile salt, glycodeoxycholate (Appendix Figs. 2.28 & 2.29). This bile salt has a fold change (HFFG/HF) of 2.6 and p-value below 0.06.

Liver metabolite profiles in the WD study also display small, but significant alterations resulting from FG supplementation. From the metabolomics data, 3,247 unique spectral features were detected, of which 130 metabolites were identified (Table 2.2). Eight identified metabolites and 190 features were determined to be significantly different with FG supplementation to WD. While minimal separation is apparent in the PLS-DA plots for the liver metabolome (Appendix Fig. 2.30), 16% of features detected in all diets (410 features) were significantly altered in WD compared to LF_{WD} diet. The majority of these features (362) were elevated in WD, all of which were significantly lower in WDFG relative to WD (Fig. 2.11).

Serum

Metabolomics data display minimal differences in the serum metabolome resulting from fenugreek supplementation in the HF study. A total of 1,772 spectral features were detected in the serum samples, with 120 metabolites identified (Table 2.1). From the unidentified spectral features, only 88 features were determined to be significantly different between HF and HFFG, and only two

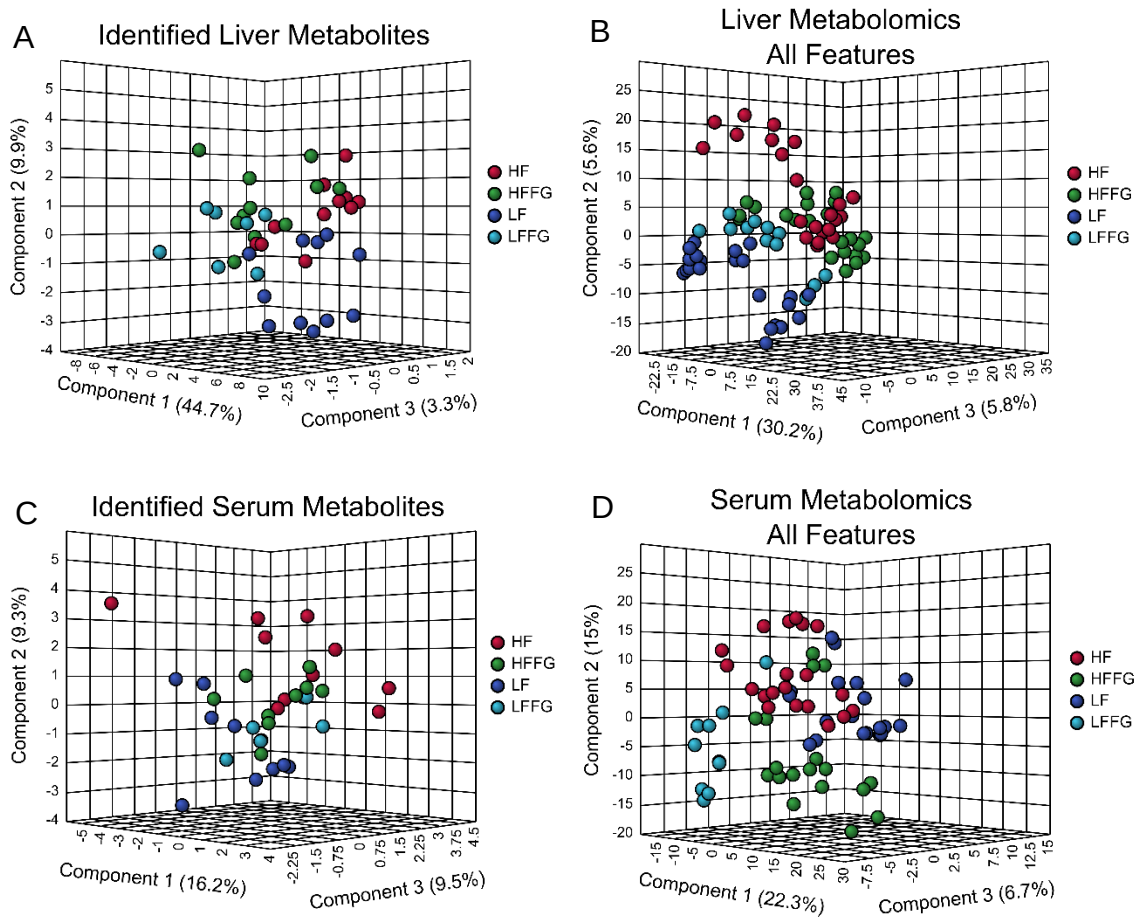


Figure 2.10 PLS-DA of liver and serum samples reveal subtle distinctions between the metabolic profiles associated with each diet, more notably in the unidentified features. Untargeted metabolomics was performed on the liver samples from mice fed either HF, HFFG, LF_{HF}, or $LF_{HF}FG$ diets. PLS-DA were performed for (A) identified liver metabolites, (B) all liver spectral features, (C) identified serum metabolites, and (D) all serum spectral features. Experimental replicates are shown; HF samples are shown in red, HFFG samples are shown in green, LF_{HF} samples are shown in dark blue, and $LF_{HF}FG$ samples are shown in light blue.

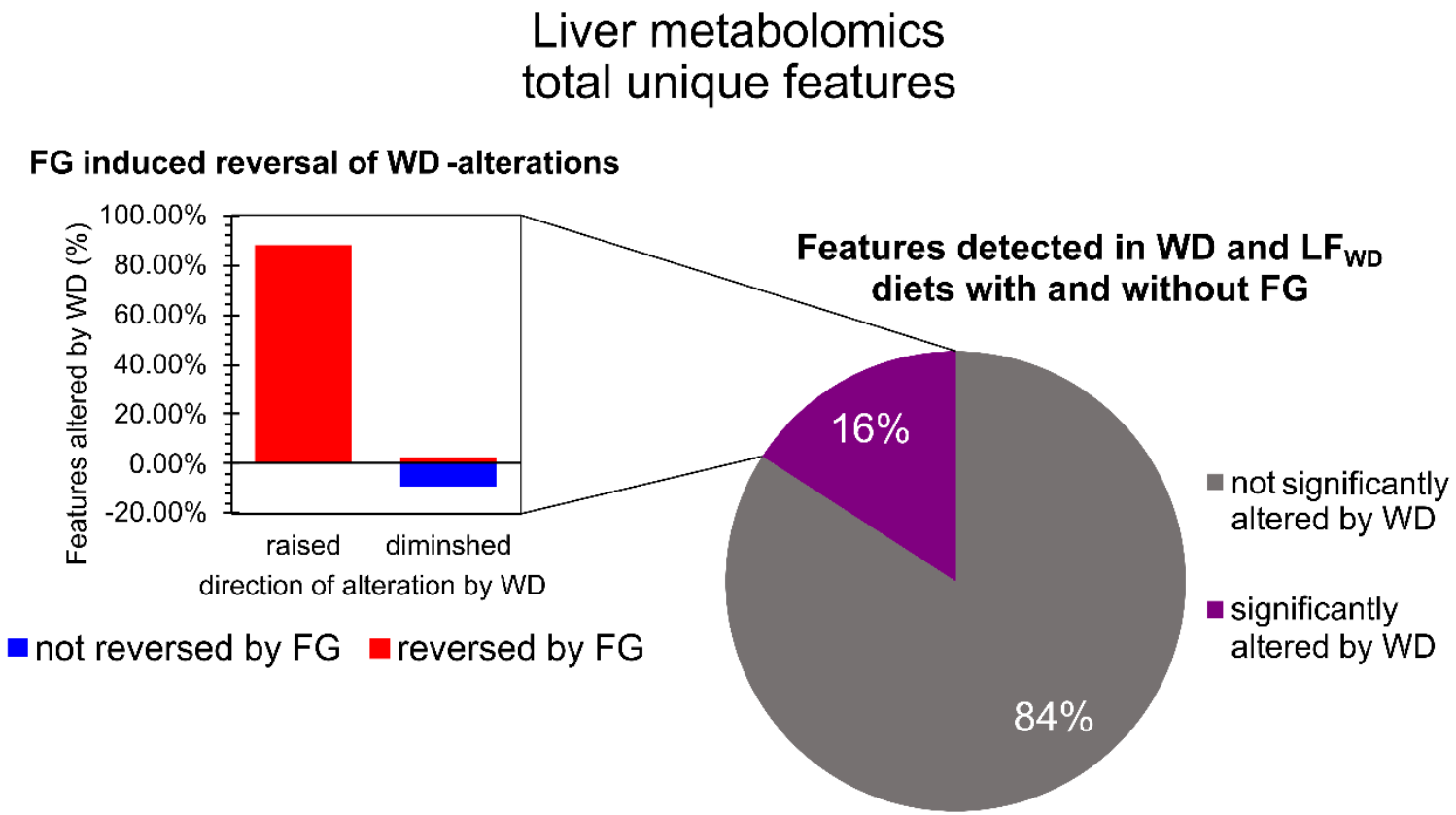


Figure 2.11 16% of unique spectral features detected in metabolomics investigations of livers of mice were significantly different in WD-fed mice compared to LF_{WD} fed mice. Of these features, nearly 90% were detected with higher abundance in WD-fed mice relative to LF-fed mice, but lower abundance in WDFG-fed mice relative to WD-fed mice.

identified metabolites were significantly altered (Table 2.1). Neither PLS-DA of identified or unidentified metabolites show obvious separation, however a small degree of separation can be observed in both (Fig. 2.10C & D). In the PLS-DA of identified metabolites (Fig. 2.10C), there is slight separation between groups as a result of the diet, with FG having little to no influence. Despite this, the PLS-DA of unidentified features (Fig. 2.10D), indicates there is separation, albeit small, resulting from the addition of fenugreek to the diets.

From the metabolomics analysis of serum in the WD study, 1,750 spectral features were detected, and 117 metabolites were identified (Table 2.2). PLS-DA analysis of identified metabolites reveal minimal separation between WD and LF_{WD} groups, although no separation resulting from FG was present (Fig. 2.12A). However, in the PLS-DA analysis of all features, the WD group was slightly separated from the other groups, indicating that the metabolic profile associated with the WDFG diet was more similar to the LF_{WD} and LF_{WD}FG metabolic profile than the WD profile (Fig. 2.12B). Additionally, 38% (494) of features detected in all diets were significantly altered in WD relative to LF_{WD} diet. Of these 494 features, 274 or 55% were reversed by FG (Fig. 2.13). In contrast to the intestinal contents and liver features, the majority (270) of features reversed by FG were detected in lower abundance in WD, and higher abundance in WDFG relative to WD.

2.3.3 Fenugreek supplementation modulates HDL balance and total cholesterol in both HF diet- and WD-fed mice

This study expands on previous research at Pennington Biomedical Research Center showing that fenugreek diet supplementation improved markers of metabolic health as well as countered dysbiotic effects in mice fed a high-fat diet.[80-81] Since a previous study demonstrated an attenuated ability of fenugreek to counter HF-diet induced metabolic dysfunction when mice were supplemented for 16 weeks, in the present study the treatment time was decreased to 14 weeks.

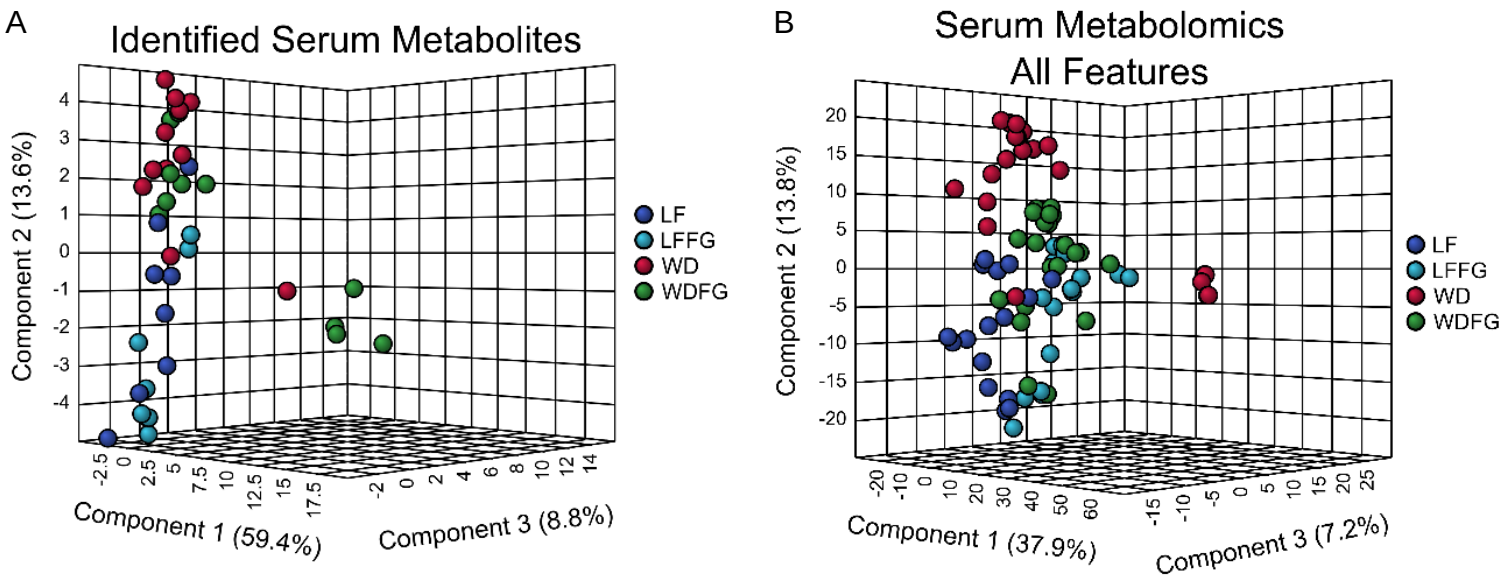


Figure 2.12 PLS-DA of serum samples reveal distinctions, although minimal, between the metabolic profiles associated with each diet, more noticeably in the unidentified features. Untargeted metabolomics was performed on the liver samples from mice fed either WD, WDFG, LF_{WD}, or $LF_{WD}FG$ diets. PLS-DA were performed for (A) identified serum metabolites and (B) all serum spectral features. Experimental replicates are shown; WD samples are shown in red, WDFG samples are shown in green, LF_{WD} samples are shown in dark blue, and $LF_{WD}FG$ samples are shown in light blue.

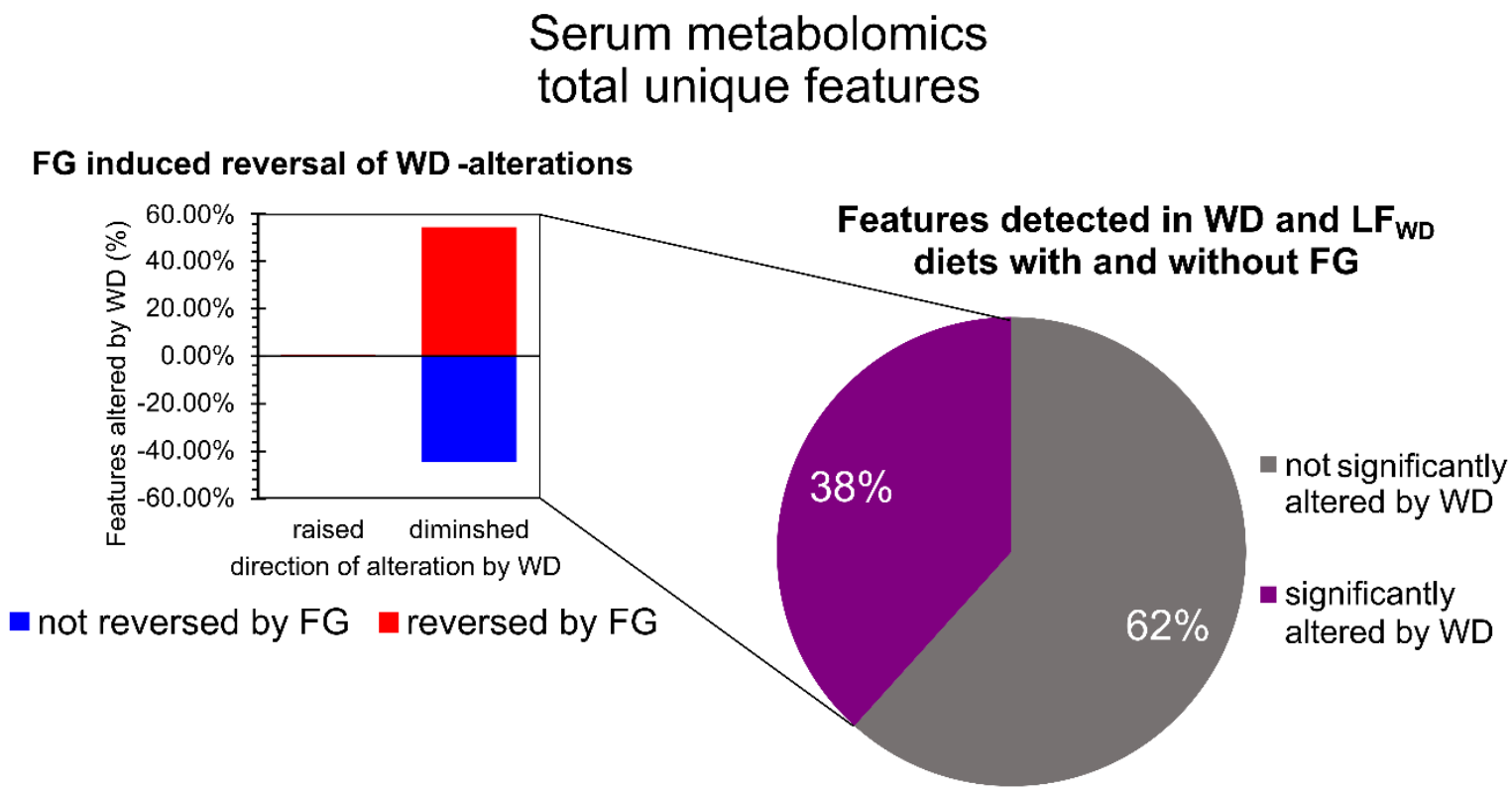


Figure 2.13 Nearly 40% of unique spectral features detected in metabolomics investigations of livers of mice were significantly different in WD-fed mice compared to LF_{WD} fed mice. Of these features, over 50% were detected with lower abundance in WD-fed mice relative to LF-fed mice, but higher abundance in WDFG-fed mice relative to WD-fed mice.

As shown in Figure 2.14, the expected increases in total cholesterol and high-density lipoprotein (HDL) and low-density lipoprotein (LDL) cholesterol in HF- versus LF_{HF}-fed mice were observed. Fenugreek supplementation decreased total cholesterol levels in HF-fed mice (Fig. 2.14C), but this attenuation did not reach statistical significance ($p = 0.0627$). When HDL was expressed as a percent of total cholesterol, HF diet decreased the percent HDL compared to LF_{HF} diet in the absence of fenugreek but not in the presence of fenugreek (compare LF_{HF}FG and HFFG) (Fig. 2.14A & B). Concordant with previous results,[80] fenugreek supplementation improved the HDL cholesterol composition in HF-fed mice without altering body weight or body fat (Appendix Table 2.4).

Similar trends were apparent in the WD study. In particular, the absolute levels of HDL, LDL, and total cholesterol were increased in WD-fed mice relative to LF_{WD}-fed mice (Fig. 2.15). Liver weight, body weight, and body fat also increased as expected in WD-fed mice relative to LF_{WD}-fed mice (Appendix Table 2.5). However, fenugreek had a more significant influence in the WD study than in the HF study. Specifically, the percent HDL of total cholesterol was significantly increased from WD- to WDFG-fed mice (Fig 2.15A), but minimal change in the percent LDL of total cholesterol (Fig. 2.15B). In contrast to the HF study, FG supplementation was found to significantly decrease the liver weight in WD-fed mice (Appendix Table 2.5).

2.4 Discussion

Fenugreek has traditionally been used in herbal remedies to treat disorders such as hyperlipidemia and diabetes, however the mechanisms by which these benefits arise are largely unknown. While several mechanisms have been proposed, a compelling theory is that at least some beneficial effects are a result of fenugreek altered gut microbiomes. Specifically, a previous study determined that while HF diet has detrimental effects such as reducing alpha diversity and inducing gut

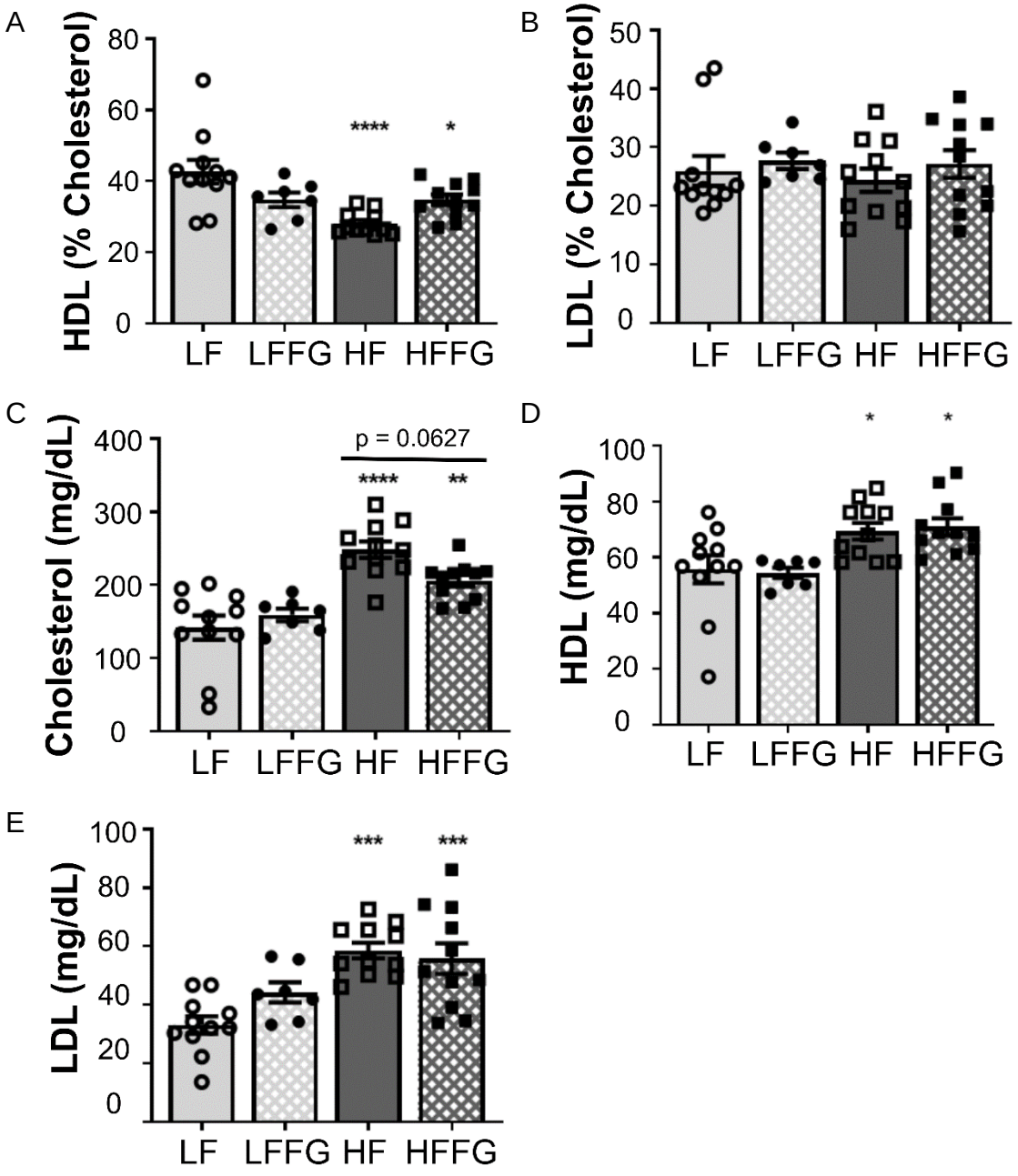


Figure 2.14 Fenugreek supplementation improves cholesterol levels and high-density lipoprotein (HDL) balance in HF diet-fed mice. Whole blood was collected from fasted mice following 14 weeks on LF_{HF}, $LF_{HF}FG$, HF, or HFFG diet, and serum was separated and analyzed for total cholesterol, HDL, and low-density lipoprotein (LDL). (A) and (B) HDL and LDL are represented as percent cholesterol. (C – E) show the absolute levels of total cholesterol, HDL, and LDL. Results are presented as mean ± SEM for each group – LF_{HF}, HF and HFFG (n = 11); $LF_{HF}FG$ (n = 7). Statistical significance was determined using Tukey's multiple comparison test following a one-way ANOVA. Significance is represented as *p < 0.05, **p < 0.01, ***p < 0.001, and ****p < 0.0001 for comparisons against the LF_{HF} group.

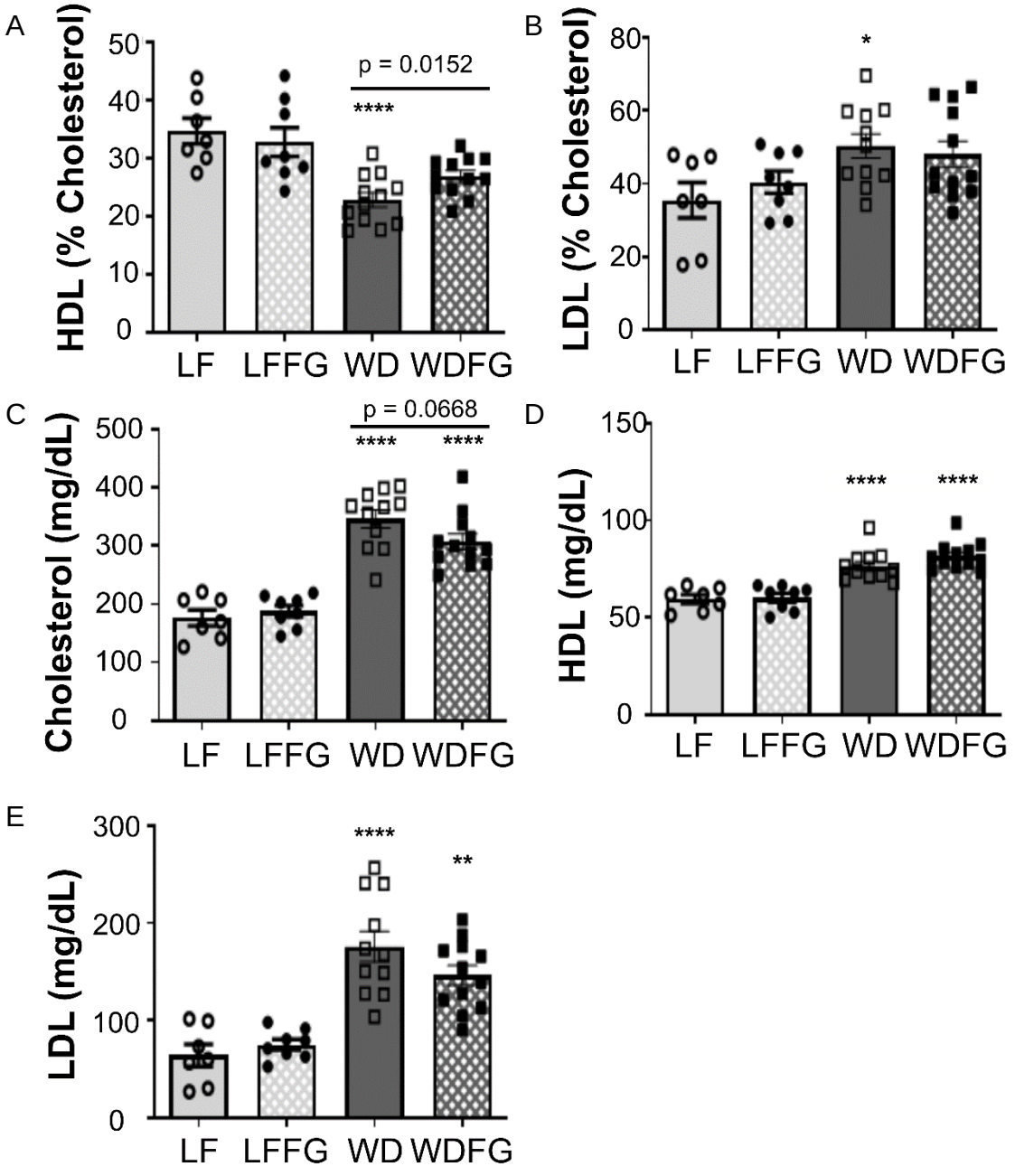


Figure 2.15 Fenugreek supplementation improves cholesterol levels and high-density lipoprotein (HDL) balance in WD-fed mice. Whole blood was collected from fasted mice following 14 weeks on LF_{WD}, $LF_{WD}FG$, WD, or WDFG diet, and serum was separated and analyzed for total cholesterol, HDL, and low-density lipoprotein (LDL). (A) and (B) HDL and LDL are represented as percent cholesterol. (C – E) show the absolute levels of total cholesterol, HDL, and LDL. Results are presented as mean ± SEM for each group – LF_{WD} and $LF_{WD}FG$ (n = 8); WD and WDFG (n = 12). Statistical significance was determined using Tukey's multiple comparison test following a one-way ANOVA. Significance is represented as *p < 0.05, **p < 0.01, ***p < 0.001, and ****p < 0.0001 for comparisons against the LF_{WD} group.

dysbiosis, fenugreek was able to reverse some of the harmful effects.[81] This is important as gut dysbiosis has been seen to be sufficient to impair metabolic and neurologic function of the mammalian host.[42, 81, 90-94] In particular, studies have shown that fenugreek is an efficient treatment for hyperlipidemia, cholesterolemia, and hyperglycemia which maybe a result of the microbial alterations.[81, 95-98]

This study however, focused on the changes in the metabolome resulting from fenugreek supplementation. As fenugreek and the microbiome both contribute to metabolic health, and the metabolome serves as a way to increase understanding of phenotypes, it follows that metabolomics is an important addition to fenugreek studies. Untargeted mass spectrometry-based metabolomics allows for the analysis of all detectable, water-soluble small molecules, rather than limiting the analysis to known central carbon metabolites, which are only a fraction of the total metabolites. This study demonstrates, using high throughput mass analysis, that fenugreek, not only alters the microbiome, but also significantly alters the intestinal, liver, and serum metabolomes of mice in a diet dependent manner.

As anticipated, metabolomics data reveal distinctly different metabolic profiles in the small intestine, large intestines, liver, and serum which arise from the different microbial activity and physiological function of these tissues and biofluids. For the small and large intestine samples, while it is expected that the metabolome will be differentiated, it is not guaranteed that there will be clear and obvious distinctions in metabolomics since certain metabolites are common to many cells and organisms. However, substantial distinctions are present in this study, which is an indicator of high-quality data. Regardless of diet, the sum of the normalized abundance displays a higher abundance for the identified metabolites in the liver and small intestine regions than in the large intestinal regions or serum (Appendix Fig. 2.31), however, there were thousands more unidentified spectral features in the cecum and colon as compared to other regions (Tables 2.1 and 2.2). It is interesting that while the large intestines have a lower abundance of identified metabolites, there are significantly more features, which likely leads to greater diversity in the spectral features in this region.

2.4.1 High fat diet influences purine metabolite abundances

The alterations in the relative abundance of purine metabolites within the large intestine contents of mice from the HF study are intriguing as these compounds are the building blocks for nucleic acids and cofactors, which are important for energy metabolism. Additionally, a previous study, which investigated the impact of various diets on both male and female mice found that purine metabolites were impacted in liver tissues.[88] Purine metabolites are regulated in mammalian cells primarily through salvage pathways, but also *de novo* biosynthesis and purine degradation pathways.[99] However, as the metabolites leading into these pathways (ex. AICAR, IMP, and uric acid) are not significantly different between HF and LF_{HF} diets in this study, alterations in mammalian purine metabolite regulation seems an unlikely explanation. Another possible reason for these alterations is different abundances of purine metabolites in the diets, but as the diets in this study were nutritionally matched, this also seems an unlikely. While these metabolites are altered between HF and LF_{HF} diets, and an integral part of primary metabolism, there is not sufficient evidence in this study to suggest a causative relationship between these metabolite abundances and the negative effects of HF diet.

2.4.2 Fenugreek induces considerable changes in the large intestines

Although fenugreek-induced alterations are less obvious in the small intestines, the large intestines display fenugreek-induced alterations which are undeniable. PLS-DA analyses of the metabolite profiles associated with the four diets from the HF study for each intestinal region highlight the significant differences in the metabolome of the cecum and colon metabolites between mice fed either HF or LF_{HF} diet and each supplemented with fenugreek. These PLS-DA analyses (Fig. 2.5) show very similar separation, and from the VIP scores (Appendix Fig. 2.18), it was determined that of the top 10 metabolites contributing most to the separations, five metabolites are shared between cecum and colon. From these data, it can be concluded that fenugreek has a dramatic effect on the metabolome of the large intestines in conjunction with a HF diet. In these same PLS-DA analyses of

identified metabolites (Fig. 2.5A & C) while HF and LF_{HF} diet groups are separated, the greater separation is found as a result of FG supplementation. This reiterates that fenugreek has a significant influence on the metabolome of the large intestines. The metabolome is representative of and informs about the phenotype, thus the similarities between the HF study metabolite profiles in the cecum and colon are suggestive of similar microbial activity and response to fenugreek in these regions.

As in the HF study, the metabolite profiles from the large intestinal contents in the WD study reveal significant alterations as a result of fenugreek supplementation. The PLS-DA analyses of the identified metabolites from either cecum or colon contents, and total features from the cecum contents show distinct groupings between WD and WDFG groups (Figs. 2.8). Interestingly, in these same PLS-DA plots, there is no separation between the LF_{WD} and LF_{WD}FG groups. Additionally, the WDFG group tends to be more similar to the LF_{WD} groups than the WD group, but this trend is not present in the PLS-DA analysis of the total features from the colon contents (Fig. 2.8D). In another similarity with the HF study, five of the top ten VIP scored metabolites are shared between the two regions, revealing the comparable effect of fenugreek in the cecum and colon (Appendix Fig. 26). These results suggest that fenugreek may be providing some resiliency to the negative effects of WD, and that this effect could be more substantial in the cecum contents than in the colon contents.

The metabolomics data correspond with microbial data described previously, in which the fecal microbiome populations were sequenced after exposure to fenugreek.[81] In this former study, which was designed similar to the present study, mice were given either HF or LF diet each with and without fenugreek (2% w/w) for 16 weeks. After fecal microbiome samples were sequenced, 410 operational taxonomic units (OTUs) were found to be common to all mice. HF diet significantly altered 147 OTUs, but 50 OTUs were restored by fenugreek supplementation. Further analyses of these OTUs found that many were from the Firmicutes phylum and are predictive of metabolic function.[81] While metabolites cannot be traced to

specific bacterial or intestinal origins, the differences observed in the metabolome often parallel changes in the microbiome. Additionally, as the microbiome is well known to alter the mammalian host function and the most significant metabolome differences were in the large intestine, it follows that fenugreek more significantly alters the metabolic function in the large intestines than the small intestines.

2.4.3 Liver and serum metabolomes are affected by fenugreek

While the metabolic profile changes in the livers of mice given diets supplemented with fenugreek are less dramatic than in the intestine, it is a significant observation. Despite well-regulated pathways found in the liver regardless of dietary changes, our analysis revealed distinct metabolic profiles indicating that fenugreek does alter the liver metabolome in the HF and WD studies. These global metabolome changes are more likely due to relative abundance differences than different metabolites detected. In fact, the sum of the relative abundance of all identified metabolites is lower in livers of the HFFG-fed mice, than the HF-fed mice, however in contrast, the sum of the relative abundance of all identified metabolites is higher in the livers of WDFG-fed mice, than the WD-fed mice (Appendix Fig. 2.31). Of the metabolites with significant p-values, there are more that have decreased than increased with fenugreek in HF-fed mice, but more that have increased with fenugreek in WD-fed mice (Tables 2.1 & 2.2). These contrasting results highlight that fenugreek may influence the mammalian host metabolism, particularly in the liver, in a diet dependent fashion.

When considering the effects of particular diets or supplements, it is important to assess the availability of nutrients in circulation. This study included the analysis of the metabolites and small molecules found in both the serum and the liver. It is beneficial to consider both, as the liver works to detoxify blood from the intestines before entering circulation. Nearly all detected metabolites from the liver display lower abundance in HFFG-fed mice as compared to HF-fed mice, while more serum metabolites display higher abundance with fenugreek (Appendix Fig. 2.32). This trend is reversed in the WD study, where more metabolites detected in the

liver display higher abundance in WDFG-fed mice than in WD-fed mice, while in the serum, more metabolites were detected in lower abundance with fenugreek (Appendix Fig. 2.33). In particular, in the HF study, allantoate and 5-methyltetrahydrofolate are significantly lower abundance with fenugreek supplementation in the liver, but not in serum. Allantoate is involved with purine degradation which produces urea and is a plant metabolite which is involved in storage and transport of fixed nitrogen, while 5-methyltetrahydrofolate is involved in the synthesis of methionine and regulation of homocysteine.[100-102] A possible explanation for the decreased abundance in the liver, is increased utilization of these metabolites. However, glycodeoxycholate is a metabolite which was significantly more abundant in livers of fenugreek mice in the HF study. Again, in the serum, glycodeoxycholate was not detected, but the bile salt taurodeoxycholate was detected and in a higher abundance in HF-fed compared to HFFG-fed mice (Appendix Fig. 2.32). As these bile salts are synthesized from cholesterol, they could potentially be involved in the decrease of total cholesterol in fenugreek-supplemented mice.

In the WD study serum metabolome, one metabolite, xanthine, in particular stands out due to the large differences in abundance between the dietary groups. Xanthine was detected with nearly 20-fold higher abundance in WDFG-fed mice than in WD-fed mice (Appendix Fig. 2.34A). This is intriguing as hypoxanthine is oxidized to xanthine by xanthine oxidase, through which process reactive nitrogen and oxygen species are produced. This is significant, as reactive oxygen species can cause oxidative stress and increased xanthine oxidase activity has been correlated to hypertension, dyslipidemia, and insulin resistance.[103] However, xanthine is also involved in nitrogen, and more specifically purine metabolism and degradation. The increase in abundance of this metabolite, rather than a result of increased xanthine oxidase activity, could also be a result of decreased utilization of xanthine. Additionally, similar to the HF study liver metabolomes, a bile acid, cholate, was detected with noticeably different abundances in the livers of WD- and WDFG-fed mice (Appendix Fig. 2.34B). However, unlike the HF-fed mice,

cholate was found to be more abundant in the mice not supplemented with fenugreek. These results reported from liver and serum metabolomics provide insight to how the circulating metabolite levels may be altered by fenugreek in a diet dependent fashion.

2.4.4 Fenugreek impacts specific pathways by location and diet

A more in depth look at the metabolomics data reported in this study reveals specific pathways and metabolites that may be more significantly contributing to the beneficial effects of fenugreek. For instance, carnitine biosynthesis and its relative abundance are significantly increased by fenugreek supplementation in the large intestines of mice in the HF study. The differences in carnitine abundances is intriguing as this dipeptide, composed of methionine and lysine, has an important role in lipid transport and fatty acid metabolism.[104-106] This metabolite is synthesized in the liver, kidneys, and brain, but the majority is absorbed from dietary sources such as red meat.[104, 106] As carnitine is used for fatty acid oxidation and energy metabolism, the highest physiological concentrations of carnitine occur in muscular tissues, specifically cardiac and skeletal muscle.[105-106] However, nearly all carnitine is absorbed through the small intestine and the remaining fraction is metabolized by bacteria in the large intestine, making it uncommon to detect carnitine in the large intestine.[104] Excess carnitine in the intestines can be problematic as gut microbiota degrade carnitine into trimethylamine (TMA) which is oxidized to trimethylamine *N*-oxide (TMAO) which promotes atherosclerosis.[107] However, due to technical limitations, TMA and TMAO were not included in this study. Carnitine deficiency, can also be concerning as it has been associated with diabetes, cardiomyopathy, and obesity, as well as other conditions.[106] Further studies will be needed to focus more on this metabolite and how it specifically relates to the beneficial effects of fenugreek.

Similar to the HF study, the metabolism of another dipeptide, carnosine which is composed of alanine and histidine, was influenced by fenugreek. In the large intestinal samples, homocarnosine is significantly decreased in WD-fed mice

relative to LF_{WD}-fed mice and reversed (increased) by fenugreek supplementation to WD-fed mice. This metabolite is suggested to have antioxidant properties, and is commonly found in brain cells.[108-109] However, other metabolites which are reduced in the large intestinal contents of WD-fed mice relative to LF_{WD}-fed mice, and then reversed with fenugreek supplementation include 6-phospho-D-gluconolactone, glucose phosphate, gluconolactone, and myo-inositol. One of the defining characteristics of a western style diet is elevated sucrose consumption. As all four of these WD-altered and FG-reversed metabolites are related to glucose metabolism, a possible explanation of the anti-diabetic effects of fenugreek may be attributed to enhanced break down and metabolism of sucrose.

Besides carnitine metabolism, other pathways affected by fenugreek in the HF study include cholesterol and bile acid metabolism, as well as arginine biosynthesis and the urea cycle. While these pathways have important roles in the liver, the magnitude of the impact fenugreek had on these pathways varies by sample location. Using MetaboAnalyst's pathway analysis feature, arginine biosynthesis was determined to be the most significantly impacted pathway from these studies, but glycodeoxycholate, a bile salt, most significantly contributed to differences in the metabolic profiles of the livers of HF-fed and HFFG-fed mice.[110] In particular, this indicates that cholesterol metabolism and bile acids may be of more influence and experience more modifications in the liver, but arginine biosynthesis, while affected in all samples analyzed, show the most differences in the cecum and colon contents. These pathways serve important functions and metabolic benefits, however there is no known connection between them. Bile acids and bile salts are primarily used to transport lipids through the intestines, and arginine assists in regulation of nitric oxide (NO) and nitrogen waste. L-Arginine has potential for use in treating several health conditions such as atherosclerosis and hypertension, cardiovascular disease, and Type 2 diabetes, because of its role in the urea cycle and NO regulation.[111-112] This suggests that the beneficial effects of fenugreek may not be the result of a single altered pathway, but rather a combination of pathways.

It is also significant to note the high numbers of features detected with only a fraction identified. Within this fraction, many metabolites were impacted by fenugreek, however the profiles of the unidentified features are even more distinct than the identified metabolites. This shows how important these features are and how both HF and WD diets, and fenugreek supplementation alter the small molecules, despite the lack of knowledge of these features. When both the identified and unidentified features are considered, it is clear that the small molecule metabolome is shaped by fenugreek which implies alterations within the microbiome, and thus impacting the overall host function due to fenugreek supplementation.

2.5 Methods

2.5.1 Animals and diets

Eighty male C57BL/6J mice were randomly divided between two studies investigating the effects of fenugreek on unhealthy diets, specifically a 60% high fat diet study and a western style diet study. The mice were purchased from Jackson Laboratories at 8 weeks of age (WOA) and fed chow diet until they were randomized at 9 WOA into the experimental diet groups. In the HF diet study, the groups were: 1) 60% high fat diet (HF; n=11), 2) HF diet with fenugreek (HFFG; n=11), 3) nutritionally matched (to HF) low fat diet (LF_{HF}; n=11), or 4) LF diet with fenugreek ($LF_{HF}FG$; n=7). For the WD study the groups were: 1) a Western style diet (WD; n=12), 2) WD with fenugreek (WDFG; n=12), 3) nutritionally matched (to WD) low fat diet (LF_{WD}; n=8), or 4) LF diet with fenugreek ($LF_{WD}FG$; n=8). As previously described,[80-81] fenugreek-supplemented diets were prepared at Research Diets Inc. by adding 2% w/w ground fenugreek seed powder to the respective experimental and control diets prior to pelleting (Table 2.3).

Table 2.3 Summary of diets and animals per diet for fenugreek studies

Diets with and without fenugreek supplementation

No. of replicates	Diet	Fenugreek	Research Diets p/n
11	HF	no	D12492i
11	HF	yes	D18121403i
11	LF_{HF}	no	D12450Ji
7	LF_{HF}	yes	D18121402i
12	WD	no	D12079Bi
12	WD	yes	D18121405i
8	LF_{WD}	no	D14042701i
8	LF_{WD}	yes	D17121404i

The fenugreek seeds used were fully characterized at Rutgers University by the Botanical Dietary Supplements Research Center (http://www.botanical.pbrc.edu/institutions.html). The mice were fed the indicated diets for 14 weeks prior to euthanasia and subjected to assessment of metabolic parameters including weight gain, adiposity, total cholesterol, high-density lipoprotein (HDL), and low-density lipoprotein (LDL). Body weight/adiposity data were collected regularly throughout the study. Serum, liver, and intestine sections were collected at euthanasia. Intestinal contents were isolated from the jejunum, ileum, cecum, and colon for metabolomics. These studies were conducted in strict accordance with the National Institutes of Health guidelines on the care and use of laboratory animals, and all experimental protocols were approved by the Institutional Animal Care and Use Committee at Pennington Biomedical Research Center.

2.5.2 Metabolic phenotyping

Body composition was measured using a Bruker minispec LF110 NMR analyzer (Bruker Optics, Billerica, MA) as previously described.[80] All mice were fed indicated diets for 14 weeks and then euthanized by decapitation under deep isoflurane anesthesia following a 5-hour fast. Fasting levels of HDL and LDL cholesterol as well as total cholesterol were measured using colorimetric assays (Wako Chemicals, Richmond, VA) from serum samples collected at euthanasia.

2.5.3 Metabolite extractions

Prior to extraction of water-soluble metabolites, serum samples and pulverized liver samples, jejunum contents, ileum contents, cecum contents, and colon contents were pre-weighed. The extraction procedure was adapted from Rabinowitz and Kimball.[57] All solvents used were HPLC grade. The pre-weighed samples were mixed with 1.3 mL of extraction solvent (4:4:2 acetonitrile: methanol: water with 0.1 M formic acid). The mixture was allowed to extract for 20 minutes at -20 °C. The mixture was centrifuged, and the supernatant collected. To the

remaining pellet, an additional 200 µL of extraction solvent was added and extracted for 20 minutes at -20 °C. This mixture was centrifuged and supernatants from both extraction steps were combined and dried under nitrogen. The dried samples were resuspended in 300 µL of water prior to mass analysis.

2.5.4 UHPLC-HRMS

The chromatographic and mass spectral analysis was performed according to an established method using ultra-high performance liquid chromatography coupled to high resolution mass spectrometry (UHPLC-HRMS).[58] The resuspended metabolites were stored at 4°C in an UltiMate 3000 RS autosampler (Dionex, Sunnyvale, CA) until analysis. Samples were analyzed with duplicate injections. All solvents used were HPLC grade (Fisher Scientific, Hampton, NH). Reversed phase separations were carried out using a Synergi 2.6 µm Hydro RP column (100 mm x 2.1 mm, 100 Å; Phenomenex, Torrance, CA) and an UltiMate 3000 pump (Dionex). The chromatography utilized a 25-minute gradient elution as described previously[58] with a water:methanol solvent system and a tributylamine ion pairing reagent. The separated metabolites were ionized via negative mode electrospray ionization prior to analysis on an Exactive Plus Orbitrap MS (Thermo Scientific, San Jose, CA). The full scan analysis was performed as described previously.[58]

2.5.5 Metabolomics Data Processing

Initial raw spectral files, which were generated by Thermo's Xcalibur software, were converted to mzML format using the msConvert package from ProteoWizard.[59] After converting these files, Metabolomic Analysis and Visualization Engine (MAVEN) (Princeton University) was used for data processing.[60-61] This software was used for retention time correction and peak alignment. Metabolites were manually identified and annotated by comparing the exact mass (±5 ppm) and retention times to an in-house standard library. The unidentified spectral features were automatically selected, and isotope and adduct

peaks annotated using XCMS and CAMERA R packages.[62-63, 113] Before further processing the adduct and isotope peaks were removed, and only features with a signal/blank ratio of 3 or greater in at least half of the biological replicates for at least one diet were used for further analyses and are reported here.

2.5.6 Statistical Analysis

All spectral data were normalized according to mass and background subtracted. Heatmaps display $\log_2$ fold changes and p-values determined by a Student's T-test and were prepared using R (version 4.0.3).[64] The normalized data were filtered via interquartile range (IQR), log transformed, and Pareto scaled via MetaboAnalyst 5.0 before partial least squares discriminant analysis (PLS-DA) was performed using the same software.[65, 110] After PLS-DA was performed, the plots were cross validated using 10-fold cross validation via MetaboAnalyst 5.0.[114-115] Venn diagrams were prepared using an open source software, Venny 2.1.[116] Bar graphs were prepared using R version 4.0.3. For the unidentified spectral features, those with a fold change greater than 1.5 or less than 0.667 and p-value below 0.05, were used for Fiehn's Seven Golden Rules analysis to determine potential molecular formulas.[117] Formulas were constricted to a mass accuracy of 5 ppm and only the following elements: C, H, N, O, P, S, and Cl.

2.6 Conclusions

The metabolic profile of the contents of four intestinal regions (jejunum, ileum, cecum, and colon), the liver tissues, and serum of mice were analyzed to determine the effects of fenugreek on the structure and function on the mammalian host. However, this study was limited in that only male mice were used, preventing analysis of sex-based differences in the impact of fenugreek. The results from this study reveal insight into the effects of fenugreek on the gut metabolome, in the presence of either HF or WD diets. Specifically, the most metabolic alterations were found to occur in the large intestines and small, but significant metabolic alterations were found in the liver and serum. Additionally, discrete pathways were

more significantly affected by fenugreek, including carnitine biosynthesis, antioxidant activity, glucose metabolism, bile acid and cholesterol metabolism, and arginine biosynthesis.

Appendix

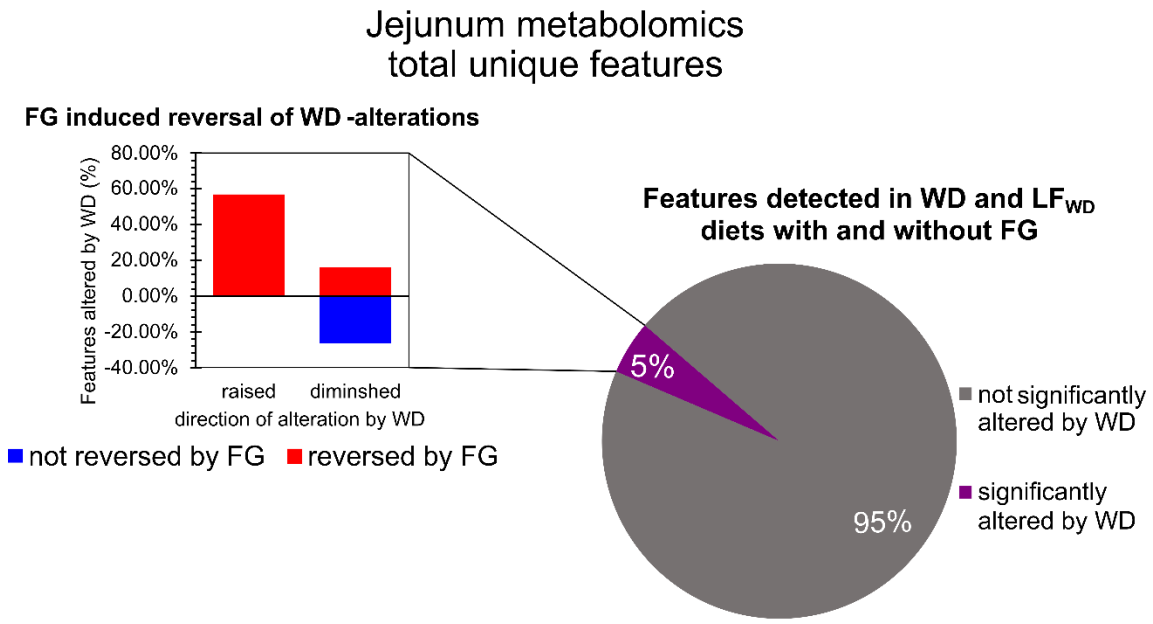


Figure 2.16 Only 5% of unique spectral features detected in metabolomics investigations of jejunum contents of mice were significantly different in WD-fed mice compared to LF_{WD} fed mice. Of these features, over 50% were detected with higher abundance in WD-fed mice relative to LF-fed mice, but lower abundance in WDFG-fed mice relative to WD-fed mice.

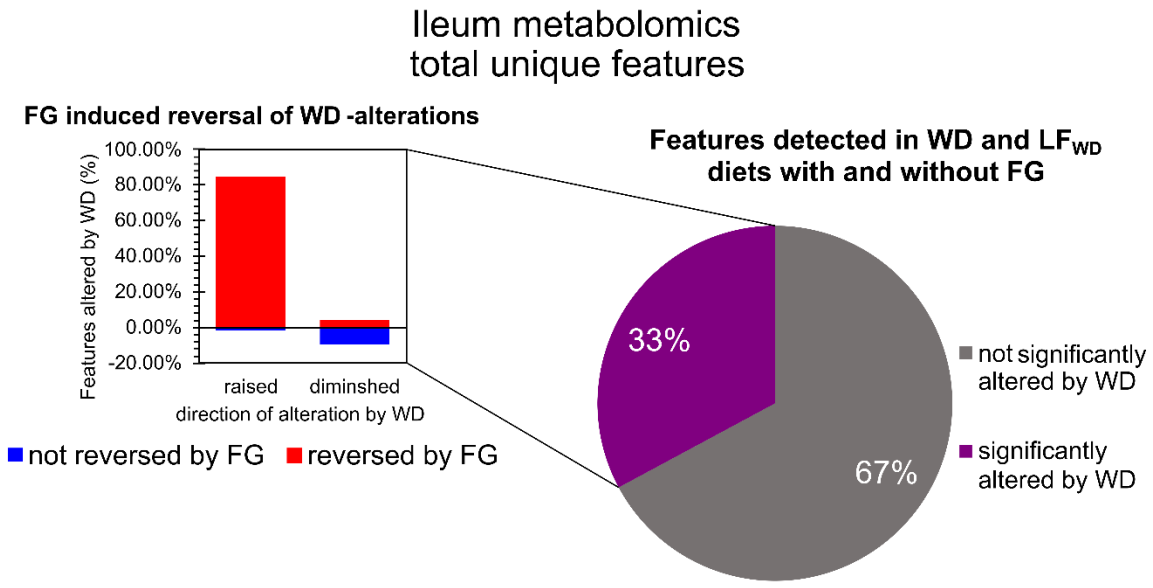


Figure 2.17 A third of unique spectral features detected in metabolomics investigations of ileum contents of mice were significantly different in WD-fed mice compared to LF_{WD} fed mice. Of these features, over 80% were detected with higher abundance in WD-fed mice relative to LF-fed mice, but lower abundance in WDFG-fed mice relative to WD-fed mice.

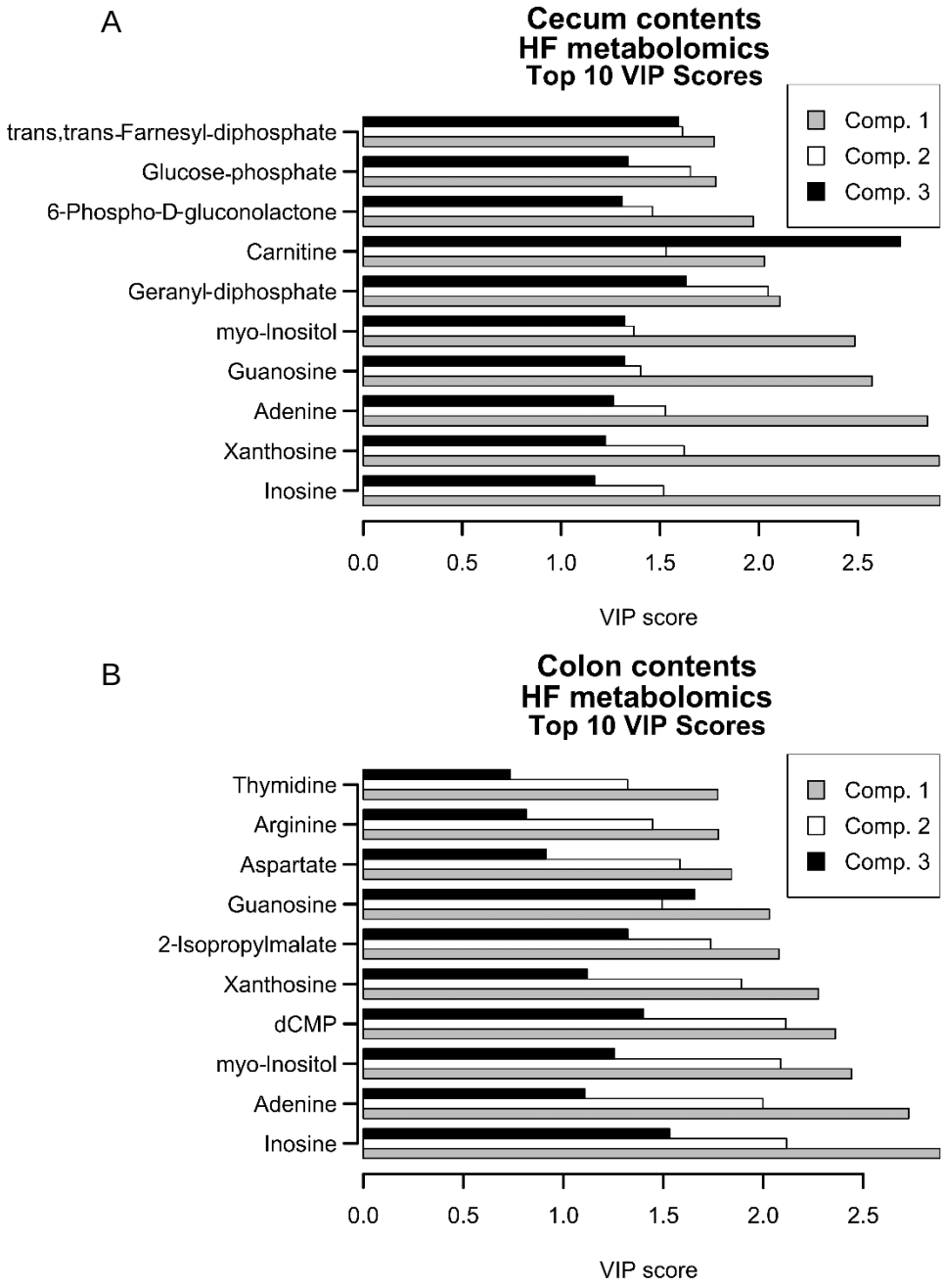


Figure 2.18 Top 10 metabolites with the highest VIP scores from PLS-DA of (A) cecum contents and (B) colon contents comparing LF_{HF}, $LF_{HF}FG$, HF and HFFG diets. VIP scores for components 1-3 are shown.

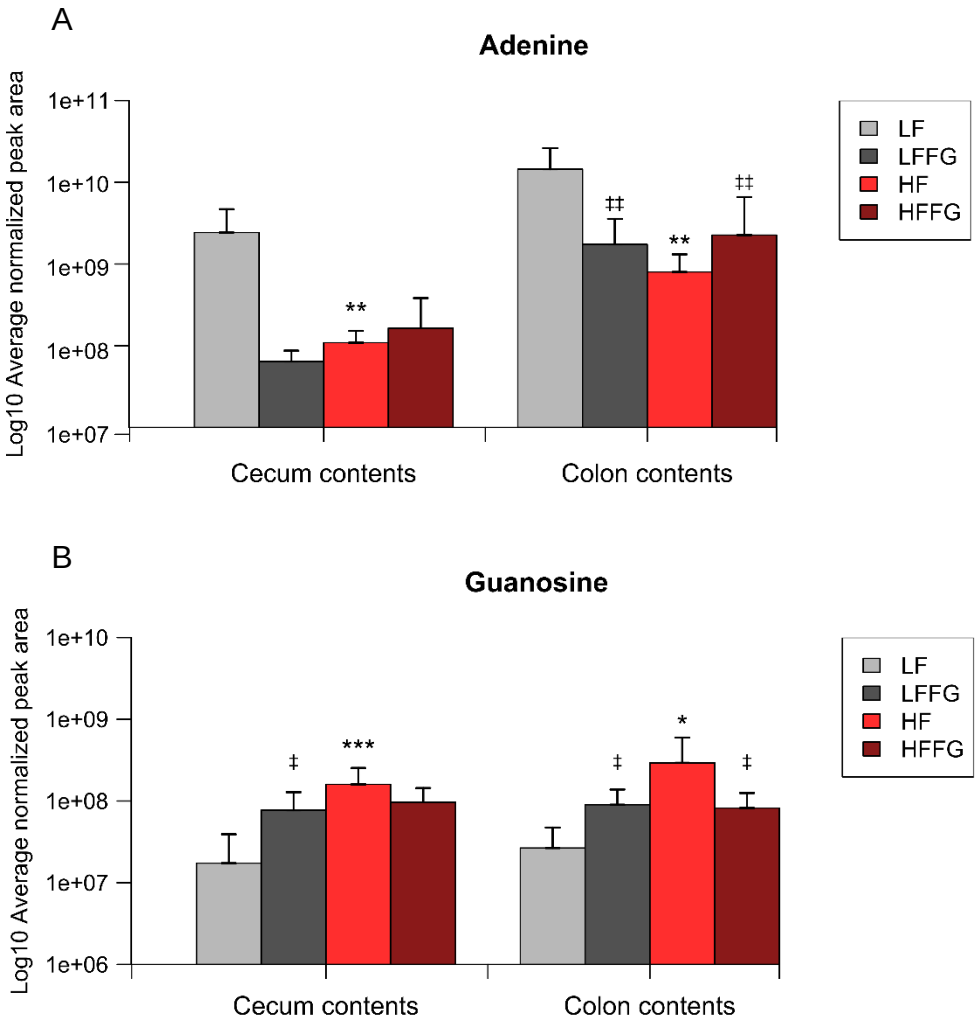


Figure 2.19 Normalized intensities of (A) adenine and (B) guanosine from both cecum and colon data from HF-, HFFG-, LF_{HF}-, and $LF_{HF}FG$-fed mice. Data was normalized according to mass and the normalized peak area is represented on a $\log_{10}$ scale as mean ± standard deviation. Significance was determined using a Student's t-test. Significance is represented as *p<0.05, **p<0.01, ***p<0.001, and ****p<0.0001 for comparisons against respective LF groups or ‡ p<0.05, ‡‡ p<0.01, ‡‡‡ p<0.001, and ‡‡‡‡ p<0.0001 for comparisons against either HF or LF_{HF}, respectively.

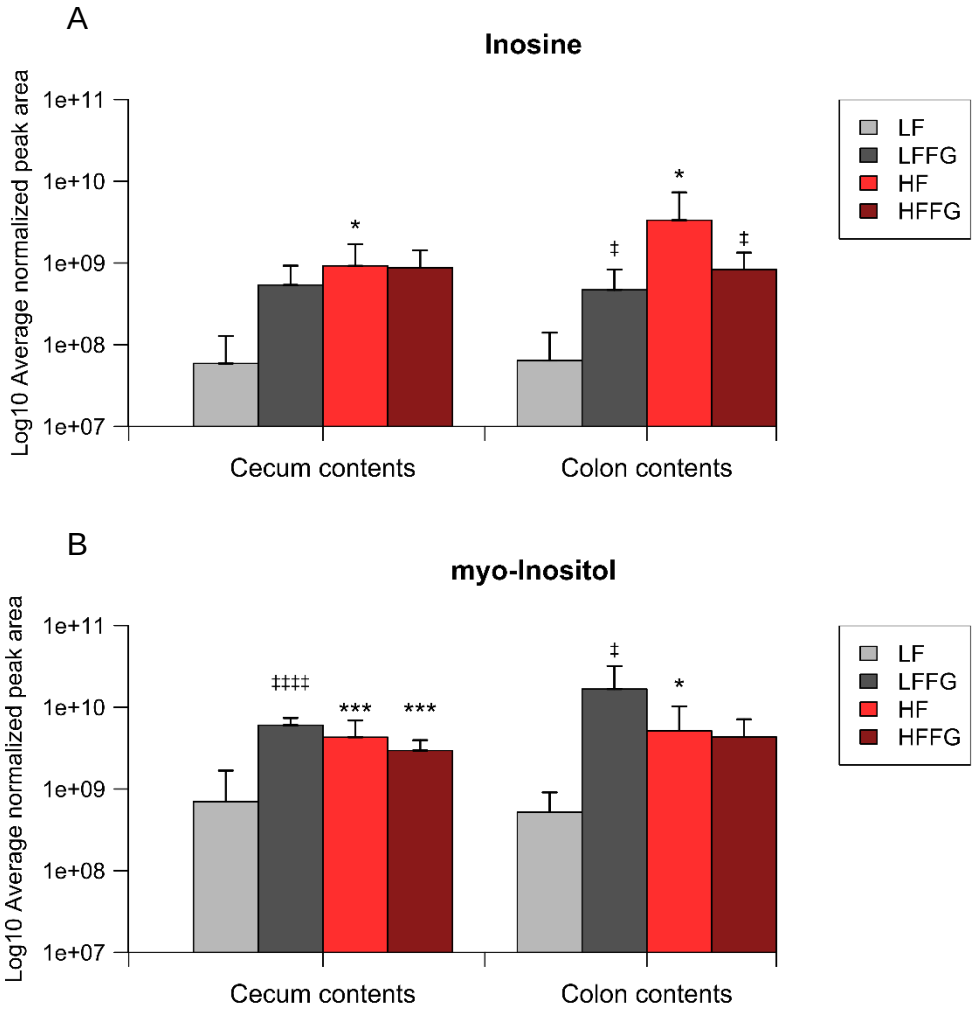


Figure 2.20 Normalized intensities of (A) inosine and (B) myo-inositol from both cecum and colon data from HF-, HFFG-, LF_{HF}-, and $LF_{HF}FG$-fed mice. Data was normalized according to mass and the normalized peak area is represented on a log_{10} scale as mean ± standard deviation. Significance was determined using a Student's t-test. Significance is represented as *p<0.05, **p<0.01, ***p<0.001, and ****p<0.0001 for comparisons against respective LF groups or ‡ p<0.05, ‡‡ p<0.01, ‡‡‡ p<0.001, and ‡‡‡‡ p<0.0001 for comparisons against either HF or LF_{HF}, respectively.

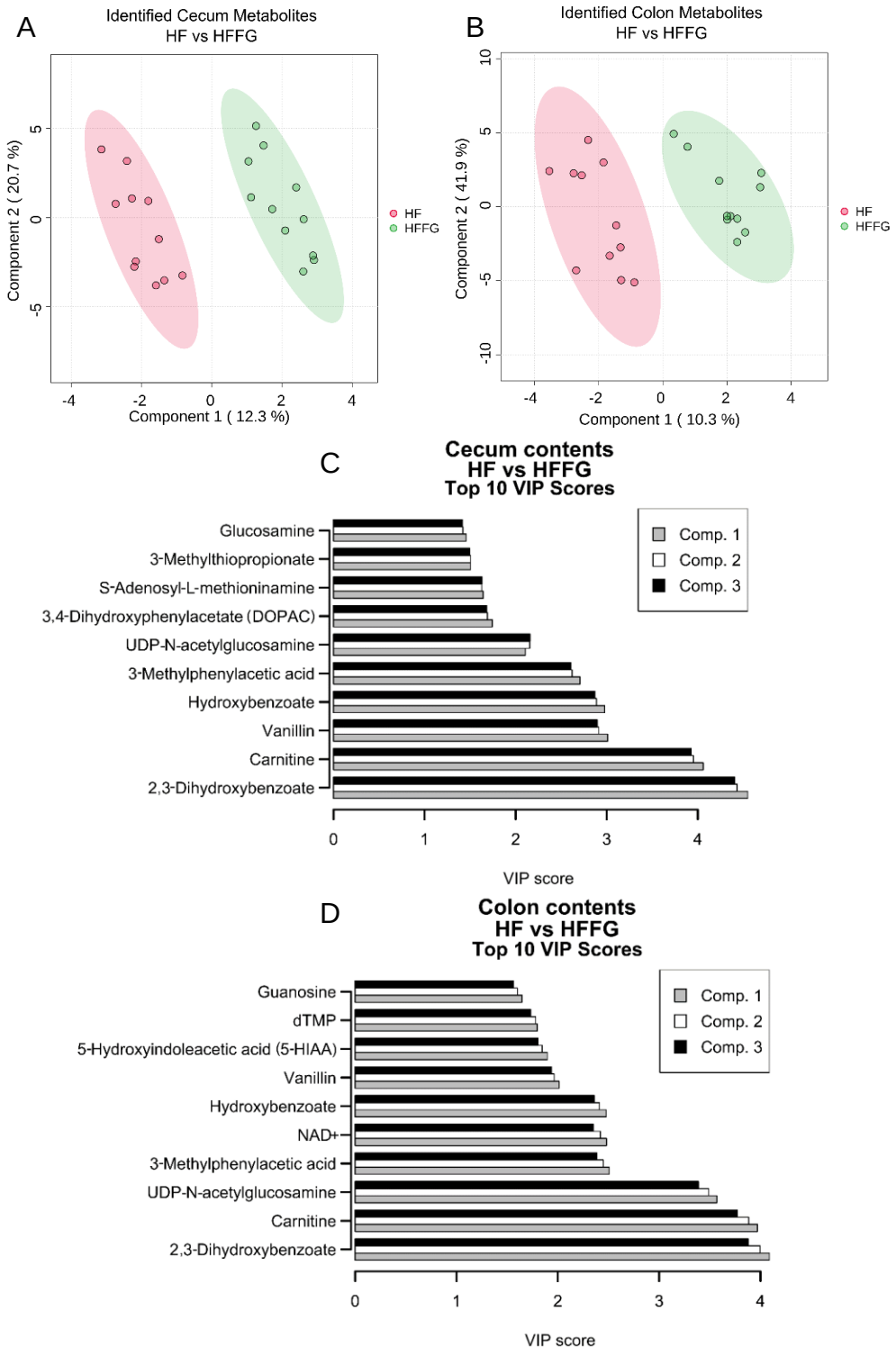


Figure 2.21 Pairwise PLS-DA of identified metabolites from (A) cecum contents and (B) colon contents of HF- and HFFG-fed mice. Experimental replicates and 95% confidence intervals are shown. Top 10 metabolites with highest VIP scores are shown for (C) cecum contents and (D) colon contents.

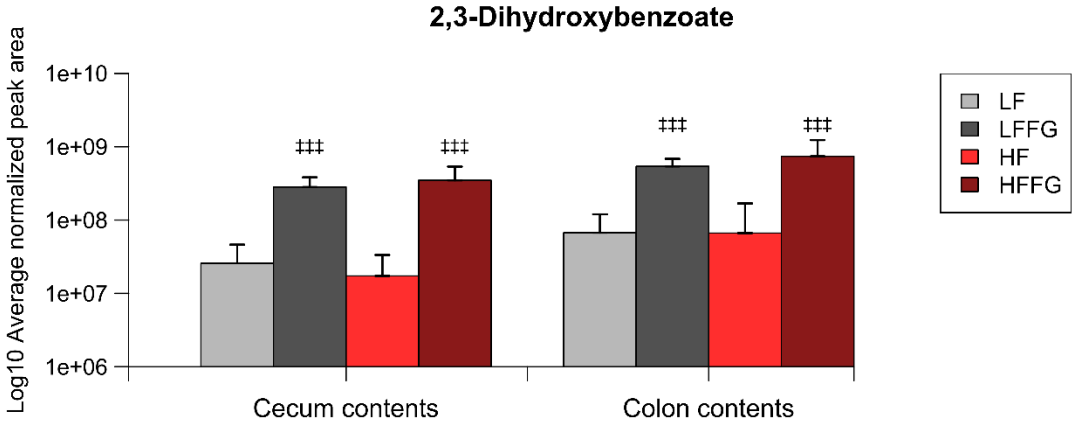


Figure 2.23 Normalized intensities of 2,3-dihydroxybenzoate from both cecum and colon data from HF-, HFFG-, LF_{HF}-, and $LF_{HF}FG$-fed mice. Data was normalized according to mass and the normalized peak area is represented on a log_{10} scale as mean ± standard deviation. Significance was determined using a Student's t-test. Significance is represented as *p<0.05, **p<0.01, ***p<0.001, and ****p<0.0001 for comparisons against respective LF groups or ‡ p<0.05, ‡‡ p<0.01, ‡‡‡ p<0.001, and ‡‡‡‡ p<0.0001 for comparisons against either HF or LF, respectively.

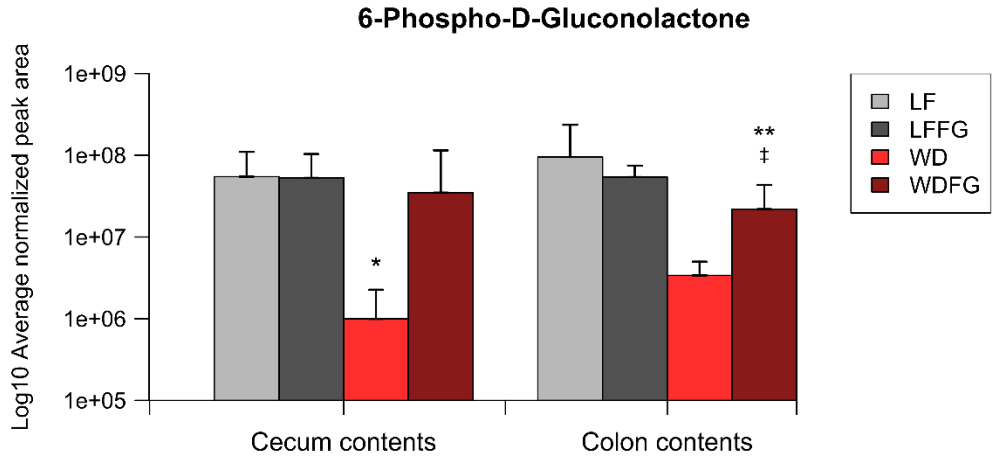


Figure 2.22 Normalized intensities of 6-phospho-D-gluconolactone from both cecum and colon data from WD-, WDFG-, LF_{WD}-, and $LF_{WD}FG$-fed mice. Data was normalized according to mass and the normalized peak area is represented on a log_{10} scale as mean ± standard deviation. Significance was determined using a Student's t-test. Significance is represented as *p<0.05, **p<0.01, ***p<0.001, and ****p<0.0001 for comparisons against respective LF groups or ‡ p<0.05, ‡‡ p<0.01, ‡‡‡ p<0.001, and ‡‡‡‡ p<0.0001 for comparisons against either HF or LF, respectively.

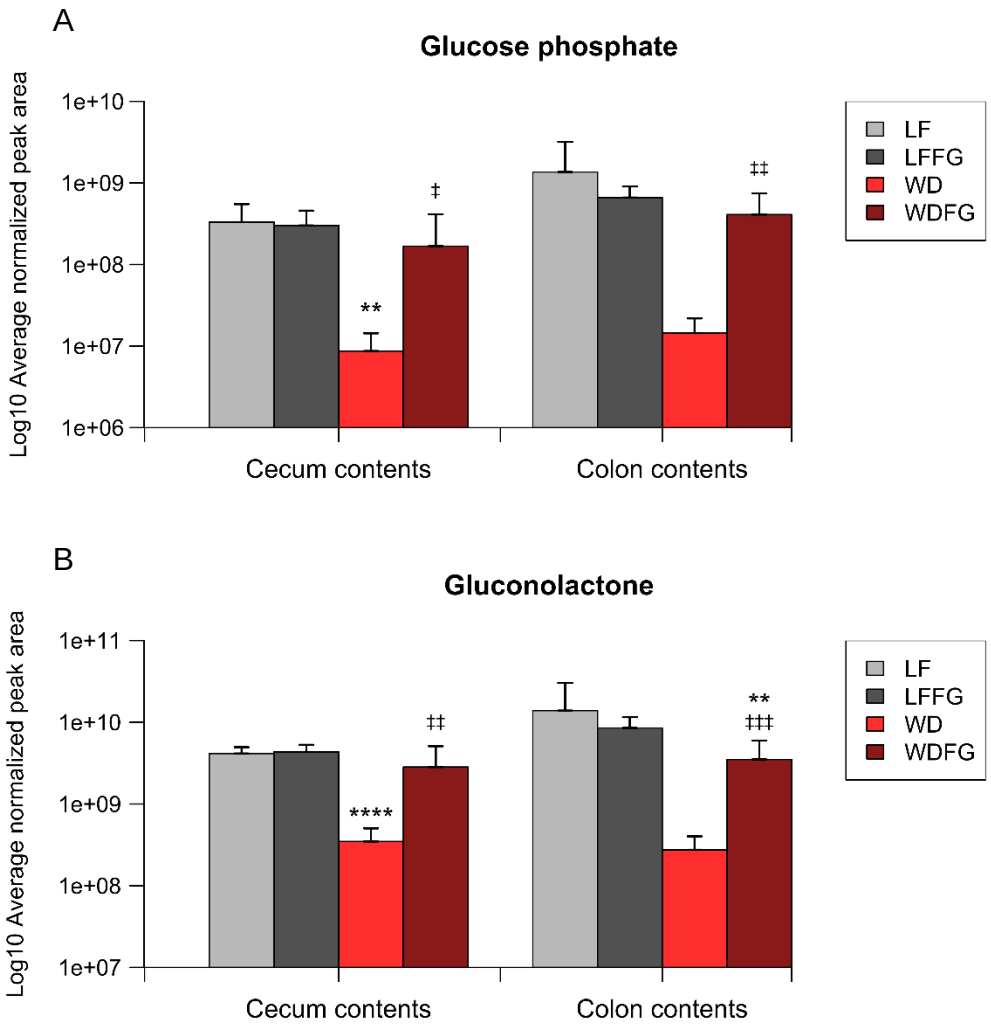


Figure 2.24 Normalized intensities of (A) glucose phosphate and (B) gluconolactone from both cecum and colon data from WD-, WDFG-, LF_{WD}-, and $LF_{WD}FG$-fed mice. Data was normalized according to mass and the normalized peak area is represented on a log_{10} scale as mean ± standard deviation. Significance was determined using a Student's t-test. Significance is represented as *p<0.05, **p<0.01, ***p<0.001, and ****p<0.0001 for comparisons against respective LF groups or ‡ p<0.05, ‡‡ p<0.01, ‡‡‡ p<0.001, and ‡‡‡‡ p<0.0001 for comparisons against either WD or LF_{WD}, respectively.

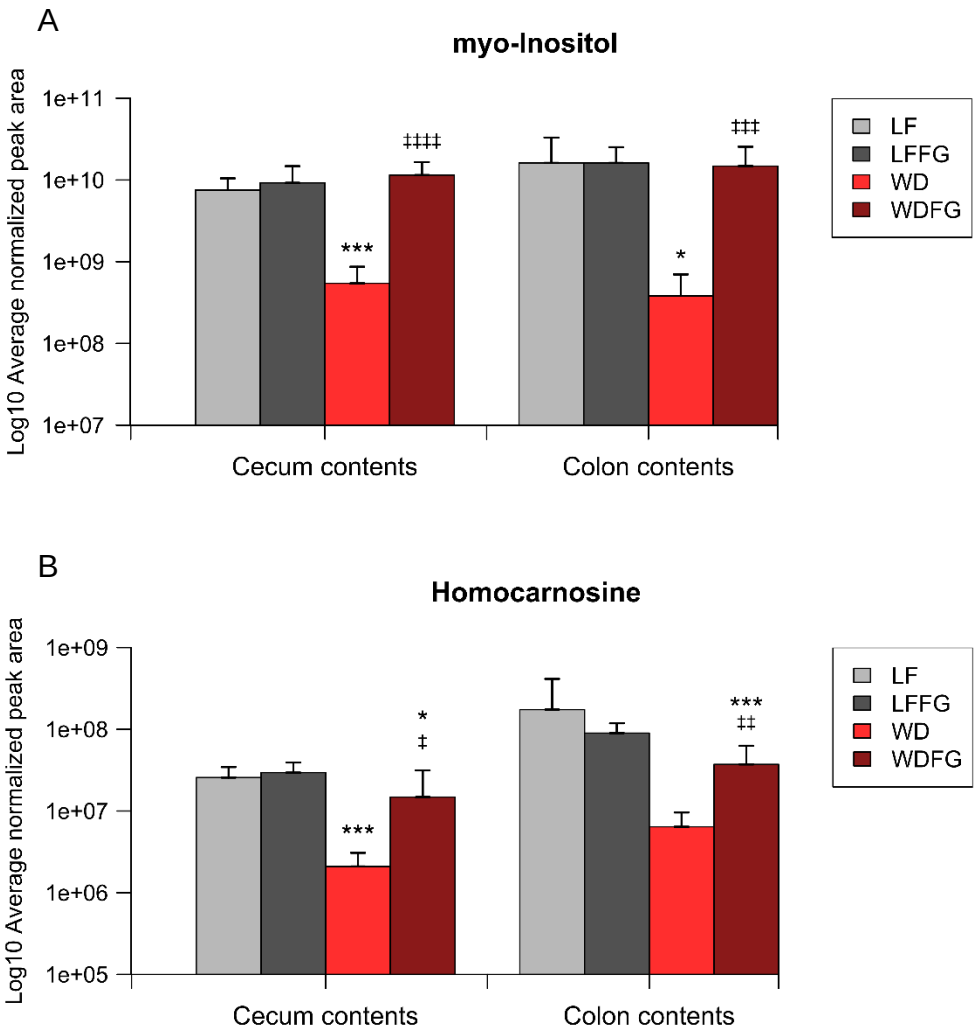


Figure 2.25 Normalized intensities of (A) myo-inositol and (B) homocarnosine from both cecum and colon data from WD-, WDFG-, LF_{WD}-, and $LF_{WD}FG$-fed mice. Data was normalized according to mass and the normalized peak area is represented on a log_{10} scale as mean ± standard deviation. Significance was determined using a Student's t-test. Significance is represented as *p<0.05, **p<0.01, ***p<0.001, and ****p<0.0001 for comparisons against respective LF groups or ‡ p<0.05, ‡‡ p<0.01, ‡‡‡ p<0.001, and ‡‡‡‡ p<0.0001 for comparisons against either WD or LF_{WD}, respectively.

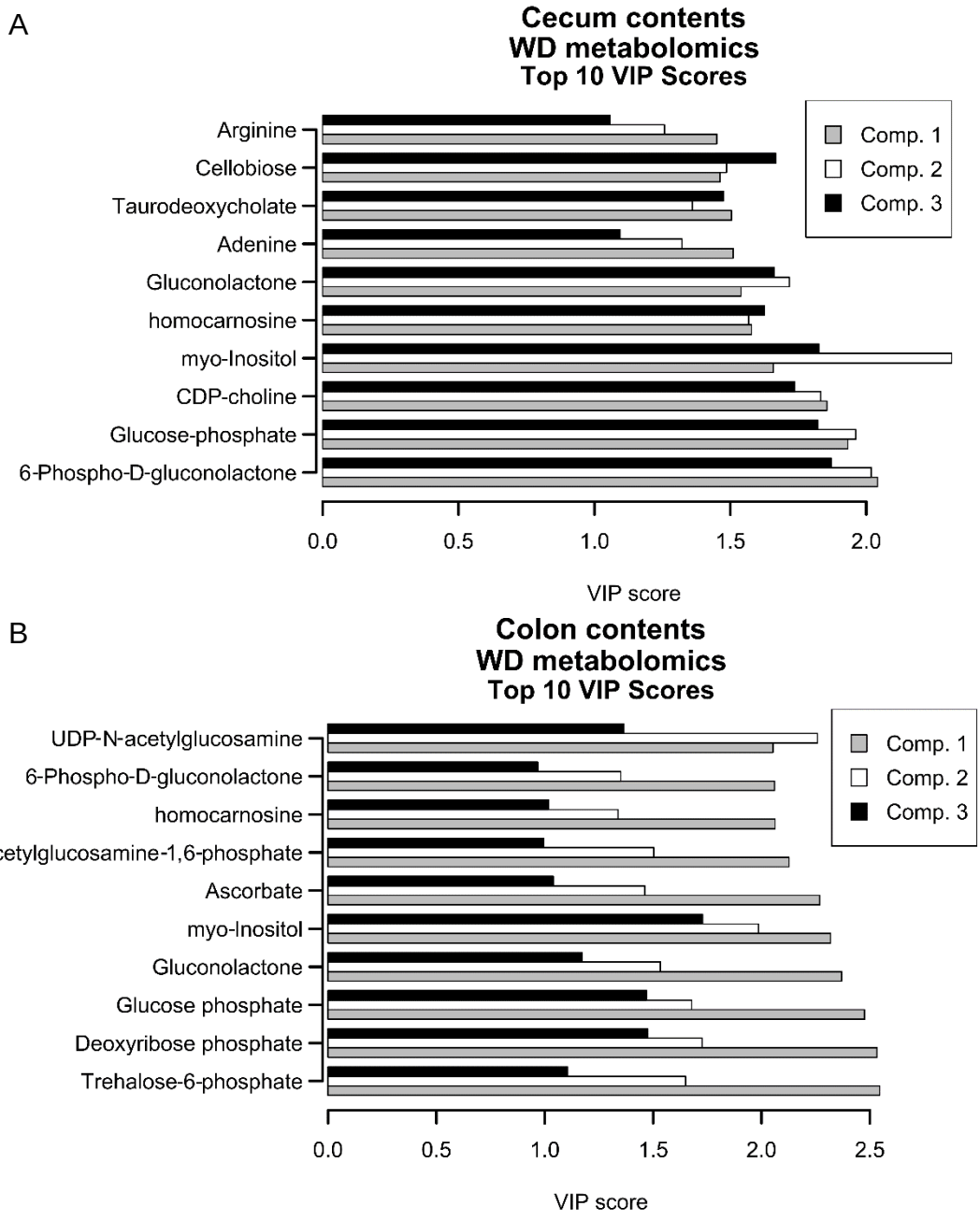


Figure 2.26 Top 10 metabolites with the highest VIP scores from PLS-DA of (A) cecum contents and (B) colon contents comparing LF_{WD}, $LF_{WD}FG$, WD and WDFG diets. VIP scores for components 1-3 are shown.

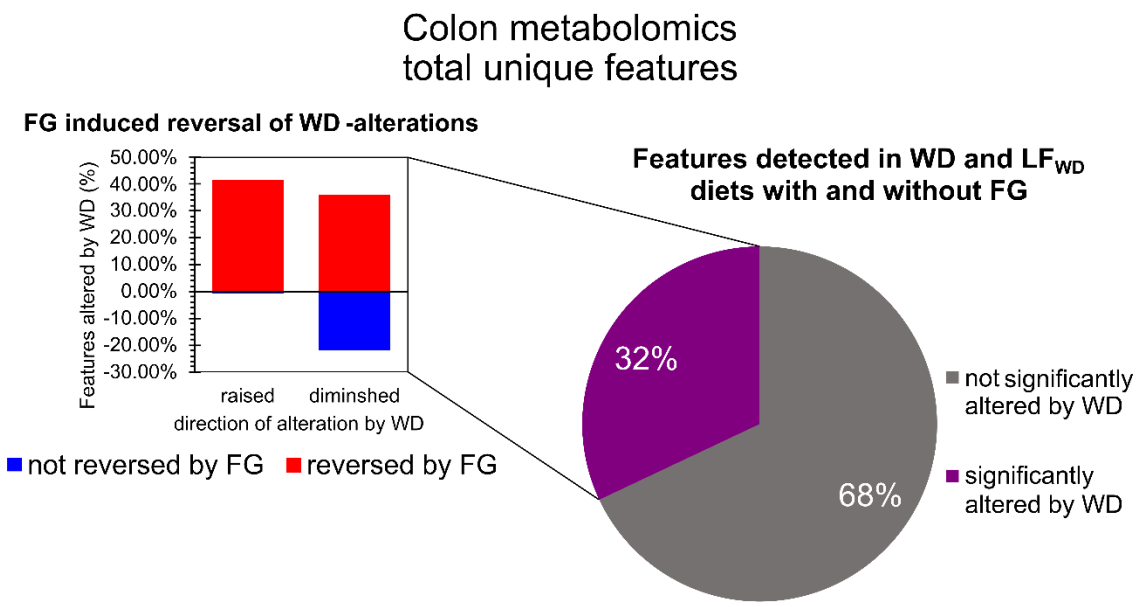


Figure 2.27 Nearly one third of unique spectral features detected in metabolomics investigations of colon contents of mice were significantly different in WD-fed mice compared to LF_{WD} fed mice. Of these features, around 40% were detected with higher abundance in WD-fed mice relative to LF-fed mice, but lower abundance in WDFG-fed mice relative to WD-fed mice.

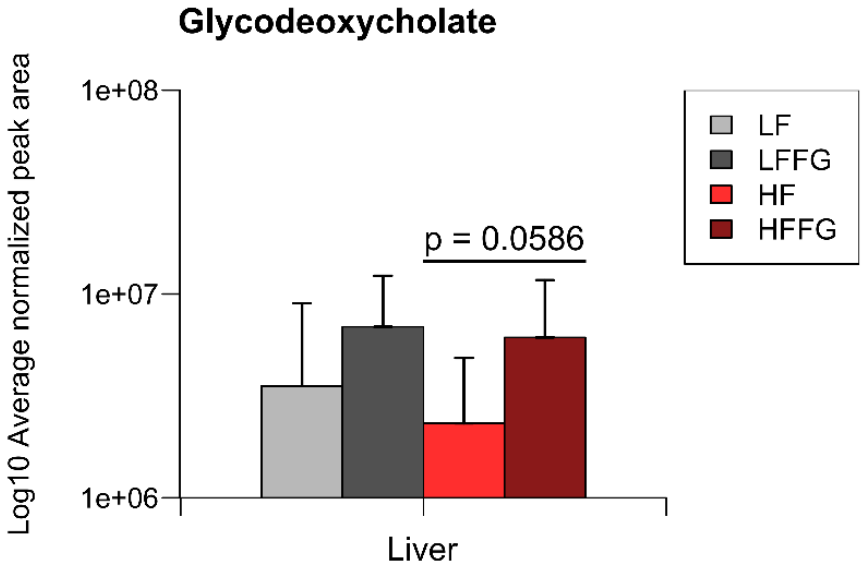


Figure 2.28 Normalized intensities of glycodeoxycholate detected in liver samples of LF_{HF}, $LF_{HF}FG$, HF and HFFG fed mice. Data was normalized according to mass and the normalized peak area is represented on a log_{10} scale as mean ± standard deviation. Significance was determined using a Student's t-test.

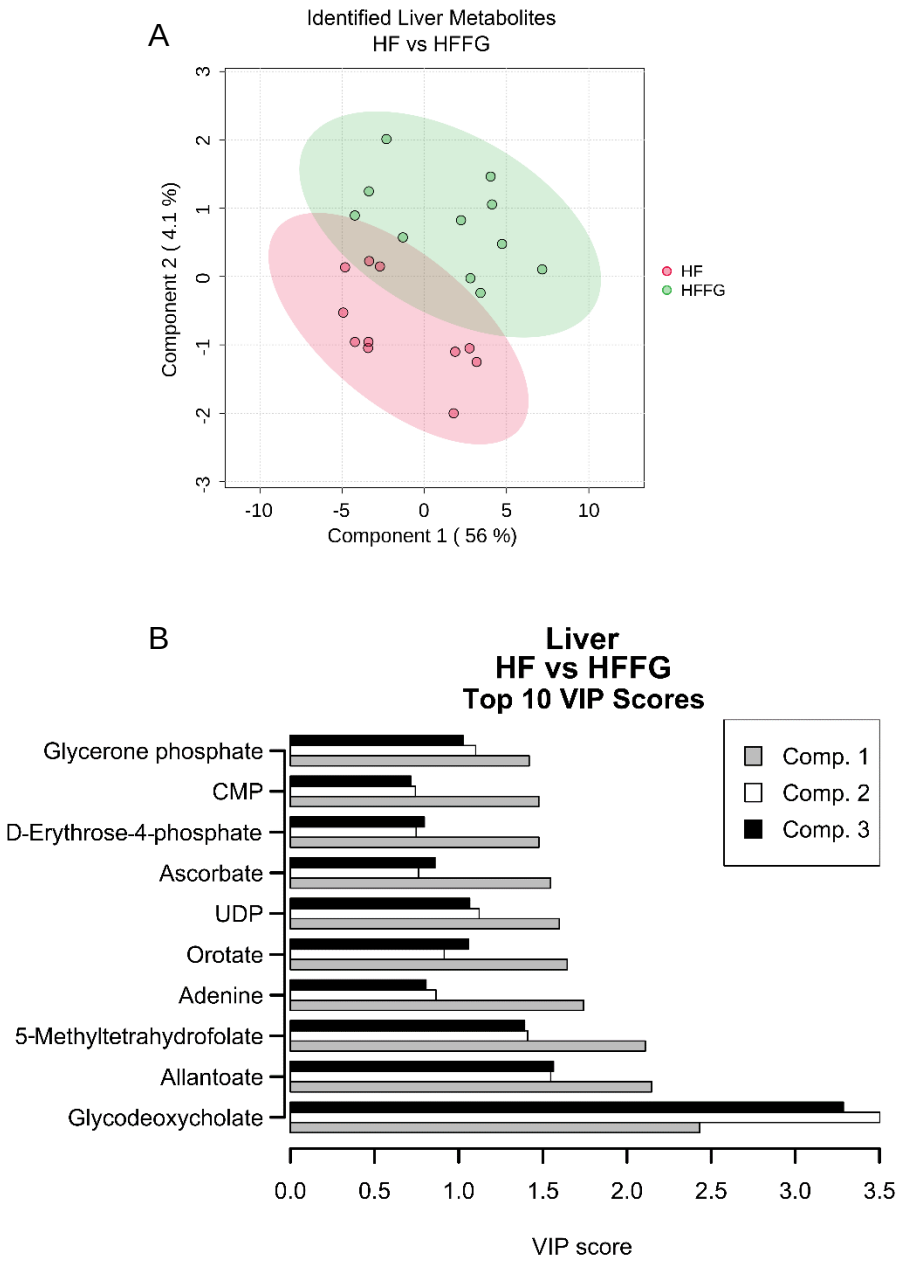


Figure 2.29 Pairwise (A) PLS-DA of identified metabolites from liver samples of HF- and HFFG-fed mice, and (B) Top 10 metabolites with highest VIP scores. Experimental replicates and 95% confidence intervals are shown.

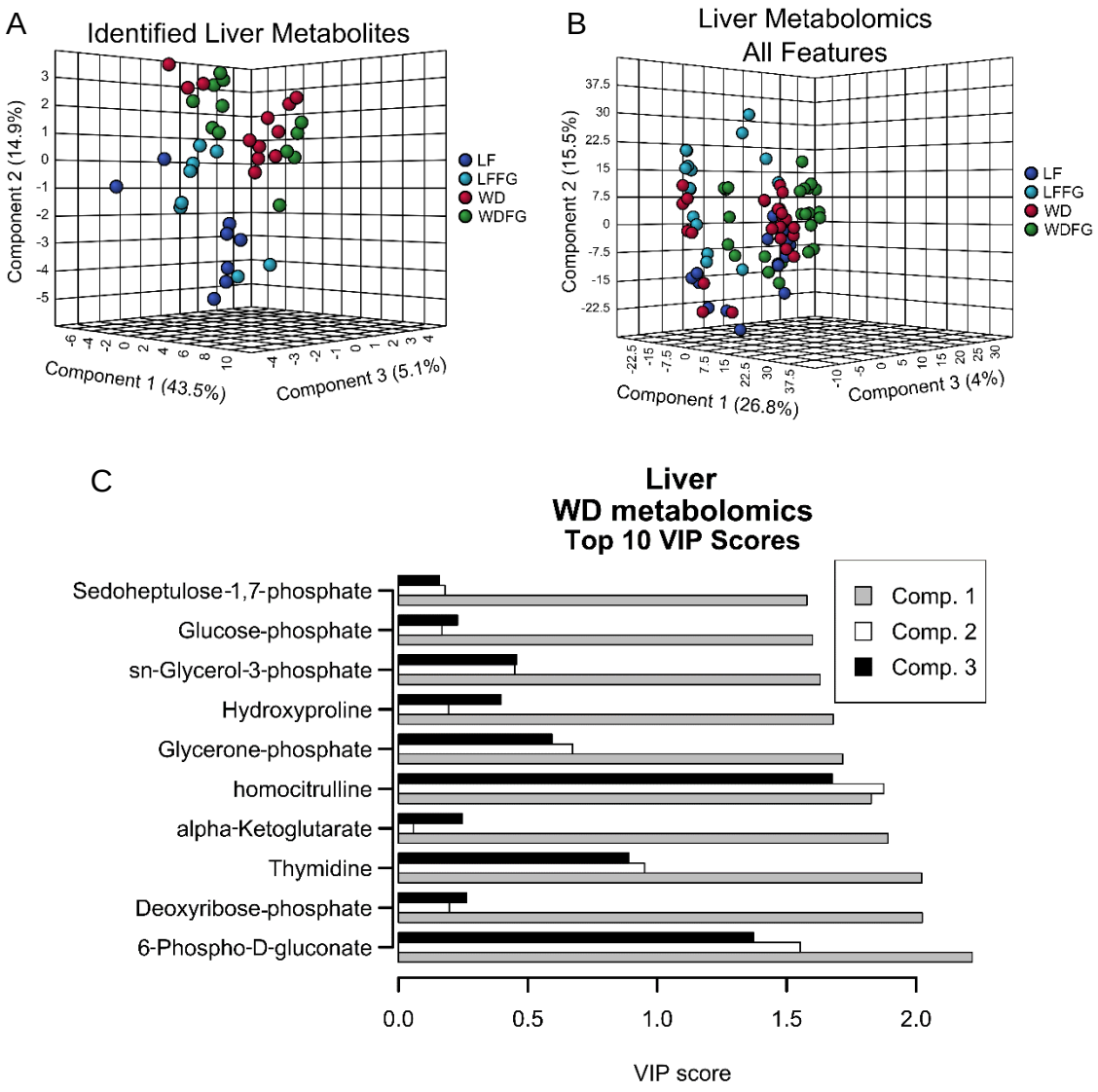
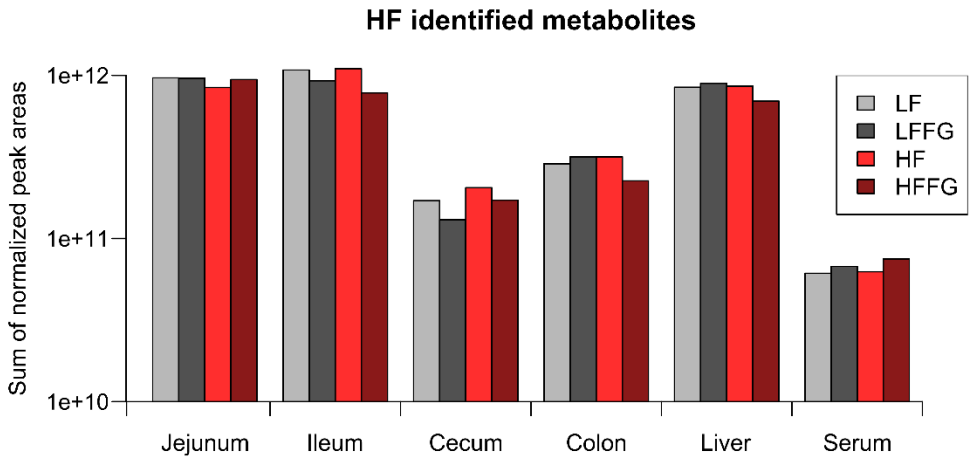


Figure 2.30 PLS-DA of (A) identified metabolites and (B) total unique features from the liver of mice fed WD, WDFG, LF_{WD}, or $LF_{WD}FG$ diets for 14 weeks. Experimental replicates are shown. Top 10 metabolites with highest VIP scores for components 1-3 from PLS-DA of identified metabolites are shown in (C).

A



B

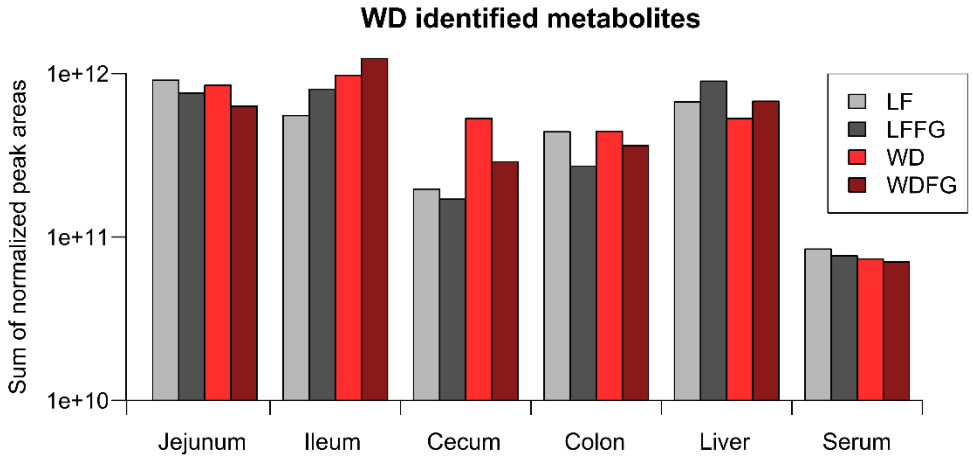


Figure 2.31 Sum of the average intensity for each metabolite identified from the contents of the jejunum, ileum, cecum, and colon, and liver and serum samples of mice fed (A) HF or LF_{HF} with and without fenugreek (FG; 2% w/w) or (B) WD or LF_{WD} with and without FG (2% w/w). The intensities were normalized by mass prior to being averaged and summed. Data is shown on a $\log_{10}$ scale.

Table 2.4 Fenugreek supplementation does not alter body weight, body composition or liver weight in mice fed a LF_{HF} or HF diet. Group comparisons were made using a one-way ANOVA, and statistical significance was determined using Tukey's multiple comparisons test. Significance is donated by ***p < 0.001 and ****p < 0.0001 for comparisons against the LF group.

High fat diet study metabolic assessments

	LF_{HF} (n=11)	LF_{HF}FG (n=7)	HF (n=11)	HFFG (n=11)
Body Weight (g)	35.1 ± 0.9	33.0 ± 0.8	46.5 ± 1.2****	49.0 ± 0.6****
Body Fat (g)	4.7 ± 0.4	5.2 ± 0.6	13.9 ± 0.5****	14.5 ± 0.3****
Liver Weight (g)	1.21 ± 0.06	1.45 ± 0.06	1.89 ± 0.1***	2.31 ± 0.17****

Table 2.5 Fenugreek supplementation does not alter body weight or body composition in mice fed a LF_{WD} or WD diet but does alter liver weight in mice fed a WD diet. Group comparisons were made using a one-way ANOVA, and statistical significance was determined using Tukey's multiple comparisons test. Significance is donated by ***p < 0.001 and ****p < 0.0001 for comparisons against the LF group, and #p < 0.05 for comparisons against non-supplemented groups.

Western diet study metabolic assessments

	LF_{WD} (n=8)	LF_{WD}FG (n=8)	WD (n=12)	WDFG (n=12)
Body Weight (g)	33.2 ± 1.0	29.6 ± 0.5	45.6 ± 1.1***	43.4 ± 0.7
Body Fat (g)	4.6 ± 0.6	4.4 ± 0.4	12.6 ± 0.4***	11.4 ± 0.6
Liver Weight (g)	1.26 ± 0.1	1.25 ± 0.4	3.23 ± 0.2***	2.64 ± 0.19#

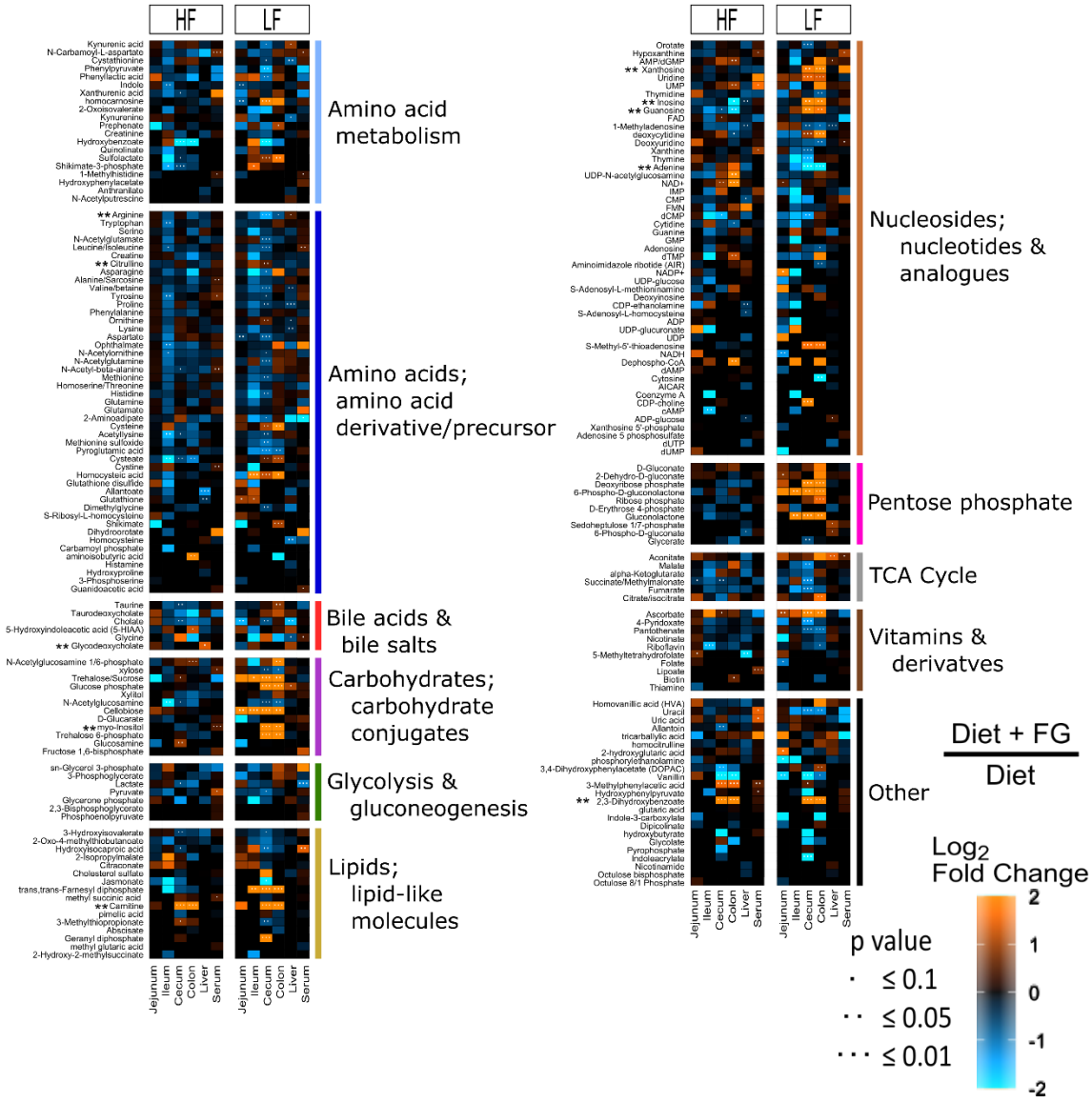


Figure 2.32 Heatmap analysis of metabolomics data from HF study. Fold changes are shown as HFFG vs HF and $LF_{HF}FG$ vs LF_{HF}. Each column represents either HF or LF_{HF} diets and each sample type, and are (left to right) jejunum contents, ileum contents, cecum contents, colon contents, liver, and serum, first for HF diet, followed by LF_{HF} diet. The fold changes are displayed on a log 2 scale and p-values denoted by dots (* = p<0.1; ** = p<0.5; *** = p<0.01). All data was normalized by mass.

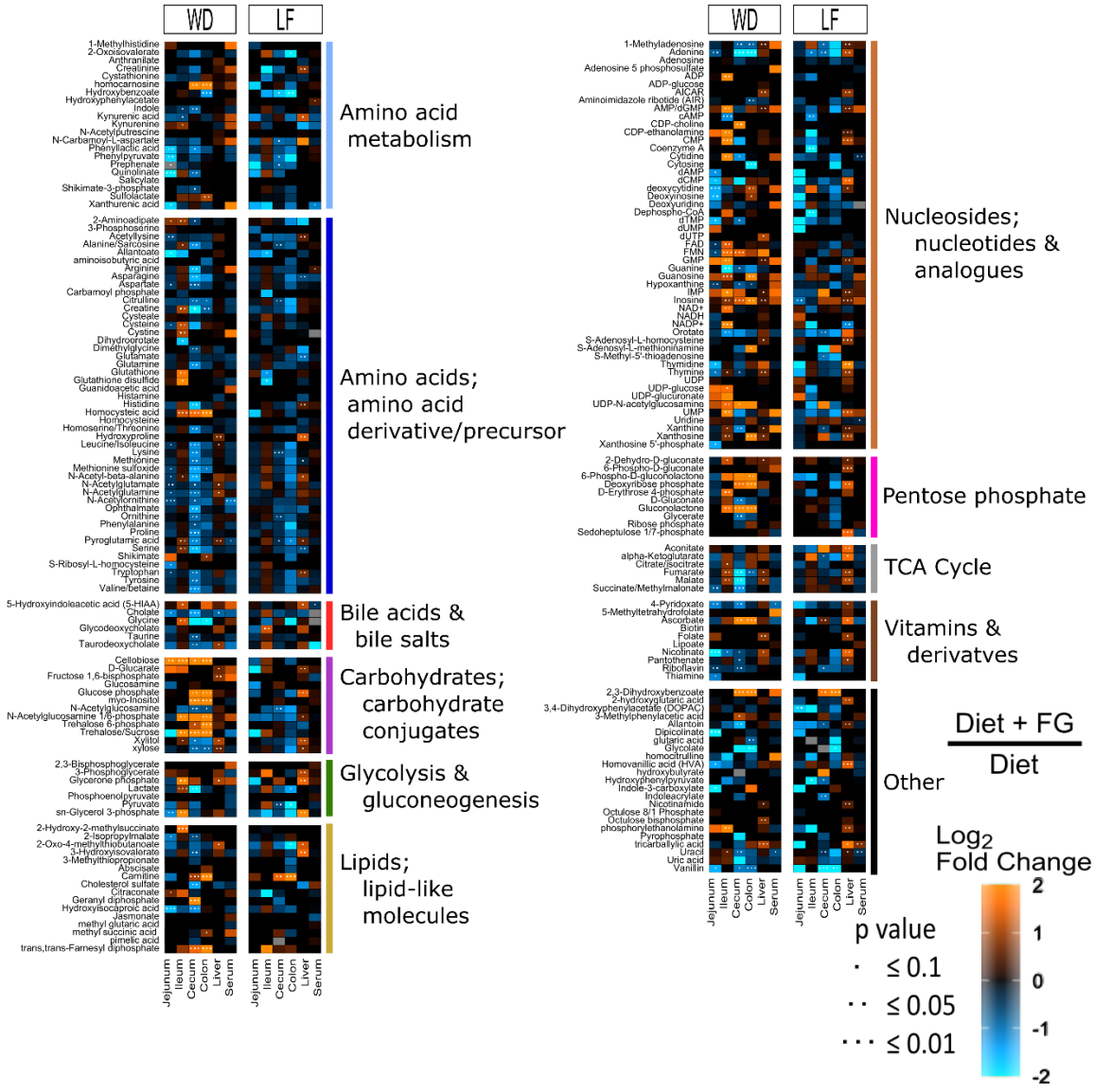


Figure 2.33 Heatmap analysis of metabolomics data from WD study. Fold changes are shown as WDFG vs WD and $LF_{WD}FG$ vs LF_{WD}. Each column represents either WD or LF_{WD} diets and each sample type, and are (left to right) jejunum contents, ileum contents, cecum contents, colon contents, liver, and serum, first for WD diet, followed by LF_{WD} diet. The fold changes are displayed on a log 2 scale and p-values denoted by dots (* = p<0.1; ** = p<0.5; *** = p<0.01). All data was normalized by mass.

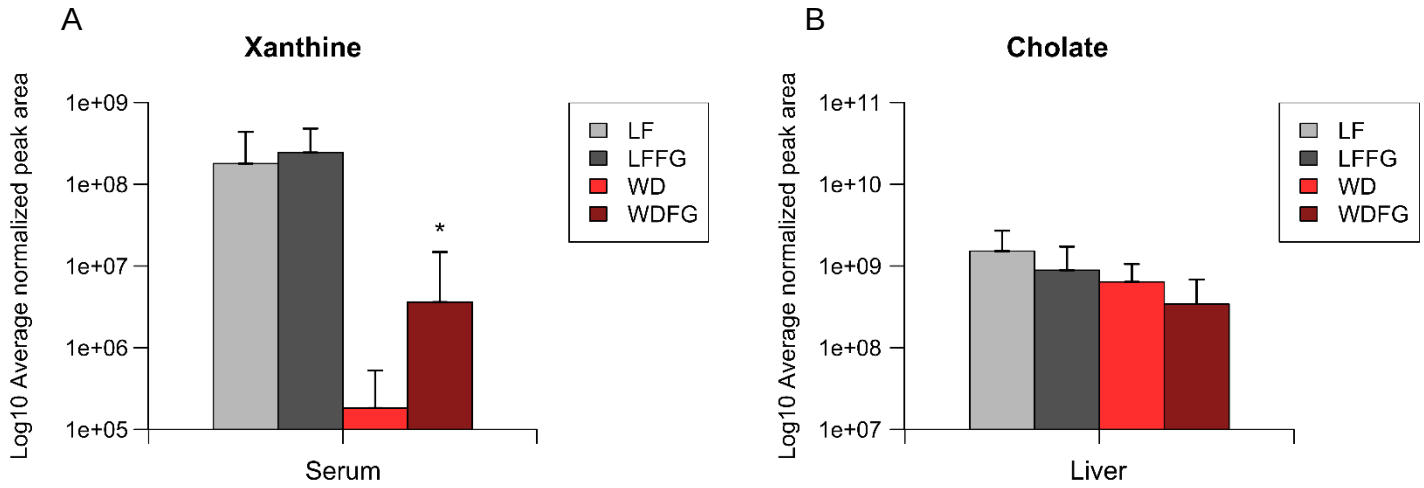


Figure 2.34 Normalized intensities of (A) xanthine detected in serum and (B) cholate detected in liver samples of LF_{WD}, $LF_{WD}FG$, WD and WDFG fed mice. Data was normalized according to mass and the normalized peak area is represented on a $\log_{10}$ scale as mean ± standard deviation. Significance was determined using a Student's t-test.

Chapter 3 Metabolomics And Lipidomics Demonstrate Two Genetically Similar Lysogens Influence Host Metabolism Based on Growth Substrate

Preface

In the following chapter a project using ultra-high performance liquid chromatography high resolution mass spectrometry to determine relative abundances of both polar metabolites and amphiphilic lipids in *Sulfitobacter* sp. Strains CB-D and CB-A will be described. While the methods used are not novel, this project is unique in using metabolomics and lipidomics methods to study two genetically similar lysogens. From this approach, the current state of the cells can be examined. While metabolism is rapidly changing and influenced by both intrinsic and extrinsic factors, lipid alterations take more time and are influenced by metabolism. By combining metabolomics and lipidomics in this study, a more complete understanding of that actual state of the cells can be elucidated.

This project was done in collaboration with Dr. Alison Buchan and her former graduate student Dr. Jonelle Basso and undergraduate student Kaylee Jacobs. The Buchan lab has focused their research on host-phage interactions using a roseobacter-roseophage model system. A previous collaboration between the Buchan lab and Campagna lab employed a metabolomics approach to study host-phage interactions between *Sulfitobacter* sp. Strain CB-D and a lytic phage ϕB. This initial study increased understanding about this system, specifically that phage infection did not lead to alterations in one specific metabolic pathway, but generally increased host metabolic activity. Additionally, it was determined that the living cells recycled the nutrients released by the lysed cells in the same culture. As well as the metabolomic results, this study found that both the lytic phage ϕB and the lysogenic phage ϕD were produced. Due to remaining viable cells present at the final timepoint, it was found that a fraction of the cells were resistant to lysis. It was theorized that the lysogenic infection by ϕD may have provided protection from lysis. These informative results prompted the study reported in this chapter.

With the prevalence of lysogeny in nature, but the lack of research focusing on lysogenic infection, temperate phages became the focus for this work. The Buchan lab had previously isolated two genetically similar lysogens which a single

host is infected by one of two temperate phages, and thus are 97% similar at the nucleotide level. Despite the similarity, these lysogens, *Sulfitobacter* sp. Strains CB-D and CB-A display marked differences in cell size and spontaneous prophage induction. For the project described in the following chapter, this one-host-two-temperate-phage model system was utilized. Furthermore, combined with the results from the previous metabolomics studies and the constant flux of nutrients in marine environments, the effects of specific nutrients were of interest. For this purpose, a complex growth media and two carbon growth substrates were selected for this study. By analyzing the differences between the strains grown with specific nutrients, a greater understanding of the phages and their influence on the host can be determined.

In this growth substrate study, the Buchan and Campagna labs worked together to achieve a greater biochemical understanding of combined influence of nutrients and phage on the host. To accomplish this goal, it was decided to probe both metabolites and lipids to gather information regarding both the functional alterations and structural changes. Untargeted methods were selected for global analysis for both the polar metabolites and amphiphilic lipids. Because of this, detection of largely unknown and uncharacterized lipid classes, such as amino lipids, was possible. Using all ion fragmentation (AIF) capabilities of Orbitrap mass spectrometers allowed for not only the detection of the parent masses of these amino lipids, but also confirmation based on fragment masses and retention time matching. While the metabolomics data was consistent with the previous study in that there was not one single pathway most impacted by phage infection, but the phages did have an impact when nutrients were limited. This trend was also apparent in the lipids, with significant alterations in the composition of the lipidome between growth substrates and varying degrees of differences in the abundances between strains. These results revealed that while growth substrates and available nutrients have strong influence on the structure and function of the cells, the phages have a notable impact in a nutrient dependent manner.

A version of this chapter will be a part of a future publication titled:

Growth Substrate and Host-Phage Interactions Collectively Influence Metabolite and Lipid Profiles in a Marine Bacterium.

Proposed authors:

Jonelle T.R. Basso*, Katarina A. Jones*, Kaylee R. Jacobs, Courtney J. Christopher, Haley B. Fielland, Shawn R. Campagna, Alison Buchan

Author contributions

JTRB, KAJ, SRC and AB designed the experiment and wrote and edited the manuscript. JTRB and KRJ cultured cells and analyzed growth dynamics and spontaneous prophage induction. KAJ performed metabolomics extractions, mass spectral analysis, and data processing and analysis. CJC and HBF assisted in metabolomics extraction and analysis.

3.1 Abstract

Bacterial growth substrates influence a variety of biological functions, including the biosynthesis and regulation of lipid intermediates. The extent of this rewiring is not well understood, nor has it been considered in the context of virally-infected cells. Here, a one-host-two-temperate phage model system was used to probe the combined influence of growth substrate and phage infection on host carbon and lipid metabolism. Using untargeted metabolomics and lipidomics, the detection of a suite of metabolites and lipid classes for two Sulfitobacter lysogens provided three growth substrates of differing complexity and nutrient composition (yeast extract/tryptone [complex], glutamate and acetate) are reported. Growth medium led to dramatic differences in the detectable intracellular metabolites, with only 15% of 175 measured metabolites showing overlap by growth substrate. Between-strain differences were most evident in the cultures grown on acetate, followed by glutamate then complex medium. Lipid distribution profiles were also distinct between cultures grown on different substrates as well as between the two

lysogens grown in the same medium. Five phospholipid classes, three amino lipid classes, and one class of unknown lipid-like features were identified. Most (≥ 94%) of these 75 lipids were quantifiable in all samples. Metabolite and lipid profiles were strongly determined by growth medium composition and modestly by strain type. As fluctuations in availability and form of carbon substrates and nutrients as well as virus pressure are common features of natural systems, the influence of these intersecting factors will undoubtedly be imprinted in the metabolome and lipidomes of resident bacteria.

3.2 Introduction

The macromolecular composition of bacterial cells is the product of both external and internal factors. The concentrations and chemical forms of carbon and nutrients, such as nitrogen, oxygen, sulfur, and phosphorus, influence bacterial physiology in a strain-specific fashion. For instance, growth substrates affect cellular growth rates, size, morphology and other dynamic biological functions.[118] The processing of growth substrates through central metabolism (e.g., the tricarboxylic acid [TCA] cycle) influences the synthesis and regulation of many important macromolecules, including key lipid biosynthesis intermediates.[118-119] However, the extent to which substrates and nutrients utilized for growth directly relate to cell lipid composition is not fully understood. This knowledge gap presents challenges to application of lab-based studies of isolates to interpretation of field-based measurements of natural microbial populations.

Lipids are key constituents of bacterial cell membranes and are organized into a few broad classes, including the common phospholipids: phosphatidylethanolamine (PE), phosphatidylglycerol (PG), cardiolipin (CL), phosphatidylcholine (PC), phosphatidylinositol (PI) and phosphatidylserine (PS).[120-123] Despite the diversity of phospholipid head groups recognized amongst bacteria, a single key precursor to all of these molecules is phosphatidic acid (PA).[124] Other lipid classes, such as amino lipids and other phosphorous-free lipids (e.g., sulfoquinovosyldiacylglycerol (SQDG)) have been documented in diverse

bacteria where they have been linked to environmental stress, most notably phosphorous limitation.[125-127]

Lipid composition tends to be a deeply conserved feature of bacteria. The model organism Escherichia coli has been used for the elucidation of bacterial lipid composition, but exhibits less complexity than other bacterial species with regards to lipid classes it possesses.[126] In E. coli, PE, PG and CL are the primary membrane glycerophospholipids, compromising ~75%, ~20% and ~1-5%, respectively, of the total pool.[128-129] Similarly, PG, PE and CL are frequently produced by Alpha-Proteobacteria. However, PC and amino lipid species have also been identified in subsets of this bacterial class, such as strains within the marine Sulfitobacter genus and Rhodobacter sphaeroides, both of the Rhodobacterales order.[120, 123, 126, 130-131]

Cellular lipid composition can be viewed as an adaptive response. It is non-static and favors forms which provide the necessary structural features for cells under specified environmental conditions.[126] Cellular modulation of lipid composition has been linked to temperature, pH, as well as production and accumulation of metabolites and nutrient levels.[126, 132] As lipid biosynthesis is intrinsically linked to central metabolism, factors influencing central metabolism, including viral infection, may also be expected to affect lipid composition.

Lytic phage infection has been shown to alter host metabolism, the nature and extent of which appears to be host-virus specific. Phage-dependent manipulation of host metabolic processes can occur through redirection of pathway-specific mechanisms, including alterations in central carbon metabolism, nucleotide and/or lipid biosynthesis pathways.[133-137] Though rare, examples providing direct linkages between phage infection and host lipid composition provide further insight into the varied fitness strategies employed by viruses. For instance, cyanophage-encoded auxiliary metabolic genes (AMGs), specifically fatty acid desaturases, have been implicated in alterations to host cyanobacterial membrane fluidity, which are suggested to lead to host photoprotection.[138] While AMGs have been involved in virus-mediated host metabolic remodeling and their

identification can lead researchers to specific targeted pathways, the presence of such genes does not appear to be a requirement for metabolic redirection. However, in the absence of obvious AMGs, the specific mechanism of such redirection is not easily elucidated from viral genetic signatures alone.[139-140]

Previous work in the Buchan lab has shown that the influx of nutrients from viral lysis of neighboring cells leads to both the accumulation and rapid utilization of these resources by the remaining viable cells for cultures of a Sulfitobacter strain.[139] These data are consistent with the notion that members of this group of abundant marine bacteria are well adapted to a feast or famine lifestyle. The prior work also highlighted the importance of nitrogen recycling in host-phage interactions which was predicted to arise from a stoichiometric imbalance between host and phage (i.e., phage are nitrogen rich relative to their hosts). However, the prior study did not examine the impact of phage infection on lipid metabolism. This study took advantage of a unique one-host-two-temperate phage roseobacter-roseophage model system to assess the intersection of growth substrate, or nutrients, and prophage activation on both host metabolism and lipid composition.

3.3 Results

A previously developed a one-host-two-phage system, in which a single Sulfitobacter host is lysogenized with one of two temperate phages (denoted ϕA and ϕD) and the resulting lysogens, termed CB-A and CB-D was used throughout this study. The two phages share an integration site in their host and 97% identity at the nucleotide level. These genetically similar temperate phages have been demonstrated to have divergent influence on their shared hosts' competitiveness. It is hypothesized that this is due, in part, to differences in the lysogenic-lytic switches of their resident prophage, with CB-A showing measurable prophage induction not evident in CB-D when these strains are grown in a complex medium.[141] However, it is recognized that other factors may contribute to observed fitness differences between the strains. Thus, to better define the nature of these host-phage interactions and influence on host physiology, this study compared the

metabolite and lipid profiles of each host-phage pair (CB-A and CB-D) grown on different carbon sources. The three media types utilized represent a range of complexity of nutrients, particularly with respect to carbon (C) and nitrogen (N). Specifically, the carbon sources ranged from simple to complex (acetate < glutamate < tryptone + yeast extract). However, inorganic N, as ammonium chloride, was supplied in all media, while organic N was only available in the complex and glutamate containing media. Organic carbon in the complex medium was 8.55 times greater (171 mM C) than either the glutamate or acetate containing media (both supplied at 20 mM C). Combining organic and inorganic N sources, the complex medium (at 27 mM N) had 1.6 or 2.2 times greater total N than either the glutamate (14 mM N) or acetate (10 mM N) media, respectively. The C:N ratio for the three media ranged from 1.4 to 6.3 (glutamate to complex) (Appendix Table 3.1). In our experiments, phosphorus was provided in non-limiting concentrations. Inorganic phosphorus was provided as 1 mM potassium phosphate, a non-limiting concentration for roseobacters, in all media.[142] Organic phosphorus was only available in the complex medium, as a component of both tryptone and yeast extract.

3.3.1 Growth physiologies of strains are different across substrates.

Growth of both strains was most robust on the complex substrate, followed by glutamate then acetate (Fig. 3.1). Free phage, indicative of prophage induction, were present in all CB-A cultures, but undetectable in the CB-D cultures (Appendix Tables 3.2-3.4).[141] Only the acetate grown cultures showed significant differences in host viability, presumably as a result of greater prophage induction. By the final (24 hr) timepoint, viable counts for CB-D were ~250% greater than CB-A in acetate grown cultures relative to the other treatments (Appendix Tables 3.5-3.7). Cell size, estimated by flow cytometry, revealed significantly larger CB-D cells relative to CB-A cells for glutamate grown cells (Fig. 3.1D). No differences were evident between the strains grown on the other two substrates (Fig. 3.1B & F).

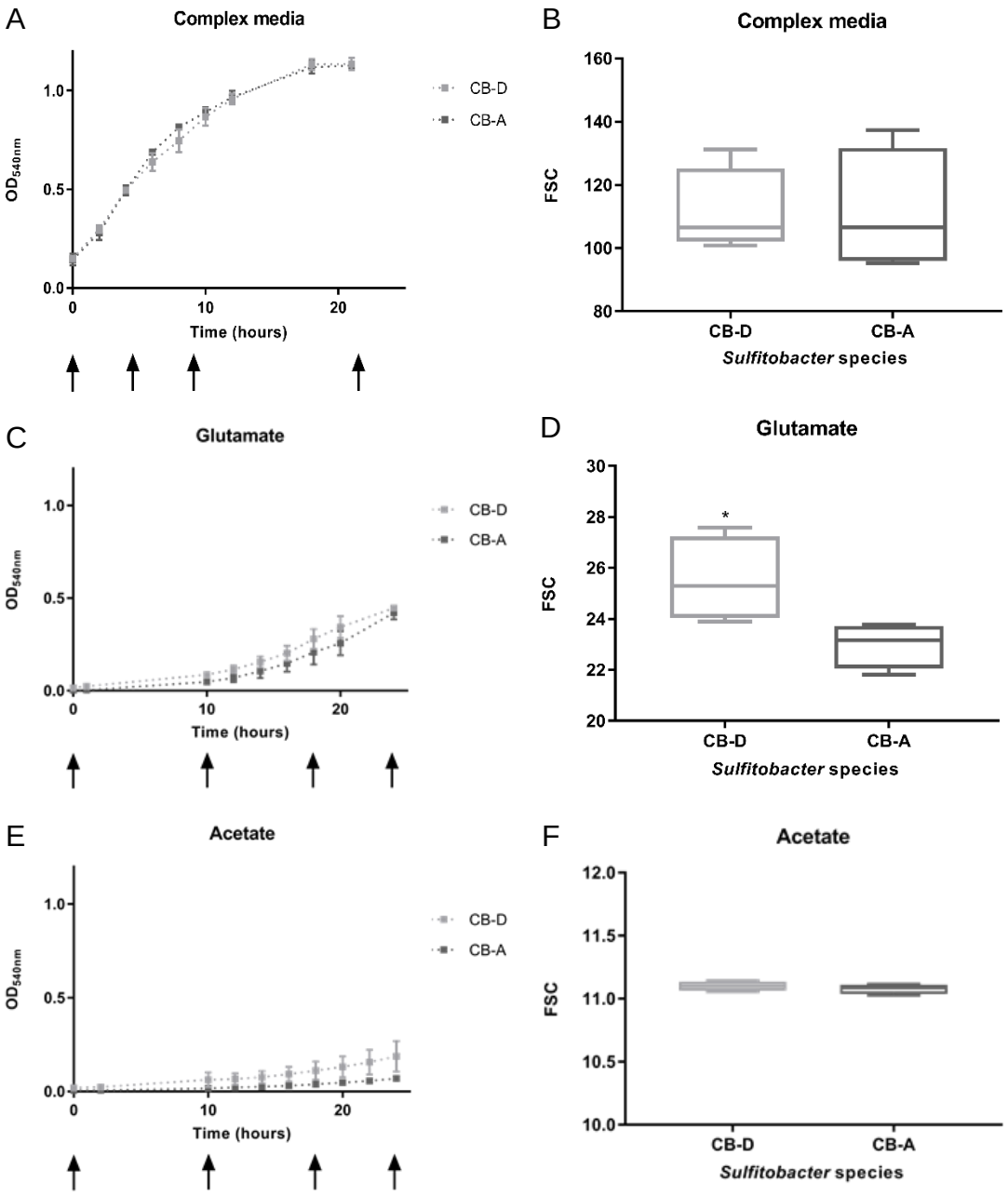


Figure 3.1 Growth dynamics and cell size data for *Sulfitobacter* sp. strains CB-D (light gray) and CB-A (dark gray) in (A) Standard Marine Media (SMM), (C) glutamate and (E) acetate. Cell size was measured by forward scatter through flow cytometry for cells grown in (B) SMM, (D) glutamate and (F) acetate. Averages and standard deviations were calculated for CFU/ml. Final timepoint average viable counts of each substrate per strain is as follows: SMM CB-A 5.36E+09 (± 5.11E+08); CB-D 4.37E+09 (± 4.9E+08). Glutamate CB-A 1.54E+09 (± 4.90E+08); CB-D 2.02E+09 (± 7.16E+08). Acetate CB-A 2.85E+08 (± 1.07E+08); CB-D 1.02E+09 (± 6.85E+08). Significant difference in cell size (Student's T-tests) is denoted by asterisks (* = $p<0.05$). Averages of biological replicates are reported for all treatments (n= 3 in SMM grown cells; n= 5 in glutamate and acetate grown cells). Plating was done in technical replicates. Arrows denote time points at which samples were taking from each media type.

3.3.2 Diversity of metabolites detected varies strongly with growth substrate.

All cultures were sampled for metabolomics and lipidomics analyses at four discrete time points over the course of the growth curve. Using ultra-high performance liquid chromatography—high resolution mass spectrometry (UHPLC-HRMS) based untargeted metabolomics, a total of 175 metabolites were identified across all samples, with only 27 (15%) detected in all growth conditions (Fig. 3.2). The greatest number of metabolites were detected in glutamate grown cells (127 of the identified metabolites; 73%). Complex-grown cells and acetate-grown cells had similar numbers of detectable metabolites (75 and 72 identified metabolites, respectively; ~40%). There was some overlap of individual metabolites that were detected in cultures grown on these two substrates (31 metabolites), but more overlap was evident with glutamate-grown cells and either complex- or acetate-grown cells (40 and 63 metabolites, respectively). Partial least squares discriminant analysis (PLS-DA) showed strong separation of samples by growth substrate, with little to no difference between strains (Fig. 3.3A). Where evident, variation between strains was greatest at discrete timepoints. For example, for both glutamate and acetate grown cultures, the greatest number of significant differences (fold change >1.5 and p-value <0.05) was observed at 10 hr post inoculation (57% of metabolites for glutamate, 47% of metabolites for acetate). These between-strain differences in metabolite profiles diminished by the final sampling timepoint, but still comprised a third of measurable metabolites in the acetate-grown cultures (8% and 31% for glutamate- and acetate-grown cells) (Appendix Fig 3.7A). The greatest differences in metabolite profiles for complex-grown cultures was 5% at 21 hr.

3.3.3 Lipid profiles vary with growth substrate and strain.

A total of 75 lipids from nine lipid classes were identified across all samples via UHPLC-HRMS-based untargeted lipidomics. Five phospholipids classes (phosphatidic acid [PA], phosphatidylethanolamine [PE], phosphatidylcholine [PC],

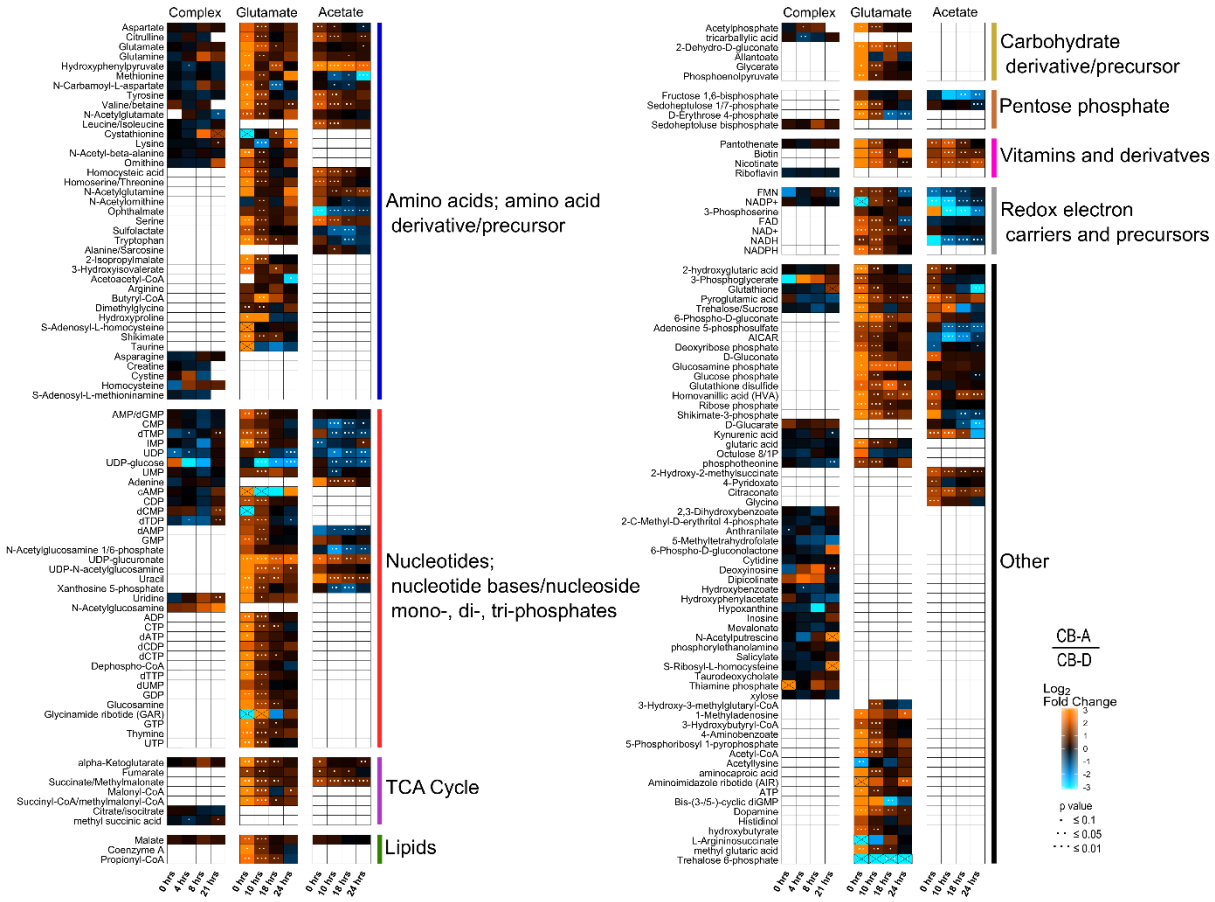


Figure 3.2 Metabolomics heatmap analysis of SMM, glutamate and acetate grown cells. Heat maps for these three media grown cells display fold change between *Sulfitobacter* sp. strain CB-D and CB-A over time (orange denotes more CB-A; blue denotes more CB-D). All data are normalized according to optical density. Significant differences are denoted by asterisks (* = p<0.1; ** = p<0.05; *** = p<0.01). Crossed out boxes denote that there was only detected in one strain, which is indicated by the color. Averages of biological replicates are reported for all treatments (n= 3 in SMM grown cells; n= 5 in glutamate and acetate grown cells).

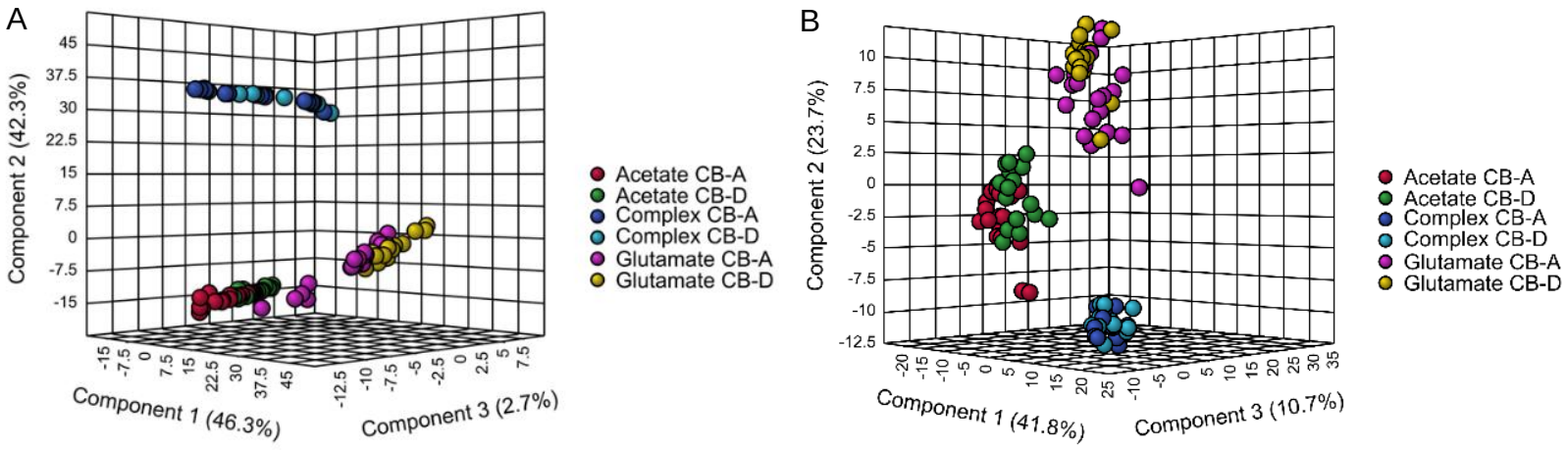


Figure 3.3 Partial least squares discriminant analysis (PLSDA) plots illustrate significant clustering by substrate, and to a lesser extent, by strain. (A) *Sulfitobacter* sp. strains CB-D and CB-A metabolites comparison and (B) lipids comparison were analyzed using MetaboAnalyst. The following color scheme was used to denote samples: pink circles = acetate grown CB-A cells; green circles = acetate grown CB-D cells; dark blue circles = complex media grown CB-A cells; light blue circles = complex media grown CB-D grown cells; purple circles = glutamate grown CB-A cells; yellow circles = glutamate grown CB-D cells. All data are normalized according to optical density. Averages of biological replicates are reported for all treatments (n= 3 in SMM grown cells; n= 5 in glutamate and acetate grown cells).

phosphatidylglycerol [PG], and acyl-phosphatidylglycerol [APG]), three amino lipid classes (AL; lysine lipid [KL], ornithine lipid [OL], and glutamine lipid [QL]) and one class of Unknown lipid-like features (Unk) were detected. Unlike the metabolite profiles, the majority of these lipids (94-97%) were detected in all samples, regardless of growth medium or strain type (Fig. 3.4). Thus, the differences between these profiles are principally due to alterations in the relative abundance of specific lipids.

While the samples principally clustered by growth substrate (Fig. 3.3B), greater variation between strains raised on either glutamate or acetate was evident amongst these lipid profiles. For example, upwards of 45% of lipids showed significantly different distributions between the two strains grown on acetate (at 24 hr) and 63% of lipids varied between the strains when grown on glutamate (at 18 hr) (Appendix Fig. 3.7B). In contrast, only 8% of lipids were significantly different between the strains when grown on complex media (0 hr). Regardless of growth substrate, significant changes were observed within the phospholipid profiles over time. When grown on complex media, the ratio of PG to the total phospholipids detected generally increased with time for both strains, while the ratio of PE to total phospholipids decreased (Fig. 3.5). However, acetate-grown cells demonstrated the opposite trend. Glutamate-grown cells showed the ratio of PG increasing over time for CB-D, however, a consistent trend was not observed for CB-A (Fig. 3.5). In addition to the obvious variation between growth substrates and temporal changes, a subset of lipid classes that showed significant variation between the two strains were the amino lipids.

3.3.4 Presence of amino lipids correlates with nutrients.

Previous work characterized ornithine (OL) and glutamine lipids (QL) from Rhodobacter sphaeroides, an organism belonging to the same Rhodobacteraceae family as the host strain used in this study.[131] Here, the identification of AL determined through exact mass and proposed structures were confirmed using all ion fragmentation (Fig. 3.6G & H; Appendix Fig. 3.8D).[142] The MS-based

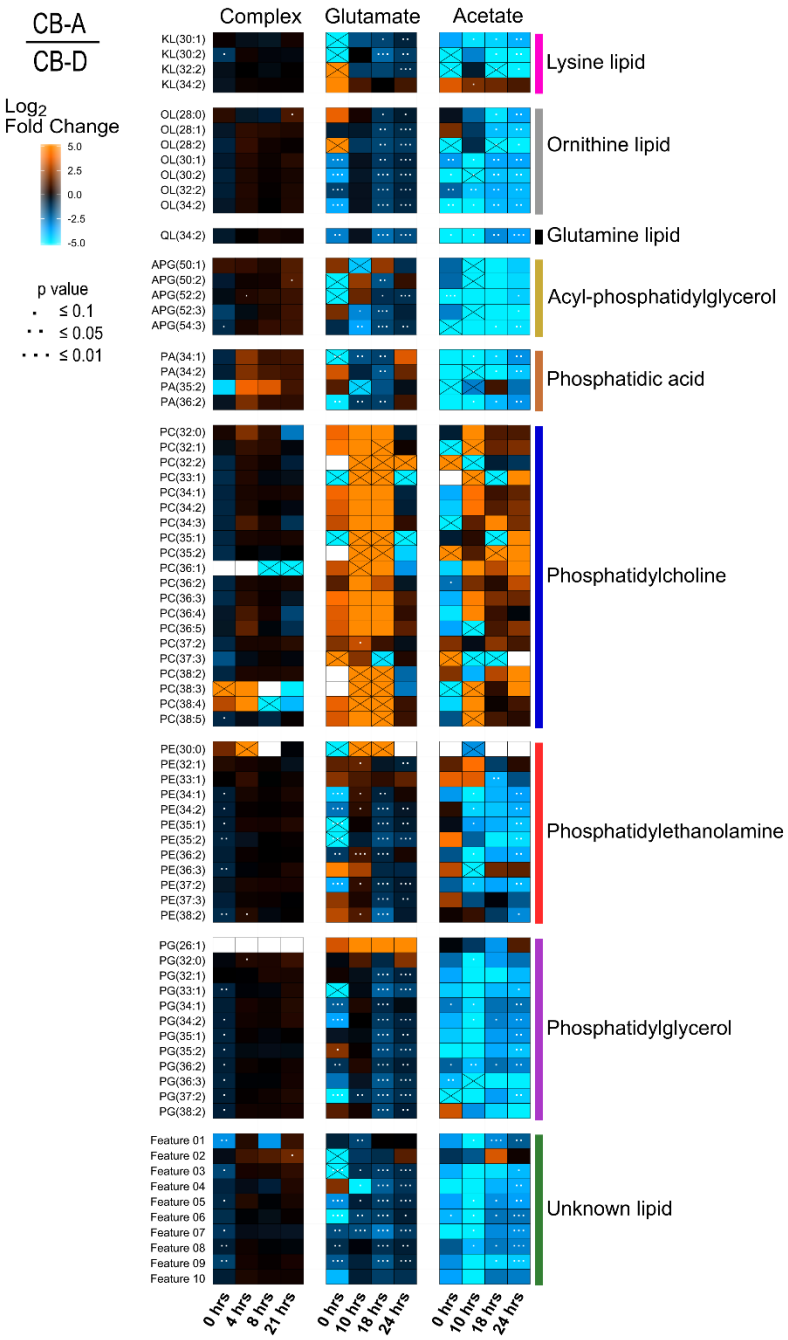


Figure 3.4 Lipidomics heatmap analysis of SMM, glutamate and acetate grown cells. Heat maps for these three media grown cells display fold change between *Sulfitobacter* sp. strain CB-D and CB-A over time (orange denotes more CB-A; blue denotes more CB-D). Lipids are ordered according to amino- and phospholipid categories. All data are normalized according to optical density. Significant differences are denoted by asterisks (* = p<0.1; ** = p<0.05; *** = p<0.01). Crossed out boxes denote that there was only detected in one strain, which is indicated by the color. Averages of biological replicates are reported for all treatments (n= 3 in SMM grown cells; n= 5 in glutamate and acetate grown cells).

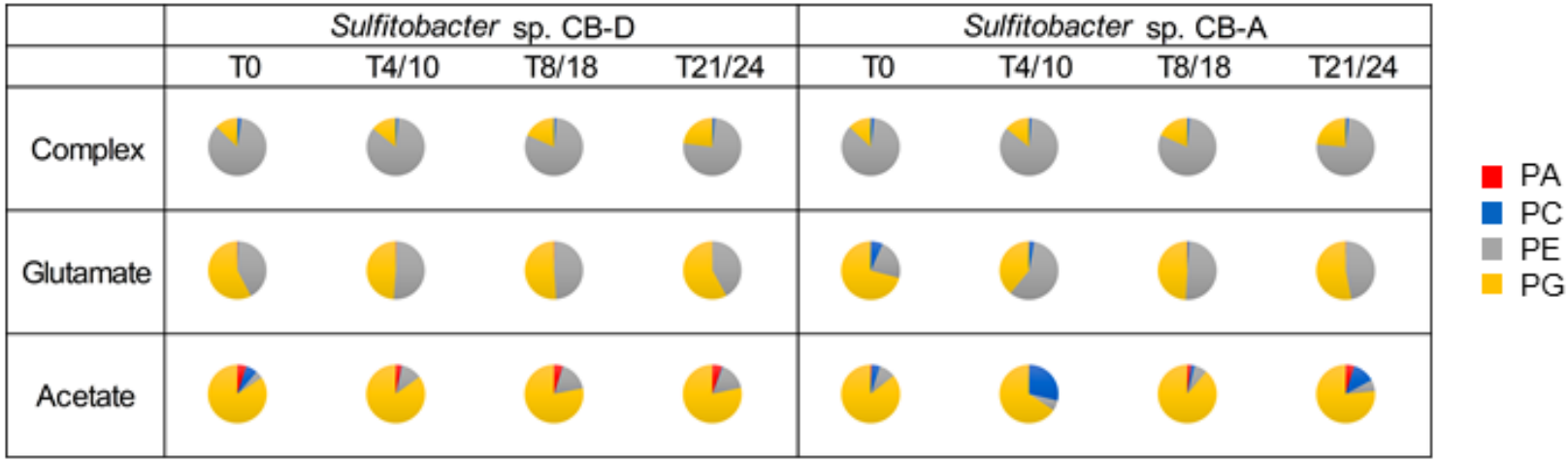


Figure 3.5 Pie charts display relative proportions of the sum of phospholipid concentrations in *Sulfitobacter* sp. strains CB-D and CB-A for each timepoint and substrate. Phospholipid concentrations were determined using external calibration curves for phosphatidic acid, phosphatidylcholine, phosphatidylethanolamine, and phosphatidylglycerol. All data are normalized according to optical density. Averages of biological replicates are reported for all treatments (n= 3 in SMM grown cells; n= 5 in glutamate and acetate grown cells) and are within 2 standard deviations.

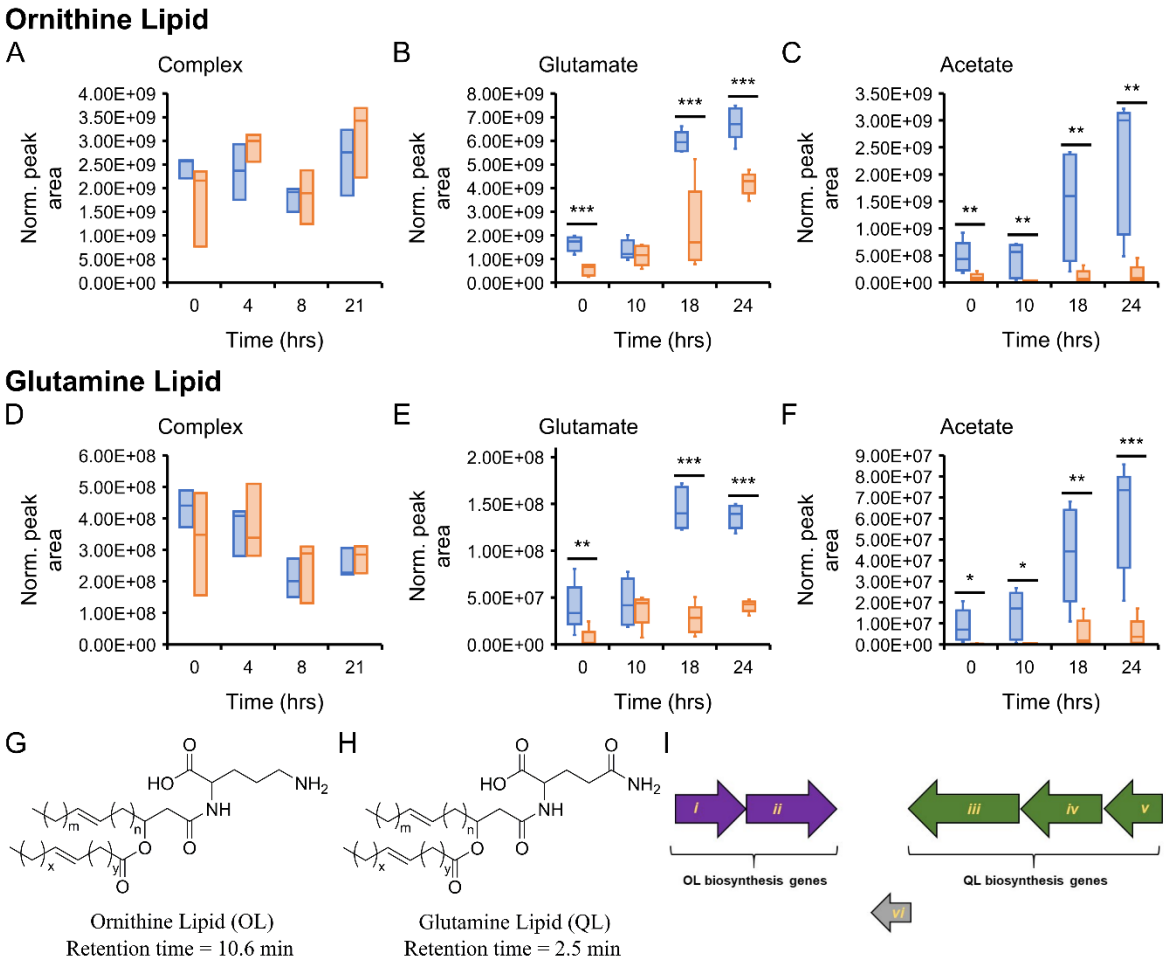


Figure 3.6 Ornithine Lipid (OL) and glutamate lipid (QL) in *Sulfitobacter* sp. strains CB-A (orange) and CB-D (blue). Box & whisker plots highlight differences between strains and time, and between substrates. These plots are shown for all substrates for (A), (B), (C) ornithine lipid (OL) and (D), (E), (F) glutamine (QL) lipid. Significant differences are denoted by asterisks (* = p<0.1; ** = p<0.05; *** = p<0.01). Averages of biological replicates are reported for all treatments (n= 3 in SMM grown cells; n= 5 in glutamate and acetate grown cells). All data are normalized according to optical density. Structures of (G) ornithine lipid (OL) and (H) glutamine lipid (QL), with respective retention times. (I) OL and QL biosynthesis gene organization in *Sulfitobacter* sp. strains CB-D and CB-A. ***i*** = GNAT family N-acetyltransferase [unclassified *Sulfitobacter*] (Accession: WP 037944303.1), ***ii*** = 1-acyl-sn-glycerol-3-phosphate acyltransferase [unclassified *Sulfitobacter*] (Accession: WP 037944304.1) ***iii*** = ATP-binding cassette domain containing protein [*Sulfitobacter*] (Accession: WP 037944390.1) ***iv*** = ornithine-acyl-ACP acyltransferase [*Sulfitobacter* sp. CB2047] Accession: KFC26427.1) ***v*** = outer membrane protein assembly factor BamE [*Sulfitobacter*] (Accession: WP 037944392) ***vi*** = phosphate regulon transcriptional regulatory protein PhoB [*Sulfitobacter*] (Accession: WP 005853599.1).

identification of these lipids is supported by genome analyses that indicate both strains possess homologs of genes previously shown to be essential for OL and QL biosynthesis in Silicibacter pomeroyi DSS-3, a close relative of sulfitobacters (Fig. 3.6I).

Of these lipids, a single glutamine lipid (QL 34:2), seven ornithine lipids (OL) and four lysine lipids (KL) were detected, with significant differences between strains when grown on glutamate or acetate (Fig. 3.4). Complex medium-grown cells showed relatively constant OL abundance over time (Fig. 3.6A). By contrast, in glutamate- and acetate-grown cultures, OL generally increased over time (Fig. 3.6B & C). In complex medium-grown cells, QL (34:2) was detected with decreasing abundance over time (Fig. 3.6D), but with increasing abundance over time in glutamate- and acetate-grown cells (Fig. 3.6E & F). Additionally, OL and QL were detected with significantly higher abundance for CB-D than CB-A in glutamate-grown cells at 0, 18, and 24 hr and acetate-grown cells (all time points) (Fig. 3.6B, C, E, F). In contrast, no KL were detected in glutamate-grown CB-A cells (Appendix Fig. 3.8B) but followed a similar trend as OL and QL in acetate-grown cells with significantly higher abundance for CB-D than CB-A at 10, 18 and 24 hr (Appendix Fig. 3.8C). In complex medium-grown cells, no difference in KL was evident between the strains, and abundance remained more constant until 21 hr when an increase was observed (Appendix Fig. 3.8A).

3.3.5 Detection of an abundant, but unidentified lipid class.

In addition to the aforementioned phospholipids and amino lipids, a class of unidentified spectral features with characteristics of lipids (subsequently termed “unidentified lipid class”) was detected in both CB-D and CB-A. This unidentified lipid class was highly abundant in glutamate- and acetate-grown cells. This lipid class was most abundant at the earliest sampling time point (0 hr), with the ratio of this lipid class to the total detected lipids reaching values of ~35% in glutamate-grown cultures of both strains and 52% and 56% in acetate-grown CB-D and CB-

A cultures, respectively (Appendix Fig. 3.9). This lipid class remained highly abundant with the lowest ratios reaching values of ~20% for CB-D and CB-A grown on glutamate (18 hr), and 40% for CB-D (24 hr) and 33% for CB-A (10 hr) when grown on acetate (Appendix Fig. 3.9). However, this lipid class was not as abundant in the complex medium-grown cultures of either strain, with ratios of only 3% at 0 hr, and a maximum ratio at 21 hr of ~13% (Appendix Fig. 3.9). This unknown lipid class displayed significant differences between strains grown on either of the defined carbon substrate conditions, but not on the complex medium (Fig. 3.4), with the most significant differences in glutamate-grown cells. Between-strain differences on glutamate were ≥60% at all time points, except 10 hr at which only 10% of features were significantly different (Fig. 3.4). Acetate-grown cells showed less deviation throughout the growth curve but had dramatic differences (70% of this class of features) at 24 hr (Fig. 3.4).

To gain a better understanding of these features, relative abundances of mass spectral isotope peaks were compared to the natural abundance of carbon-13 (1.1%). The mass-to-charge (m/z) ratios for these features ranged from 702.4363 to 816.5776 m/z (±5 ppm), with the most abundant species at 802.5621 m/z, all in negative ionization mode for the [M-H]- ion. The corresponding masses for the [M+H]+ ion were detected using positive ionization mode. From these observed masses, using the nitrogen rule, it was suggested that the lipid-like features contained an odd number of nitrogen atoms. To gain further understanding of this class of features, further fragmentation experiments were performed using a Q Exactive quadrupole-orbitrap hybrid mass spectrometer. Using Fiehn's seven golden rules, 137 potential molecular formulae were determined for the most abundant feature (802.5621 m/z), containing carbon, hydrogen, nitrogen, oxygen, phosphorus, or sulfur.[117] These features were compared with online lipid databases, including LipidMaps, but currently elude identification.[143]

3.4 Discussion

The ability of bacteria to modulate the lipid composition of their cellular membranes is cited as a common adaptive mechanism to environmental fluctuations. From a biogeochemical standpoint, much of the existing knowledge regarding factors influencing lipid composition in marine bacteria focuses on the role of phosphorus (P) availability, revealing widespread capacity for marine microbes to remodel their membrane lipids in response to P starvation.[144-145] However, lipid biosynthesis is intrinsically linked to central metabolism. As such, the role of primary growth substrates can be predicted to be a critical factor in shaping cellular lipid composition. This research sought to obtain a more holistic picture of the relationship between growth regimes, metabolism, and lipid composition in a representative heterotrophic marine bacterium of the Roseobacter clade of marine bacteria. A secondary goal was to assess the contribution of phage activity on the host cell metabolome and lipidome. To this end, a one-host-two-phage system was employed. This system is comprised of two genetically similar host-phage pairs, with different intrinsic levels of spontaneous induction i.e. CB-A cultures produce measurable free phage particles in the absence of obvious stressors, CB-D does not.[141] While recognizing that disentangling responses due to growth condition, host physiology and viral activity are difficult due to interdependencies, the data presented here reveal stark differences in metabolite and lipid profiles which appear to be driven by phages, but in a nutrient dependent manner.

The three growth substrates used herein represent a spectrum from simple to complex nutrients, particularly with respect to carbon substrates and variation in concentration and form (inorganic vs. organic) of N as well as P. The C:N ratios for the complex-, glutamate- and acetate-containing substrates were ~ 6:1, 1.4:1 and 2:1, respectively (Appendix Table 3.1). While the C:N ratio of heterotrophic marine bacteria can vary with nutrient availability, it typically ranges between 4-7 when bacteria are grown on organic matter with a C:N approaching that of the

Redfield ratio (6.6:1).[146-147] Consequently, for those cultures grown on glutamate and acetate, N was in high abundance relative to C when compared to most environments. However, C:N stoichiometry may not alone tell the story as bacteria can show preference for different N sources.[148-151] Indeed, the *Sulfitobacter* strains used in these studies may prefer the organic N present in both the complex and glutamate media over the inorganic form, ammonium chloride, provided in the base medium.[139] The absence of an exogenous source of organic N in the acetate-based medium, may have contributed to the strains' poor growth on this substrate. While the N:P ratio of marine bacteria is typically 16:1, the N:P ratio of the defined media used in this study was ~20:1.[152] The N:P of the complex substrate was more difficult to assess due to the lack of elemental composition data for tryptone and yeast extract in the literature, but neither is expected to be limiting in this medium.

Sulfitobacter metabolite profiles are more defined by provided nutrients than strain-phage pair. Across the three media types, there was little (15%) overlap in the metabolites that were detected and identified. This is comparable to a recent study in *Pseudomonas aeruginosa*, in which only 40% of 145 detectable metabolites were found across all strains raised on six distinct carbon substrates but contrasts findings in *Bacillus subtilius* raised on three different carbon mixtures, where >90% of the 46 measured metabolites were present across all growth conditions.[153-154] Moreover, the intracellular metabolomes of these *B. subtilis* cultures were largely indistinguishable. However, in that study all media types contained glucose, varying only by addition of a secondary carbon substrate (malate, fumarate, or citrate), making the comparison to this work less relevant.

Metabolome differences between-strains raised under the same growth conditions were evident and most pronounced in glutamate- and acetate-grown cultures. The most divergent metabolomes between the two strains were the acetate-grown cultures, where the metabolite profiles of both strains became increasingly divergent throughout growth. This result is consistent with the influence of phage-mediated cell lysis, which was strongly evident in the CB-A cultures, on host cell metabolism.[139] In contrast, significant differences in

metabolite pools for the glutamate-grown cultures were greatest in early and mid-exponential phases, but the metabolomes were largely similar as the cells reached stationary phase. This suggests prophage-related effects in this growth medium were most apparent in actively growing cells. As was seen with the acetate-grown cultures, the between-strain comparisons indicate the overwhelming majority of these differences were the result of an increase in a given metabolite in the CB-A cells relative to CB-D. Additionally, a size difference in the two strains is apparent when grown on glutamate, specifically CB-D is significantly larger than CB-A. This is relevant since metabolites are normalized to OD which correlates to cell number, so that the strains can be more appropriately compared. Though accurate biovolumes for these two strains were not determined, it can be anticipated that the metabolite concentration differences between the two strains, on a per cell basis, is greater than what is reported here as the smaller cells had higher cell-number normalized concentrations. Furthermore, these results are consistent with earlier studies in the same *Sulfitobacter* host strain that revealed a generalized increase in most measurable metabolites in response to an obligately lytic viral infection.[139] The morphological difference of the two lysogens on glutamate is intriguing and may be related to differential N quota needed by each lysogen: CB-A has intrinsically higher rates of spontaneous induction than CB-D and thus is anticipated to have a higher N demand due to viral production.[139, 141] Detection of infectious phage particles in the culture medium is an indication of cell lysis. However, despite the detection of infectious particles in CB-A cultures, the cell viability was indistinguishable from CB-D over the course of the growth curves. This was also true for the strains grown on complex medium. However, the metabolomes from the complex medium grown strains were far less divergent than those grown on the two defined substrates. As both the glutamate and complex media contain organic forms of N, these results suggest that supplemental organic N may reduce the fitness costs associated with prophage induction in the CB-A strain.

The lipid profiles support the metabolite data in that strains can be discriminated by growth medium and strain-phage pairs. Unlike the metabolite profiles, nearly all detected lipids were present across all samples. Mirroring the metabolite profiling, strain level differences were not strongly apparent in complex medium-grown cultures, but significant between strains grown on either of the defined media, resulting in upwards of 50% and 60% variation in lipid profiles between the strains when grown on acetate and glutamate, respectively. The observed variation was noted in both the overall composition of the lipid classes as well as in the composition of the acyl moieties. Temporal variation in lipid profiles for batch grown cultures is expected and anticipated to be the result of changing environmental conditions that occur in a closed system (e.g., changes in nutrient concentrations, accumulation of metabolite waste products, alterations in oxygen levels).[126] As such, caution should be given against drawing summative conclusions regarding the temporal variation evident in these lipid profiles, but the observed variation demonstrates a flexibility in lipid composition in these strains that warrants further study.

The lipid classes identified in this study are the same major (PC, PG, PE) and minor (APG, AL) classes found in other characterized *Sulfitobacter* species reared in a complex medium[155]. A common bacterial phospholipid class, cardiolipin, has been reported as a minor lipid in Roseobacters, including *Sulfitobacter* species [156], but was not detected in our strains. The presence of an unidentified lipid class in our strains is consistent with findings in other sulfitobacters [155]. However, the methods of lipid identification employed (TLC vs UHPLC-HRMS) prevent direct comparisons here, representing an area for future study.

The most striking difference in lipid composition across media types occurs within the phospholipid classes. Most notable is the relative abundance of PE and PG. Lipids within these two classes typically co-occur in diverse bacteria. Molecular simulations suggest interactions between the two influence membrane integrity; increases in PG relative to PE are predicted to increase membrane

stability and decrease membrane permeability [157]. PE was the dominant phospholipid in complex medium-grown cells whereas PG dominated in the glutamate- and acetate-grown cells, suggestive of a fundamentally different membrane architecture when these strains are grown on defined vs complex media. Given common parameters influencing lipid composition in bacteria were held static across the medium types (i.e., pH, salinity, and temperature), a likely interpretation is that the differences are due to other components of the medium, namely the primary growth substrate(s) and/or nutrients. The extent to which the relative proportions of the identified phospholipid classes change in response to primary growth components in this and other groups of marine bacteria does not appear to be well understood, with examples in the literature difficult to identify. Studies in the non-marine bacterium, *E. coli*, reveal no significant difference in phospholipid composition in strains grown on the complex medium Luria Broth versus a minimal medium, M9, supplemented with glucose.[158] Early work conducted in *Bacillus subtilis* identified alterations in phospholipid composition that were ultimately linked to pH differences between media types, one supplemented with glucose.[159] In contrast, membrane phospholipid reconfiguration has been demonstrated in response to supplies of exogenous fatty acids, which can be directly incorporated into membrane lipids. This is a well-studied phenomenon in many human pathogens, including *Vibrio cholerae, Enterococcus faecalis* and *E. coli*, where it has been linked to virulence.[160-162]

Lipid remodeling, specifically the fatty acid tail component, by marine bacteria is a widespread strategy for dealing with nutrient limitation, particularly P.[163-165] Amino lipids are a common class of non-P containing lipids found amongst Roseobacters where their production has been linked to P limitation.[126, 142] However, they are also common in many *Sulfitobacter* species grown under non-limiting P conditions (i.e. in complex media).[155] Amino lipid head groups include ornithine, glutamine and lysine, all of which were identified in our strains. [131, 142, 166-167] The genes required for the production of glutamine and ornithine lipid in roseobacters has been elucidated and are present in the strains.[142] Amino lipids

were identified in all growth conditions tested here, which suggest their production is not exclusively linked to P status. This finding, coupled with the prevalence of this lipid class in members of the *Sulfitobacter* genus, indicates amino lipids play an integral physiological role in this group of bacteria.

Differences in lipid profiles between the strains were most evident in the ornithine (OL) and glutamine lipid (QL) classes and when grown on glutamate and acetate. The general trend was an increased abundance of these ALs in CB-D relative to CB-A. Silvano and coworkers reported an increase in OL in Roseobacter strains in response to P starvation; the strains under study did not produce QL.[165] The data collected in this study indicates phage activity may play a previously unrecognized role in alteration of AL composition. It has been proposed that OL may lead to enhanced membrane stability, and this lipid is required for optimal c-type cytochrome function in the alpha-Proteobacterium *Rhodobacter capsulatus*, comprehensive functional characterization of bacterial amino lipids is relatively limited.[168-169] As a consequence, interpretation of the results from this system is presently challenging. In an unexpected finding, a highly significant, and abundant (upwards of 50% of the total lipids in CB-A cultures grown on acetate) lipid-like class of spectral features was detected. As with the aforementioned amino lipids, these features displayed notable differences between strains raised on the same growth medium. As such, these features are intriguing and would be of interest for future studies. Once this class of lipid-like features is identified, more work can be done to determine the biological role of these compounds and how they relate to growth conditions, phage activity, and cell stress.

The bacterial metabolome comprises only a small fraction of the total cellular dry weight (~3%), and this collection of molecules primarily exists to provide energy and building blocks for macromolecular biosynthesis.[170] Bacterial metabolism is highly responsive to substrate and nutrient availability, but it is also known to be influenced by viral infection. However, these forces are not unidirectional: viral infection is sensitive and responsive to cellular metabolism, as it is often wholly dependent upon the host cell processes to produce viral

progeny.[171] As both nutrient fluctuations and virus pressure are common features of most natural ecosystems, including the coastal oceans where Roseobacters dominate, the physiologies of resident bacteria are anticipated to be shaped by these intersecting factors. The metabolic and lipid profiling presented here provides a first look at the complexity of these interactions and lays the foundation for future studies that relate cellular composition with function.

3.5 Materials and Methods

3.5.1 Bacterial propagation in different growth conditions.

Sulfitobacter sp. strains CB-A and C-D (formerly Sulfitobacter sp. strain CB2047) [141] were inoculated and incubated overnight in 10ml cultures at 25^{o}C at 200rpm.[141] Strains were grown in Standard Marine Media (SMM) [4.1 M NaCl; 950 mM KCl; 700 mM $CaCl_2$; 20 mM H_3BO_3; 2.1 mM $MgSO_4$ ($7H_2O$); 2.0 M $MgCl_2$; 1.0 M Tris (Tris-HCl and Tris-Base; pH 7.5); 800 mM $NaHCO_3$; 5.0 M NH_4Cl; 150 mM K_2HPO_4. 1.125g yeast extract, 2g tryptone, Fe, vitamins and minerals], or Roseobacter Marine Media (RMM) [4 M NaCl; 0.2 M KCl; 0.2M CaCl2; 1.0 M $MgSO_4$ ($7H_2O$); 1.0 M Tris-HCl (pH 7.5); 0.5M NH_4Cl; 50 mM K_2HPO_4, Fe, vitamins and minerals] supplemented with either (4 mM L-glutamic acid [glutamate], or 10 mM sodium acetate [acetate]. The concentrations of acetate and glutamate contain comparable amounts of carbon. Overnight cultures were sub-cultured, and 0 hr samples were taken at $OD_{540nm} \approx 0.17$. Growth was monitored every two hours for 24 hr. Samples were taken at 0, 4, 8 and 21 hr for SMM grown cells, and 0, 10, 18 and 24 hr for glutamate and acetate grown cells. Both strains were initially grown in SMM in biological triplicate, then grown in glutamate and acetate in five 200ml biological replicates. Growth dynamics, viable counts, and Spontaneous Prophage Induction (SPI) data were recorded for these growth conditions.

3.5.2 Sampling methodology.

Five milliliters of bacterial culture were filtered at each time point and taken for metabolomics processing and analysis. 5 mL of bacterial culture was

centrifuged at 4,000 rpm for 5 minutes at 4°C, then taken for lipidomics processing and analysis. Blanks were used as negative controls, and 0 hr data was used as reference points for data normalization. All data were normalized by optical density. 1 ml of bacterial culture was taken for serial dilutions (plating 10^{-5}, 10^{-6}, 10^{-7} dilutions), to obtain viable counts data and CFU/ml. Serial dilutions were plated in technical triplicate. Optical density readings and viable counts were conducted for the five biological replicates at OD_{540nm}. 12 mL of bacterial culture was filtered at each time point, flash frozen in liquid nitrogen, and archived at -80°C for future transcriptomics analysis. 2 mL of culture was taken for flow cytometry. All sampling was conducted for five biological replicates for all time points. For complex media cultures, all sampling was conducted in biological triplicate.

3.5.3 Metabolomics.

Water-soluble metabolites were extracted from filtered samples using 4:4:2 acetonitrile:methanol:water with 0.1 M formic acid as previously described.[172] Analysis of the extracted metabolites was carried out using UHPLC-HRMS (Thermo Scientific, San Jose, CA, USA) with a previously validated untargeted metabolomics method.[173] The metabolites were separated using reversed phase chromatography utilizing a Synergi Hydro RP column (100mmx 2.1 mm, 2.6 µm, 100 Å; Phenomenex, Torrance, CA) and an UltiMate 3000 pump (Thermo Scientific). All solvents used were HPLC grade. An Exactive Plus Orbitrap MS (Thermo Scientific) was used for the full scan mass analysis. For the glutamate- and acetate-grown cells, each biological replicate was analyzed by UHPLC-HRMS in triplicate. Following the mass analysis, metabolites were identified by exact mass and retention time from an in-house standard library using the open source software package, Metabolomics Analysis and Visualization Engine (MAVEN).[174-175] Area under the curve (AUC) was integrated and normalized according to OD prior to being used for further statistical analyses.

3.5.4 Lipidomics.

Lipids were extracted from cell pellets using 15:15:5:1:0.18 95% ethanol, water, diethyl ether, pyridine, and 4.2 N ammonium hydroxide followed by a water saturated butanol extraction according to the protocol for glycerophospholipids and sphingolipids described by Guan and coworkers.[176] The extracted lipids were dried under a steady stream of nitrogen, resuspended in 300 µl of a 9:1 ratio of methanol:chloroform prior to UHPLC-HRMS analysis. Extracted lipids were analyzed by UHPLC-HRMS using an established untargeted lipidomics method.[177] The chromatographic separations were performed using a Kinetex HILIC column (150 mm × 2.1 mm, 2.6 µm, 100 Å; Phenomenex) and an UltiMate 3000 pump (Thermo Scientific). The full scan mass analysis was carried out in both positive and negative ionization modes with an Exactive Plus Orbitrap MS (Thermo Scientific). Glutamate- and acetate-grown cells were analyzed in triplicate by UHPLC-HRMS. The phospholipids were then identified by exact mass and retention time by comparison to an in-house standard library using MAVEN. Amino lipids were also identified by exact mass using MAVEN. Amino lipids were confirmed using isotopic patterns as well as fragmentation data gathered by all ion fragmentation utilizing high energy collision dissociation (HCD). Amino lipids KL, OL, and QL were detected at retention times of 10.7, 10.6, and 2.5 minutes, respectively. Statistical analyses were performed on the OD normalized AUC.

3.5.5 Spot plating assays for SPI detection.

1 mL of bacterial culture was taken for Spontaneous Prophage Induction (SPI) detection. *Sulfitobacter* sp. strains CB-A and CB-D were inoculated in duplicate and incubated overnight in 10 mL of SMM, glutamate or acetate, at 200 rpm at 25^{o}C. *Sulfitobacter* sp. strains were sub-cultured in SMM, glutamate or acetate, and at an optical density of 0.10-0.17 (OD_{540nm}), 500 µL of bacterial culture was added to 3 mL top agar aliquots and plated. Top agar was prepared ahead of time using 0.55-0.6 g (0.55-0.60%) noble agar. Once this top layer dried, 10 µl of ϕ-D and ϕ-A lysate were spot plated in technical triplicate. Serial dilutions were

done for viral lysate of ϕ-A and ϕ-D, ranging from undiluted to 10^{-4} for ϕ-A, and from undiluted to 10^{-2} for ϕ-D. The schematic included a media only control. Plates were incubated at room temperature, and zones of clearing were observed 24-48 hours after plating.

3.5.6 Statistical analysis.

All data were normalized according to OD. Five replicates were done per time point. Heat maps show fold change of CB-A relative to CB-D and significant differences denoted by asterisks (* = $p<0.1$; ** = $p<0.05$; *** = $p<0.01$). Partial least squares discriminant analysis (PLS-DA) was performed using MetaboAnalyst 4.0.[110] Prior to PLS-DA data was filtered using interquartile range (IQR), normalized by optical density, log 2 transformed, and Pareto scaled. PLS-DA was used to determine the relationship between two matrices to visualize differences between organism groups and substrates. Heatmaps were prepared using R statistical program (version 3.5.1). Fold changes were log 2 transformed. The JGI IMG portal was used to search for the OL and QL biosynthesis gene organization in the *Sulfitobacter* sp. strains CB-D and CB-A genomes.

3.6 Conclusions

In conclusion, the metabolic and lipidomic profiles of *Sulfitobacter* sp. strains CB-D and CB-A were analyzed in three different growth conditions. The growth conditions varied by the available nutrients, specifically one had a complex mixture of organic carbon and nitrogen sources, provided in tryptone and yeast extract. The second growth condition contained a single organic carbon and nitrogen source, namely glutamate. The final growth condition contained only acetate as a single organic carbon source, and no organic nitrogen. Between these three growth substrates there were dramatic differences between the metabolome, but only small scale differences between the strains when provided the same nutrient. In contrast, depending on the nutrient provided, there were vast differences between the lipid profiles of the two strains. Specifically, when grown on acetate, the strains displayed the greatest differences, while only minimal

differences were apparent when the strains were grown on complex substrates. In addition to the broad scale differences between the global lipid profiles, specific lipid classes were investigated, including the largely uncharacterized amino lipids. From this class of lipids, three different head groups were detected, ornithine lipid, glutamine lipid, and lysine lipid. Analysis of these lipids revealed significant differences between the strains when grown on either glutamate or acetate. These growth substrate dependent alterations between strains indicate that there may be differences nutrient preferences of the phages, warranting further research.

Appendix

Table 3.1 Media comparisons for complex, glutamate, and acetate carbon sources. Total carbon, organic nitrogen, inorganic nitrogen, and combined nitrogen molar concentrations are calculated for all substrates. C:N ratios are calculated for all substrates.

Totals (mM)			
	Complex	Glutamate	Acetate
Carbon	171.72	20	20
Organic N	22.31	4	0
Inorganic N	5	10	10
Combined N	27.31	14	10
Ratios			
	Complex	Glutamate	Acetate
C:N	6.29	1.43	2
C:N (organic N)	7.7	5	0
C:N (inorganic N)	34.34	2	2

Table 3.2 Incidence of SPI from *Sulfitobacter* sp. strains CB-D and CB-A cells grown in SMM were detected through spot plating assays using serial dilutions ranging from 10^0 to 10^{-3}. Data for biological replicates are reported for all treatments and time points (n= 3 in SMM grown cells; n= 5 in glutamate and acetate grown cells). Plating was done in technical triplicate. Detection of SPI is denoted by asterisks (* = detection at 10^0 dilution; ** = detection at 10^{-1} dilution; *** = detection at 10^{-2} dilution; **** = detection at 10^{-3} dilution; n.d. = not detected).

SMM

Time	Treatment	Biological Replicate	SPI detected	Time	Treatment	Biological Replicate	SPI detected
T0	CB-A (addition of 0.2um filter sterilized CB-A spent media to host CB-D)	A	*	T10	CB-A (addition of 0.2um filter sterilized CB-A spent media to host CB-D)	A	*
		B	*			B	n.d.
		C	*			C	n.d.
	CB-D (addition of 0.2um filter sterilized CB-D spent media to host CB-A)	A	n.d.		CB-D (addition of 0.2um filter sterilized CB-D spent media to host CB-A)	A	n.d.
		B	n.d.			B	n.d.
		C	n.d.			C	n.d.
T8	CB-A (addition of 0.2um filter sterilized CB-A spent media to host CB-D)	A	n.d.	T24	CB-A (addition of 0.2um filter sterilized CB-A spent media to host CB-D)	A	*
		B	*			B	*
		C	n.d.			C	*
	CB-D (addition of 0.2um filter sterilized CB-D spent media to host CB-A)	A	n.d.		CB-D (addition of 0.2um filter sterilized CB-D spent media to host CB-A)	A	n.d.
		B	n.d.			B	n.d.
		C	n.d.			C	n.d.

Table 3.3 Incidence of SPI from *Sulfitobacter* sp. strains CB-D and CB-A cells grown in glutamate were detected through spot plating assays using serial dilutions ranging from 10^0 to 10^{-3}. Data for biological replicates are reported for all treatments and time points (n= 3 in SMM grown cells; n= 5 in glutamate and acetate grown cells). Plating was done in technical triplicate. Detection of SPI is denoted by asterisks (* = detection at 10^0 dilution; ** = detection at 10^{-1} dilution; *** = detection at 10^{-2} dilution; **** = detection at 10^{-3} dilution; n.d. = not detected).

4mM glutamate

Time	Treatment	Biological Replicate	SPI detected	Time	Treatment	Biological Replicate	SPI detected
T0	CB-A (addition of 0.2um filter sterilized CB-A spent media to host CB-D)	A	**	T18	CB-A (addition of 0.2um filter sterilized CB-A spent media to host CB-D)	A	***
		B	**			B	**
		C	**			C	**
		D	**			D	***
		E	**			E	***
	CB-D (addition of 0.2um filter sterilized CB-D spent media to host CB-A)	A	n.d.		CB-D (addition of 0.2um filter sterilized CB-D spent media to host CB-A)	A	n.d.
		B	n.d.			B	n.d.
		C	n.d.			C	n.d.
		D	n.d.			D	n.d.
		E	n.d.			E	n.d.
T10	CB-A (addition of 0.2um filter sterilized CB-A spent media to host CB-D)	A	**	T24	CB-A (addition of 0.2um filter sterilized CB-A spent media to host CB-D)	A	***
		B	**			B	***
		C	**			C	n.d.
		D	**			D	n.d.
		E	**			E	***
	CB-D (addition of 0.2um filter sterilized CB-D spent media to host CB-A)	A	n.d.		CB-D (addition of 0.2um filter sterilized CB-D spent media to host CB-A)	A	n.d.
		B	n.d.			B	n.d.
		C	n.d.			C	n.d.
		D	n.d.			D	n.d.
		E	n.d.			E	n.d.

Table 3.4 Incidence of SPI from *Sulfitobacter* sp. strains CB-D and CB-A cells grown in acetate were detected through spot plating assays using serial dilutions ranging from 10^0 to 10^{-3}. Data for biological replicates are reported for all treatments and time points (n= 3 in SMM grown cells; n= 5 in glutamate and acetate grown cells). Plating was done in technical triplicate. Detection of SPI is denoted by asterisks (* = detection at 10^0 dilution; ** = detection at 10^{-1} dilution; *** = detection at 10^{-2} dilution; **** = detection at 10^{-3} dilution; n.d. = not detected).

10mM acetate

Time	Treatment	Biological Replicate	SPI detected	Time	Treatment	Biological Replicate	SPI detected
T0	CB-A (addition of 0.2um filter sterilized CB-A spent media to host CB-D)	A	*	T18	CB-A (addition of 0.2um filter sterilized CB-A spent media to host CB-D)	A	**
		B	*			B	*
		C	*			C	*
		D	n.d.			D	*
		E	***			E	****
	CB-D (addition of 0.2um filter sterilized CB-D spent media to host CB-A)	A	n.d.		CB-D (addition of 0.2um filter sterilized CB-D spent media to host CB-A)	A	n.d.
		B	n.d.			B	n.d.
		C	n.d.			C	n.d.
		D	n.d.			D	n.d.
		E	n.d.			E	n.d.
T10	CB-A (addition of 0.2um filter sterilized CB-A spent media to host CB-D)	A	**	T24	CB-A (addition of 0.2um filter sterilized CB-A spent media to host CB-D)	A	*
		B	**			B	n.d.
		C	*			C	*
		D	***			D	****
		E	*			E	*
	CB-D (addition of 0.2um filter sterilized CB-D spent media to host CB-A)	A	n.d.		CB-D (addition of 0.2um filter sterilized CB-D spent media to host CB-A)	A	n.d.
		B	n.d.			B	n.d.
		C	n.d.			C	n.d.
		D	n.d.			D	n.d.
		E	n.d.			E	n.d.

Table 3.5 Optical density and viable counts data for *Sulfitobacter* sp. strains CB-A and CB-D grown in SMM. Averages and standard deviations data for biological replicates are reported for all treatments and time points (n= 3).

Complex medium								
	CB-A				CB-D			
	optical density		viable counts		optical density		viable counts	
Time	Av	Stdev	Av	Stdev	Av	Stdev	Av	Stdev
-1	0.07	0.01			0.07	0.01		
0	0.14	0.03	2.93E+08	6.67E+07	0.15	0.02	4.59E+08	7.38E+07
2	0.28	0.04			0.3	0.02		
4	0.49	0.03	1.37E+09	1.80E+08	0.5	0.02	1.25E+09	1.82E+08
6	0.69	0.01			0.64	0.04		
8	0.81	0.01	3.67E+09	3.68E+08	0.75	0.06	2.80E+09	2.35E+08
10	0.89	0.02			0.87	0.05		
12	0.97	0.03			0.96	0.03		
18	1.12	0.03			1.13	0.03		
21	1.13	0.01	5.36E+09	5.11E+08	1.14	0.03	4.37E+09	4.94E+08

Table 3.6 Optical density and viable counts data for *Sulfitobacter* sp. strains CB-A and CB-D grown on glutamate. Averages and standard deviations data for biological replicates are reported for all treatments and time points (n= 5).

4mM glutamate medium								
	CB-A				CB-D			
	optical density		viable counts		optical density		viable counts	
Time	Av	Stdev	Av	Stdev	Av	Stdev	Av	Stdev
0	0	0	1.89E+07	1.57E+07	0.02	0	9.23E+07	2.88E+07
1	0	0			0.02	0		
10	0.05	0.01	1.13E+08	3.51E+07	0.09	0.02	2.04E+08	4.10E+07
12	0.07	0.02			0.12	0.02		
14	0.11	0.04			0.16	0.03		
16	0.15	0.05			0.2	0.04		
18	0.21	0.07	5.93E+08	2.43E+08	0.28	0.05	7.69E+08	2.00E+08
20	0.26	0.06			0.34	0.06		
24	0.42	0.04	1.54E+09	4.90E+08	0.45	0.01	2.02E+09	7.16E+08

Table 3.7 Optical density and viable counts data for *Sulfitobacter* sp. strains CB-A and CB-D grown on acetate. Averages and standard deviations data for biological replicates are reported for all treatments and time points (n= 5).

10mM acetate medium								
	CB-A				CB-D			
	optical density		viable counts		optical density		viable counts	
Time	Av	Stdev	Av	Stdev	Av	Stdev	Av	Stdev
0	0.01	0	1.50E+07	5.32E+06	0.02	0.01	6.46E+07	2.19E+07
2	0.01	0			0.02	0.01		
10	0.02	0	7.48E+07	3.95E+07	0.06	0.04	1.44E+08	7.60E+07
12	0.02	0			0.07	0.03		
14	0.03	0.01			0.08	0.03		
16	0.03	0.01			0.09	0.04		
18	0.04	0.01	1.40E+08	5.28E+07	0.11	0.05	4.63E+08	2.14E+08
20	0.05	0.01			0.13	0.06		
24	0.07	0.02	2.85E+08	1.07E+08	0.19	0.08	1.02E+09	6.85E+08

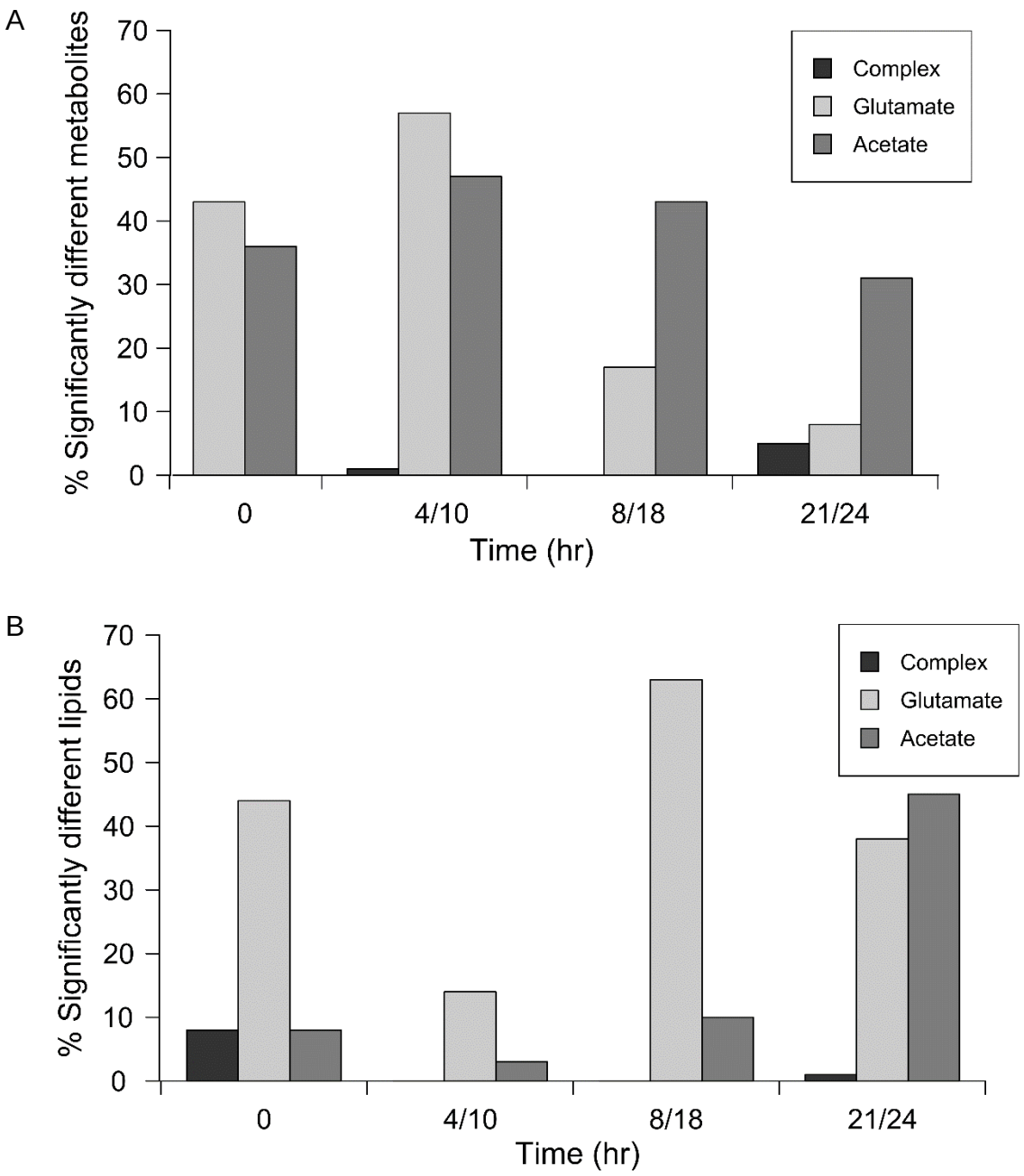


Figure 3.7 Percentages of significantly different (A) metabolites and (B) lipids of SMM (dark gray), glutamate (light gray) and acetate grown cells (medium gray). Significant difference is defined as fold change > 1.5 and p-value < 0.05. All data are normalized according to optical density. Averages of biological replicates are reported for all treatments (n= 3 in SMM grown cells; n= 5 in glutamate and acetate grown cells).

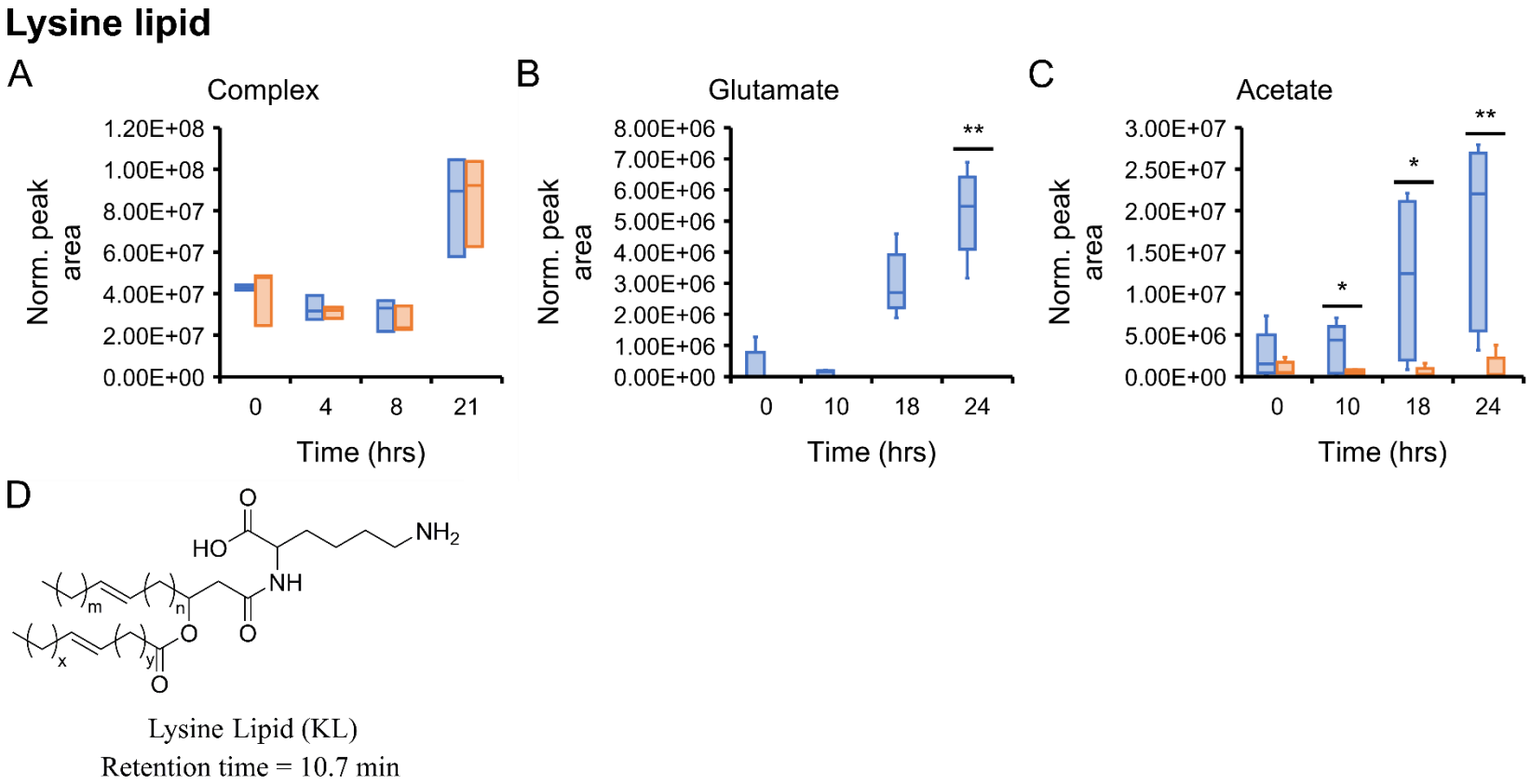


Figure 3.8 Lysine lipid (KL) in *Sulfitobacter* sp. strains CB-A (orange) and CB-D (blue). Box & whisker plots highlight differences between strains and time, and between substrates. These plots are shown for all substrates, (A) standard marine media (SMM), (B) glutamate, and (C) acetate. Significant differences are denoted by asterisks (* = $p<0.1$; ** = $p<0.05$). Averages of biological replicates are reported for all treatments (n= 3 in SMM grown cells; n= 5 in glutamate and acetate grown cells). All data are normalized according to optical density. Structures of (D) lysine lipid (KL), with respective retention time.

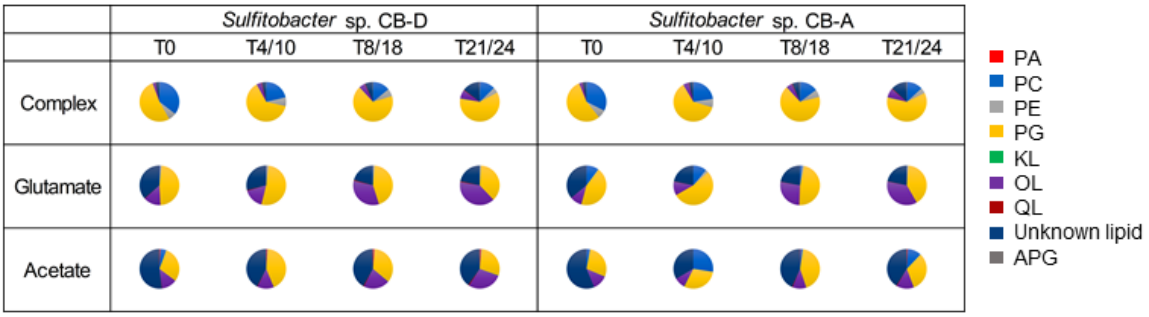


Figure 3.9 Pie charts display relative proportions of the sum of lipid intensities to total detected lipid intensities in *Sulfitobacter* sp. strains CB-D and CB-A for each timepoint and substrate. Ratios are shown for phosphatidic acid, phosphatidylcholine, phosphatidylethanolamine, phosphatidylglycerol, lysine lipid, ornithine lipid, glutamine lipid, an unidentified class of lipid-like features, and acyl-phosphatidylglycerol. All data are normalized according to optical density. Averages of biological replicates are reported for all treatments (n= 3 in SMM grown cells; n= 5 in glutamate and acetate grown cells) and are within 2 standard deviations.

Conclusion

The benefits of including metabolomics in nutritional studies has been highlighted in this dissertation. Nutrition and metabolism are intrinsically connected, and with mass spectrometry based metabolomics, a broad range of molecules can be detected. Because of this metabolomics can help to increase the understanding of the underlying mechanisms behind specific nutrients and factors influencing metabolic health of biological organisms. However, due to the complexity of metabolism and intertwined nature of metabolic pathways, frequently there is not one specific pathway that displays alterations, but rather multiple pathways exhibit changes. Despite these challenges metabolomics remains a useful tool for nutrition based studies.

In the first chapter of this dissertation, metabolomics was used to investigate the underlying metabolic alterations caused by exercise and western diet. Many metabolomics studies focus on only one variable at a time to reduce the complexity. However, as many different factors can influence metabolism and the gut microbiome, this study investigated both the impact of unhealthy diet and short-term voluntary exercise. From this study it was determined that dietary choices have a greater influence on the circulating and intestinal metabolism than short term voluntary exercise. Nevertheless, there were some metabolic alterations induced by exercise, particularly in the cecum contents. As noticeable alterations were present after short term exercise, long term exercise is likely to increase the metabolic differences.

The second chapter of this dissertation utilized metabolomics to analyze the effect of fenugreek, an herbal dietary supplement, in the presence of either a high fat or western diet. These studies analyzed liver, serum, and intestinal contents of mice exposed to high fat, western (high fat and high sucrose), or respective low fat control diets each with and without fenugreek seeds for 14 weeks. From these analyses, it was determined that fenugreek impacts several metabolic pathways, rather than a single isolated pathway. Fenugreek was observed to have the greatest impact on the large intestinal contents, however, the liver and serum metabolic profiles displayed differences with fenugreek supplementation. This

suggests that fenugreek alters the metabolites absorbed through the small intestines, which in turn impacts the circulating metabolome.

While it is well known that nutrition is vital for mammalian health, it is also important for environmental systems. For this purpose, the third and final chapter of this dissertation transitioned from mammalian nutrition and health applications to environmental studies. Specifically, the effect of nutrients on host-phage interactions was examined in lysogens from the environmentally relevant *Roseobacter* clade. The three nutrients included a complex medium with unlimited organic carbon, nitrogen, and phosphorus sources, and minimal media with either glutamate, an organic carbon and nitrogen source, or acetate, a carbon source only. Using these three growth substrates allowed for greater insight into not only the carbon utilization, but also to the preferred nitrogen sources. To analyze the impact of these nutrients, metabolomics and lipidomics were employed. Metabolomics did not reveal substantial differences between the strains within nutrients but did reveal metabolome distinctions based on growth substrate. However, the lipidomics displayed dramatic differences between the strains when grown on acetate. This revealed that the lipid profiles of the strains are significantly influenced by the phage in a nutrient dependent manner. Additionally, in this study, the presence of a minor class of lipids, the aminolipids, was confirmed and these lipids were determined to significantly differ between strains in glutamate and acetate grown cultures. The results of this study revealed that the host-phage interactions are heavily influenced by the available nutrients. These results increase the understanding of host-phage interactions and are particularly relevant as lysogeny is highly prevalent in nature, and nutrients are often in flux in marine environments.

These three chapters contribute to the understanding of nutrition at a molecular level in different applications. While the first two chapters focus on health applications and relate to the obesity epidemic and malnutrition, the third chapter highlights the broad scope of nutritional and metabolomic investigations. Future researchers can build upon these studies to answer further questions, whether

about the specific roles of the gut microbiome, or nutrient recycling and bacteriophages.

References

1. Micha, R.; Peñalvo, J. L.; Cudhea, F.; Imamura, F.; Rehm, C. D.; Mozaffarian, D., Association Between Dietary Factors and Mortality From Heart Disease, Stroke, and Type 2 Diabetes in the United States. *JAMA* **2017,** *317* (9), 912-924.

2. Mozaffarian, D., Dietary and Policy Priorities for Cardiovascular Disease, Diabetes, and Obesity. *Circulation* **2016,** *133* (2), 187-225.

3. O'Neil, A.; Quirk, S. E.; Housden, S.; Brennan, S. L.; Williams, L. J.; Pasco, J. A.; Berk, M.; Jacka, F. N., Relationship Between Diet and Mental Health in Children and Adolescents: A Systematic Review. *American Journal of Public Health* **2014,** *104* (10), e31-e42.

4. Felice N. Jacka, Ph.D. ,; Julie A. Pasco, Ph.D. ,; Arnstein Mykletun, Ph.D. ,; Lana J. Williams, Ph.D. ,; Allison M. Hodge, Ph.D. ,; Sharleen Linette O'Reilly, Ph.D. ,; Geoffrey C. Nicholson, M.D., Ph.D. ,; Mark A. Kotowicz, M.D. , and; Michael Berk, M.D., Ph.D., Association of Western and Traditional Diets With Depression and Anxiety in Women. *American Journal of Psychiatry* **2010,** *167* (3), 305-311.

5. Sánchez-Villegas, A.; Verberne, L.; De Irala, J.; Ruíz-Canela, M.; Toledo, E.; Serra-Majem, L.; Martínez-González, M. A., Dietary Fat Intake and the Risk of Depression: The SUN Project. *PLOS ONE* **2011,** *6* (1), e16268.

6. Beisel, W. R., Nutrition and Immune Function: Overview. *The Journal of nutrition* **1996,** *126* (suppl_10), 2611S-2615S.

7. De Rosa, V.; Galgani, M.; Santopaolo, M.; Colamatteo, A.; Laccetti, R.; Matarese, G., Nutritional control of immunity: Balancing the metabolic requirements with an appropriate immune function. *Seminars in Immunology* **2015,** *27* (5), 300-309.

8. Wang, J.; Suo, Y.; Zhang, J.; Zou, Q.; Tan, X.; Yuan, T.; Liu, Z.; Liu, X., Lycopene supplementation attenuates western diet-induced body weight gain through increasing the expressions of thermogenic/mitochondrial functional genes and improving insulin resistance in the adipose tissue of obese mice. *The Journal of Nutritional Biochemistry* **2019,** *69*, 63-72.

9. Cordeiro, M. M.; Biscaia, P. B.; Brunoski, J.; Ribeiro, R. A.; Franco, G. C. N.; Scomparin, D. X., Vitamin D supplementation decreases visceral adiposity

and normalizes leptinemia and circulating TNF-α levels in western diet-fed obese rats. *Life Sciences* **2021,** *278*, 119550.

10. Noble, E. E.; Hsu, T. M.; Kanoski, S. E., Gut to Brain Dysbiosis: Mechanisms Linking Western Diet Consumption, the Microbiome, and Cognitive Impairment. *Frontiers in Behavioral Neuroscience* **2017,** *11* (9).

11. Mazzone, G.; Morisco, C.; Lembo, V.; D'Argenio, G.; D'Armiento, M.; Rossi, A.; Giudice, C. D.; Trimarco, B.; Caporaso, N.; Morisco, F., Dietary supplementation of vitamin D prevents the development of western diet-induced metabolic, hepatic and cardiovascular abnormalities in rats. *United European Gastroenterology Journal* **2018,** *6* (7), 1056-1064.

12. Liu, J.; He, Z.; Ma, N.; Chen, Z.-Y., Beneficial Effects of Dietary Polyphenols on High-Fat Diet-Induced Obesity Linking with Modulation of Gut Microbiota. *Journal of Agricultural and Food Chemistry* **2020,** *68* (1), 33-47.

13. Milne, S. B.; Mathews, T. P.; Myers, D. S.; Ivanova, P. T.; Brown, H. A., Sum of the Parts: Mass Spectrometry-Based Metabolomics. *Biochemistry* **2013,** *52* (22), 3829-3840.

14. Ryan, D.; Robards, K., Metabolomics: The Greatest Omics of Them All? *Analytical Chemistry* **2006,** *78* (23), 7954-7958.

15. Putri, S. P.; Nakayama, Y.; Matsuda, F.; Uchikata, T.; Kobayashi, S.; Matsubara, A.; Fukusaki, E., Current metabolomics: Practical applications. *Journal of Bioscience and Bioengineering* **2013,** *115* (6), 579-589.

16. Reily, M. D.; Tymiak, A. A., Metabolomics in the pharmaceutical industry. *Drug Discovery Today: Technologies* **2015,** *13*, 25-31.

17. Cevallos-Cevallos, J. M.; Reyes-De-Corcuera, J. I.; Etxeberria, E.; Danyluk, M. D.; Rodrick, G. E., Metabolomic analysis in food science: a review. *Trends in Food Science & Technology* **2009,** *20* (11), 557-566.

18. Lu, W.; Bennett, B. D.; Rabinowitz, J. D., Analytical strategies for LC–MS-based targeted metabolomics. *Journal of Chromatography B* **2008,** *871* (2), 236-242.

19. Woodall, B. M.; Harp, J. R.; Brewer, W. T.; Tague, E. D.; Campagna, S. R.; Fozo, E. M., Enterococcus faecalis Readily Adapts Membrane Phospholipid

Composition to Environmental and Genetic Perturbation. *Frontiers in Microbiology* **2021,** *12* (1118).

20. Ibáñez, C.; Mouhid, L.; Reglero, G.; Ramírez de Molina, A., Lipidomics Insights in Health and Nutritional Intervention Studies. *Journal of Agricultural and Food Chemistry* **2017,** *65* (36), 7827-7842.

21. Hills, R. D.; Pontefract, B. A.; Mishcon, H. R.; Black, C. A.; Sutton, S. C.; Theberge, C. R., Gut Microbiome: Profound Implications for Diet and Disease. *Nutrients* **2019,** *11* (7), 1613.

22. Zinöcker, M. K.; Lindseth, I. A., The Western Diet–Microbiome-Host Interaction and Its Role in Metabolic Disease. *Nutrients* **2018,** *10* (3), 365.

23. Moco, S.; Martin, F.-P. J.; Rezzi, S., Metabolomics View on Gut Microbiome Modulation by Polyphenol-rich Foods. *Journal of Proteome Research* **2012,** *11* (10), 4781-4790.

24. Tu, P.; Bian, X.; Chi, L.; Gao, B.; Ru, H.; Knobloch, T. J.; Weghorst, C. M.; Lu, K., Characterization of the Functional Changes in Mouse Gut Microbiome Associated with Increased Akkermansia muciniphila Population Modulated by Dietary Black Raspberries. *ACS Omega* **2018,** *3* (9), 10927-10937.

25. Han, S.; Van Treuren, W.; Fischer, C. R.; Merrill, B. D.; DeFelice, B. C.; Sanchez, J. M.; Higginbottom, S. K.; Guthrie, L.; Fall, L. A.; Dodd, D.; Fischbach, M. A.; Sonnenburg, J. L., A metabolomics pipeline for the mechanistic interrogation of the gut microbiome. *Nature* **2021,** *595* (7867), 415-420.

26. Stražar, M.; Temba, G. S.; Vlamakis, H.; Kullaya, V. I.; Lyamuya, F.; Mmbaga, B. T.; Joosten, L. A. B.; van der Ven, A. J. A. M.; Netea, M. G.; de Mast, Q.; Xavier, R. J., Gut microbiome-mediated metabolism effects on immunity in rural and urban African populations. *Nature Communications* **2021,** *12* (1), 4845.

27. Bäckhed, F.; Ley, R. E.; Sonnenburg, J. L.; Peterson, D. A.; Gordon, J. I., Host-Bacterial Mutualism in the Human Intestine. *Science* **2005,** *307* (5717), 1915-1920.

28. Tremaroli, V.; Bäckhed, F., Functional interactions between the gut microbiota and host metabolism. *Nature* **2012,** *489* (7415), 242-249.

29. Quiroga, R.; Nistal, E.; Estébanez, B.; Porras, D.; Juárez-Fernández, M.; Martínez-Flórez, S.; García-Mediavilla, M. V.; de Paz, J. A.; González-Gallego, J.; Sánchez-Campos, S.; Cuevas, M. J., Exercise training modulates the gut microbiota profile and impairs inflammatory signaling pathways in obese children. *Experimental & Molecular Medicine* **2020,** *52* (7), 1048-1061.

30. Cronin, O.; Barton, W.; Skuse, P.; Penney, N. C.; Garcia-Perez, I.; Murphy, E. F.; Woods, T.; Nugent, H.; Fanning, A.; Melgar, S.; Falvey, E. C.; Holmes, E.; Cotter, P. D.; O'Sullivan, O.; Molloy, M. G.; Shanahan, F.; Gilbert, J. A., A Prospective Metagenomic and Metabolomic Analysis of the Impact of Exercise and/or Whey Protein Supplementation on the Gut Microbiome of Sedentary Adults. *mSystems* **2018,** *3* (3), e00044-18.

31. Martin, F.-P. J.; Sprenger, N.; Yap, I. K. S.; Wang, Y.; Bibiloni, R.; Rochat, F.; Rezzi, S.; Cherbut, C.; Kochhar, S.; Lindon, J. C.; Holmes, E.; Nicholson, J. K., Panorganismal Gut Microbiome−Host Metabolic Crosstalk. *Journal of Proteome Research* **2009,** *8* (4), 2090-2105.

32. Louis-Jean, S.; Martirosyan, D., Nutritionally Attenuating the Human Gut Microbiome To Prevent and Manage Metabolic Syndrome. *Journal of Agricultural and Food Chemistry* **2019,** *67* (46), 12675-12684.

33. Hasegawa, Y.; Chen, S.-Y.; Sheng, L.; Jena, P. K.; Kalanetra, K. M.; Mills, D. A.; Wan, Y.-J. Y.; Slupsky, C. M., Long-term effects of western diet consumption in male and female mice. *Scientific Reports* **2020,** *10* (1), 14686.

34. Febbraio, M. A., Health benefits of exercise — more than meets the eye! *Nature Reviews Endocrinology* **2017,** *13* (2), 72-74.

35. Allen, J. M.; Miller, M. E. B.; Pence, B. D.; Whitlock, K.; Nehra, V.; Gaskins, H. R.; White, B. A.; Fryer, J. D.; Woods, J. A., Voluntary and forced exercise differentially alters the gut microbiome in C57BL/6J mice. *Journal of Applied Physiology* **2015,** *118* (8), 1059-1066.

36. Campbell, S. C.; Wisniewski, P. J.; Noji, M.; McGuinness, L. R.; Häggblom, M. M.; Lightfoot, S. A.; Joseph, L. B.; Kerkhof, L. J., The Effect of Diet and Exercise on Intestinal Integrity and Microbial Diversity in Mice. *PLOS ONE* **2016,** *11* (3), e0150502.

37. Cerdá, B.; Pérez, M.; Pérez-Santiago, J. D.; Tornero-Aguilera, J. F.; González-Soltero, R.; Larrosa, M., Gut Microbiota Modification: Another Piece in

the Puzzle of the Benefits of Physical Exercise in Health? *Frontiers in Physiology* **2016,** *7* (51).

38. Kern, T.; Blond, M. B.; Hansen, T. H.; Rosenkilde, M.; Quist, J. S.; Gram, A. S.; Ekstrøm, C. T.; Hansen, T.; Stallknecht, B., Structured exercise alters the gut microbiota in humans with overweight and obesity—A randomized controlled trial. *International Journal of Obesity* **2020,** *44* (1), 125-135.

39. Nicholson, J. K.; Holmes, E.; Kinross, J.; Burcelin, R.; Gibson, G.; Jia, W.; Pettersson, S., Host-Gut Microbiota Metabolic Interactions. *Science* **2012,** *336* (6086), 1262-1267.

40. Wikoff, W. R.; Anfora, A. T.; Liu, J.; Schultz, P. G.; Lesley, S. A.; Peters, E. C.; Siuzdak, G., Metabolomics analysis reveals large effects of gut microflora on mammalian blood metabolites. *Proceedings of the National Academy of Sciences* **2009,** *106* (10), 3698-3703.

41. Hariharan, D.; Vellanki, K.; Kramer, H., The Western Diet and Chronic Kidney Disease. *Current Hypertension Reports* **2015,** *17* (3), 16.

42. Bruce-Keller, A. J.; Salbaum, J. M.; Berthoud, H.-R., Harnessing Gut Microbes for Mental Health: Getting From Here to There. *Biological Psychiatry* **2018,** *83* (3), 214-223.

43. Bruce-Keller, A. J.; Fernandez-Kim, S.-O.; Townsend, R. L.; Kruger, C.; Carmouche, R.; Newman, S.; Salbaum, J. M.; Berthoud, H.-R., Maternal obese-type gut microbiota differentially impact cognition, anxiety and compulsive behavior in male and female offspring in mice. *PLOS ONE* **2017,** *12* (4), e0175577.

44. Rooks, M. G.; Garrett, W. S., Gut microbiota, metabolites and host immunity. *Nature Reviews Immunology* **2016,** *16* (6), 341-352.

45. Cani, P. D., Microbiota and metabolites in metabolic diseases. *Nature Reviews Endocrinology* **2019,** *15* (2), 69-70.

46. Kasahara, K.; Rey, F. E., The emerging role of gut microbial metabolism on cardiovascular disease. *Current Opinion in Microbiology* **2019,** *50*, 64-70.

47. Cook, M. D.; Allen, J. M.; Pence, B. D.; Wallig, M. A.; Gaskins, H. R.; White, B. A.; Woods, J. A., Exercise and gut immune function: evidence of

alterations in colon immune cell homeostasis and microbiome characteristics with exercise training. *Immunology & Cell Biology* **2016,** *94* (2), 158-163.

48. van den Bogert, B.; Leimena, M. M.; de Vos, W. M.; Zoetendal, E. G.; Kleerebezem, M., Functional Intestinal Metagenomics. In *Handbook of Molecular Microbial Ecology II*, 2011; pp 175-190.

49. Zulli, A.; Widdop, R. E.; Hare, D. L.; Buxton, B. F.; Black, M. J., High Methionine and Cholesterol Diet Abolishes Endothelial Relaxation. *Arteriosclerosis, Thrombosis, and Vascular Biology* **2003,** *23* (8), 1358-1363.

50. Chaturvedi, P.; Kamat, P. K.; Kalani, A.; Familtseva, A.; Tyagi, S. C., High Methionine Diet Poses Cardiac Threat: A Molecular Insight. *Journal of Cellular Physiology* **2016,** *231* (7), 1554-1561.

51. Glier, M. B.; Green, T. J.; Devlin, A. M., Methyl nutrients, DNA methylation, and cardiovascular disease. *Molecular Nutrition & Food Research* **2014,** *58* (1), 172-182.

52. McBean, G. J., The transsulfuration pathway: a source of cysteine for glutathione in astrocytes. *Amino Acids* **2012,** *42* (1), 199-205.

53. Christ, A.; Lauterbach, M.; Latz, E., Western Diet and the Immune System: An Inflammatory Connection. *Immunity* **2019,** *51* (5), 794-811.

54. Arulselvan, P.; Fard, M. T.; Tan, W. S.; Gothai, S.; Fakurazi, S.; Norhaizan, M. E.; Kumar, S. S., Role of Antioxidants and Natural Products in Inflammation. *Oxid Med Cell Longev* **2016,** *2016*, 5276130-5276130.

55. Jin, Z.; Liu, Y., DNA methylation in human diseases. *Genes & Diseases* **2018,** *5* (1), 1-8.

56. Muscella, A.; Stefàno, E.; Marsigliante, S., The effects of exercise training on lipid metabolism and coronary heart disease. *American Journal of Physiology-Heart and Circulatory Physiology* **2020,** *319* (1), H76-H88.

57. Rabinowitz, J. D.; Kimball, E., Acidic Acetonitrile for Cellular Metabolome Extraction from Escherichia coli. *Analytical chemistry* **2007,** *79* (16), 6167-6173.

58. Bazurto, J. V.; Dearth, S. P.; Tague, E. D.; Campagna, S. R.; Downs, D. M., Untargeted metabolomics confirms and extends the understanding of the

impact of aminoimidazole carboxamide ribotide (AICAR) in the metabolic network of Salmonella enterica. *Microbial cell (Graz, Austria)* **2017,** *5* (2), 74-87.

59. Chambers, M. C.; Maclean, B.; Burke, R.; Amodei, D.; Ruderman, D. L.; Neumann, S.; Gatto, L.; Fischer, B.; Pratt, B.; Egertson, J.; Hoff, K.; Kessner, D.; Tasman, N.; Shulman, N.; Frewen, B.; Baker, T. A.; Brusniak, M.-Y.; Paulse, C.; Creasy, D.; Flashner, L.; Kani, K.; Moulding, C.; Seymour, S. L.; Nuwaysir, L. M.; Lefebvre, B.; Kuhlmann, F.; Roark, J.; Rainer, P.; Detlev, S.; Hemenway, T.; Huhmer, A.; Langridge, J.; Connolly, B.; Chadick, T.; Holly, K.; Eckels, J.; Deutsch, E. W.; Moritz, R. L.; Katz, J. E.; Agus, D. B.; MacCoss, M.; Tabb, D. L.; Mallick, P., A cross-platform toolkit for mass spectrometry and proteomics. *Nature Biotechnology* **2012,** *30* (10), 918-920.

60. Melamud, E.; Vastag, L.; Rabinowitz, J. D., Metabolomic analysis and visualization engine for LC-MS data. *Analytical chemistry* **2010,** *82* (23), 9818-9826.

61. Clasquin, M. F.; Melamud, E.; Rabinowitz, J. D., LC-MS Data Processing with MAVEN : A Metabolomic Analysis and Visualization Engine. *Current Protocols in Bioinformatics* **2012,** (March), 1-23.

62. Tautenhahn, R.; Patti, G. J.; Rinehart, D.; Siuzdak, G., XCMS Online: A Web-Based Platform to Process Untargeted Metabolomic Data. *Analytical Chemistry* **2012,** *84* (11), 5035-5039.

63. Kuhl, C.; Tautenhahn, R.; Böttcher, C.; Larson, T. R.; Neumann, S., CAMERA: An Integrated Strategy for Compound Spectra Extraction and Annotation of Liquid Chromatography/Mass Spectrometry Data Sets. *Analytical Chemistry* **2012,** *84* (1), 283-289.

64. Team, R. C. *R: A Language and Environment for Statistical Computing*, 4.0.3; R Foundation for Statistical Computing: Vienna, Austria, 2020.

65. Xia, J.; Psychogios, N.; Young, N.; Wishart, D. S., MetaboAnalyst: a web server for metabolomic data analysis and interpretation. *Nucleic Acids Research* **2009,** *37* (suppl_2), W652-W660.

66. Pang, Z.; Chong, J.; Zhou, G.; de Lima Morais, D. A.; Chang, L.; Barrette, M.; Gauthier, C.; Jacques, P.-É.; Li, S.; Xia, J., MetaboAnalyst 5.0: narrowing the gap between raw spectra and functional insights. *Nucleic Acids Research* **2021,** *49* (W1), W388-W396.

67. Caballero, B., Humans against Obesity: Who Will Win? *Advances in Nutrition* **2019,** *10*, S4-S9.

68. Rao, S. V.; Donahue, M.; Pi-Sunyer, F. X.; Fuster, V., Obesity as a risk factor in coronary artery disease. *American Heart Journal* **2001,** *142* (6), 1102-1107.

69. Khaodhiar, L.; McCowen, K. C.; Blackburn, G. L., Obesity and its comorbid conditions. *Clinical Cornerstone* **1999,** *2* (3), 17-31.

70. Gregor, M. F.; Hotamisligil, G. S., Inflammatory Mechanisms in Obesity. *Annual Review of Immunology* **2011,** *29* (1), 415-445.

71. Simon, G. E.; Von Korff, M.; Saunders, K.; Miglioretti, D. L.; Crane, P. K.; van Belle, G.; Kessler, R. C., Association Between Obesity and Psychiatric Disorders in the US Adult Population. *Archives of General Psychiatry* **2006,** *63* (7), 824-830.

72. Ma, J.; Xiao, L., Obesity and Depression in US Women: Results From the 2005–2006 National Health and Nutritional Examination Survey. *Obesity* **2010,** *18* (2), 347-353.

73. Nissen, S. E.; Wolski, K., Effect of Rosiglitazone on the Risk of Myocardial Infarction and Death from Cardiovascular Causes. *New England Journal of Medicine* **2007,** *356* (24), 2457-2471.

74. Filippatos, T. D.; Panagiotopoulou, T. V.; Elisaf, M. S., Adverse Effects of GLP-1 Receptor Agonists. *Rev Diabet Stud* **2014,** *11* (3-4), 202-230.

75. Piette, J. D.; Heisler, M.; Wagner, T. H., Problems Paying Out-of-Pocket Medication Costs Among Older Adults With Diabetes. *Diabetes Care* **2004,** *27* (2), 384-391.

76. Payab, M.; Hasani-Ranjbar, S.; Shahbal, N.; Qorbani, M.; Aletaha, A.; Haghi-Aminjan, H.; Soltani, A.; Khatami, F.; Nikfar, S.; Hassani, S.; Abdollahi, M.; Larijani, B., Effect of the herbal medicines in obesity and metabolic syndrome: A systematic review and meta-analysis of clinical trials. *Phytotherapy Research* **2020,** *34* (3), 526-545.

77. Fuller, S.; Stephens, J. M., Diosgenin, 4-Hydroxyisoleucine, and Fiber from Fenugreek: Mechanisms of Actions and Potential Effects on Metabolic Syndrome. *Advances in Nutrition* **2015,** *6* (2), 189-197.

78. Garg, R. C., Chapter 44 - Fenugreek: Multiple Health Benefits. In *Nutraceuticals*, Gupta, R. C., Ed. Academic Press: Boston, 2016; pp 599-617.

79. Nagulapalli Venkata, K. C.; Swaroop, A.; Bagchi, D.; Bishayee, A., A small plant with big benefits: Fenugreek (Trigonella foenum-graecum Linn.) for disease prevention and health promotion. *Mol Nutr Food Res.* **2017,** *61* (6), 1600950.

80. Knott, E. J.; Richard, A. J.; Mynatt, R. L.; Ribnicky, D.; Stephens, J. M.; Bruce-Keller, A., Fenugreek supplementation during high-fat feeding improves specific markers of metabolic health. *Scientific Reports* **2017,** *7* (1), 12770.

81. Bruce-Keller, A. J.; Richard, A. J.; Fernandez-Kim, S.-O.; Ribnicky, D. M.; Salbaum, J. M.; Newman, S.; Carmouche, R.; Stephens, J. M., Fenugreek Counters the Effects of High Fat Diet on Gut Microbiota in Mice: Links to Metabolic Benefit. *Scientific Reports* **2020,** *10* (1), 1245.

82. Zentek, J.; Gärtner, S.; Tedin, L.; Männer, K.; Mader, A.; Vahjen, W., Fenugreek seed affects intestinal microbiota and immunological variables in piglets after weaning. *British Journal of Nutrition* **2013,** *109* (5), 859-866.

83. Shtriker, M. G.; Hahn, M.; Taieb, E.; Nyska, A.; Moallem, U.; Tirosh, O.; Madar, Z., Fenugreek galactomannan and citrus pectin improve several parameters associated with glucose metabolism and modulate gut microbiota in mice. *Nutrition* **2018,** *46*, 134-142.e3.

84. Antharam, V. C.; McEwen, D. C.; Garrett, T. J.; Dossey, A. T.; Li, E. C.; Kozlov, A. N.; Mesbah, Z.; Wang, G. P., An Integrated Metabolomic and Microbiome Analysis Identified Specific Gut Microbiota Associated with Fecal Cholesterol and Coprostanol in Clostridium difficile Infection. *PLOS ONE* **2016,** *11* (2), e0148824.

85. Cornejo-Pareja, I.; Muñoz-Garach, A.; Clemente-Postigo, M.; Tinahones, F. J., Importance of gut microbiota in obesity. *European Journal of Clinical Nutrition* **2019,** *72* (1), 26-37.

86. Sekirov, I.; Russell, S. L.; Antunes, L. C. M.; Finlay, B. B., Gut Microbiota in Health and Disease. *Physiological Reviews* **2010,** *90* (3), 859-904.

87. Shen, W.; Gaskins, H. R.; McIntosh, M. K., Influence of dietary fat on intestinal microbes, inflammation, barrier function and metabolic outcomes. *The Journal of Nutritional Biochemistry* **2014,** *25* (3), 270-280.

88. Wells, A.; Barrington, W. T.; Dearth, S.; May, A.; Threadgill, D. W.; Campagna, S. R.; Voy, B. H., Tissue Level Diet and Sex-by-Diet Interactions Reveal Unique Metabolite and Clustering Profiles Using Untargeted Liquid Chromatography–Mass Spectrometry on Adipose, Skeletal Muscle, and Liver Tissue in C57BL6/J Mice. *Journal of Proteome Research* **2018,** *17* (3), 1077-1090.

89. Pendyala, S.; Walker, J. M.; Holt, P. R., A High-Fat Diet Is Associated With Endotoxemia That Originates From the Gut. *Gastroenterology* **2012,** *142* (5), 1100-1101.e2.

90. Douglas-Escobar, M.; Elliott, E.; Neu, J., Effect of Intestinal Microbial Ecology on the Developing Brain. *JAMA Pediatrics* **2013,** *167* (4), 374-379.

91. Dinan, T. G.; Quigley, E. M., Probiotics in the Treatment of Depression: Science or Science Fiction? *Australian & New Zealand Journal of Psychiatry* **2011,** *45* (12), 1023-1025.

92. Tillisch, K., The effects of gut microbiota on CNS function in humans. *Gut Microbes* **2014,** *5* (3), 404-410.

93. Neufeld, K. M.; Kang, N.; Bienenstock, J.; Foster, J. A., Reduced anxiety-like behavior and central neurochemical change in germ-free mice. *Neurogastroenterology & Motility* **2011,** *23* (3), 255-e119.

94. Heijtz, R. D.; Wang, S.; Anuar, F.; Qian, Y.; Björkholm, B.; Samuelsson, A.; Hibberd, M. L.; Forssberg, H.; Pettersson, S., Normal gut microbiota modulates brain development and behavior. *Proceedings of the National Academy of Sciences* **2011,** *108* (7), 3047-3052.

95. Hannan, J. M. A.; Rokeya, B.; Faruque, O.; Nahar, N.; Mosihuzzaman, M.; Azad Khan, A. K.; Ali, L., Effect of soluble dietary fibre fraction of Trigonella foenum graecum on glycemic, insulinemic, lipidemic and platelet aggregation status of Type 2 diabetic model rats. *Journal of Ethnopharmacology* **2003,** *88* (1), 73-77.

96. Narender, T.; Puri, A.; Shweta; Khaliq, T.; Saxena, R.; Bhatia, G.; Chandra, R., 4-Hydroxyisoleucine an unusual amino acid as antidyslipidemic and

antihyperglycemic agent. *Bioorganic & Medicinal Chemistry Letters* **2006,** *16* (2), 293-296.

97. Hamden, K.; Jaouadi, B.; Carreau, S.; Bejar, S.; Elfeki, A., Inhibitory effect of fenugreek galactomannan on digestive enzymes related to diabetes, hyperlipidemia, and liver-kidney dysfunctions. *Biotechnology and Bioprocess Engineering* **2010,** *15* (3), 407-413.

98. Jiang, W.; Gao, L.; Li, P.; Kan, H.; Qu, J.; Men, L.; Liu, Z.; Liu, Z., Metabonomics study of the therapeutic mechanism of fenugreek galactomannan on diabetic hyperglycemia in rats, by ultra-performance liquid chromatography coupled with quadrupole time-of-flight mass spectrometry. *Journal of Chromatography B* **2017,** *1044-1045*, 8-16.

99. Pedley, A. M.; Benkovic, S. J., A New View into the Regulation of Purine Metabolism: The Purinosome. *Trends in Biochemical Sciences* **2017,** *42* (2), 141-154.

100. Díaz-Leal, J. L.; Torralbo, F.; Antonio Quiles, F.; Pineda, M.; Alamillo, J. M., Molecular and functional characterization of allantoate amidohydrolase from Phaseolus vulgaris. *Physiologia Plantarum* **2014,** *152* (1), 43-58.

101. Witte, C.-P., Urea metabolism in plants. *Plant Science* **2011,** *180* (3), 431-438.

102. Finkelstein, J. D.; Martin, J. J.; Harris, B. J., Methionine metabolism in mammals. The methionine-sparing effect of cystine. *Journal of Biological Chemistry* **1988,** *263* (24), 11750-11754.

103. Battelli, M. G.; Bortolotti, M.; Polito, L.; Bolognesi, A., Metabolic syndrome and cancer risk: The role of xanthine oxidoreductase. *Redox Biology* **2019,** *21*, 101070.

104. Hoppel, C., The role of carnitine in normal and altered fatty acid metabolism. *American Journal of Kidney Diseases* **2003,** *41*, S4-S12.

105. Bene, J.; Hadzsiev, K.; Melegh, B., Role of carnitine and its derivatives in the development and management of type 2 diabetes. *Nutrition & Diabetes* **2018,** *8* (1), 8.

106. Flanagan, J. L.; Simmons, P. A.; Vehige, J.; Willcox, M. D. P.; Garrett, Q., Role of carnitine in disease. *Nutrition & Metabolism* **2010,** *7* (1), 30.

107. Koeth, R. A.; Wang, Z.; Levison, B. S.; Buffa, J. A.; Org, E.; Sheehy, B. T.; Britt, E. B.; Fu, X.; Wu, Y.; Li, L.; Smith, J. D.; DiDonato, J. A.; Chen, J.; Li, H.; Wu, G. D.; Lewis, J. D.; Warrier, M.; Brown, J. M.; Krauss, R. M.; Tang, W. H. W.; Bushman, F. D.; Lusis, A. J.; Hazen, S. L., Intestinal microbiota metabolism of l-carnitine, a nutrient in red meat, promotes atherosclerosis. *Nature Medicine* **2013,** *19* (5), 576-585.

108. Bauer, K., Carnosine and Homocarnosine, the Forgotten, EnigmaticPeptides of the Brain. *Neurochemical Research* **2005,** *30* (10), 1339-1345.

109. Kohen, R.; Yamamoto, Y.; Cundy, K. C.; Ames, B. N., Antioxidant activity of carnosine, homocarnosine, and anserine present in muscle and brain. *Proceedings of the National Academy of Sciences* **1988,** *85* (9), 3175-3179.

110. Chong, J.; Soufan, O.; Li, C.; Caraus, I.; Li, S.; Bourque, G.; Wishart, D. S.; Xia, J., MetaboAnalyst 4.0: towards more transparent and integrative metabolomics analysis. *Nucleic Acids Research* **2018,** *46* (W1), W486-W494.

111. Wu, G.; Bazer, F. W.; Davis, T. A.; Kim, S. W.; Li, P.; Marc Rhoads, J.; Carey Satterfield, M.; Smith, S. B.; Spencer, T. E.; Yin, Y., Arginine metabolism and nutrition in growth, health and disease. *Amino Acids* **2009,** *37* (1), 153-168.

112. Allerton, T. D.; Proctor, D. N.; Stephens, J. M.; Dugas, T. R.; Spielmann, G.; Irving, B. A., l-Citrulline Supplementation: Impact on Cardiometabolic Health. *Nutrients* **2018,** *10* (7).

113. Team, R. C. *R: A Language and Environment for Statistical Computing*, 3.5.1; R Foundation for Statistical Computing: Vienna, Austria, 2018.

114. Worley, B.; Powers, R., Multivariate Analysis in Metabolomics. *Curr Metabolomics* **2013,** *1* (1), 92-107.

115. Worley, B.; Powers, R., PCA as a practical indicator of OPLS-DA model reliability. *Curr Metabolomics* **2016,** *4* (2), 97-103.

116. Oliveros, J. C. *Venny. An interactive tool for comparing lists with Venn's diagrams*, 2007-2015.

117. Kind, T.; Fiehn, O., Seven Golden Rules for heuristic filtering of molecular formulas obtained by accurate mass spectrometry. *BMC Bioinformatics* **2007,** *8* (105), 1-20.

118. Westfall, C. S.; Levin, P. A., Comprehensive analysis of central carbon metabolism illuminates connections between nutrient availability, growth rate, and cell morphology in Escherichia coli. *PLOS Genetics* **2018,** *14* (2), 1-25.

119. Vadia, S.; Tse, J. L.; Lucena, R.; Yang, Z.; Kellogg, D. R.; Wang, J. D.; Levin, P. A., Fatty Acid Availability Sets Cell Envelope Capacity and Dictates Microbial Cell Size. *Current Biology* **2017,** *27* (12), 1757-1767.

120. Catucci, L.; Depalo, N.; Lattanzio, V. M. T.; Agostiano, A.; Corcelli, A., Neosynthesis of Cardiolipin in Rhodobacter sphaeroides under Osmotic Stress. *Biochemistry* **2004,** *43* (47), 15066-15072.

121. Jackson, M.; Crick, D. C.; Brennan, P. J., Phosphatidylinositol is an essential phospholipid of mycobacteria. *The Journal of biological chemistry* **2000,** *275* (39), 30092-9.

122. Nguyen, N. A.; Sallans, L.; Kaneshiro, E. S., The major glycerophospholipids of the predatory and parasitic bacterium Bdellovibrio bacteriovorus HID5. *Lipids* **2008,** *43* (11), 1053-63.

123. Park, S.; Jung, Y.-T.; Won, S.-M.; Park, J.-M.; Yoon, J.-H., Sulfitobacter undariae sp. nov., isolated from a brown algae reservoir. **2015,** *65* (Pt_5), 1672-1678.

124. Yao, J.; Rock, C. O., Phosphatidic acid synthesis in bacteria. *Biochimica et Biophysica Acta (BBA) - Molecular and Cell Biology of Lipids* **2013,** *1831* (3), 495-502.

125. Gao, J.-L.; Weissenmayer, B.; Taylor, A. M.; Thomas-Oates, J.; López-Lara, I. M.; Geiger, O., Identification of a gene required for the formation of lyso-ornithine lipid, an intermediate in the biosynthesis of ornithine-containing lipids. *Molecular Microbiology* **2004,** *53* (6), 1757-1770.

126. Sohlenkamp, C.; Geiger, O., Bacterial membrane lipids: diversity in structures and pathways. *Fems Microbiology Reviews* **2016,** *40* (1), 133-159.

127. Weissenmayer, B.; Gao, J.-L.; López-Lara, I. M.; Geiger, O., Identification of a gene required for the biosynthesis of ornithine-derived lipids. *Molecular Microbiology* **2002,** *45* (3), 721-733.

128. Raetz, C. R. H., Molecular Genetics of Membrane Phospholipid Synthesis. *Annual Review of Genetics* **1986,** *20* (1), 253-291.

129. Raetz, C. R.; Dowhan, W., Biosynthesis and function of phospholipids in Escherichia coli. *The Journal of biological chemistry* **1990,** *265* (3), 1235-1238.

130. Park, S.; Kim, I. K.; Lee, J.-S.; Yoon, J.-H., Sulfitobacter sabulilitoris sp. nov., isolated from marine sand. **2019,** *69* (10), 3230-3236.

131. Zhang, X.; Fergulson-Miller, S. M.; Reid, G. E., Characterization of Ornithine and Glutamine Lipids Extracted from Cell Membranes of Rhodobacter sphaeroides. *Journal of the American Society for Mass Spectrometry* **2009,** *20* (2), 198-212.

132. Favre, L.; Ortalo-Magne, A.; Pichereaux, C.; Gargaros, A.; Burlet-Schiltz, O.; Cotelle, V.; Culioli, G., Metabolome and proteome changes between biofilm and planktonic phenotypes of the marine bacterium Pseudoalteromonas lipolytica TC8. *Biofouling* **2018,** *34* (2), 132-148.

133. Breitbart, M.; Bonnain, C.; Malki, K.; Sawaya, N. A., Phage puppet masters of the marine microbial realm. *Nature Microbiology* **2018,** *3* (7), 754-766.

134. Hurwitz, B. L.; Hallam, S. J.; Sullivan, M. B., Metabolic reprogramming by viruses in the sunlit and dark ocean. *Genome Biol* **2013,** *14* (11), 1-14.

135. Lindell, D.; Sullivan, M. B.; Johnson, Z. I.; Tolonen, A. C.; Rohwer, F.; Chisholm, S. W., Transfer of photosynthesis genes to and from Prochlorococcus viruses. *Proceedings of the National Academy of Sciences of the United States of America* **2004,** *101* (30), 11013–11018.

136. Thompson, L. R.; Zeng, Q.; Kelly, L.; Huang, K. H.; Singer, A. U.; Stubbe, J.; Chisholm, S. W., Phage auxiliary metabolic genes and the redirection of cyanobacterial host carbon metabolism. *Proceedings of the National Academy of Sciences* **2011,** *108* (39), E757–E764.

137. Warwick-Dugdale, J.; Buchholz, H. H.; Allen, M. J.; Temperton, B., Host-hijacking and planktonic piracy: how phages command the microbial high seas. *Virology Journal* **2019,** *16* (1), 1-13.

138. Roitman, S.; Hornung, E.; Flores-Uribe, J.; Sharon, I.; Feussner, I.; Beja, O., Cyanophage-encoded lipid desaturases: oceanic distribution, diversity and function. *Isme Journal* **2018,** *12* (2), 343-355.

139. Ankrah, N. Y. D.; May, A. L.; Middleton, J. L.; Jones, D. R.; Hadden, M. K.; Gooding, J. R.; LeCleir, G. R.; Wilhelm, S. W.; Campagna, S. R.; Buchan, A., Phage infection of an environmentally relevant marine bacterium alters host metabolism and lysate composition. *Isme Journal* **2014,** *8* (5), 1089-1100.

140. De Smet, J.; Zimmermann, M.; Kogadeeva, M.; Ceyssens, P. J.; Vermaelen, W.; Blasdel, B.; Jang, H. B.; Sauer, U.; Lavigne, R., High coverage metabolomics analysis reveals phage-specific alterations to Pseudomonas aeruginosa physiology during infection. *Isme Journal* **2016,** *10* (8), 1823-1835.

141. Basso, J. T. R.; Ankrah, N. Y. D.; Tuttle, M. J.; Grossman, A. S.; Sandaa, R.-A.; Buchan, A., Genetically similar temperate phages form coalitions with their shared host that lead to niche-specific fitness effects. *The ISME Journal* **2020,** *14*, 1688–1700.

142. Smith, A. F.; Rihtman, B.; Stirrup, R.; Silvano, E.; Mausz, M. A.; Scanlan, D. J.; Chen, Y., Elucidation of glutamine lipid biosynthesis in marine bacteria reveals its importance under phosphorus deplete growth in Rhodobacteraceae. *Isme Journal* **2019,** *13* (1), 39-49.

143. Fahy, E.; Subramaniam, S.; Murphy, R. C.; Nishijima, M.; Raetz, C. R.; Shimizu, T.; Spener, F.; van Meer, G.; Wakelam, M. J.; Dennis, E. A., Update of the LIPID MAPS comprehensive classification system for lipids. *Journal of lipid research* **2009,** *50 Suppl* (Suppl), S9-14.

144. Carini, P.; Van Mooy, B. A. S.; Thrash, J. C.; White, A.; Zhao, Y.; Campbell, E. O.; Fredricks, H. F.; Giovannoni, S. J., SAR11 lipid renovation in response to phosphate starvation. *Proceedings of the National Academy of Sciences* **2015,** *112* (25), 7767–7772.

145. Van Mooy, B. A.; Fredricks, H. F.; Pedler, B. E.; Dyhrman, S. T.; Karl, D. M.; Koblízek, M.; Lomas, M. W.; Mincer, T. J.; Moore, L. R.; Moutin, T.; Rappé, M. S.; Webb, E. A., Phytoplankton in the ocean use non-phosphorus lipids in response to phosphorus scarcity. *Nature* **2009,** *458* (7234), 69-72.

146. Zimmerman, A. E.; Allison, S. D.; Martiny, A. C., Phylogenetic constraints on elemental stoichiometry and resource allocation in heterotrophic marine bacteria. *Environmental Microbiology* **2014,** *16* (5), 1398-1410.

147. Fagerbakke, K. M.; Heldal, M.; Norland, S., Content of carbon, nitrogen, oxygen, sulfur and phosphorus in native aquatic and cultured bacteria. *Aquatic Microbial Ecology* **1996,** *10* (1), 15-27.

148. Ietswaart, T.; Schneider, P. J.; Prins, R. A., Utilization of Organic Nitrogen Sources by Two Phytoplankton Species and a Bacterial Isolate in Pure and Mixed Cultures. *Applied and Environmental Microbiology* **1994,** *60* (5), 1554-1560.

149. Wheeler, P. A.; Kirchman, D. L., Utilization of inorganic and organic nitrogen by bacteria in marine systems1. *Limnology and Oceanography* **1986,** *31* (5), 998-1009.

150. Andersson, M., G. I.; Rijswijk, P. v.; Middelburg, J., J., Uptake of dissolved inorganic nitrogen, urea and amino acids in the Scheldt estuary: comparison of organic carbon and nitrogen uptake. *Aquatic Microbial Ecology* **2006,** *44* (3), 303-315.

151. Bradley, P. B.; Sanderson, M. P.; Frischer, M. E.; Brofft, J.; Booth, M. G.; Kerkhof, L. J.; Bronk, D. A., Inorganic and organic nitrogen uptake by phytoplankton and heterotrophic bacteria in the stratified Mid-Atlantic Bight. *Estuarine, Coastal and Shelf Science* **2010,** *88* (4), 429-441.

152. Jover, L. F.; Effler, T. C.; Buchan, A.; Wilhelm, S. W.; Weitz, J. S., The elemental composition of virus particles: implications for marine biogeochemical cycles. *Nature Reviews Microbiology* **2014,** *12* (7), 519-528.

153. Frimmersdorf, E.; Horatzek, S.; Pelnikevich, A.; Wiehlmann, L.; Schomburg, D., How Pseudomonas aeruginosa adapts to various environments: a metabolomic approach. *Environmental Microbiology* **2010,** *12* (6), 1734-1747.

154. Meyer, H.; Weidmann, H.; Mäder, U.; Hecker, M.; Völker, U.; Lalk, M., A time resolved metabolomics study: the influence of different carbon sources during growth and starvation of Bacillus subtilis. *Molecular BioSystems* **2014,** *10* (7), 1812-1823.

155. Zachariah, S.; Kumari, P.; Das, S. K., Sulfitobacter pontiacus subsp. fungiae subsp. nov., Isolated from Coral Fungia seychellensis from Andaman

Sea, and Description of Sulfitobacter pontiacus subsp. pontiacus subsp. nov. *Current Microbiology* **2017,** *74* (3), 404-412.

156. Pujalte, M. J.; Lucena, T.; Ruvira, M. A.; Arahal, D. R.; Macián, M. C., The Family Rhodobacteraceae. In *The Prokaryotes: Alphaproteobacteria and Betaproteobacteria*, Rosenberg, E.; DeLong, E. F.; Lory, S.; Stackebrandt, E.; Thompson, F., Eds. Springer Berlin Heidelberg: Berlin, Heidelberg, 2014; pp 439-512.

157. Zhao, W.; Róg, T.; Gurtovenko, A. A.; Vattulainen, I.; Karttunen, M., Role of phosphatidylglycerols in the stability of bacterial membranes. *Biochimie* **2008,** *90* (6), 930-938.

158. Rowlett, V. W.; Mallampalli, V. K. P. S.; Karlstaedt, A.; Dowhan, W.; Taegtmeyer, H.; Margolin, W.; Vitrac, H., Impact of Membrane Phospholipid Alterations in Escherichia coli on Cellular Function and Bacterial Stress Adaptation. *Journal of Bacteriology* **2017,** *199* (13), e00849-16.

159. Op den Kamp, J. A. F.; Redai, I.; van Deenen, L. L. M., Phospholipid Composition of Bacillus subtilis. *Journal of Bacteriology* **1969,** *99* (1), 298-303.

160. Fujita, Y.; Matsuoka, H.; Hirooka, K., Regulation of fatty acid metabolism in bacteria. *Mol Microbiol* **2007,** *66* (4), 829-39.

161. Giles, D. K.; Hankins, J. V.; Guan, Z.; Trent, M. S., Remodelling of the Vibrio cholerae membrane by incorporation of exogenous fatty acids from host and aquatic environments. *Molecular microbiology* **2011,** *79* (3), 716-728.

162. Harp, J. R.; Saito, H. E.; Bourdon, A. K.; Reyes, J.; Arias, C. A.; Campagna, S. R.; Fozo, E. M., Exogenous Fatty Acids Protect Enterococcus faecalis from Daptomycin-Induced Membrane Stress Independently of the Response Regulator LiaR. *Appl Environ Microbiol* **2016,** *82* (14), 4410-4420.

163. Sebastián, M.; Smith, A. F.; González, J. M.; Fredricks, H. F.; Van Mooy, B.; Koblížek, M.; Brandsma, J.; Koster, G.; Mestre, M.; Mostajir, B.; Pitta, P.; Postle, A. D.; Sánchez, P.; Gasol, J. M.; Scanlan, D. J.; Chen, Y., Lipid remodelling is a widespread strategy in marine heterotrophic bacteria upon phosphorus deficiency. *The ISME Journal* **2016,** *10* (4), 968-978.

164. Goutx, M.; Acquaviva, M.; Bertrand, J.-C., Cellular and extracellular carbohydrates and lipids from marine bacteria during growth on soluble substrates and hydrocarbons. *Marine ecology progress series.* **1990,** *61* (3), 291-296.

165. Silvano, E.; Yang, M.; Wolterink, M.; Giebel, H.-A.; Simon, M.; Scanlan, D. J.; Zhao, Y.; Chen, Y., Lipidomic Analysis of Roseobacters of the Pelagic RCA Cluster and Their Response to Phosphorus Limitation. **2020,** *11* (3240), 1-7.

166. Geiger, O.; González-Silva, N.; López-Lara, I. M.; Sohlenkamp, C., Amino acid-containing membrane lipids in bacteria. *Progress in Lipid Research* **2010,** *49* (1), 46-60.

167. Moore, E.; Hopmans, E.; Rijpstra, W. I.; Sanchez Andrea, I.; Villanueva, L.; Wienk, H.; Schoutsen, F.; Stams, A.; Sinninghe Damste, J., Lysine and novel hydroxylysine lipids in soil bacteria: amino acid membrane lipid response to temperature and pH in Pseudopedobacter saltans. **2015,** *6* (637), 1-12.

168. Vences-Guzman, M. A.; Geiger, O.; Sohlenkamp, C., Ornithine lipids and their structural modifications: from A to E and beyond. *Fems Microbiology Letters* **2012,** *335* (1), 1-10.

169. Aygun-Sunar, S.; Mandaci, S.; Koch, H.-G.; Murray, I. V. J.; Goldfine, H.; Daldal, F., Ornithine lipid is required for optimal steady-state amounts of c-type cytochromes in Rhodobacter capsulatus. *Molecular Microbiology* **2006,** *61* (2), 418-435.

170. Bennett, B. D.; Kimball, E. H.; Gao, M.; Osterhout, R.; Van Dien, S. J.; Rabinowitz, J. D., Absolute metabolite concentrations and implied enzyme active site occupancy in Escherichia coli. *Nature Chemical Biology* **2009,** *5* (8), 593-599.

171. Clasen, J. L.; Elser, J. J., The effect of host Chlorella NC64A carbon : phosphorus ratio on the production of Paramecium bursaria Chlorella Virus-1. *Freshwater Biology* **2007,** *52* (1), 112-122.

172. Martin, R. M.; Dearth, S. P.; LeCleir, G. R.; Campagna, S. R.; Fozo, E. M.; Zinser, E. R.; Wilhelm, S. W., Microcystin-LR does not induce alterations to transcriptomic or metabolomic profiles of a model heterotrophic bacterium. *PLOS ONE* **2017,** *12* (12), 1-19.

173. Bazurto, J. V.; Dearth, S. P.; Tague, E. D.; Campagna, S. R.; Downs, D. M., Untargeted metabolomics confirms and extends the understanding of the impact of aminoimidazole carboxamide ribotide (AICAR) in the metabolic network of Salmonella enterica. *Microbial Cell* **2018,** *5* (2), 74-87.

174. Clasquin, M. F.; Melamud, E.; Rabinowitz, J. D., LC-MS Data Processing with MAVEN: A Metabolomic Analysis and Visualization Engine. *Current Protocols in Bioinformatics* **2012,** *37* (1), 14.11.1-14.11.23.

175. Melamud, E.; Vastag, L.; Rabinowitz, J. D., Metabolomic Analysis and Visualization Engine for LC−MS Data. *Analytical Chemistry* **2010,** *82* (23), 9818-9826.

176. Guan, X. L.; Riezman, I.; Wenk, M. R.; Riezman, H., Chapter 15 - Yeast Lipid Analysis and Quantification by Mass Spectrometry. In *Methods in Enzymology*, Academic Press: 2010; Vol. 470, pp 369-391.

177. Tague, E. D.; Woodall, B. M.; Harp, J. R.; Farmer, A. T.; Fozo, E. M.; Campagna, S. R., Expanding lipidomics coverage: effective ultra performance liquid chromatography-high resolution mass spectrometer methods for detection and quantitation of cardiolipin, phosphatidylglycerol, and lysyl-phosphatidylglycerol. *Metabolomics* **2019,** *15* (4), 1-10.

Vita

Katarina Jones grew up outside of Atlanta, Georgia and discovered her love of chemistry in her sophomore year of high school. She then continued to pursue chemistry and began her journey at Berry College in Rome, Georgia in 2013. As a part of Berry's student work program, she began to work in the chemistry department as a general lab assistant. In the spring of 2015, she began undergraduate research in the lab of Dr. Alice Suroviec where she was using cyclic voltammetry to detect polyphenols in teas. Through the mentorship of Dr. Suroviec, she decided to pursue analytical chemistry in graduate school. Katarina graduated from Berry in May 2017 with her degree in chemistry. In the fall of 2017, she began her graduate school career at the University of Tennessee Knoxville, where she joined the lab of Dr. Shawn Campagna. During her time in the Campagna lab, Katarina has worked on projects using mass spectrometry to evaluate metabolite and lipid alterations in various biological systems, with particular interest in the effects of nutrients.